Earthquake analysis of quay walls

- Appendices -

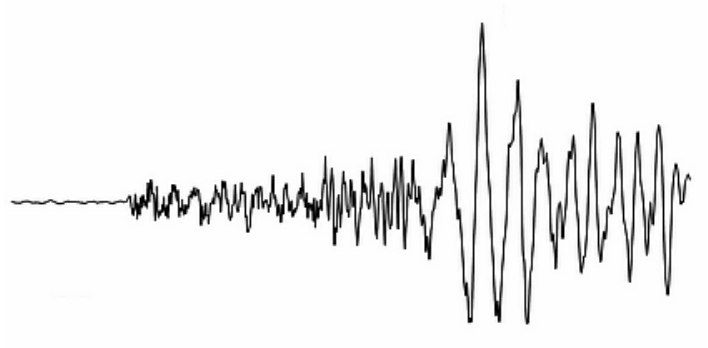

Delft University of Technology

Gemeentewerken
Gemeente Rotterdam

Appendices

Appendix A Soundings and ground profile

Behaviour of the soil takes an important part during seismic analysis. Different soil type behaves and reacts differently during an earthquake. Many soundings are available for the Euromax quay wall with a maximum distance of 25m in between and a minimum reach of NAP -40m. These soundings were used during the design and construction of the Euromax terminal by the main contractor BAM and will also be uses during this research. A notion must be made that these soundings were made before the quay wall was build. Soil near the quay wall may become denser during the pile driving. Still, these soundings were used due to the fact that no soundings after completion were available.

Based on the soundings made for the Euromax terminal, BAM (main contractor in building the quay) subdivided the total quay length into 14 sections. Within these sections, the ground profiles won't differ a lot from each other and were assumed to be the same. They also determined the ground parameters for each layer of soil for the 14 different ground profiles. The research done by the main contractor won't be questioned further and was used during this research. The notation and location of the 14 section are shown in Figure A-1 and Table A-1.

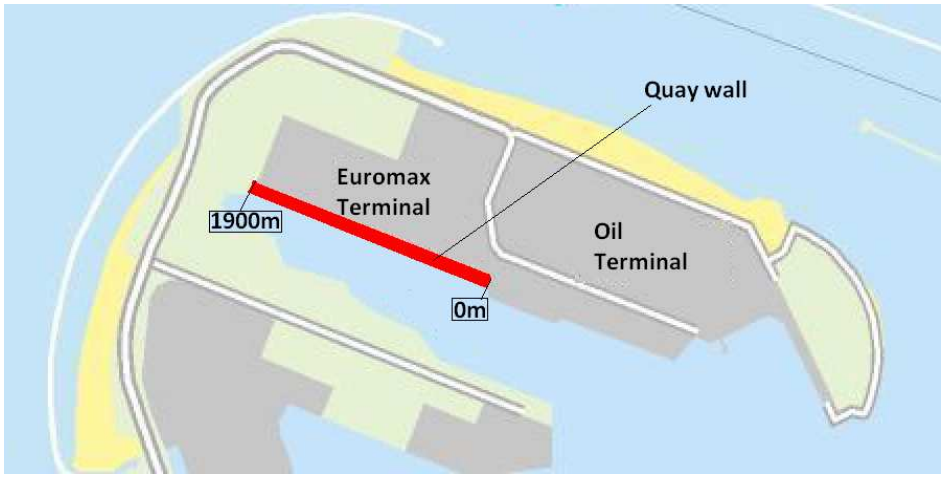

Figure A-1 Euromax terminal and his quay wall

	Location of occurence	
Section	From [m]	Till [m]
1	0	100
2	100	240
3	240	310
4	310	510
5	510	630
6	630	730
7	730	960
8	960	1085
9	1085	1130
10	1130	1250
11	1250	1410
12	1410	1500
13	1500	1800
14	1800	1900

Table A-1: Location of the 14 sections

The representative soundings and ground profiles for each section can be found in Figure A-2 till Figure A-15. Also some ground parameters determined by the main contractor are given for these ground profile in Table A-2 till Table A-15.

Figure A-2: Sounding and ground profile of section 1

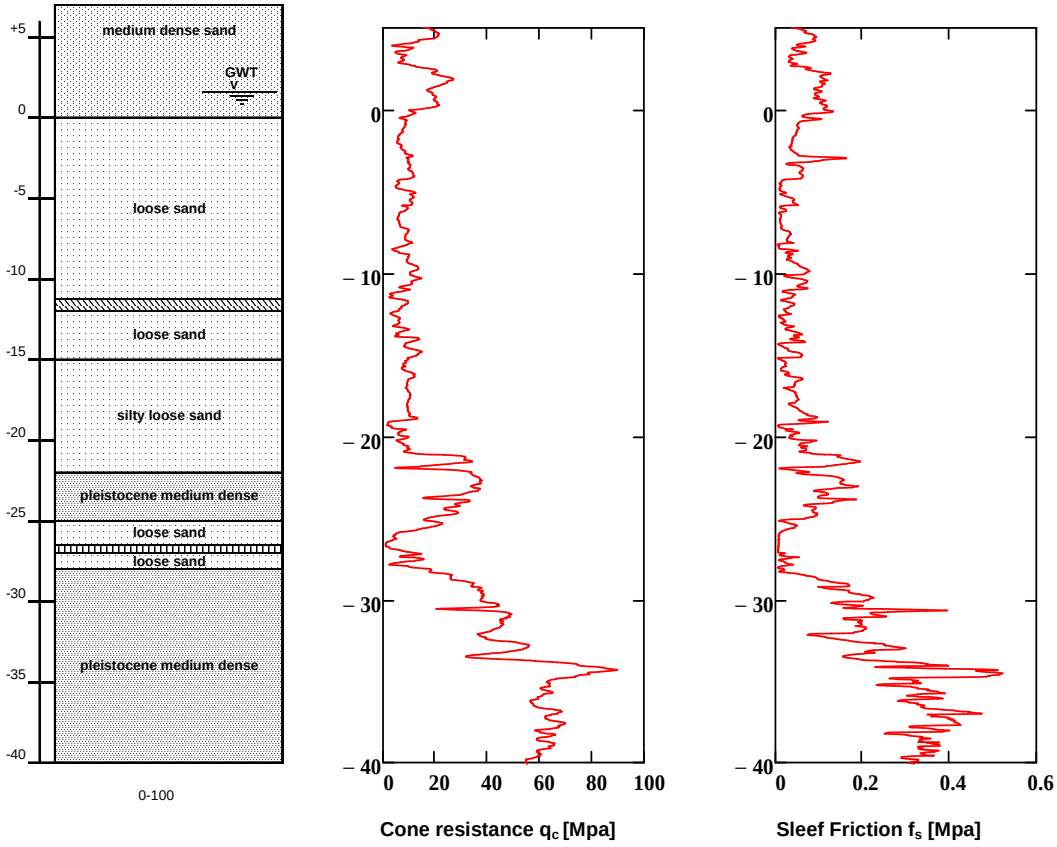

Depth [m NAP]		Layer discription	γ_{dry}	γ_{sat}
from	till		[kN/m^3]	[kN/m^3]
7	0	medium dense sand	18	20
0	-11,3	loose sand	17	19
-11,3	-12	dense sandy loam/clay	19,5	19,5
-12	-15	loose sand	17	19
-15	-22	silty loose sand	19	19
-22	-25	pleistocene medium dense	20	20
-25	-26,5	loose sand	17	19
-26,5	-27	sandy medium dense loam	20	20
-27	-28	loose sand	17	19
-28	-40	pleistocene medium dense	20	20
-40				

Table A-2: Ground parameters for sections 1

Figure A-3: Sounding and ground profile of section 2

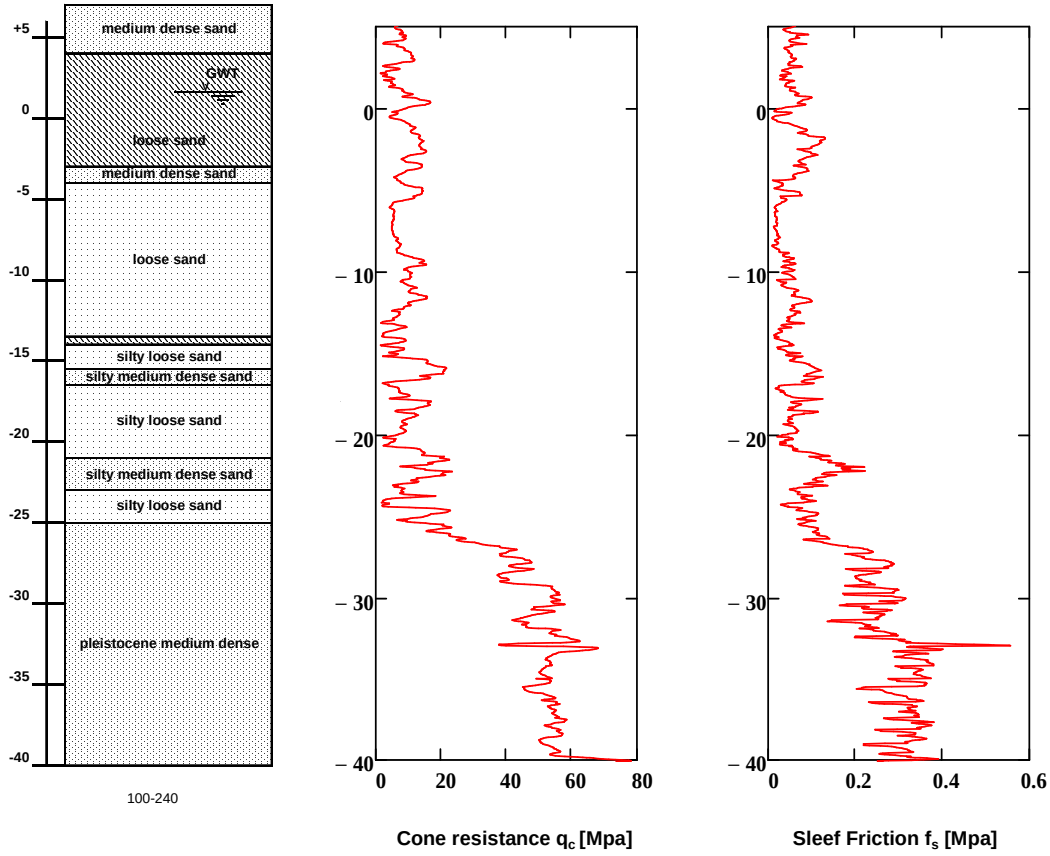

Depth [m NAP]		Layer discription	γ_{dry}	γ_{sat}
from	till		[kN/m^3]	[kN/m^3]
7	4	medium dense sand	18	20
4	-3	loose sand	17	19
-3	-4	medium dense sand	18	20
-4	-13,5	loose sand	17	19
-13,5	-14	sandy clay	18	18
-14	-15,5	silty loose sand	19	19
-15,5	-16,5	silty medium dense sand	19,5	19,5
-16,5	-21	silty loose sand	19	19
-21	-23	silty medium dense sand	19,5	19,5
-23	-25	silty loose sand	19	19
-25	-40	pleistocene medium dense	20	20
-40				

Table A-3: Ground parameters for sections 2

Figure A-4 Sounding and ground profile of section 3

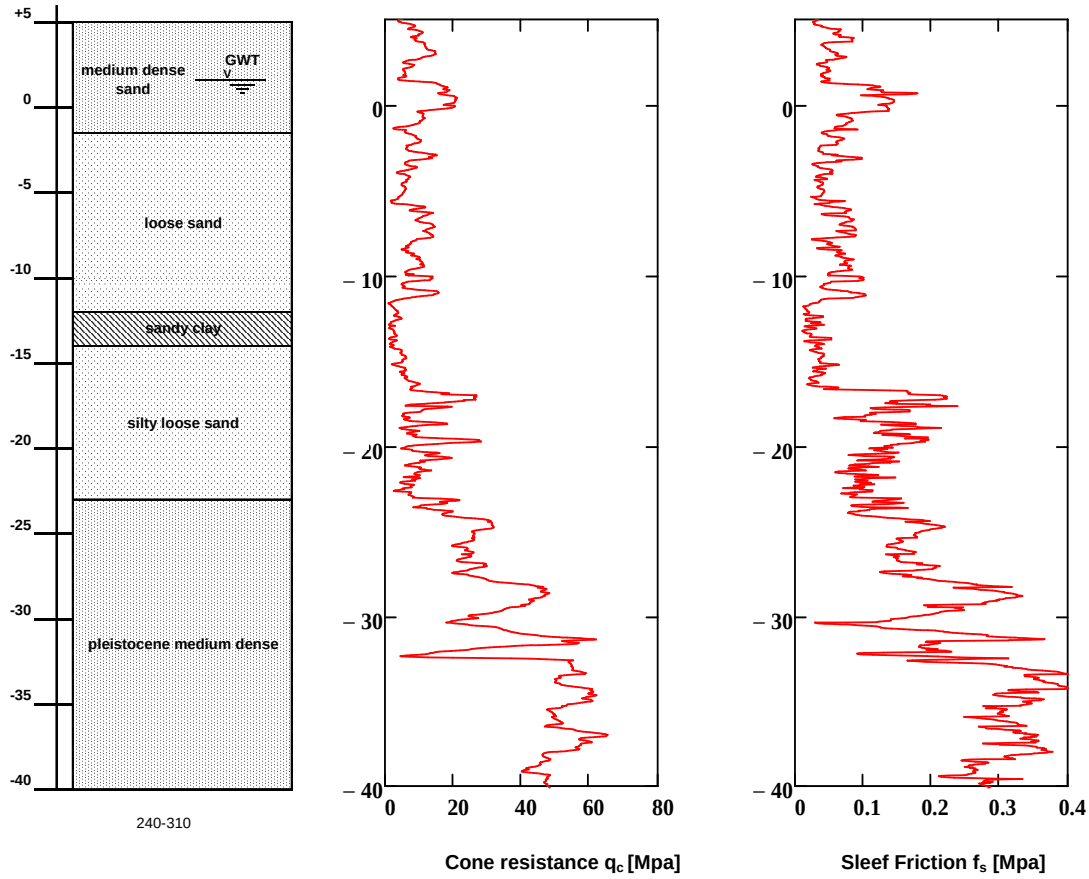

Depth [m NAP]		Layer discription	γ_{dry}	γ_{sat}
from	till		[kN/m^3]	[kN/m^3]
7	-1,5	medium dense sand	18	20
-1,5	-12	loose sand	17	19
-12	-14	sandy clay	18	18
-14	-23	silty loose sand	19	19
-23	-40	pleistocene medium dense	20	20
-40				

Table A-4: Ground parameters for sections 3

Figure A-5 Sounding and ground profile of section 4

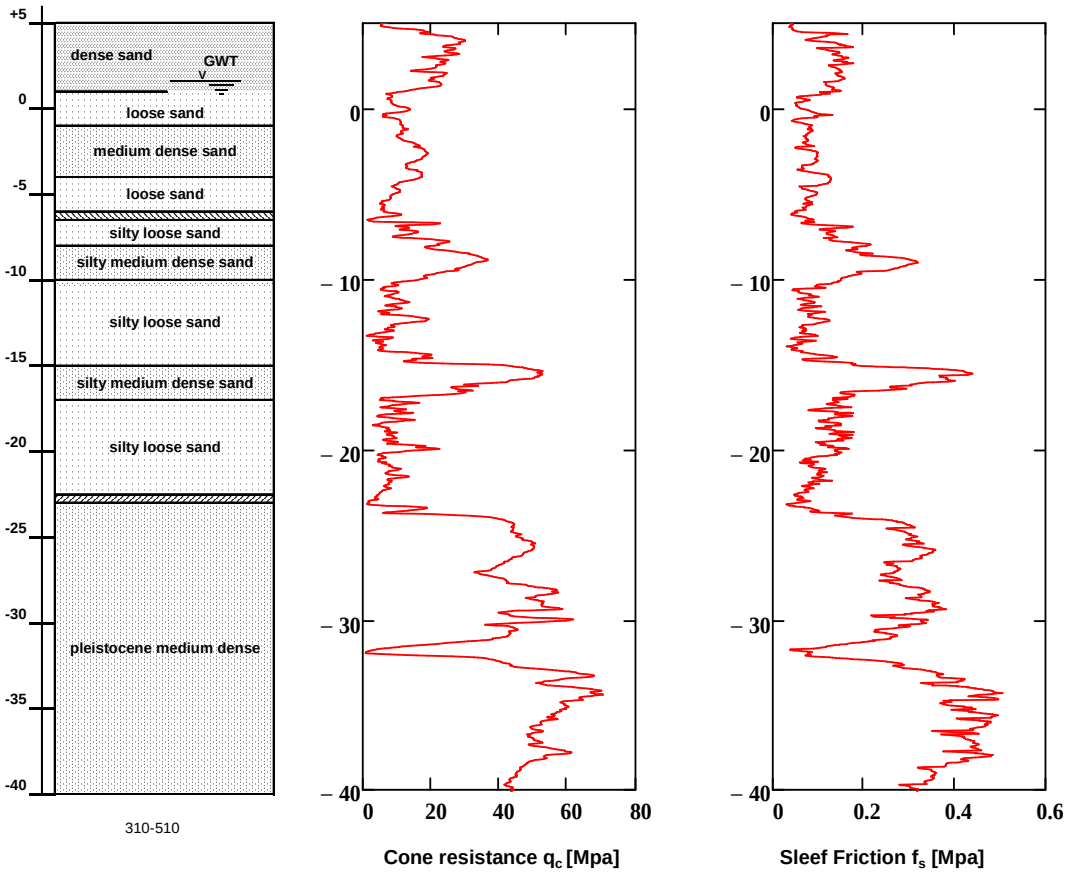

Depth [m NAP]		Layer discription	γ_{dry}	γ_{sat}
from	till		[kN/m^3]	[kN/m^3]
5	1	dense sand	19	21
1	-1	loose sand	17	19
-1	-4	medium dense sand	18	20
-4	-6	loose sand	17	19
-6	-6,4	clay	16,5	16,5
-6,4	-8	silty losse sand	19	19
-8	-10	silty medium dense sand	19,5	19,5
-10	-15	silty loose sand	19	19
-15	-17	silty medium dense sand	19,5	19,5
-17	-22,5	silty loose sand	19	19
-22,5	-23	sandy medium dense loam	20	20
-23	-40	pleistocene medium dense	20	20
-40				

Table A-5: Ground parameters for sections 4

Figure A-6 Sounding and ground profile of section 5

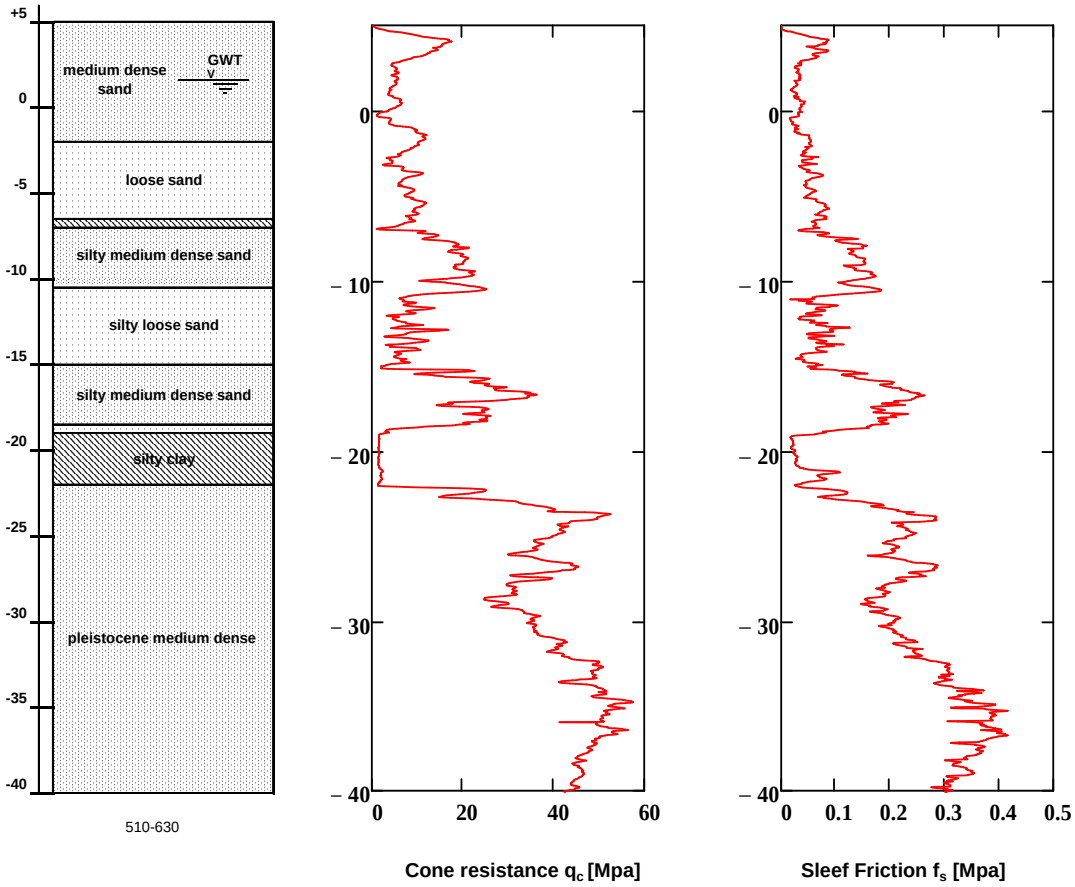

Depth [m NAP]		Layer discription	γ_{dry}	γ_{sat}
from	till		[kN/m^3]	[kN/m^3]
5	-2	medium dense sand	18	20
-2	-6,5	loose sand	17	19
-6,5	-7	clay	16,5	16,5
-7	-10,5	silty medium dense sand	19,5	19,5
-10,5	-15	silty loose sand	19	19
-15	-18,5	silty medium dense sand	19,5	19,5
-18,5	-19	silty loose sand	19	19
-19	-22	silty clay	17	17
-22	-40	pleistocene medium dense	20	20
-40				

Table A-6: Ground parameters for sections 5

Figure A-7 Sounding and ground profile of section 6

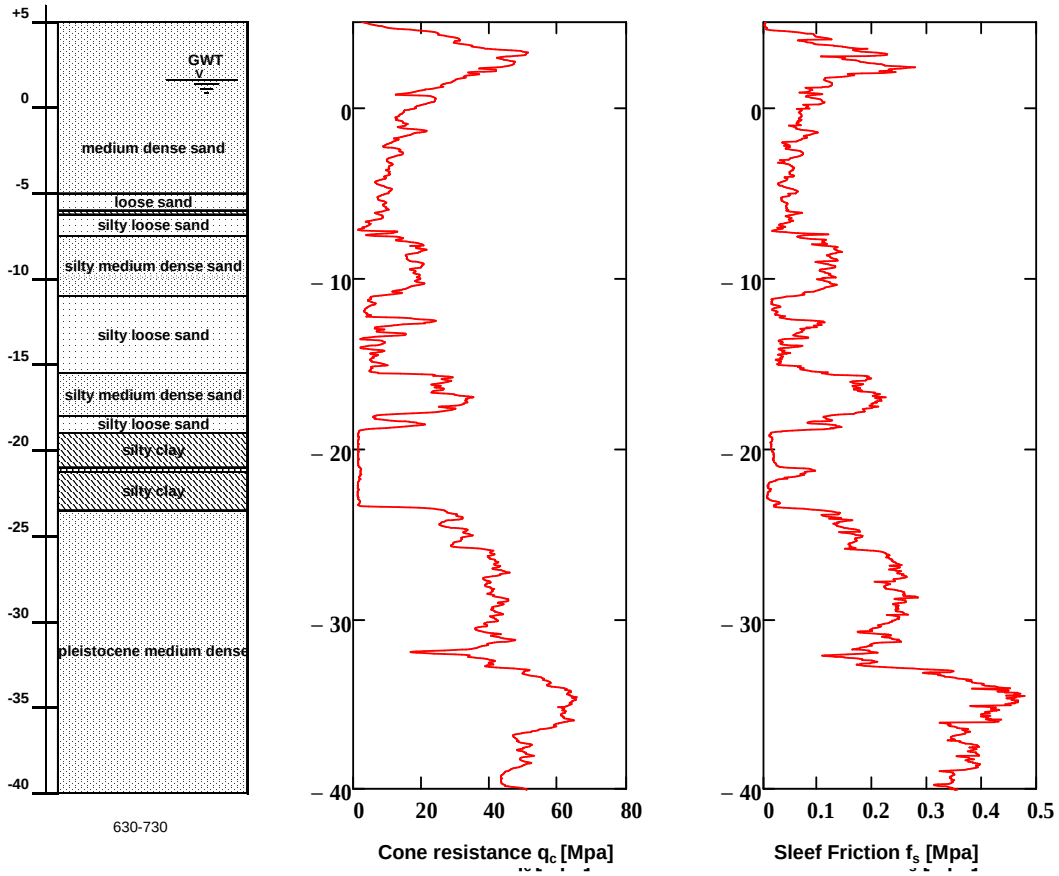

Depth [m NAP]		Layer discription	γ_{dry}	γ_{sat}
from	till		[kN/m^3]	[kN/m^3]
5	-5	medium dense sand	18	20
-5	-6	loose sand	17	19
-6	-6,3	clay	16,5	16,5
-6,3	-7,5	silti loose sand	19	19
-7,5	-11	silt medium dense sand	19,5	19,5
-11	-15,5	silty loose sand	19	19
-15,5	-18	silty medium dense sand	19,5	19,5
-18	-19	silt loose sand	19	19
-19	-21	silty clay	17	17
-21	-21,3	peat	12,5	12,5
-21,3	-23,5	silty clay	17	17
-23,5	-40	pleistocene medium dense	20	20
-40				

Table A-7: Ground parameters for sections 6

Figure A-8 Sounding and ground profile of section 7

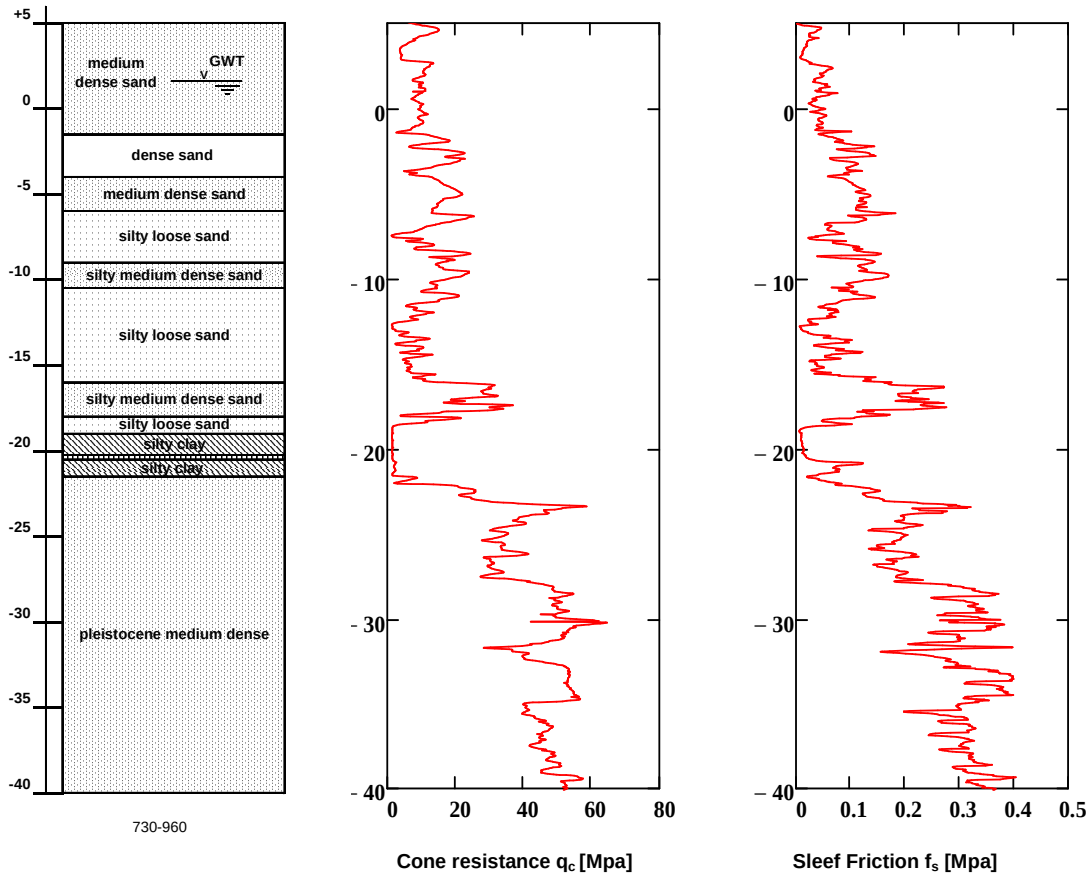

Depth [m NAP]		Layer discription	γ_{dry}	γ_{sat}
from	till		[kN/m^3]	[kN/m^3]
5	-1,5	medium dense sand	18	20
-1,5	-4	dense sand	19	21
-4	-6	medium dense sand	18	20
-6	-9	silty loose sand	19	19
-9	-10,5	silty medium dense sand	19,5	19,5
-10,5	-16	silty loose sand	19	19
-16	-18	silty medium dense sand	19,5	19,5
-18	-19	silty loose sand	19	19
-19	-20,2	silty clay	17	17
-20,2	-20,4	peat	12,5	12,5
-20,4	-21,5	silty clay	17	17
-21,5	-40	pleistocene medium dense	20	20
-40				

Table A-8: Ground parameters for sections 7

Figure A-9 Sounding and ground profile of section 8

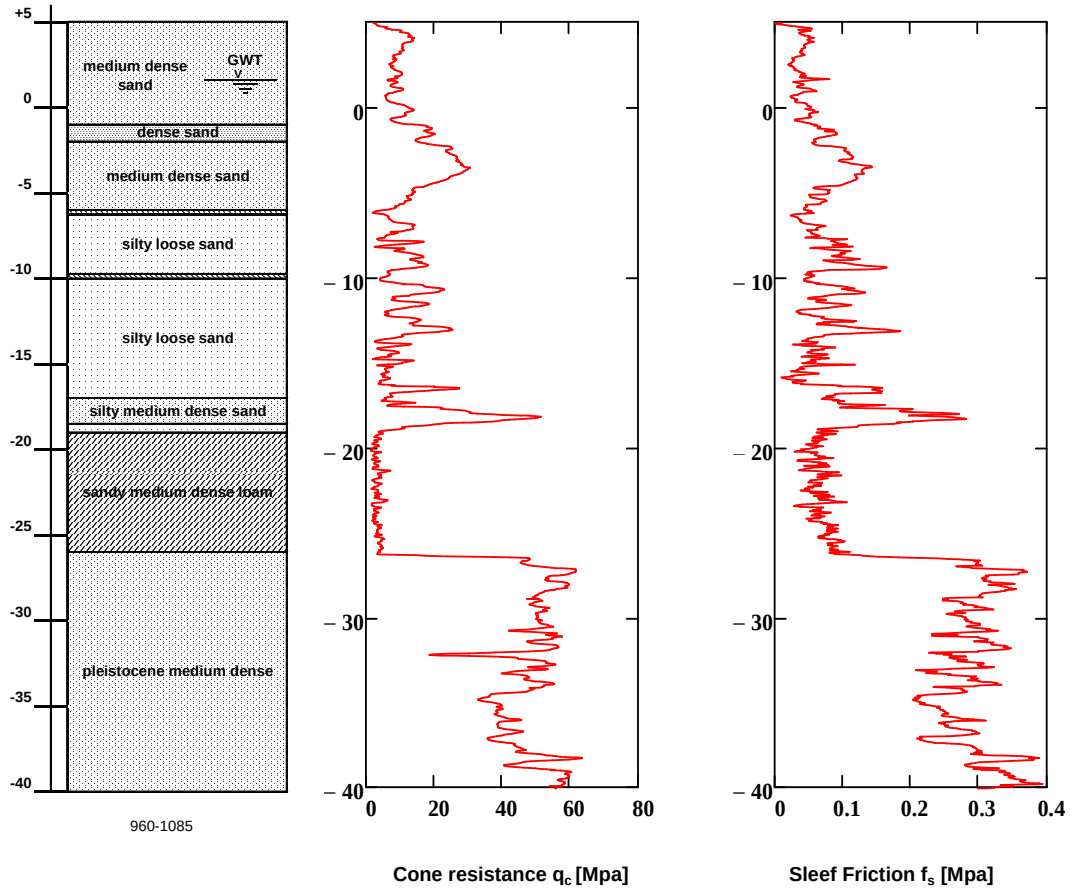

Depth [m NAP]		Layer discription	γ_{dry}	γ_{sat}
from	till		[kN/m^3]	[kN/m^3]
5	-1	medium dense sand	18	20
-1	-2	dense sand	19	21
-2	-6	medium dense sand	18	20
-6	-6,3	clay	16,5	16,5
-6,3	-9,7	silty loose sand	19	19
-9,7	-10	clay	16,5	16,5
-10	-17	silt loose sand	19	19
-17	-18,5	silt medium dense sand	19,5	19,5
-18,5	-19	silty loose sand	19	19
-19	-26	sandy medium dense loam	20	20
-26	-40	pleistocene medium dense	20	20
-40				

Table A-9: Ground parameters for sections 8

Figure A-10 Sounding and ground profile of section 9

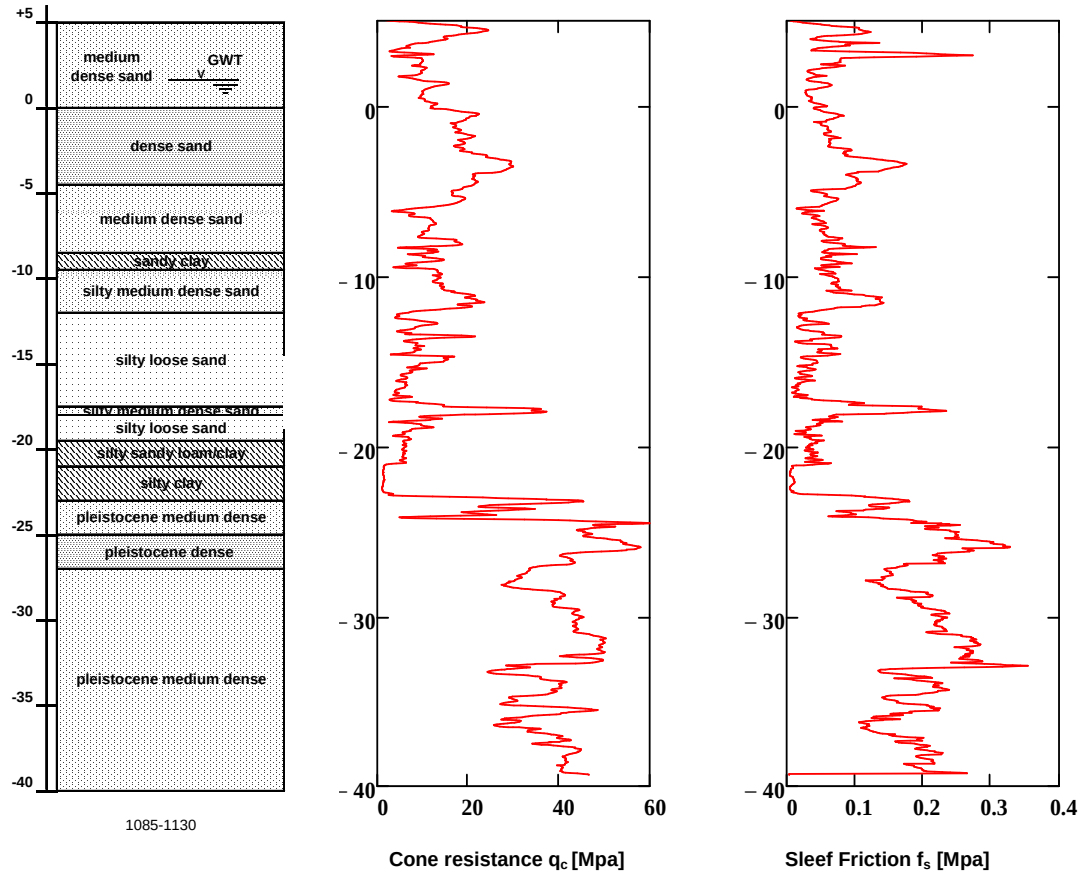

Depth [m NAP]		Layer discription	γ_{dry}	γ_{sat}
from	till		[kN/m^3]	[kN/m^3]
5	0	medium dense sand	18	20
0	-4,5	dense sand	19	21
-4,5	-8,5	medium dense sand	18	20
-8,5	-9,5	sandy clay	18	18
-9,5	-12	silty medium dense sand	19,5	19,5
-12	-17,5	silty loose sand	19	19
-17,5	-18	silty medium dense sand	19,5	19,5
-18	-19,5	silty loose sand	19	19
-19,5	-21	sandy loam/clay	19,5	19,5
-21	-23	silty clay	17	17
-23	-25	pleistocene medium dense	20	20
-25	-27	pleistocene dense	20,5	20,5
-27	-40	pleistocene medium dense	20	20
-40				

Table A-10: Ground parameters for sections 9

Figure A-11 Sounding and ground profile of section 10

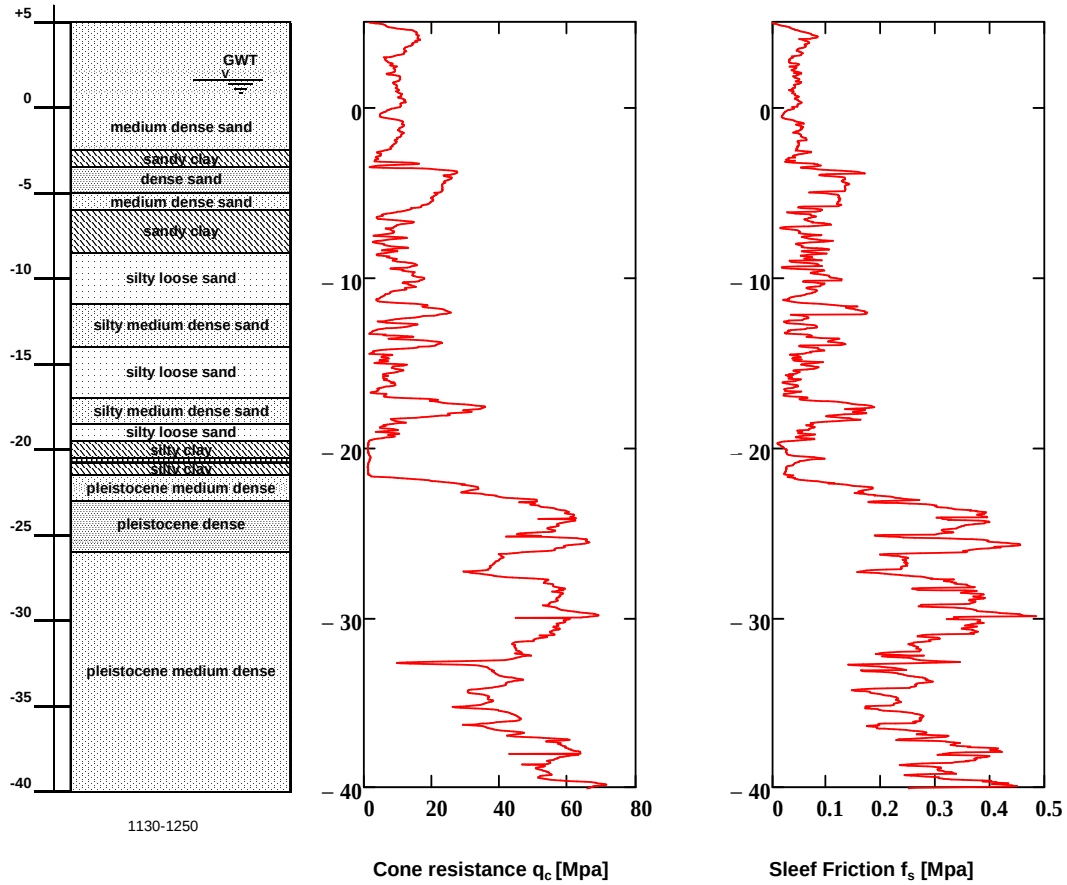

Depth [m NAP]		Layer discription	γ_{dry}	γ_{sat}
from	till		[kN/m^3]	[kN/m^3]
5	-2,5	medium dense sand	18	20
-2,5	-3,5	sandy clay	18	18
-3,5	-5	dense sand	19	21
-5	-6	medium dense sand	18	20
-6	-8,5	sandy clay	18	18
-8,5	-11,5	silty loose sand	19	19
-11,5	-14	silty medium dense sand	19,5	19,5
-14	-17	silty loose sand	19	19
-17	-18,5	silty medium dense sand	19,5	19,5
-18,5	-19,5	silty loose sand	19	19
-19,5	-20,5	silty clay	17	17
-20,5	-20,7	peat	12,5	12,5
-20,7	-21,5	silty clay	17	17
-21,5	-23	pleistocene medium dense	20	20
-23	-26	pleistocene dense	20,5	20,5
-26	-40	pleistocene medium dense	20	20
-40				

Table A-11: Ground parameters for sections 10

Figure A-12 Sounding and ground profile of section 11

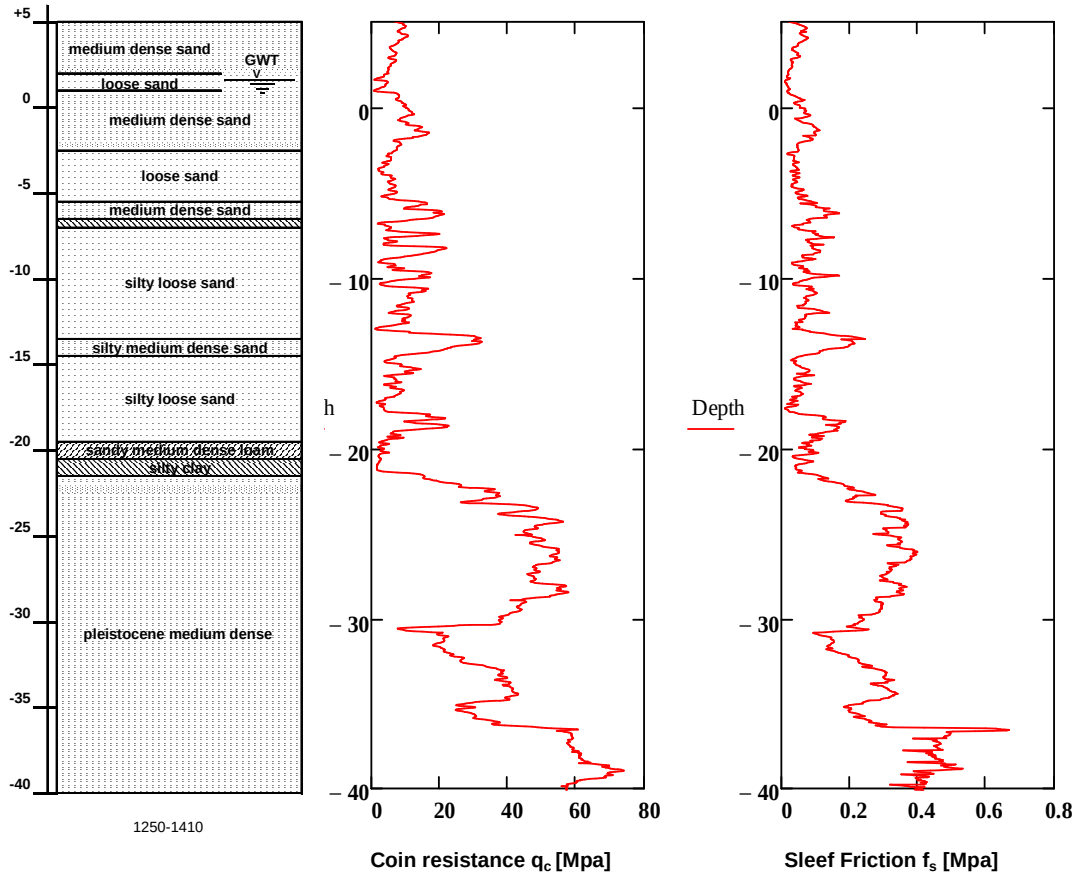

Depth [m NAP]		Layer discription	γ_{dry}	γ_{sat}
from	till		[kN/m^3]	[kN/m^3]
5	2	medium dense sand	18	20
2	1	loose sand	17	19
1	-2,5	medium dense sand	18	20
-2,5	-5,5	loose sand	17	19
-5,5	-6,5	medium dense sand	18	20
-6,5	-7	sandy clay	18	18
-7	-13,5	silty loose sand	19	19
-13,5	-14,5	silty medium dense sand	19,5	19,5
-14,5	-19,5	silt loose sand	19	19
-19,5	-20,6	sandy medium dense loam	20	20
-20,6	-21,4	silty clay	17	17
-21,4	-40	pleistocene medium dense	20	20
-40				

Table A-12: Ground parameters for sections 11

Figure A-13 Sounding and ground profile of section 12

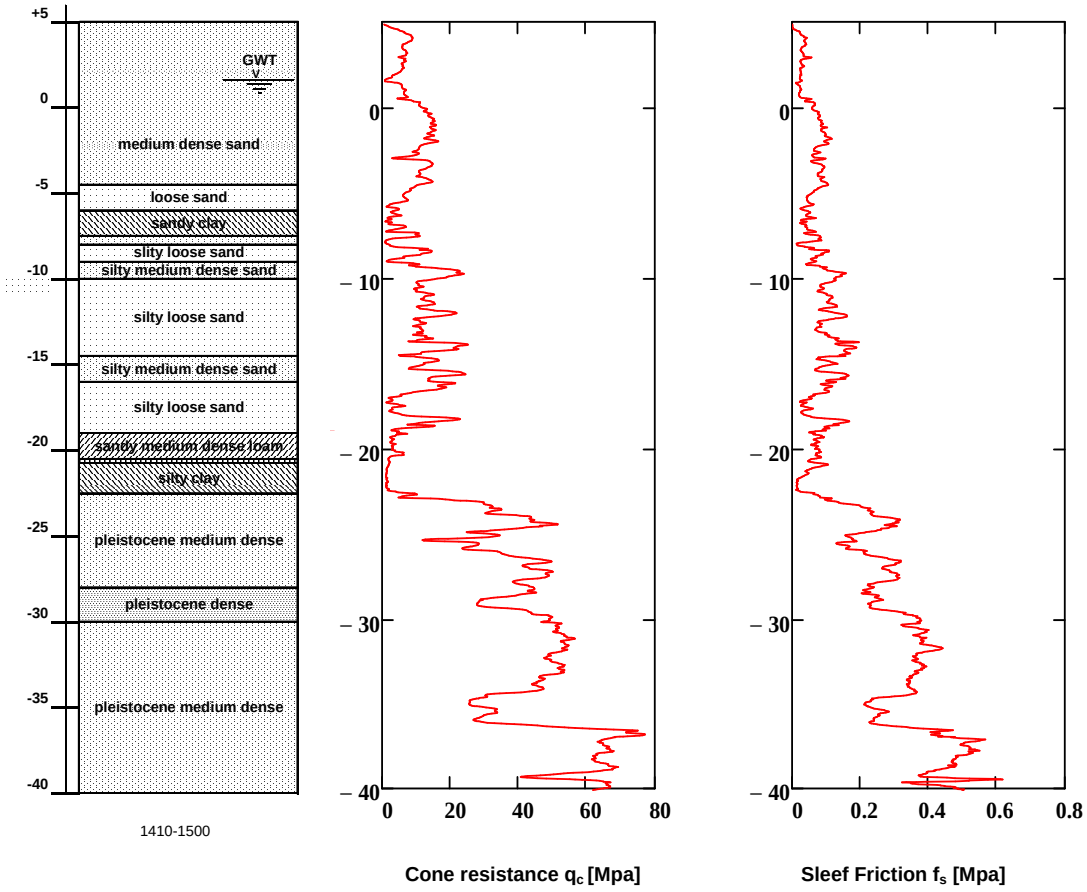

Depth [m NAP]		Layer discription	γ_{dry}	γ_{sat}
from	till		[kN/m^3]	[kN/m^3]
5	-4,5	medium dense sand	18	20
-4,5	-6	loose sand	17	19
-6	-7,5	sandy clay	18	18
-7,5	-8	clay	16,5	16,5
-8	-9	sitly loose sand	19	19
-9	-10	silt medium dense sand	19,5	19,5
-10	-14,5	silty loose sand	19	19
-14,5	-16	silt medium dense sand	19,5	19,5
-16	-19	silty loose sand	19	19
-19	-20,5	sandy medium dense loam	20	20
-20,5	-20,7	peat	12,5	12,5
-20,7	-22,5	silty clay	17	17
-22,5	-28	pleistocene medium dense	20	20
-28	-30	pleistocen dense	20,5	20,5
-30	-40	pleistocene medium dense	20	20
-40				

Table A-13: Ground parameters for sections 12

Figure A-14 Sounding and ground profile of section 13

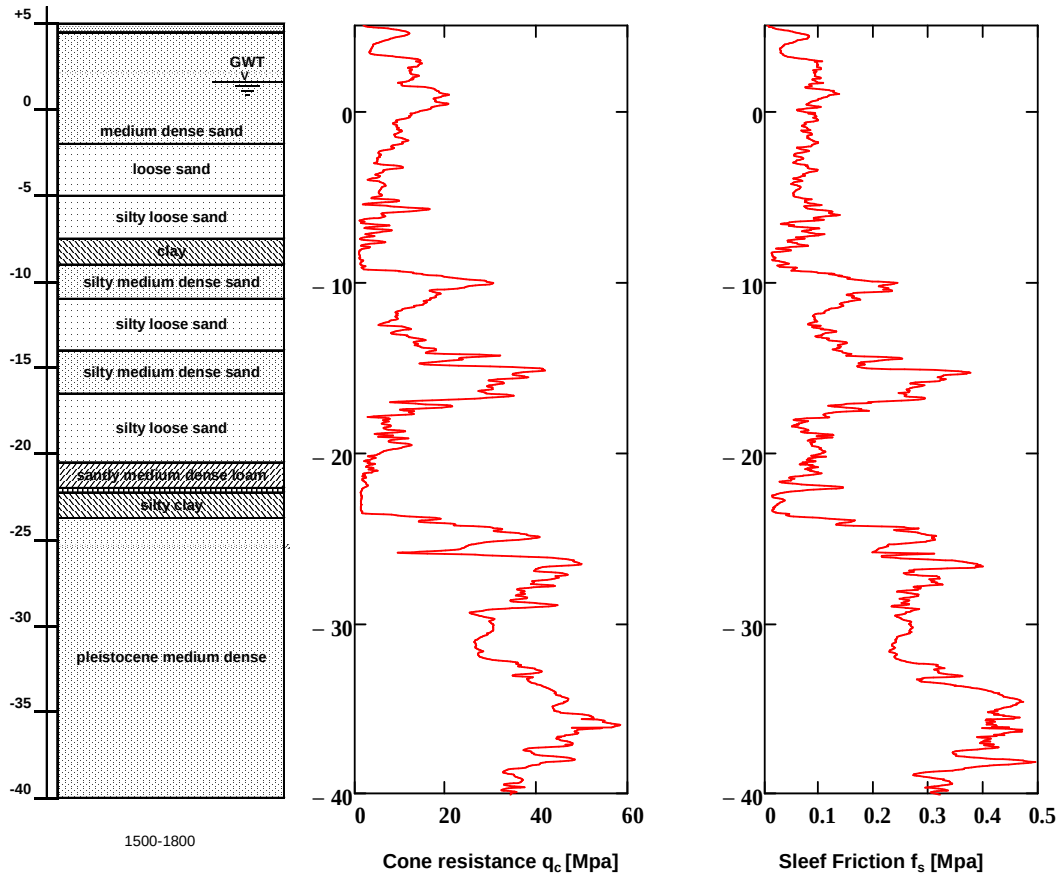

Depth [m NAP]		Layer discription	γ_{dry}	γ_{sat}
from	till		[kN/m^3]	[kN/m^3]
5	4,5	dense sand	19	21
4,5	-2	medium dense sand	18	20
-2	-5	loose sand	17	19
-5	-7,5	silty loose sand	19	19
-7,5	-9	clay	16,5	16,5
-9	-11	silty medium dense sand	19,5	19,5
-11	-14	silt loose sand	19	19
-17	-16,5	silt medium dense sand	19,5	19,5
-16,5	-20,5	silty loose sand	19	19
-20,5	-22	sandy medium dense loam	20	20
-22	-22,3	peat	12,5	12,5
-22,3	-23,7	silty clay	17	17
-23,7	-40	pleistocene medium dense	20	20
-40				

Table A-14: Ground parameters for sections 13

Figure A-15 Sounding and ground profile of section 14

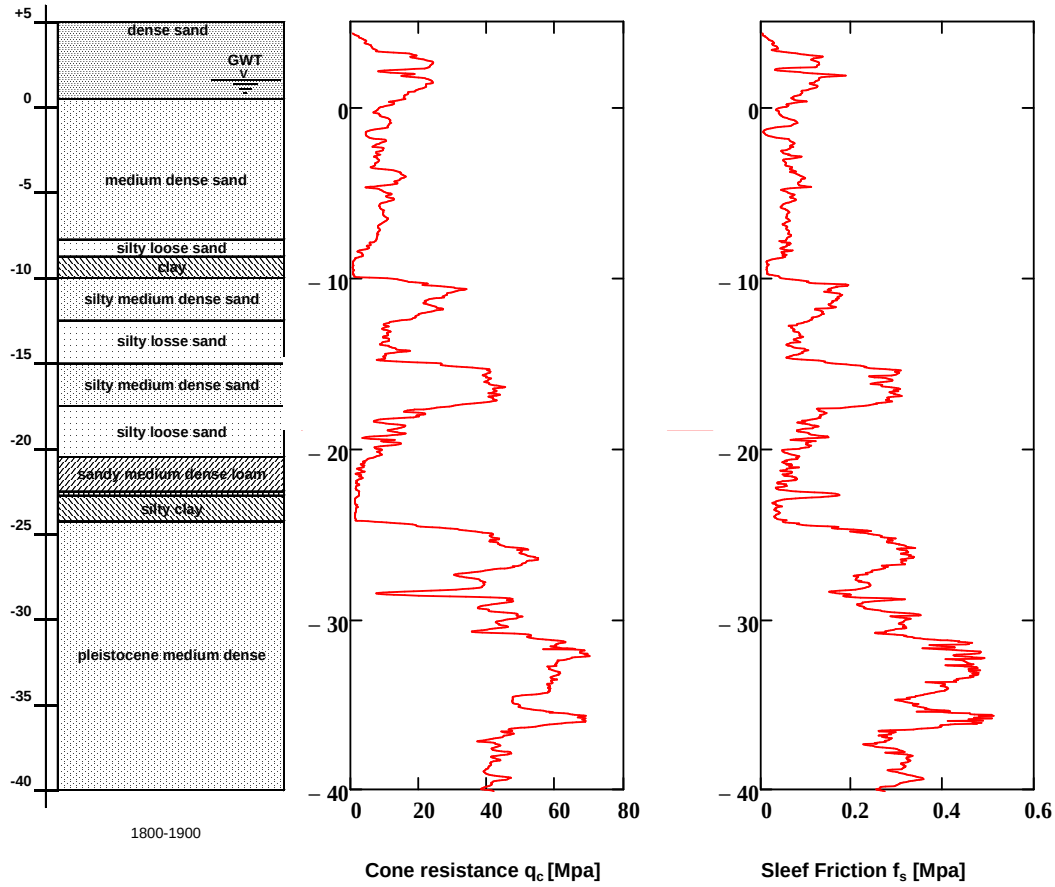

Depth [m NAP]		Layer discription	γ_{dry}	γ_{sat}
from	till		[kN/m^3]	[kN/m^3]
5	0,5	dense sand	19	21
0,5	-7,5	medium dense sand	18	20
-7,5	-8,8	silty loose sand	19	19
-8,8	-10	clay	16,5	16,5
-10	-12,5	silty meium dense sand	19,5	19,5
-12,5	-15	silty loose sand	19	19
-15	-17,5	silty meidum dense sand	19,5	19,5
-17,5	-20,5	silty loose sand	19	19
-20,5	-22,5	sandy medium dense loam	20	20
-22,5	-22,8	peat	12,5	12,5
-22,8	-24,2	silty clay	17	17
-24,2	-40	pleistocene medium dense	20	20
-40				

Table A-15: Ground parameters for sections 14

Appendix B Simplified static earth pressure approaches

B1 Rankine theory

Rankine (1857) developed the simplest procedure for computing minimum active and maximum passive earth pressures[B.1]. By making assumptions about the stress conditions and strength envelope of the soil behind a retaining wall (the backfill soil), Rankine was able to render the lateral earth pressure problem determinate and directly compute the static pressures acting on retaining walls. For minimum active conditions, Rankine expressed the pressure at a point on the back of a retaining wall as:

$$p_a = k_a \sigma'_v - 2c\sqrt{k_a} \qquad \textbf{Eq. B-1}$$

where:

k_a: active earth pressure coefficient
σ'_v: vertical effective stress at the point of interest
c: cohesive strength of the soil

When the principal stress planes are vertical and horizontal (as in the case of a smooth vertical wall retaining a horizontal backfill), the active earth pressure coefficient is given by:

$$k_a = \frac{1-\sin\varphi}{1+\sin\varphi} \qquad \text{Eq. B-2}$$

For dry homogeneous cohesionless backfill, Rankine theory predicts a triangular active pressure distribution oriented parallel to the backfill surface. The active earth pressure resultant P_a, acts at a point located H/3 above the base of a wall of height H, with magnitude:

$$P_a = \frac{1}{2} k_a \gamma H^2 \qquad \textbf{Eq. B-3}$$

Under passive conditions, Rankine theory predicts wall pressure given by:

$$p_p = k_p \sigma'_v - 2c\sqrt{k_p} \qquad \textbf{Eq. B-4}$$

Where for smooth, vertical walls retaining horizontal backfills the passive earth pressure coefficient k_p is given by equation 5-7 and the passive earth pressure resultant P_p by equation 5-8.

$$k_p = \frac{1+\sin\varphi}{1-\sin\varphi} \qquad \textbf{Eq. B-5}$$

$$P_p = \frac{1}{2} k_p \gamma H^2 \qquad \textbf{Eq. B-6}$$

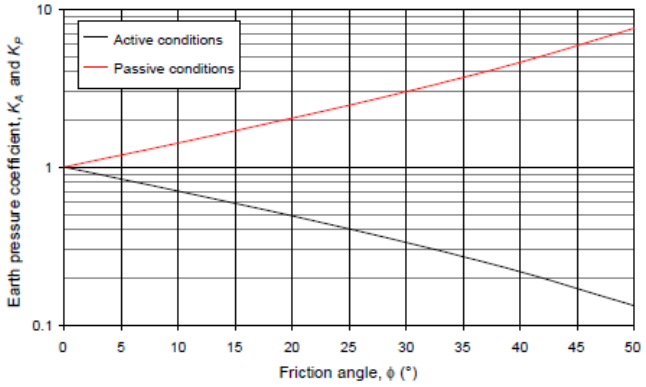

Figure B-1: Rankine active and passive earth pressure coefficient for a horizontal backfill

Figure B-1 plotted the ghraphical representations of the equations equation 5-4 and equation 5-7.

B2 Coulomb theory

Coulomb (1776) was the first to study the problem of lateral earth pressures on retaining structures[B.1]. By assuming that the forces acting on the back of the retaining wall resulted from the weight of the wedge of the soil above a planar failure plane surface, Coulomb used force equilibrium to determine the magnitude of the soil thrust acting on the wall for both minimum active and maximum passive conditions. Since the problem is indeterminate, a number of potential failure surfaces must be analyzed to identify the critical failure surface (i.e. the surface that produces the greatest active thrust or the smallest passive thrust).

Under minimum active earth pressure conditions, the active thrust on a wall with the geometry shown in Figure 5-4, is obtained from the force equilibrium. For the critical failure surface, the active thrust on a wall retaining a cohesionless soil can be expressed as:

$$P_a = \frac{1}{2} k_a \gamma H^2 \qquad \text{Eq. B-7}$$

where

$$k_a = \frac{\cos^2(\varphi - \beta)}{\cos^2\beta \cos(\delta + \beta)\left[1 + \sqrt{\frac{\sin(\delta + \varphi)\sin(\varphi - \alpha)}{\cos(\delta + \beta)\cos(\alpha - \beta)}}\right]^2} \qquad \text{Eq. B-8}$$

$$\alpha_{pfs,a} = \varphi + \arctan\left[\frac{\tan(\varphi - \alpha) + C_1}{C_2}\right] \qquad \text{Eq. B-9}$$

$$C_1 = \sqrt{\tan(\varphi - \alpha)\,[\tan(\varphi - \alpha) + \cot(\varphi - \beta)][1 + \tan(\delta + \beta)\cot(\varphi - \beta)]}$$
$$C_2 = 1 + \tan(\delta + \beta)[\tan(\varphi - \alpha) + \cot(\varphi - \beta)]$$

P_a: resultant active earth pressure on wall
k_a: active earth pressure coefficient
$\alpha_{pfs,a}$: angle of the critical active planar failure surface respect to horizontal
γ: unit weight of soil
φ: angle of internal friction of soil
δ: angle of friction structure soil
α: slope inclination
β: inclination of back of wall to vertical

Coulomb theory does not explicitly predict the distribution of active pressure, but it can be shown to be triangular for linear backfill surfaces with no surface loads. In such cases, P_a acts at a point located H/3 above the base of a wall of height H.

For maximum passive conditions in cohesionless backfills, Coulomb theory predicts a passive thrust given by:

$$P_p = \frac{1}{2} k_p \gamma H^2 \qquad \text{Eq. B-10}$$

where

$$k_p = \frac{\cos^2(\varphi + \beta)}{\cos^2\beta \cos(\delta - \beta)\left[1 - \sqrt{\frac{\sin(\delta + \varphi)\sin(\varphi + \alpha)}{\cos(\delta - \beta)\cos(\alpha - \beta)}}\right]^2} \qquad \text{Eq. B-11}$$

$$\alpha_{pfs,p} = -\varphi + \arctan\left[\frac{\tan(\varphi+\alpha)+C_3}{C_4}\right] \qquad \textbf{Eq. B-12}$$

$$C_3 = \sqrt{\tan(\varphi+\alpha)[\tan(\varphi+\alpha)+\cot(\varphi+\beta)][1+\tan(\delta-\beta)\cot(\varphi+\beta)]}$$
$$C_4 = 1+\tan(\delta-\beta)[\tan(\varphi+\alpha)+\cot(\varphi+\beta)]$$

P_p: resultant passive earth pressure on wall
k_p: passive earth pressure coefficient
$\alpha_{pfs,p}$: angle of the critical passive planar failure surface respect to horizontal
γ: unit weight of soil
φ: angle of internal friction of soil
δ: angle of friction structure soil
α: slope inclination
β: inclination of back of wall to vertical

It should be noted that the Coulomb theory gives the entire earth pressure coefficient. If the normal component to the wall is the objective of the analysis, the calculated values of the coefficients should be multiplied for cosδ.

In Figure 3-3 the values of the earth pressures coefficients calculated with the Coulomb theory for a vertical wall (β=0) that retains a horizontal backfill (α=0) for different soil-wall friction angles δ are plotted. For δ=0, the results are the same given by the Rankine theory.

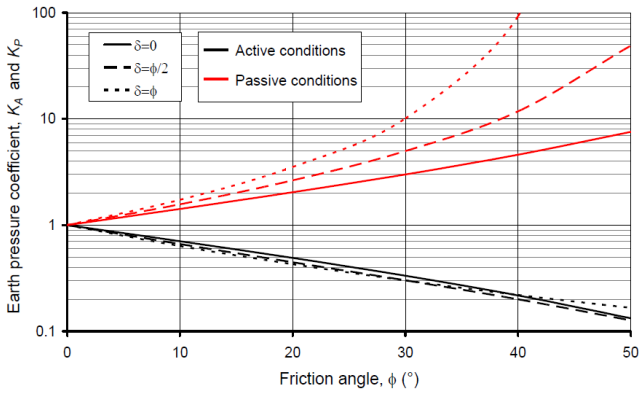

Figure B-2: Coulomb active and passive earth pressure coefficient for a horizontal backfill sustained by a vertical wall

In contrast to the Rankine approach, Coulomb theory can be used to predict soil thrust on walls with irregular backfill slopes, concentrated loads on the backfill surface, and seepage forces. By considering the soil above a potential failure plane as a free body and including forces due to concentrated loads, boundary water pressures, and so on, the magnitude of the resultant thrust can easily computed.

References

[B.1] A. Verruijt, Soil mechanics, Delft university press, 1999

Appendix C Mononobe & Okabe method

Okabe (1926) [C.1] and Mononobe & Matsuo (1929) [C.2] developed the basis of a pseudo-static analysis of seismic earth pressures on retaining structures that has become popularly known as the Mononobe-Okabe (M-O) method. The M-O method is a direct extension of the static Coulomb theory to pseudo-static conditions. In M-O method, pseudo-static accelerations are applied to a Coulomb active (or passive) wedge. The pseudo-static soil thrust is then obtained from the force equilibrium of the wedge (Figure C-1). In addition to those under static conditions, the forces acting on an active wedge in a cohesionless backfill wedge are constituted by horizontal and vertical pseudo-static forces whose magnitudes are related to the mass of the wedge by the pseudo-static accelerations $a_h = k_{h^*} g$ and $a_v = k_{v^*} g$.

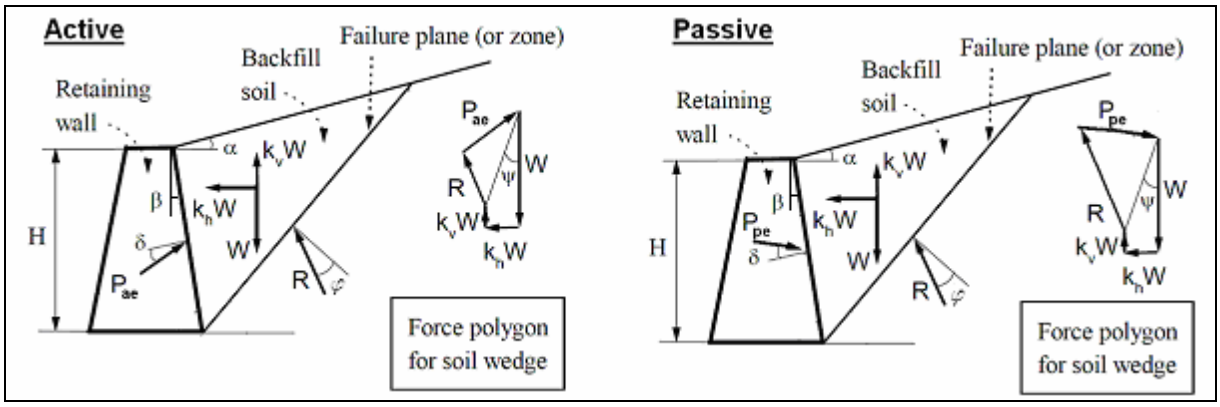

Figure C-1 The sliding wedge theory included with seismic terms of Mononobe-Okabe [Mononobe-Okabe, 1926]

The total active thrust can be expressed in a form similar to that developed for static conditions, that is:

$$P_{ae} = \frac{1}{2} k_{ae} \gamma_{eff} H^2 (1 \pm k_v) \qquad \textbf{Eq. C-1}$$

Where the dynamic active earth pressure coefficient k_{ae} and seismic inertia angle ψ is given by:

$$k_{ae} = \frac{\cos^2(\varphi - \beta - \psi)}{\cos\psi \cos^2\beta \cos(\delta + \beta + \psi)\left[1 + \sqrt{\frac{\sin(\delta+\varphi)\sin(\varphi-\alpha-\psi)}{\cos(\delta+\beta+\psi)\cos(\alpha-\beta)}}\right]^2} \qquad \textbf{Eq. C-2}$$

$$\psi = \tan^{-1}\left(\frac{k_h}{1 \pm k_v}\right) \quad for \quad dry \ soil$$

$$\psi = \tan^{-1}\left(\frac{k_h}{1 \pm k_v}\frac{\gamma_d}{\gamma - \gamma_w}\right) \quad for \quad wet \ soil \qquad \textbf{Eq. C-3}$$

The critical failure surface, which is flatter than the crititcal failure surface for static conditions, is inclined (Zarrabi-Kashini, 1979) at an angle:

$$\alpha_{pfs,ae} = \varphi - \arctan\left[\frac{-\tan(\varphi - \alpha - \psi) + C_{1e}}{C_{2e}}\right] \qquad \textbf{Eq. C-4}$$

where:
P_{ae}: resultant seismic active earth pressure on wall
k_{ae}: seismic active earth pressure coefficient (static + dynamic)
γ: unit weight of wet soil

γ_d: dry unit weight of soil
γ_w: unit weight of water
γ_{eff}: effective unit weight of soil (γ-γ_w)
φ: angle of internal friction of soil
δ: angle of friction structure soil
α: slope inclination
β: inclination of back of wall to vertical
ψ: seismic inertia angle
k_h: seismic coefficient of horizontal acceleration
k_v: seismic coefficient of vertical acceleration
$\alpha_{pfs,ae}$: angle of the critical seismic active planar failure surface respect to horizontal
H: height of the wall

$$C_{1e} = \sqrt{\tan(\varphi - \alpha - \psi)[\tan(\varphi - \alpha - \psi) + \cot(\varphi - \beta - \psi)][1 + \tan(\delta + \beta + \psi)\cot(\varphi - \beta - \psi)]}$$
$$C_{2e} = 1 + \tan(\delta + \beta + \psi)[\tan(\varphi - \alpha - \psi) + \cot(\varphi - \beta - \psi)]$$

Altough the M-O method implies that the total active thrust should act at a point H/3 above the base of a wall of height H, experimental results suggest that it actually acts at a higher points under dynamic loading conditions. The total active thrust, P_{ae}, can be divided into a static component, P_a, and a dynamic component, ΔP_{ae}:

$$P_{ae} = P_a + \Delta P_{ae} \qquad \textbf{Eq. C-5}$$

The static component is known to act at H/3 above the base of the wall. Seed & Whitman (1970) recommended that the dynamic component be taken to act at approximately 0.6 H. On this basis, the total active thrust will act at a height *h*:

$$h = \frac{P_a \cdot H/3 + \Delta P_{ae}(0.6H)}{P_{ae}} \qquad \textbf{Eq. C-6}$$

The total passive thrust on a wall retaining a cohesionless backfill is given by:

$$P_{pe} = \frac{1}{2} k_{pe} \gamma_{eff} H^2 (1 \pm k_v) \qquad \textbf{Eq. C-7}$$

Where the dynamic passive earth pressure coefficient k_{pe} and the critical passive seismic failure surface $\alpha_{pfs,pe}$ is given by:

$$k_{pe} = \frac{\cos^2(\varphi + \beta - \psi)}{\cos\psi \cos^2\beta \cos(\delta - \beta + \psi)\left[1 + \sqrt{\frac{\sin(\delta + \varphi)\sin(\varphi + \alpha - \psi)}{\cos(\delta - \beta + \psi)\cos(\alpha - \beta)}}\right]^2} \qquad \textbf{Eq. C-8}$$

$$\alpha_{pfs,pe} = \psi - \varphi + \arctan\left[\frac{-\tan(\varphi + \alpha + \psi) + C_{3e}}{C_{4e}}\right] \qquad \textbf{Eq. C-9}$$

Where:
P_{pe}: resultant seismic active earth pressure on wall
K_{pe}: seismic active earth pressure coefficient (static + dynamic)
φ: angle of internal friction of soil
δ: angle of friction structure soil
α: slope inclination
β: inclination of back of wall to vertical
ψ: seismic inertia angle
k_h: seismic coefficient of horizontal acceleration

k_v: seismic coefficient of vertical acceleration
$\alpha_{pfs,pe}$: angle of the critical seismic active planar failure surface respect to horizontal
H: height of the wall

$$C_{3e} = \sqrt{\tan(\varphi+\alpha-\psi)\,[\tan(\varphi+\alpha-\psi)+\cot(\varphi+\beta-\psi)][1+\tan(\delta+\beta-\psi)\cot(\varphi+\beta-\psi)]}$$
$$C_{4e} = 1+\tan(\delta-\beta+\psi)[\tan(\varphi+\alpha-\psi)+\cot(\varphi+\beta-\psi)]$$

The Total passive thrust can also be devided into static and dynamic componets:

$$P_{pe} = P_p + \Delta P_{pe} \qquad \textbf{Eq. C-10}$$

Where P_{pe} and P_p are computed from equation C-7 and B-10 , respectively. Note that the dynamic component acts in the opposite direction of the static component, thus reducing the available passive resistance. The point of application of P_{pe} may move downward from its static point of application for anchored sheet pile walls as the value for k_h increases. However, no satisfactory procedure was found for computing the point of application of P_{pe} for this structure. Therefore, the assumption of P_{pe} acting at approximately 1/3 of the height of the soil in front of the wall is restricted to low to moderate levels of earthquake shaking (e.g. one rough index is $k_h < 0{,}1$).

Deviation of seismic forces ψ must be for active earth pressure always less or equal to the difference of the angle of internal friction and the ground surface inclination (i.e. φ - β). If the values ψ>φ – β, than the value ψ = φ – β is assumed. In case of passive earth pressure the value of deviation of seismic forces ψ must be always less or equal to the sum of the angle of internal friction and the ground surface inclination (i.e. φ + β). If the values ψ>φ + β, than the value ψ = φ + β is assumed.

Although conceptually quite simple, the M-O method provides a useful means of estimating earthquake-induced loads on retaining walls. A positive horizontal acceleration coefficient causes the total active thrust to exceed the static active thrust and the total passive thrust to be less than the static passive thrust. Since the stability of a particular wall is generally reduced by an increase in active thrust and/or a decrease in passive thrust, the M-O method produces seismic loads that are more critical than the static loads that act prior an earthquake. The effects of distributed load and discrete surface loads and irregular backfill surfaces are easily considered by modifying the free-body diagram of the active or passive wedge.

As a pseudo-static extension of the Coulomb analysis, however, the M-O method is subject to all of the limitations of pseudo-static analyses as well as the limitations of Coulomb theory. An overview of the most important limitations and assumptions is given below:

- As with the original Coulomb method, the backfill must be deforming enough so that full shear resistance is mobilized along the failure plane
- Inertia forces are assumed to act at all points of an assumed Coulomb failure wedge
- The accelerations must be constant throughout the failing wedge
- The determination of the appropriate pseudo-static coefficient is difficult and the analysis is not appropriate for soils that experience significant loss of strength during earthquake (e.g. liquefiable soils)

Terzaghi [C.3] had shown that for active earth pressure, assumption of planar rupture surface in the analysis closely matches with the actual experimental observations. But for passive case, when wall friction angle δ exceeds one-third of soil friction angle φ, then the assumption of planar failure surface seriously overestimate the passive earth pressures. Hence to correct the error in Mononobe-Okabe method for passive case, curved rupture surface can be considered for the passive case. During this research only planar failure surfaces where used which is a conservative approach.

Just as Coulomb theory does under static conditions, the M-O analysis will overpredict the actual total passive thrust, particularly for δ> 1/2. For this reason the M-O method should be used and interpreted carefully.

References

[C.1] Okabe S., General theory of earth pressure, J. Jpn. Soc. Civil Eng., 1926
[C.2] Mononobe N. and Matsuo H., On the determination of earth oressure during earthquakes, Proceedings of the World Engineering Congress, 1929
[C.3] Terzaghi K., Theoritical soil mechanics, Wiley, New York, 1943

Appendix D Liquefaction

D1 Liquefaction Process

Liquefaction is a process by which sediments below the water table temporarily lose strength and behave as a viscous liquid rather than a solid. The types of sediments most susceptible are clay-free deposits of sand and silts. The actions in the soil which produce liquefaction are as follows: seismic waves, primarily shear waves, passing through saturated granular layers, distort the granular structure, and cause loosely packed groups of particles to collapse. As the soil particle structure collapses, the loosely-packed individual soil particles attempt to move into a denser configuration. In an earthquake, however, there is not enough time for the water in the pores of the soil to be squeezed out. Instead, the water is trapped and prevents the soil particles from moving closer together. This will increase the pore water pressure between the grains if drainage is not present. The increase in pore water pressure results in a decrease of effective stress within the soil mass. If the pore water pressure rises to a level approaching the weight of the overlying soil, the granular layer temporarily behaves like a viscous liquid rather than a solid. Liquefaction has occurred.

In the liquefied condition, soil may deform with little shear resistance. Deformations large enough to cause damage to structures are called ground failures. The ease with which a soil can be liquefied depends primarily on the looseness of the soil, the amount of cementing or clay between particles, and the amount of drainage restriction. The amount of soil deformation following liquefaction depends on the looseness of the material, the depth, thickness, and extent of the liquefied layer, the ground slope, and the distribution of loads applied by structures. Liquefaction does not occur at random, but is restricted to certain geologic and hydrologic environments, primarily recently deposited sands and silts in areas with high ground water levels. Generally, the younger and looser the sediment, and the higher the water table, the more susceptible the soil is to liquefaction. Sediments most susceptible to liquefaction include Holocene (less than 10,000 year old) delta, river channel, flood plain, and aeolian deposits, and poorly compacted fills. Liquefaction has been most abundant in areas where ground water lies within 10 m of the ground surface; few instances of liquefaction have occurred in areas with ground water deeper than 20 m. Dense soils, including well compacted fills, have low susceptibility to liquefaction.

D2 Effect of liquefaction

The liquefaction phenomenon by itself may not be particularly damaging or hazardous. It is destructive to the built environment only when liquefaction is accompanied by some ground displacement or ground failure. For engineering purposes, it is not the occurrence of liquefaction that is of prime importance, but its severity or its capability to cause damage. Adverse effects of liquefaction can take many forms. These include:

- Flow failures (section D.2.1)
- Lateral spreads (section D.2.2)
- Ground oscillation (section D.2.3)
- Loss of bearing strength (section D.2.4)
- Settlement (section D.2.5)
- Increased lateral pressure on retaining walls (section D.2.6)

D.2.1 Flow Failures

Flow failures are the most catastrophic ground failures caused by liquefaction. These failures commonly displace large masses of soil laterally tens of meters and in a few instances, large masses of soil have travelled tens of kilometres down long slopes at velocities ranging up to tens of kilometres per hour. Flows may be comprised of completely liquefied soil or blocks of intact material riding on a layer of liquefied soil. Flows develop in loose saturated sands or silts on relatively steep slopes, usually greater than 3 degrees as shown in Figure D-1.

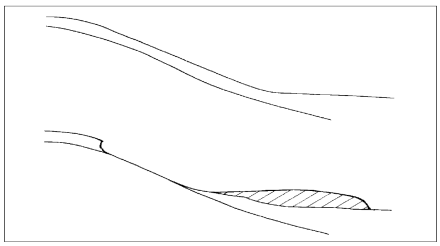

Figure D-1 Flow failure caused by liquefaction and loss of strength of soils lying on a steep slope. (Youd, 1992)

D.2.2 Lateral Spreads

Lateral spreads involve lateral displacement of large, blocks of soil at the surface as a result of liquefaction of a subsurface layer (Figure D-2). Displacement occurs in response to the combination of gravitational forces and inertial forces generated by an earthquake. Lateral spreads generally develop on gentle slopes (most commonly less than 3 degrees) and move toward a free face such as an incised river channel. Horizontal displacements commonly range up to several meters. The displaced ground usually breaks up internally, causing cracks in the ground to form on the failure surface. Lateral spreads commonly disrupt foundations of buildings built on or across the failure, sever pipelines and other utilities in the failure mass, and compress or buckle engineering structures, such as bridges, founded on the toe of the failure.

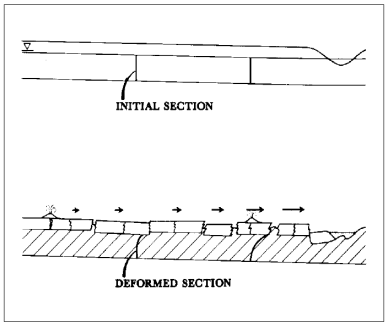

Figure D-2 Lateral spread (Youd, 1992)

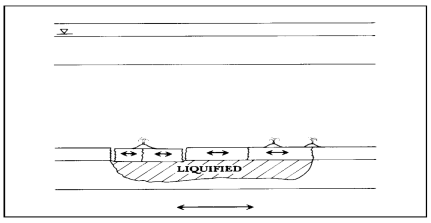

Figure D-3 Horizontal ground oscillation caused by liquefaction (Youd, 1992)

D.2.3 Ground Oscillation

When liquefaction occurs at depth but the slope is too gentle to permit lateral spreads, the soil blocks that are not liquefied may separate from one another and oscillate on the liquefied zone. The resulting ground oscillation may be accompanied by the opening and closing of cracks and sand boils (upward flowing sediment). These can potentially damage structures and underground utilities.

D.2.4 Loss of Bearing Strength

When the soil supporting a building or other structure liquefies and loses strength, large deformations can occur within the soil which may allow the structure to settle and tilt (Figure D-4). If the structure is below ground level, it may float upward. Apparently, liquefaction first developed in a sand layer several meters below ground surface and then propagated upward through overlying sand layers. The rising wave of liquefaction weakened the soil supporting the buildings and allowed the structures to slowly settle and tilt.

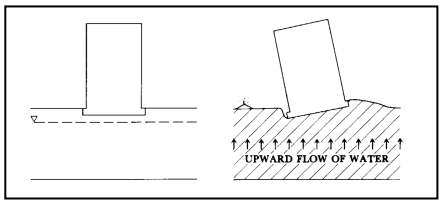

Figure D-4 Tilted structure due to lose of bearing strength caused by liquefaction in the sub soil (Youd, 1992)

D.2.5 Settlement

Small settlements may occur as soil pore water pressures dissipate and the soil consolidates after the earthquake. These settlements may be damaging, although they would tend to be much less so than the large movements accompanying flow failures, lateral spreading, and bearing capacity failures. The eruption of sand boils (fountains of water and sediment emanating from the pressurized, liquefied sand) is a common manifestation of liquefaction that can also lead to localized differential settlements.

D.2.6 Increased Lateral Pressure on Retaining Walls

If the soil behind a retaining wall liquefies, the lateral pressures on the wall may greatly increase. As a result, retaining walls may be laterally displaced, tilt, or structurally fail, as has been observed for waterfront walls retaining loose saturated sand in a number of earthquakes.

D3 Can Liquefaction Be Predicted?

Although it is possible to identify areas that have the potential for liquefaction, its occurrence cannot be predicted any more accurately than a particular earthquake can be (with a time, place, and degree of reliability assigned to it). Once these areas have been defined in general terms, it is possible to conduct site investigations that provide very detailed information regarding a site's potential for liquefaction.

Appendix E Liquefaction analysis

Appendix E-1 Determining the most liquefaction potential ground profile

Appendix E-2 Determining the liquefiable layers

E1 Determining the most liquefaction potential ground profile

For every 2 cm in depth, cone resistances and sleeve friction have been measured during the soundings which will determine the ground profile. Based on these measurements, liquefaction potential analysis has been performed using two different methods: Robertson and Wride method and the Juang et al. method. The outcome of both methods for an earthquake with a return period of 57850 and 67600 years, can be found in figure Figure E-1and Figure E-2. These figures show us that both the methods indicate the same soil layer where liquefaction may occur. Therefore both the methods are quit comparable. Figure E-3 till Figure E-16 shows us the probabilities of liquefaction for different return periods at different locations according to the two methods.

The ground profile with the highest liquefaction potential was determined based on how many measurement points are above the probability of 0.6 (P_L>0.6) and above 0.8(P_L>08) for both the methods. These measurement points were assumed to represent a ground layer with a thickness of 2 cm. The more measurement points above P_L>0.6 or P_L>08 means that occurrence of liquefaction might take place at a thicker soil layer. These results can be found in Table E-1 for a seismic return period of 57850 years and P_L>0.6. Table E-2 shows a return period of 67600 years for a P_L>0.8.

Return period (R) = 57850 years	Number of measurement point above P_L > 0.6	
Location	Robertson and Wride	Juang et al.
1900-1800 (west side)	179	86
1800-1500	54	109
1500-1410	160	138
1410-1250	398	236
1250-1130	325	177
1130-1085	436	272
1085-960	282	143
960-730	189	161
730-630	304	217
630-510	258	139
510-310	198	20
310-240	450	335
240-100	533	291
100-0 (East side)	775	354

Table E-1: results of measurement points above P_L > 0.6 for an earthquake with return period of 3000 years for both the methods

Return period (R) = 67600 years	Number of measurement point above P_L > 0.8	
Location	Robertson and Wride	Juang et al.
1900-1800 (west side)	25	46
1800-1500	6	40
1500-1410	45	74
1410-1250	46	118
1250-1130	78	82
1130-1085	167	146
1085-960	62	51
960-730	36	91
730-630	137	125
630-510	31	60
510-310	0	3
310-240	143	185
240-100	256	201
100-0 (East side)	352	225

Table E-2: Table C-1 results of measurement points above P_L > 0.8 for an earthquake with return period of 3500 years for both the methods

According to the result, ground profile in section 100-0 m on the east side of the Euromax terminal is the most sensitive to liquefaction. Number of measuring point in this profile is the highest compared to the rest. Hereby, a thicker soil layer will be subjected to liquefaction.

Figure E-1: Probability of liquefaction according to Robertson and Wride method

Return period : 67600 Years Acceleration: 0.284g Moment magnitude: 6.138
Whole quay length

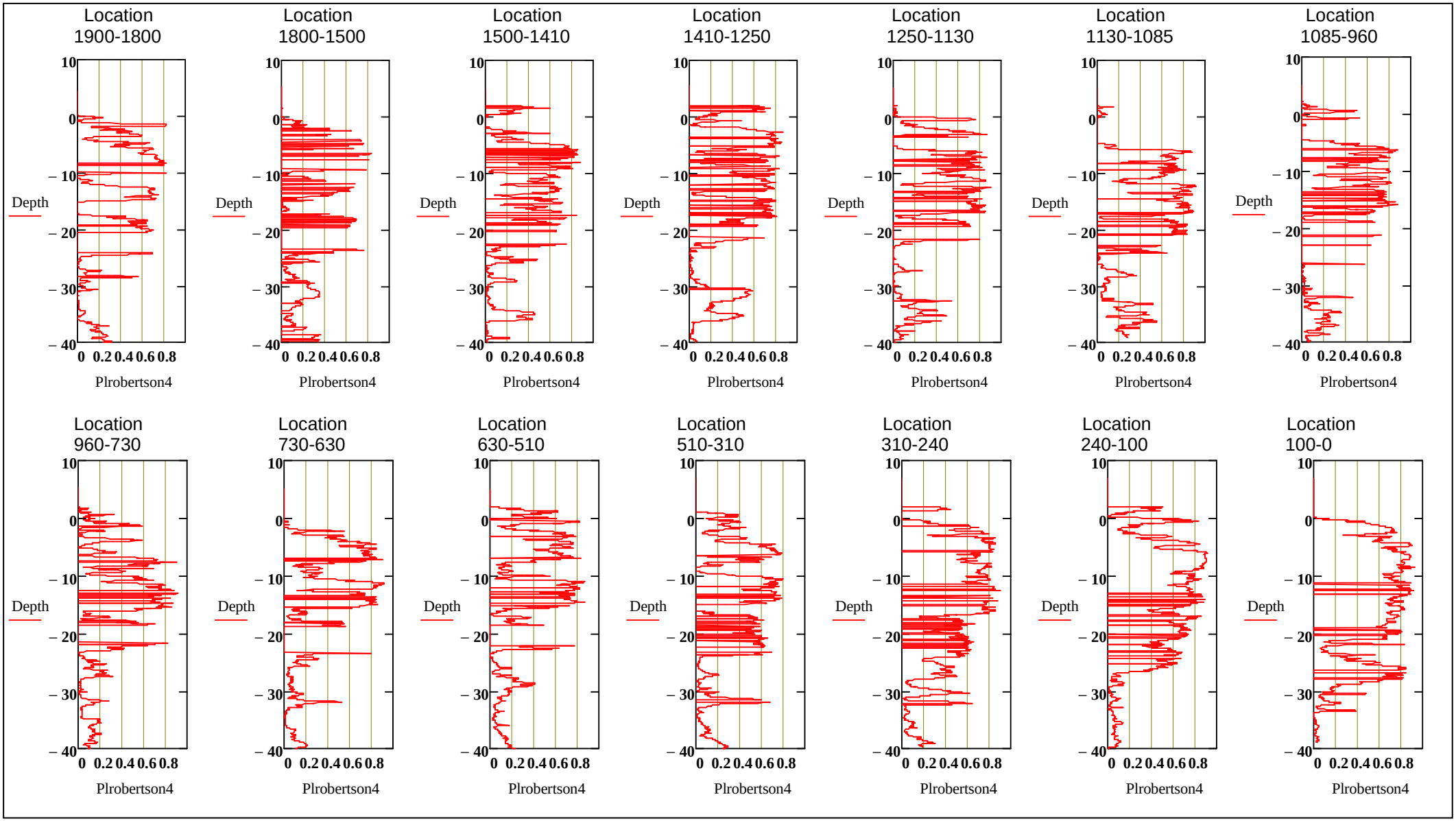

Figure E-2: Probability of liquefaction according to Robertson and Wride method

Return period : 67600 Years **Acceleration: 0.284g** **Moment magnitude: 6.138**

Whole quay length

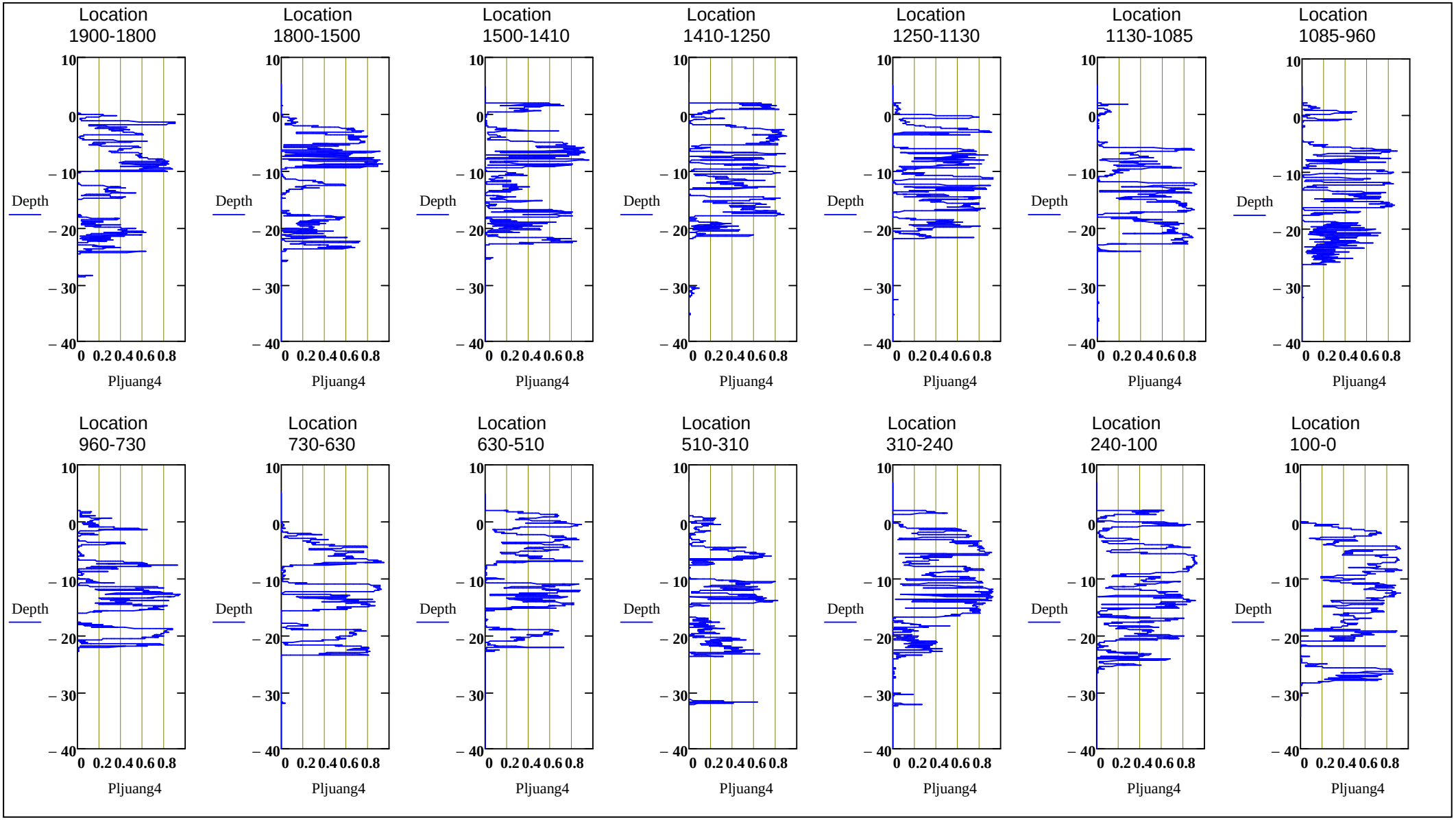

Figure E-3: Probability of liquefaction with different return periods

Methods:
Robertson and Wride (Red)
Juang et al. (Blue)

Location:
1900-1800m

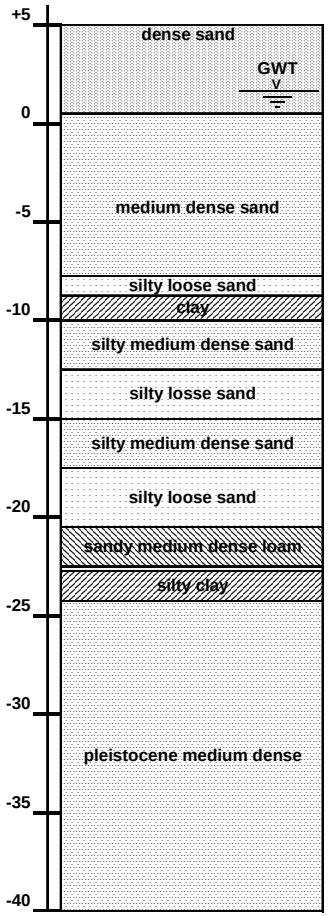

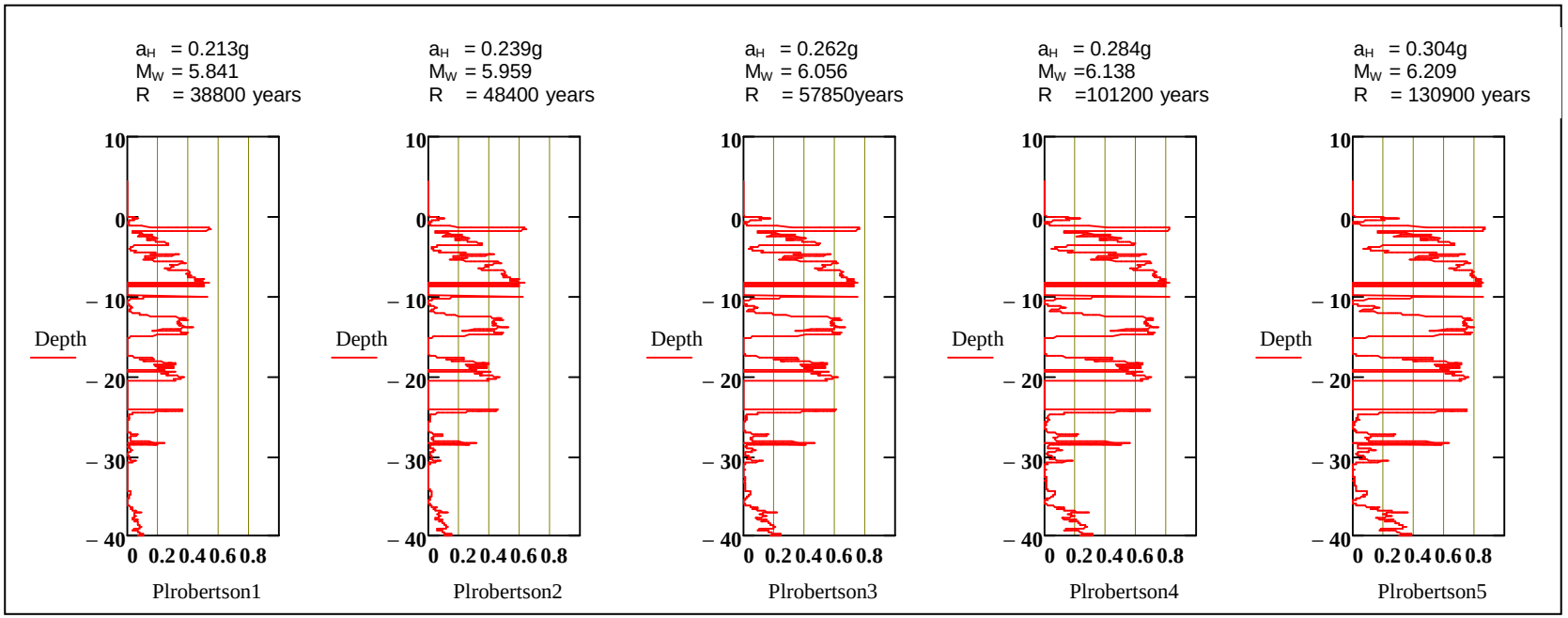

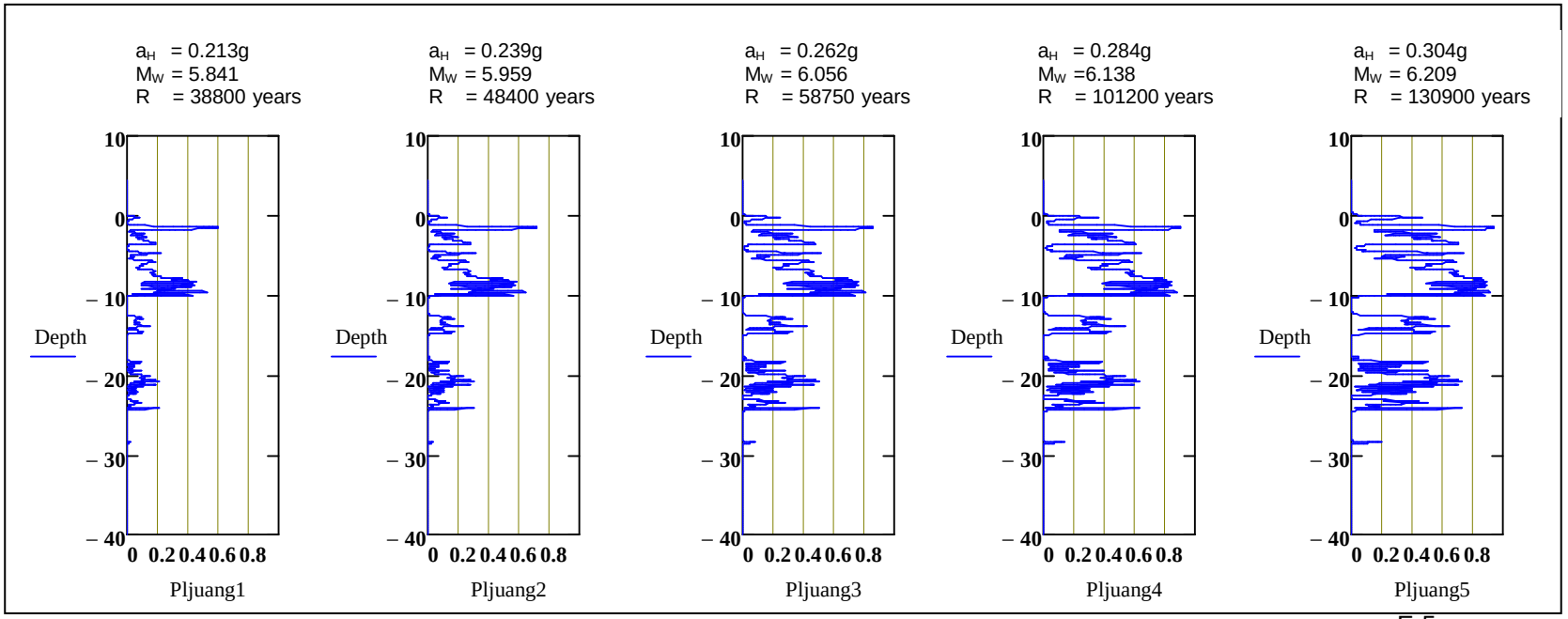

Figure E-4: Probability of liquefaction with different return periods

Methods:
Robertson and Wride (Red)
Juang et al. (Blue)

Location:
1800-1500m

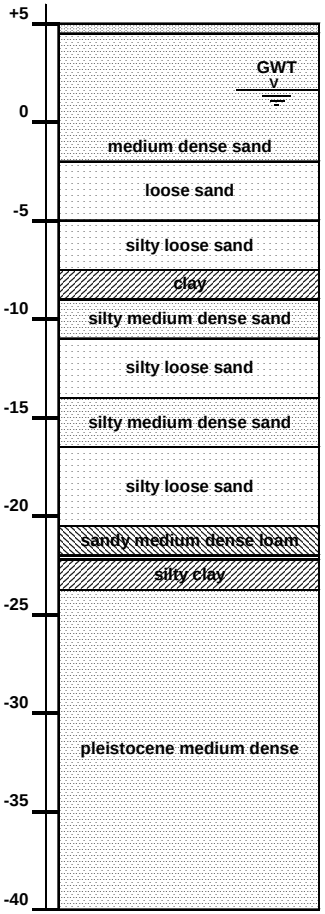

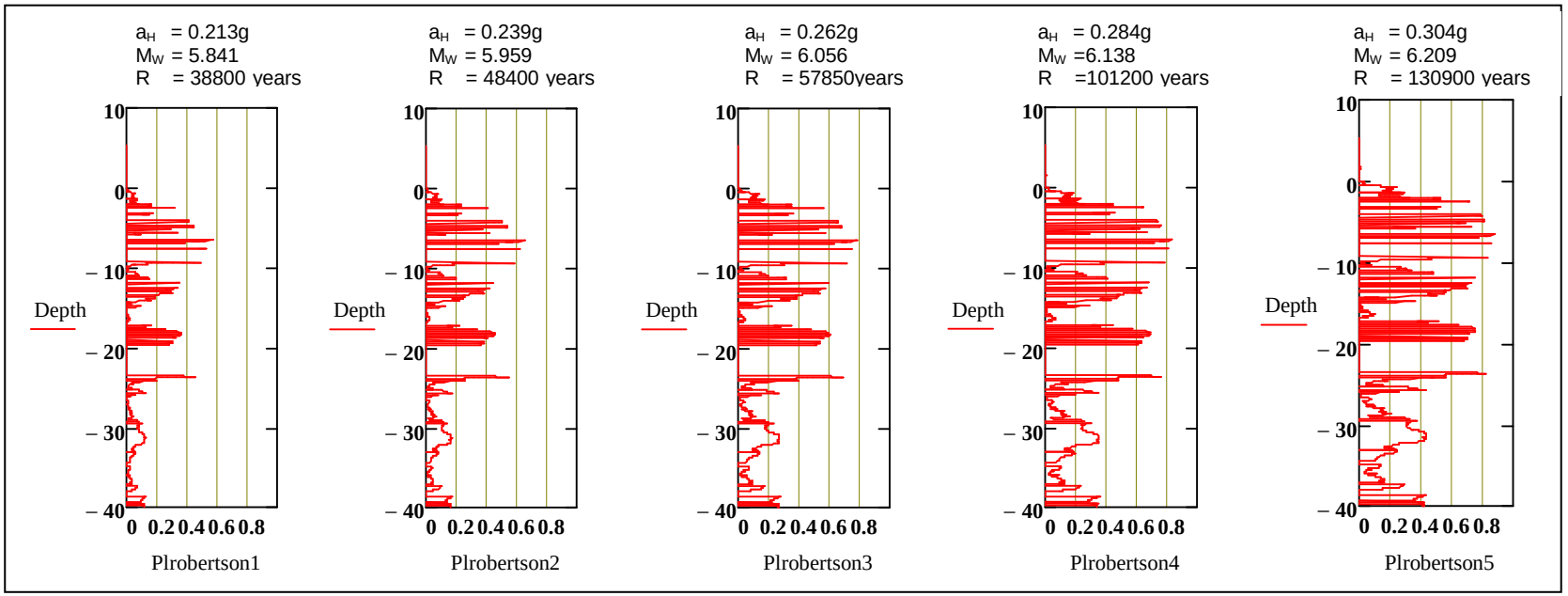

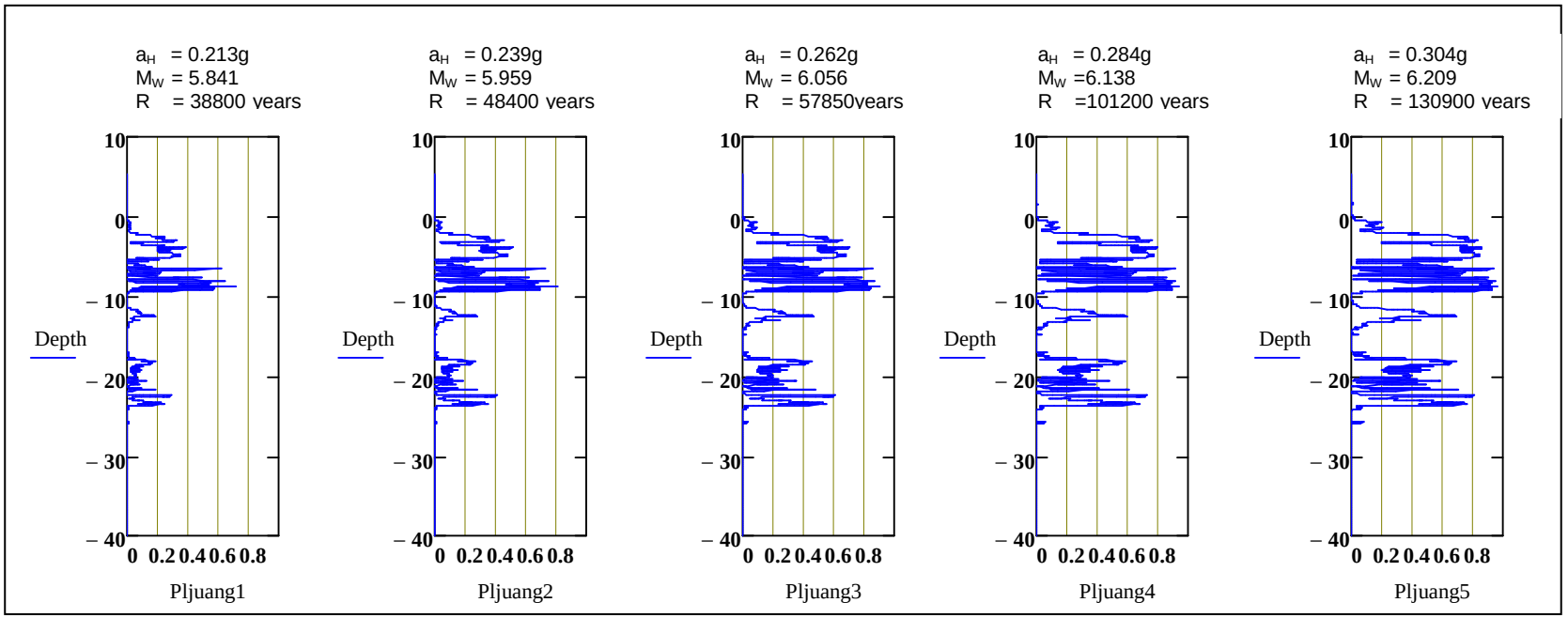

Figure E-5: Probability of liquefaction with different return periods

Methods:
Robertson and Wride (Red)
Juang et al. (Blue)

Location:
1500-1410

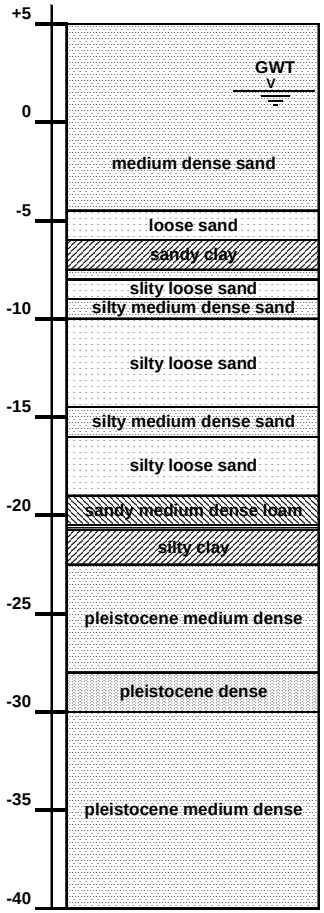

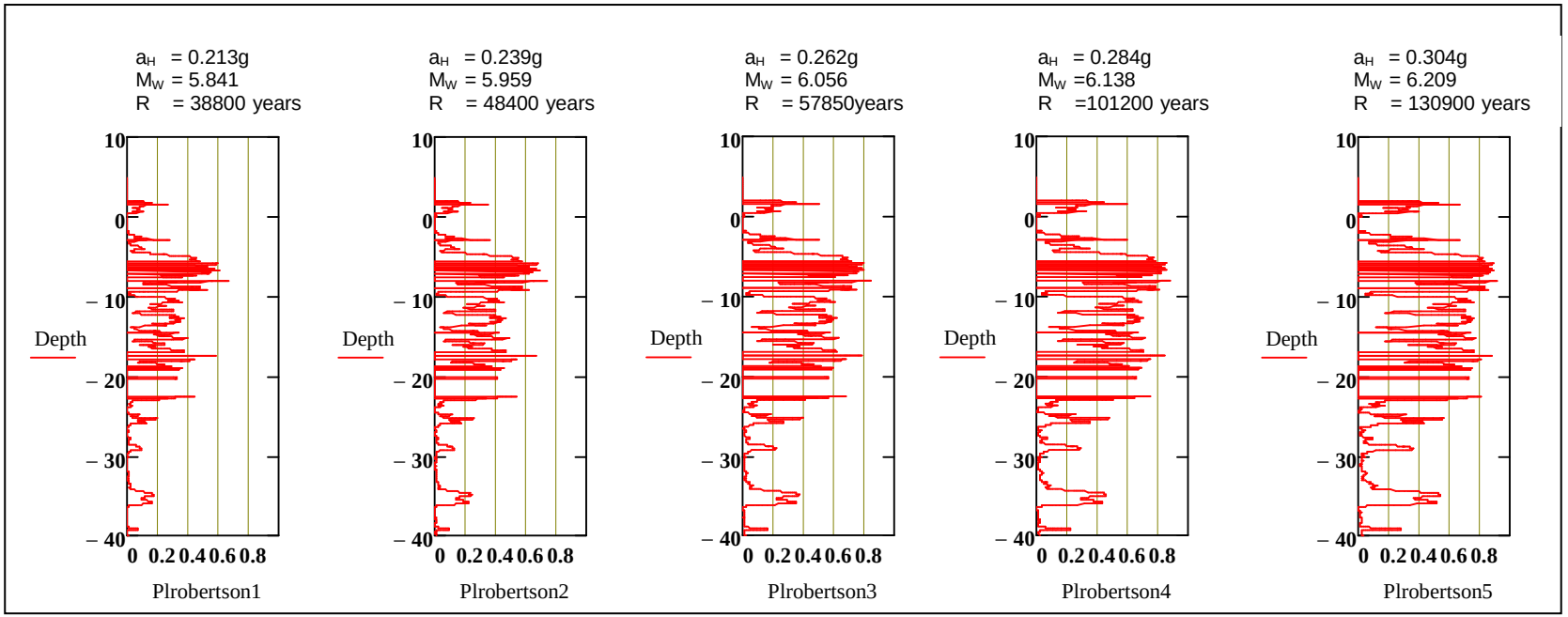

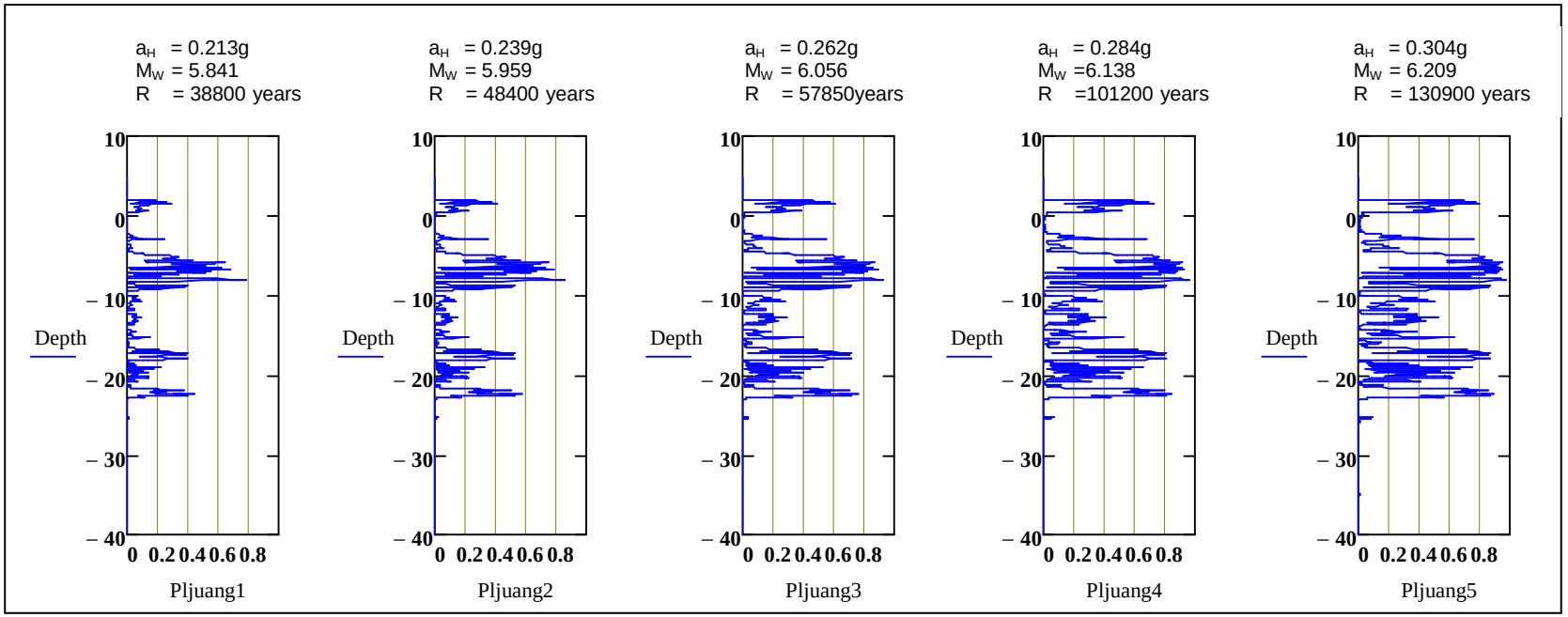

Figure E-6: Probability of liquefaction with different return periods

Methods:
Robertson and Wride (Red)
Juang et al. (Blue)

Location:
1410-1250

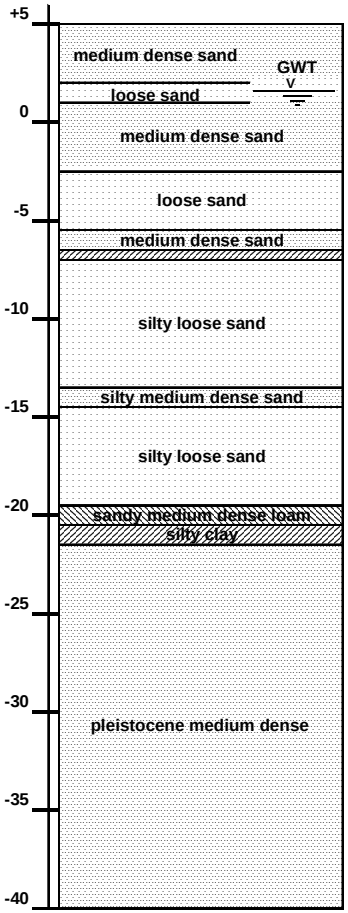

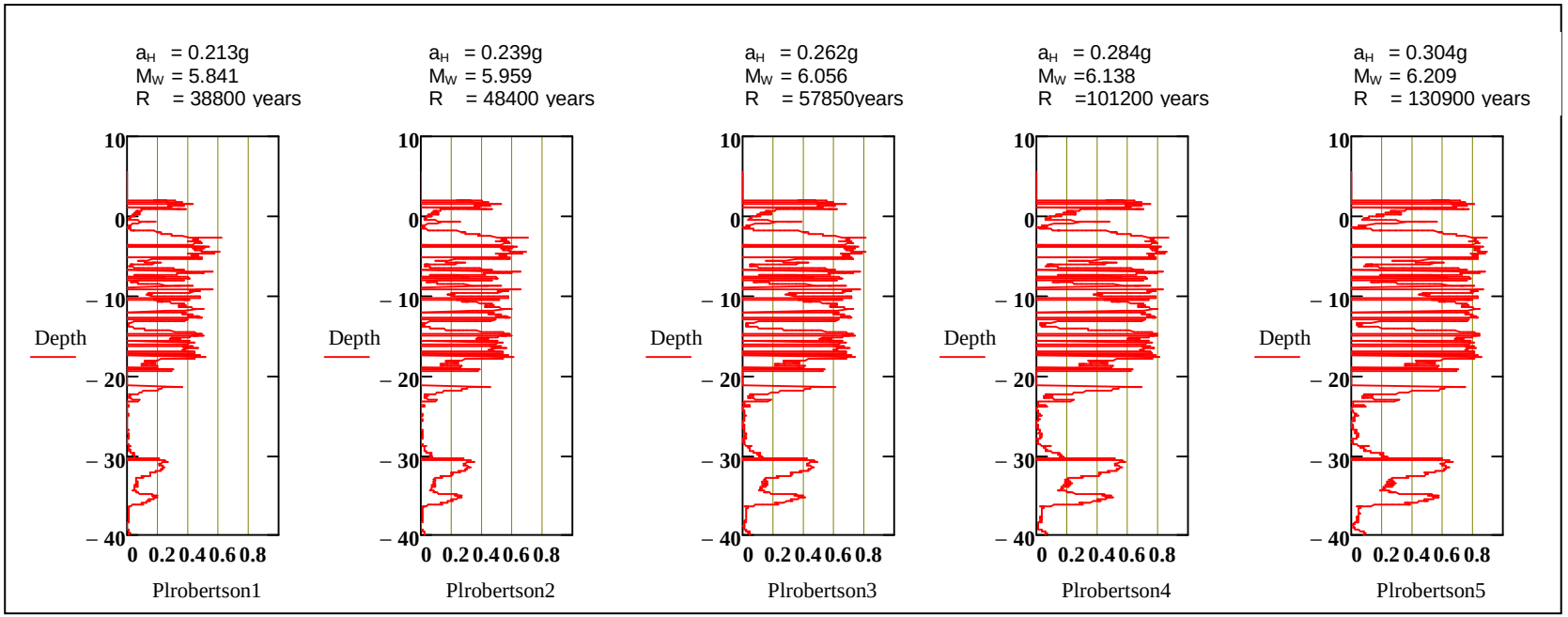

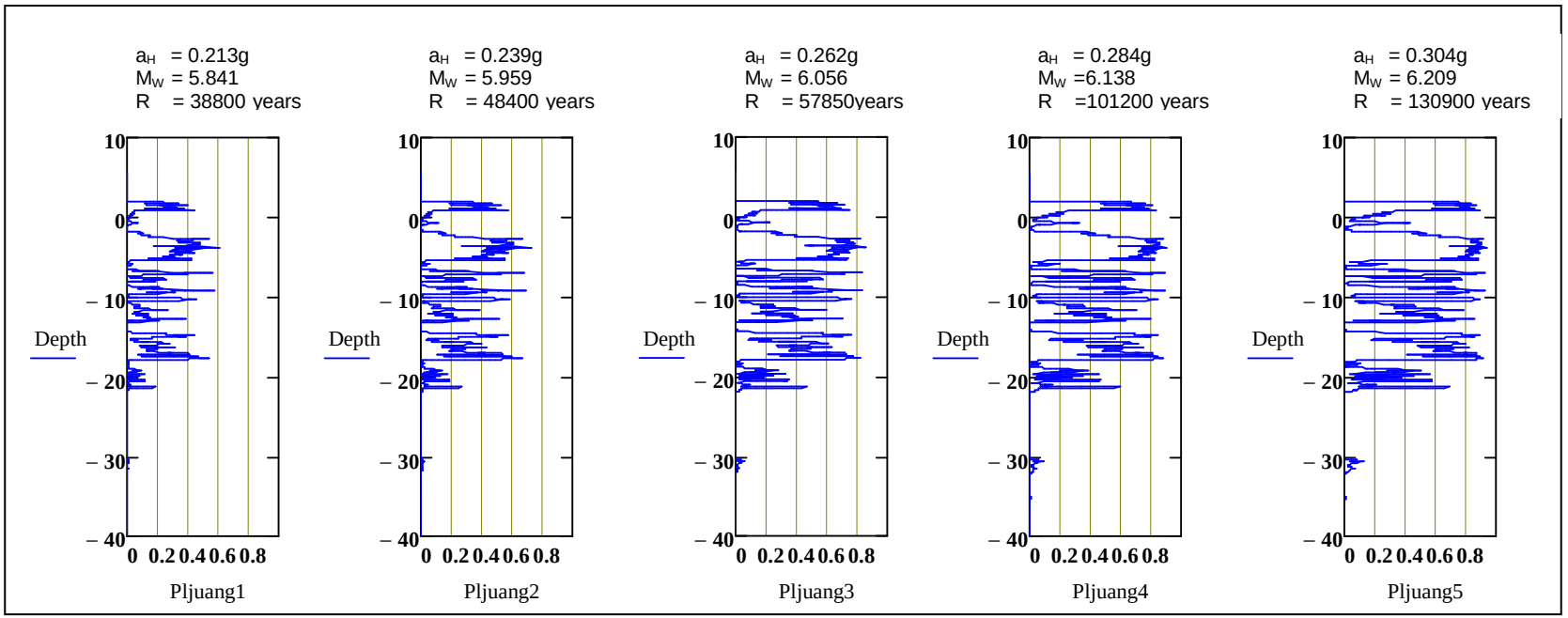

Figure E-7: Probability of liquefaction with different return periods

Methods:
Robertson and Wride (Red)
Juang et al. (Blue)

Location:
1250-1130

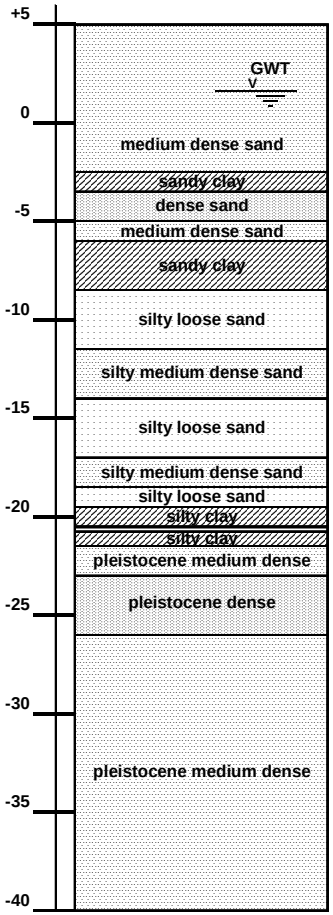

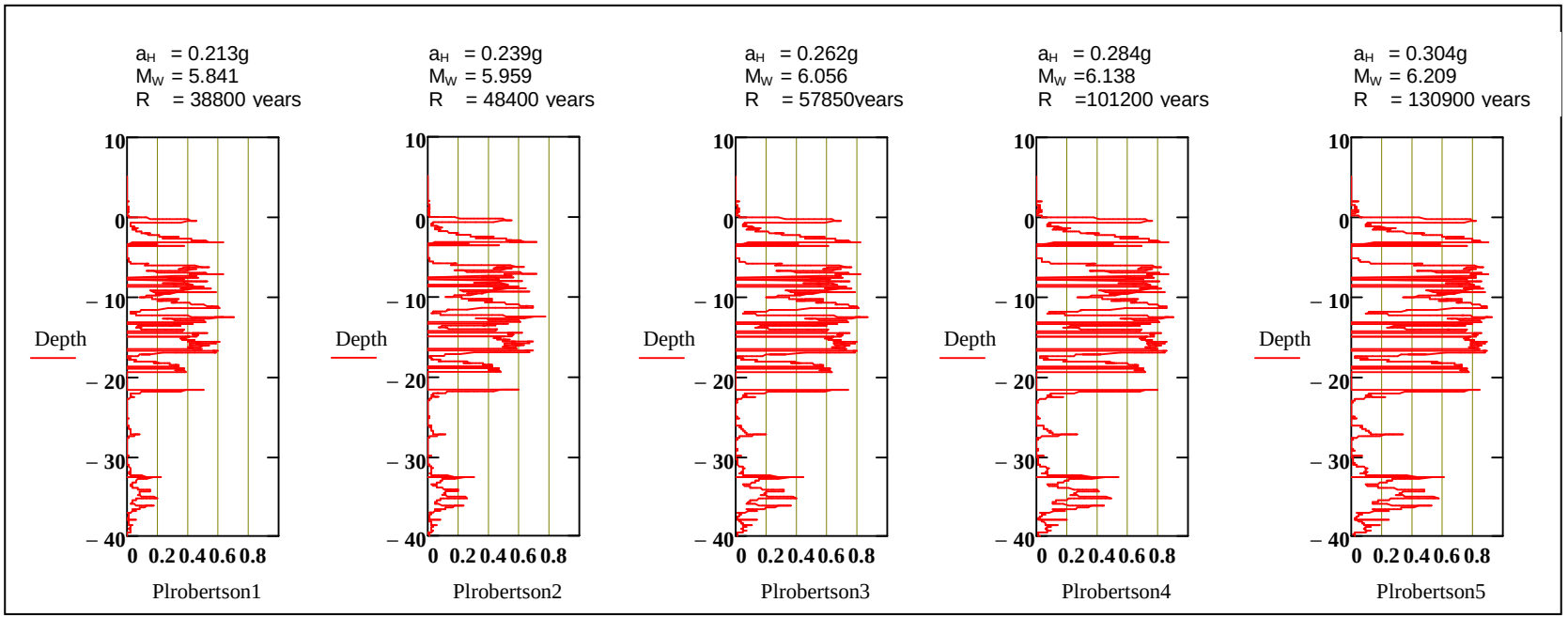

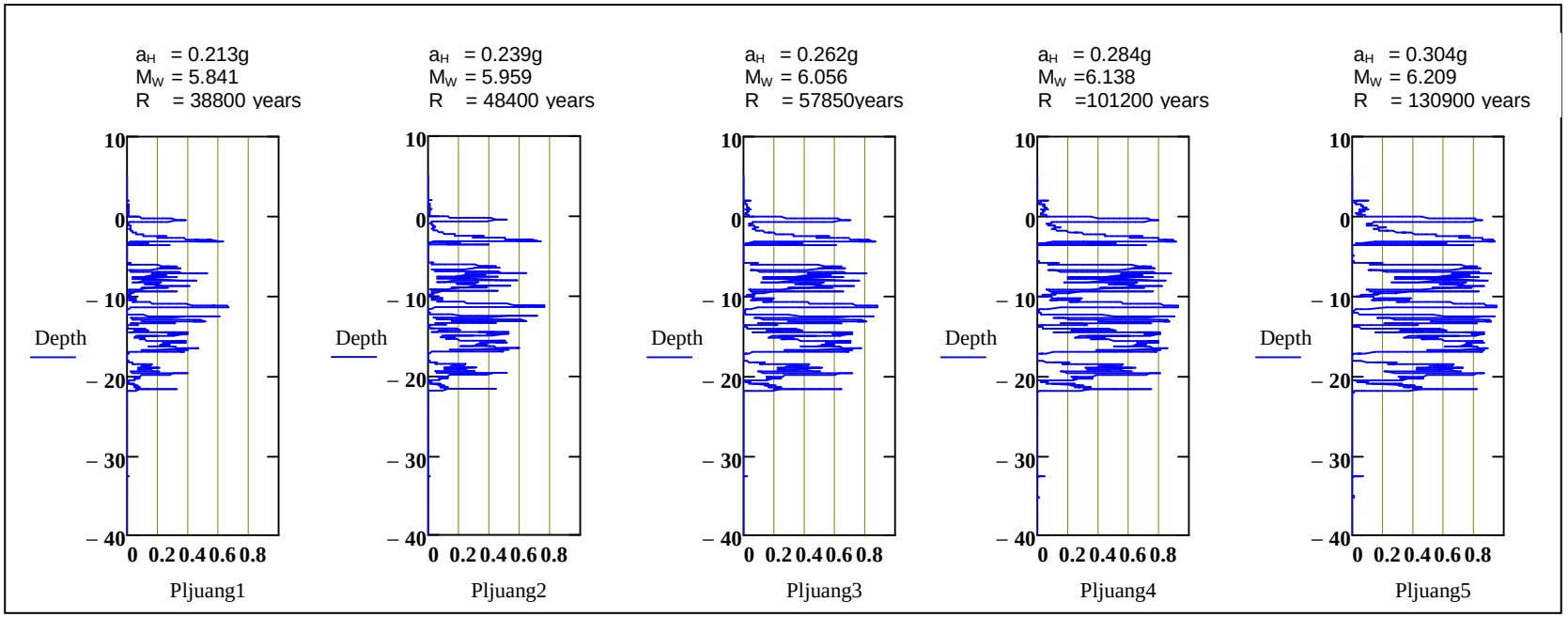

Figure E-8: Probability of liquefaction with different return periods

Methods:
Robertson and Wride (Red)
Juang et al. (Blue)

Location:
1130-1080

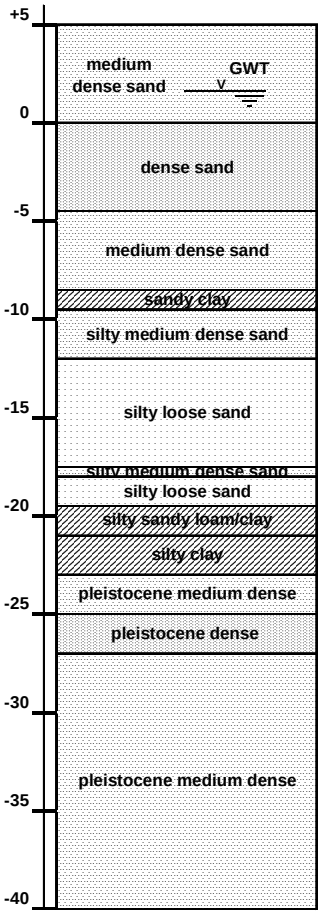

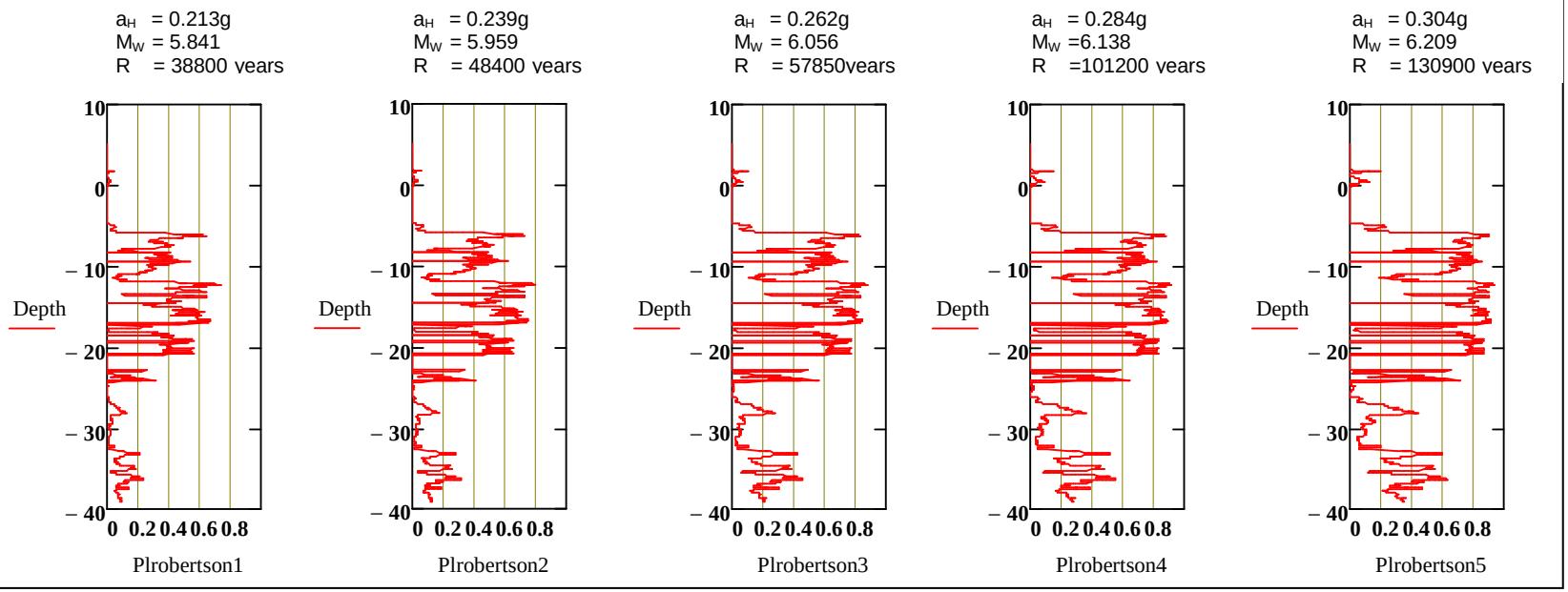

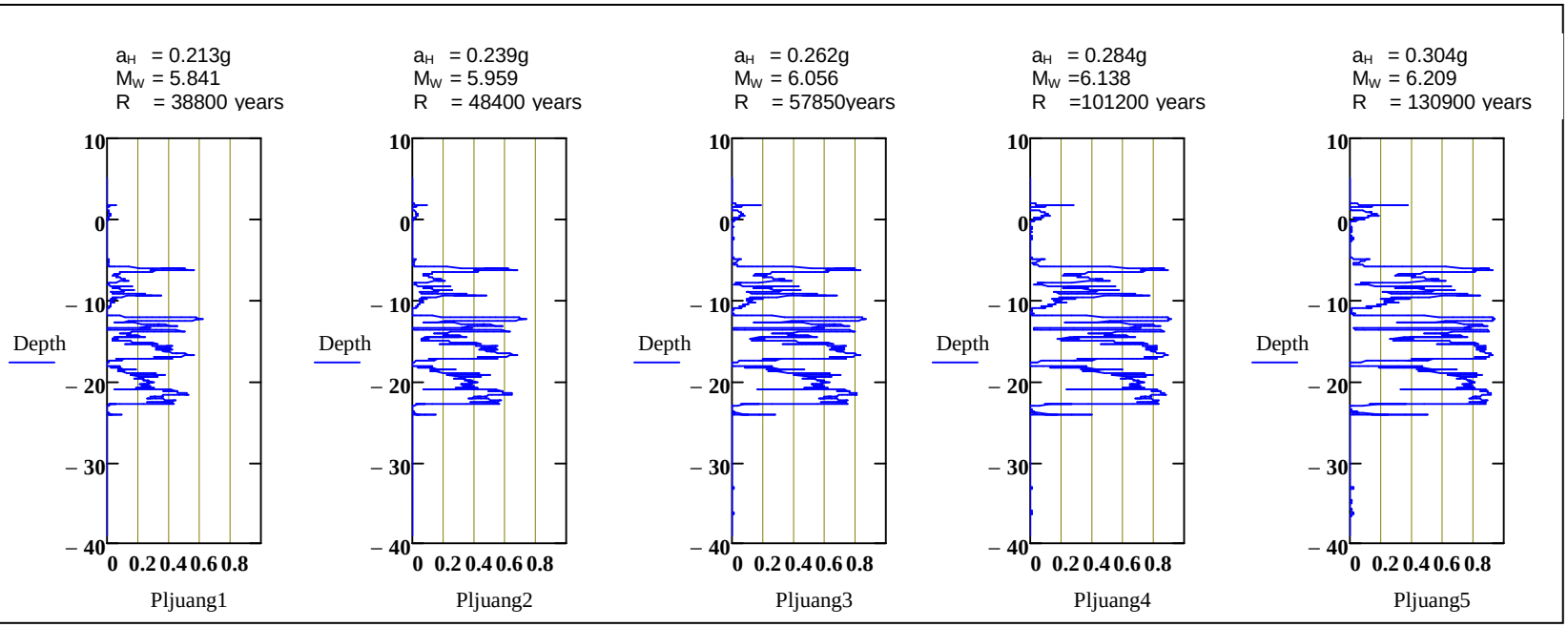

Figure E-9: Probability of liquefaction with different return periods

Methods:
Robertson and Wride (Red)
Juang et al. (Blue)

Location:
1085-960

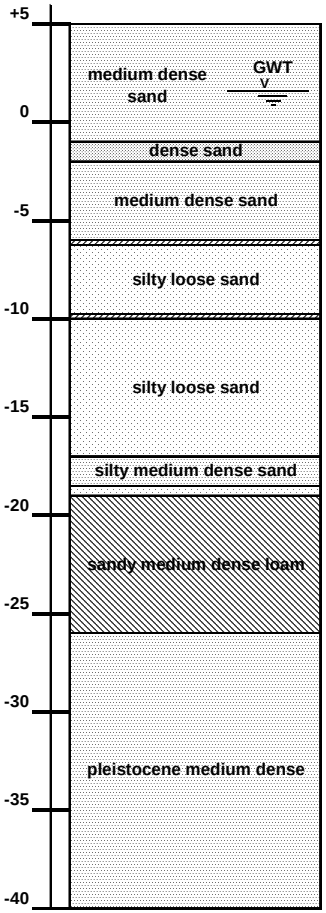

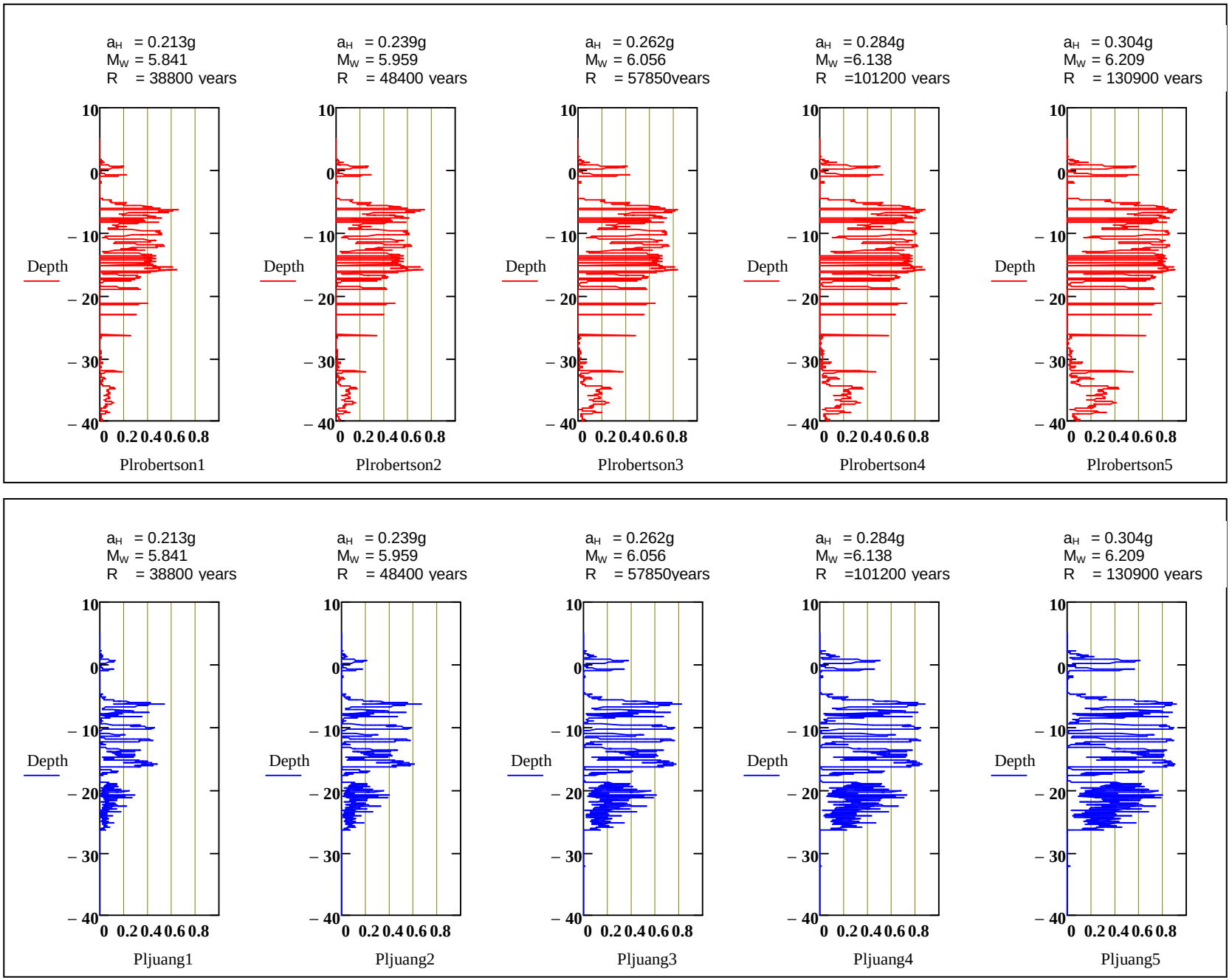

Figure E-10: Probability of liquefaction with different return periods

Methods:
Robertson and Wride (Red)
Juang et al. (Blue)

Location:
960-730

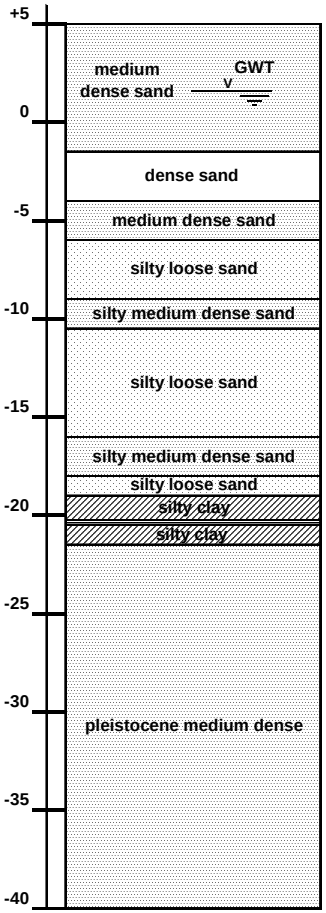

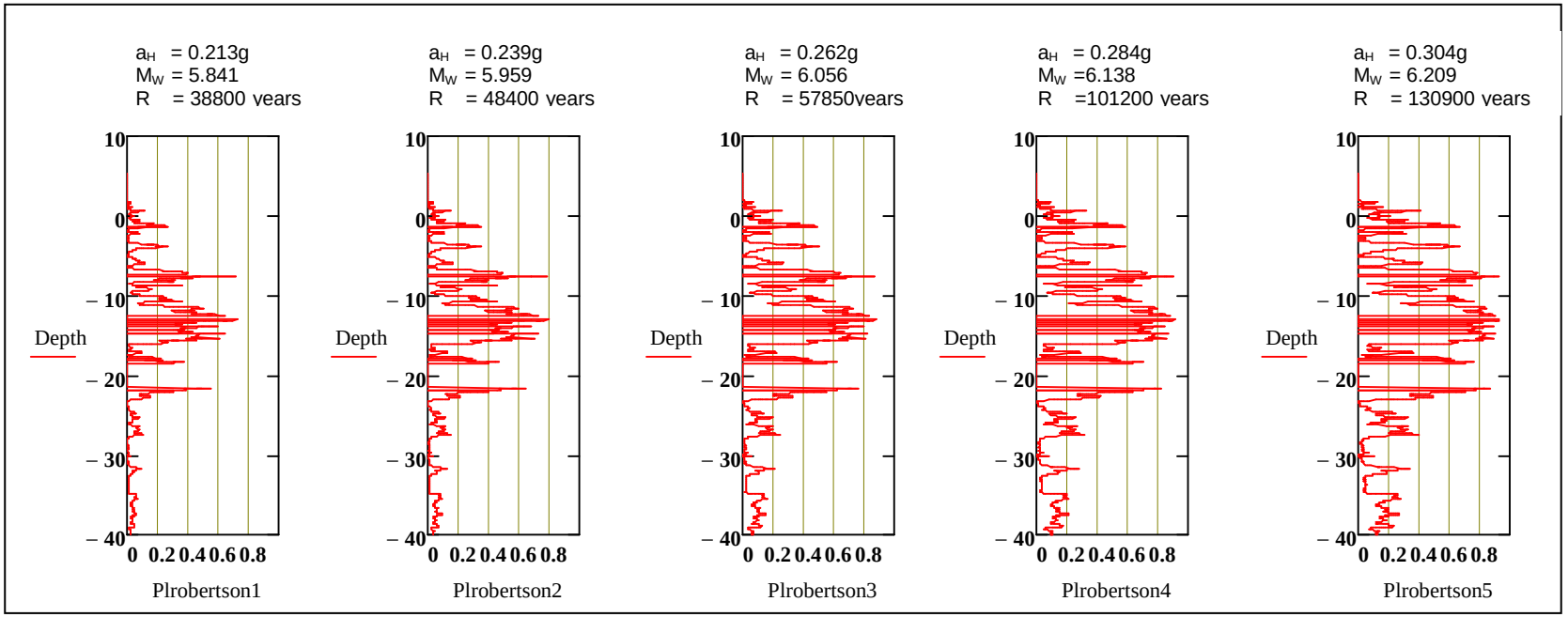

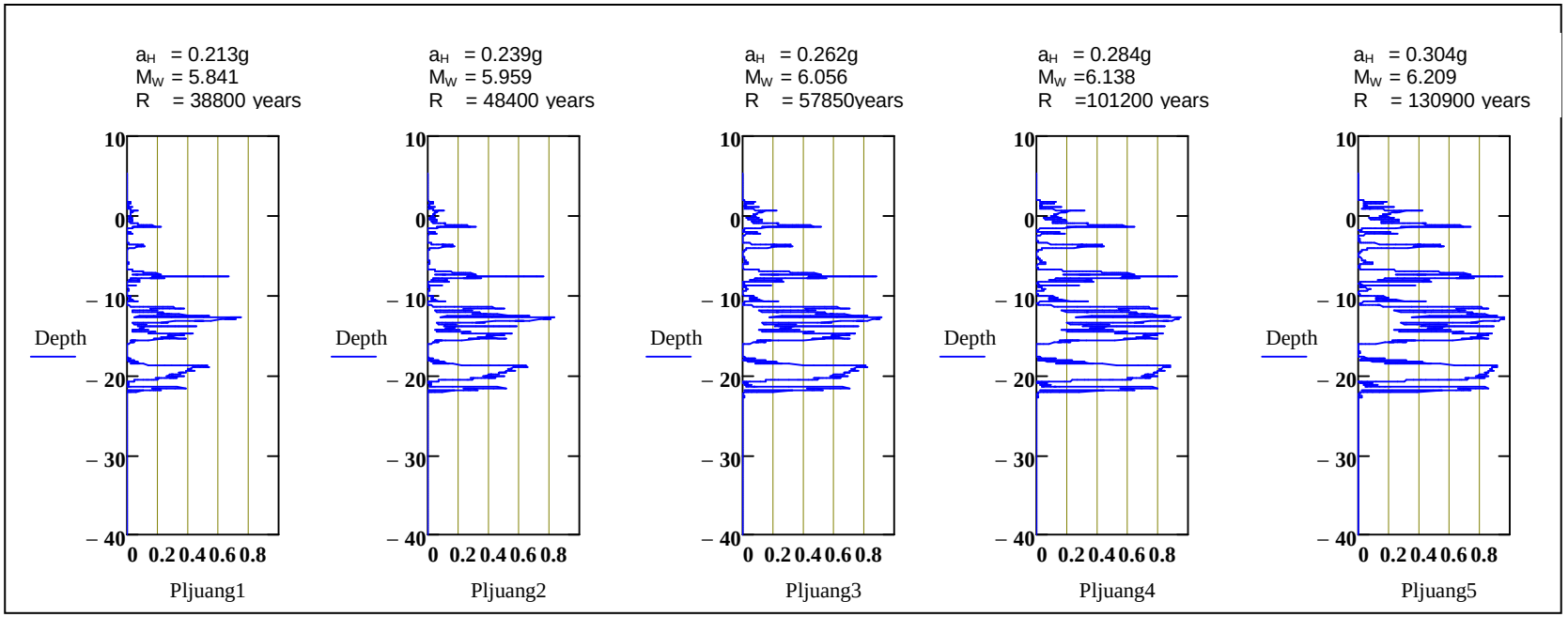

Figure E-11: Probability of liquefaction with different return periods

Methods:
Robertson and Wride (Red)
Juang et al. (Blue)

Location:
730-630

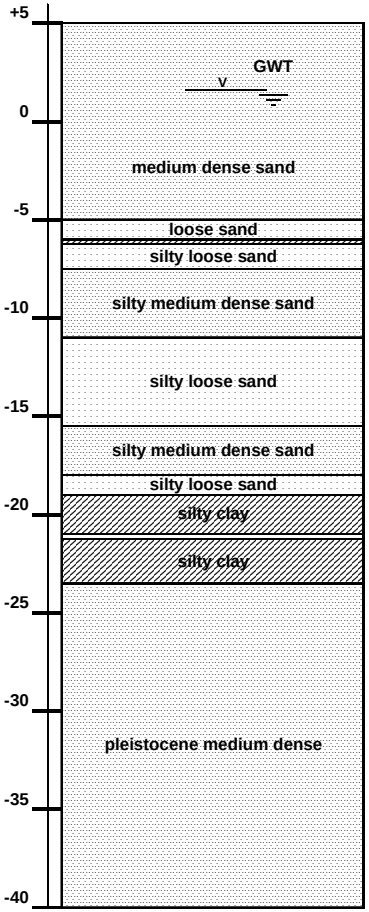

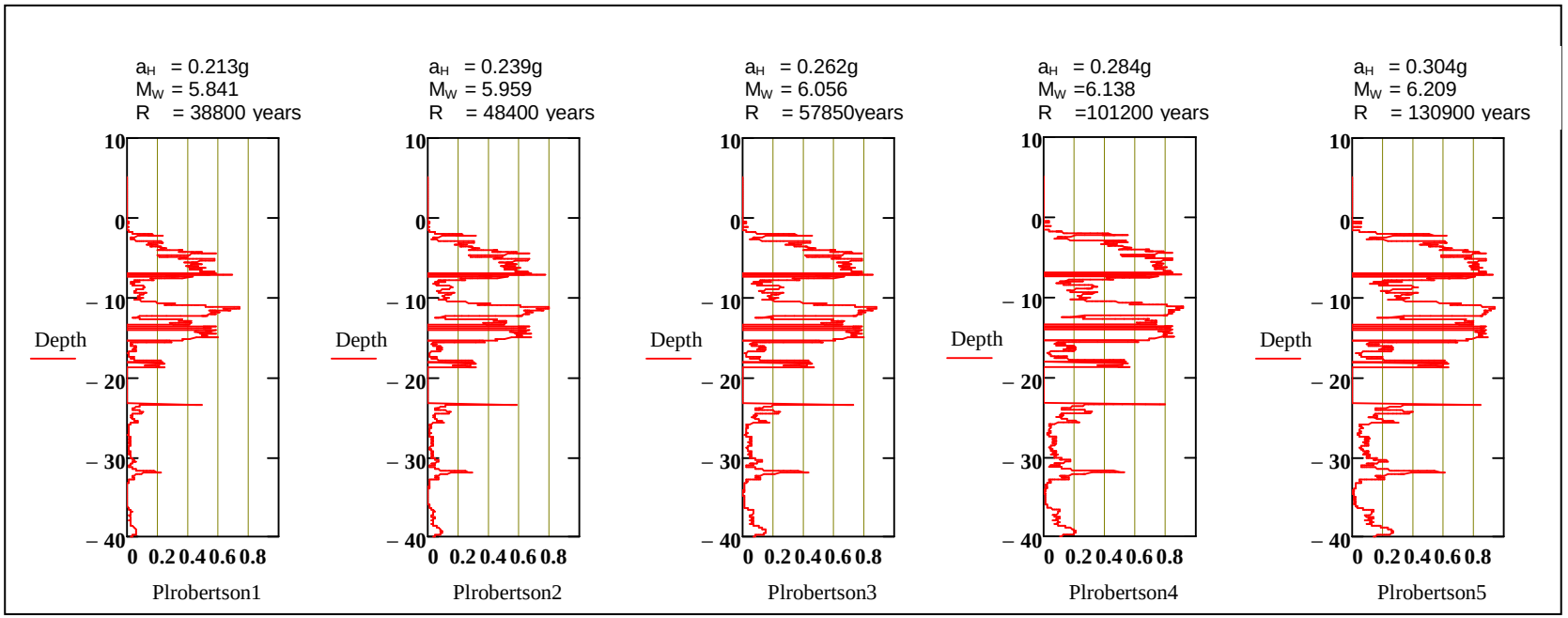

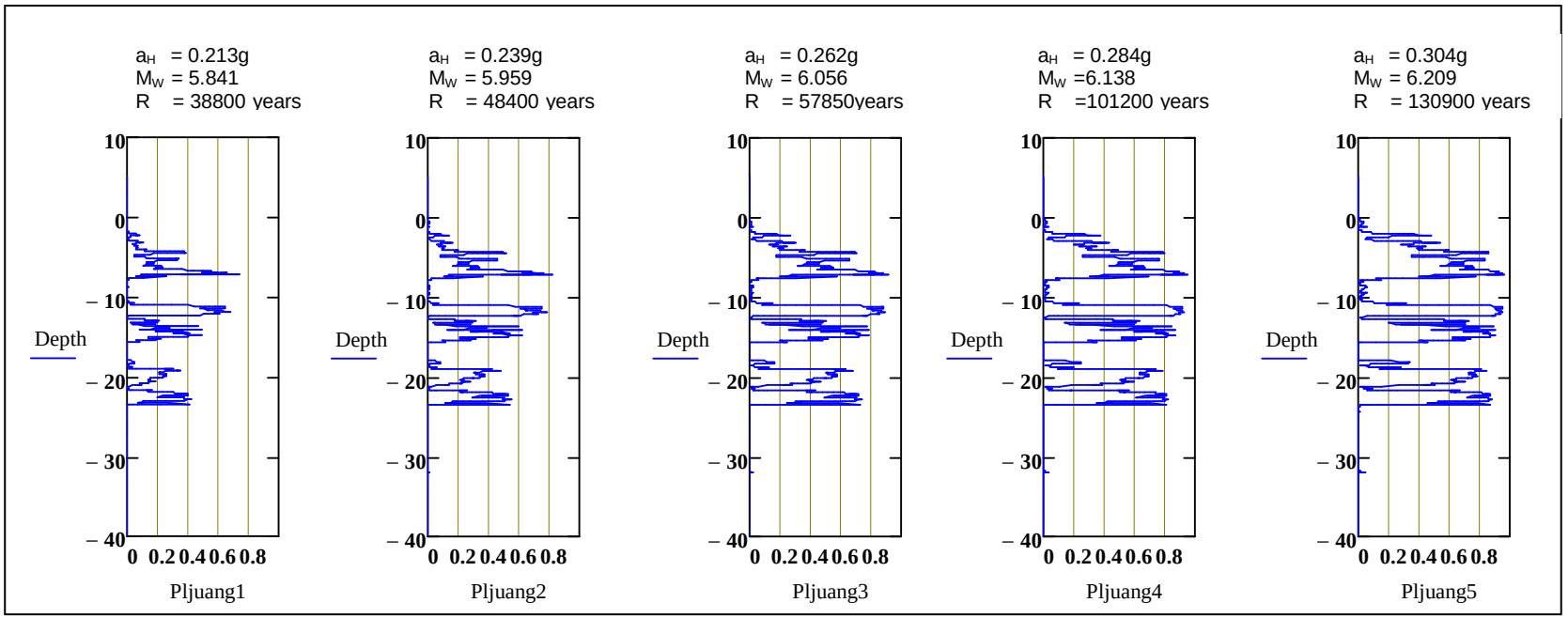

Figure E-12: Probability of liquefaction with different return periods

Methods:
Robertson and Wride (Red)
Juang et al. (Blue)

Location:
630-510

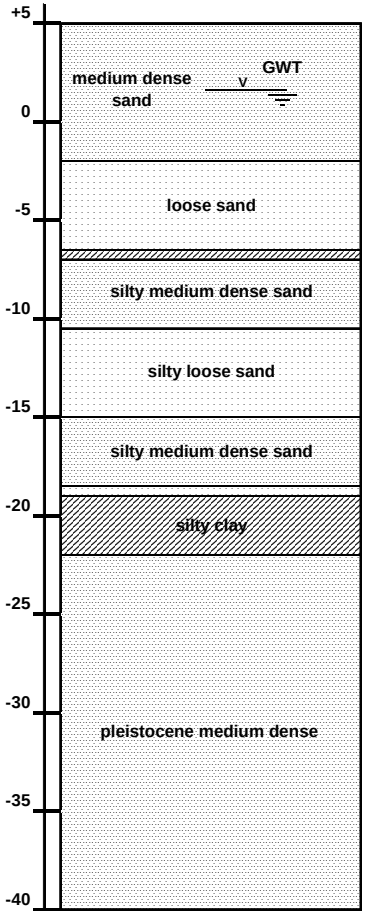

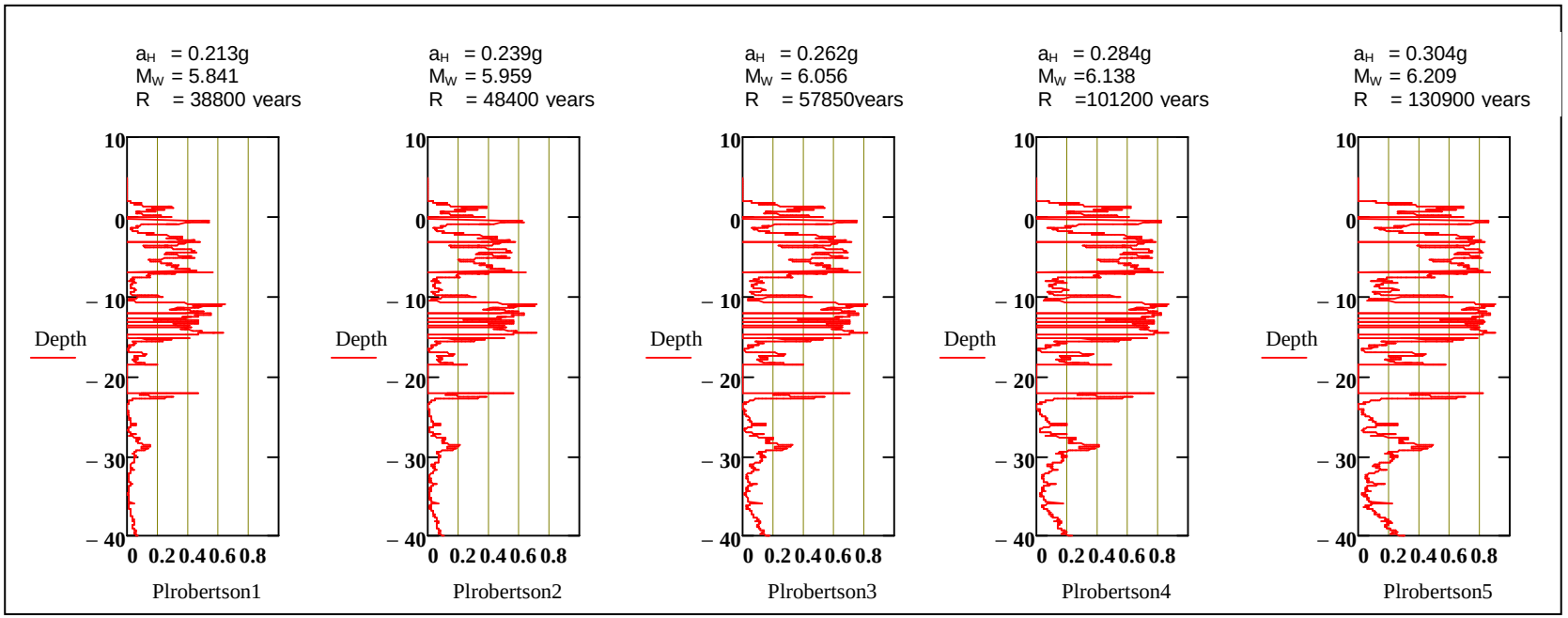

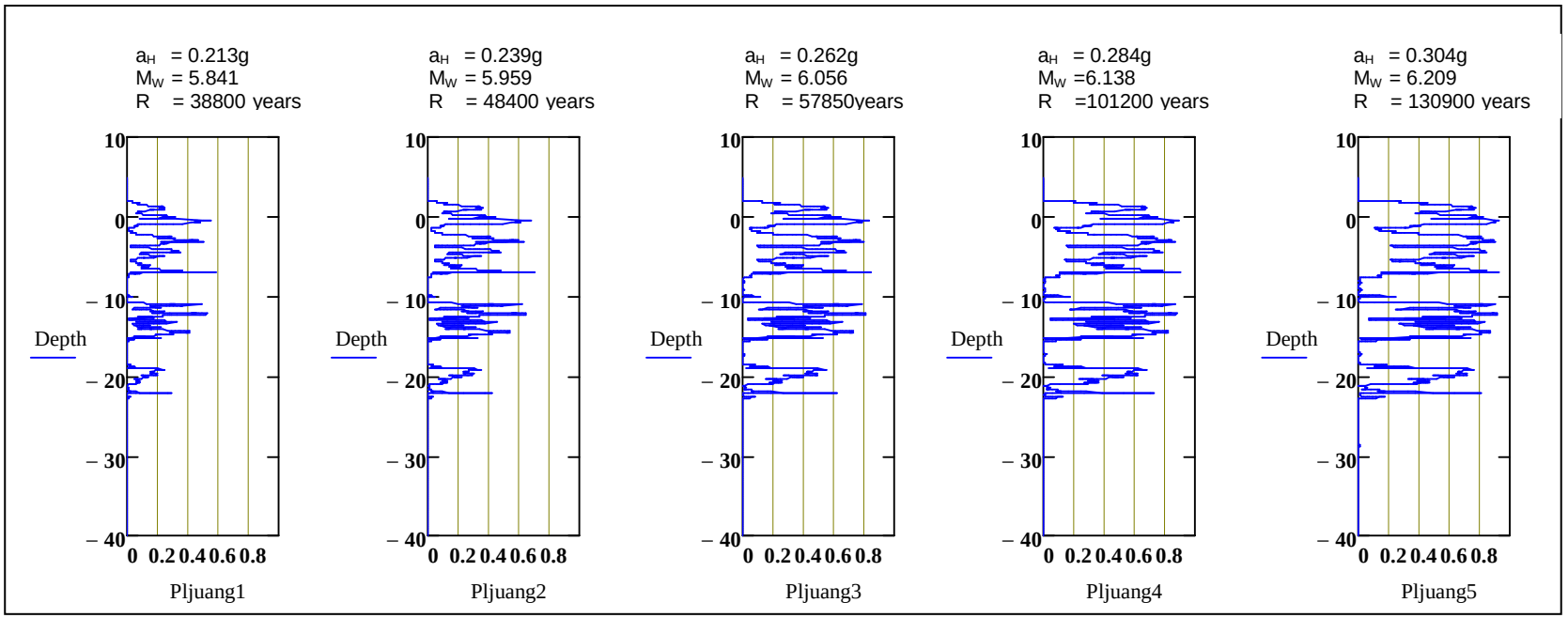

Figure E-13: Probability of liquefaction with different return periods

Methods:
Robertson and Wride (Red)
Juang et al. (Blue)

Location:
510-310

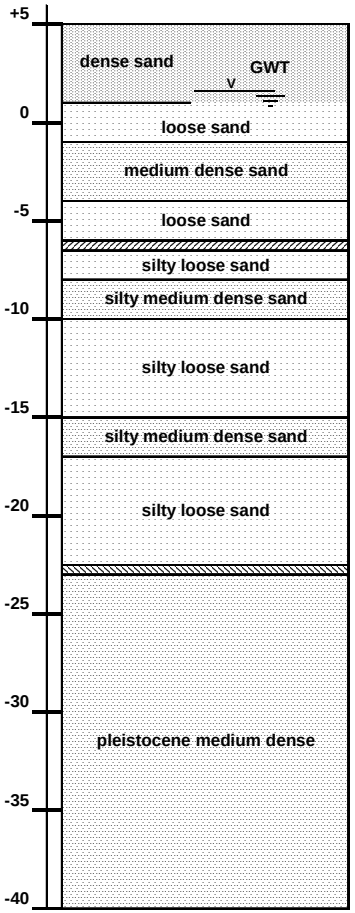

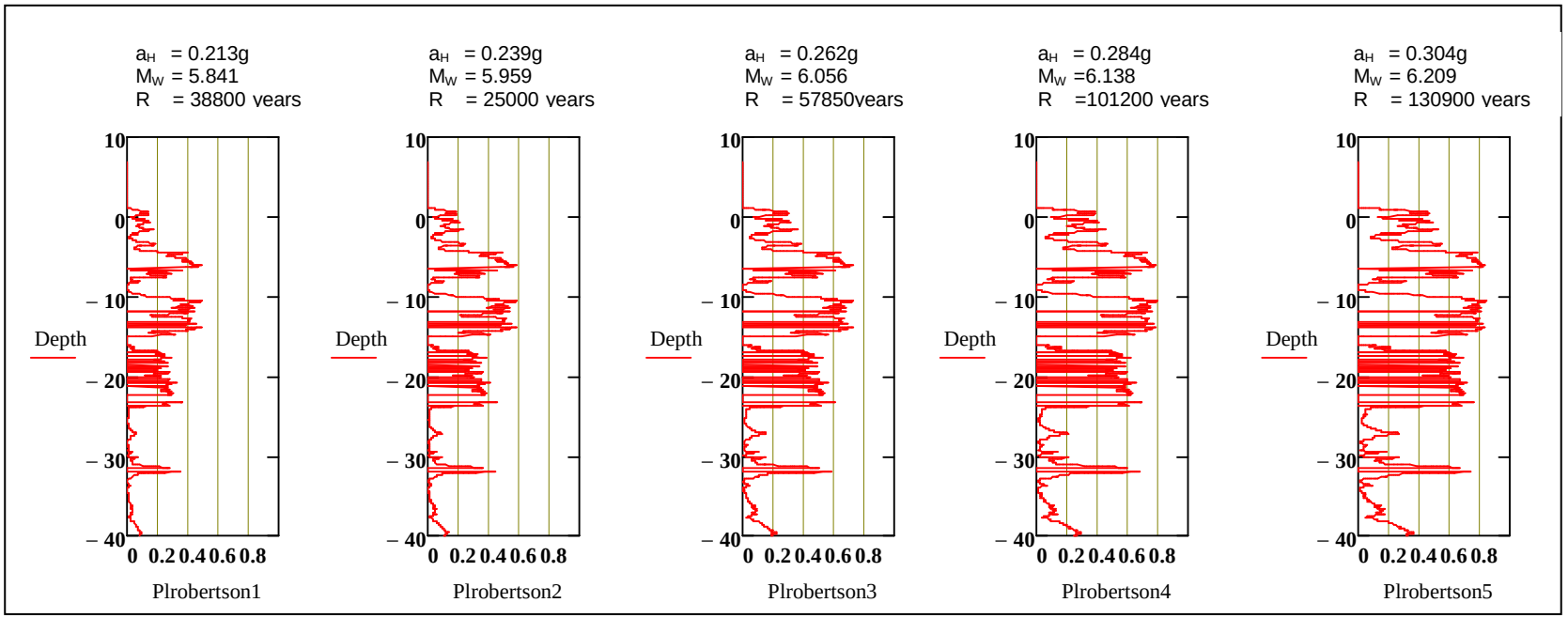

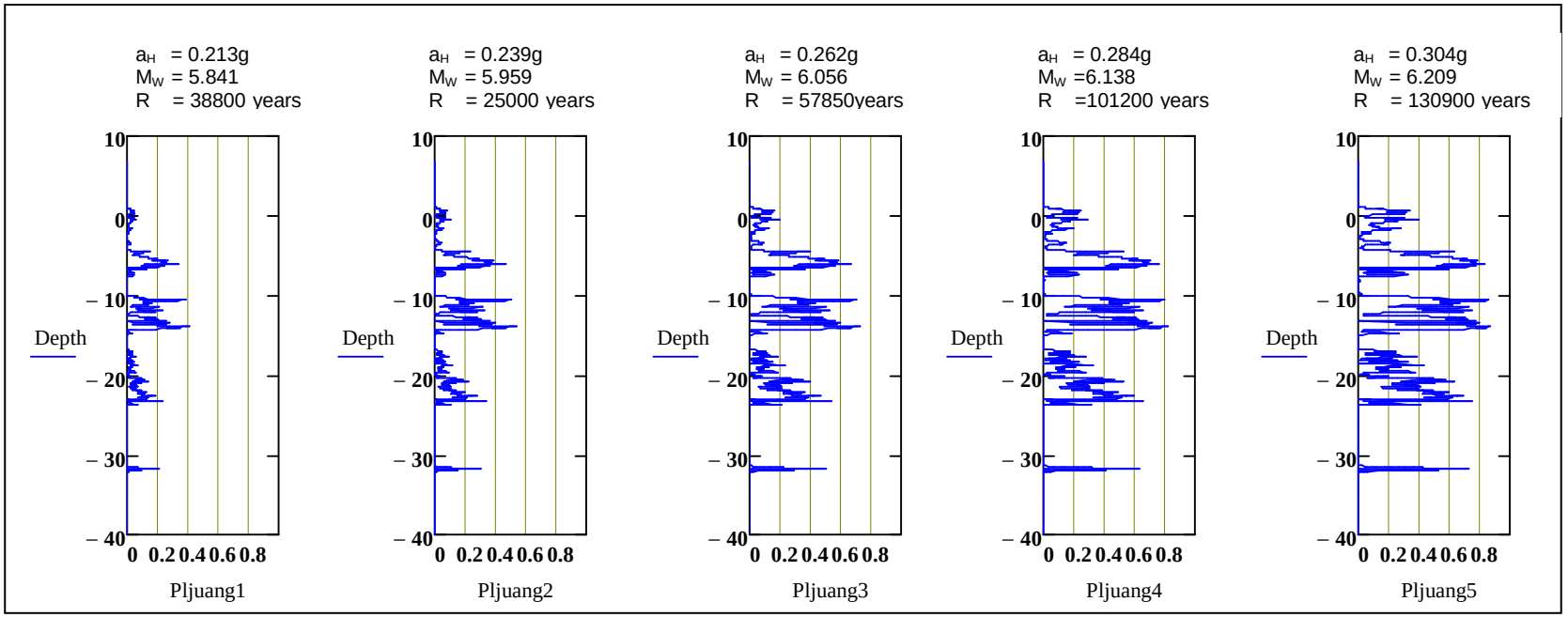

Figure E-14: Probability of liquefaction with different return periods

Methods:
Robertson and Wride (Red)
Juang et al. (Blue)

Location:
310-240

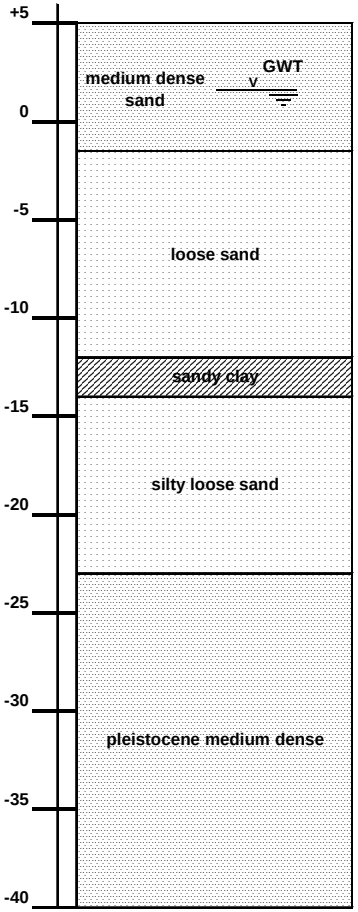

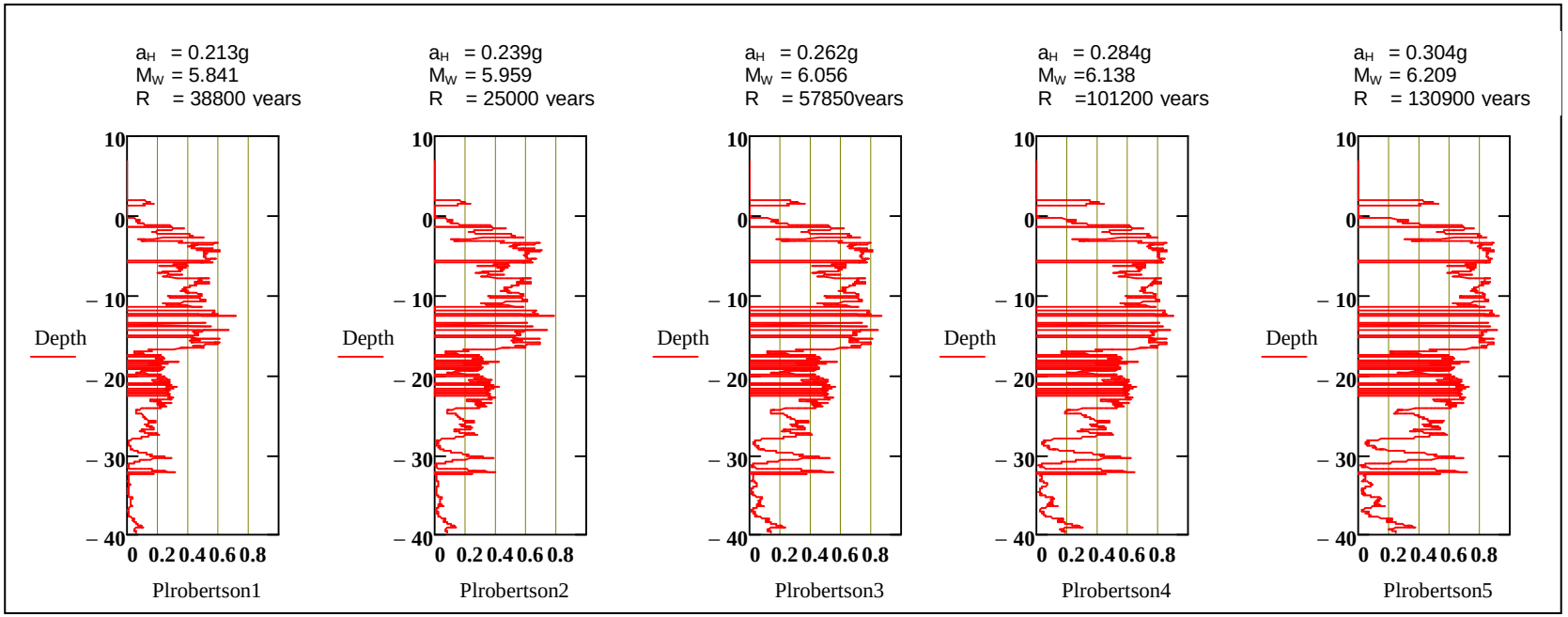

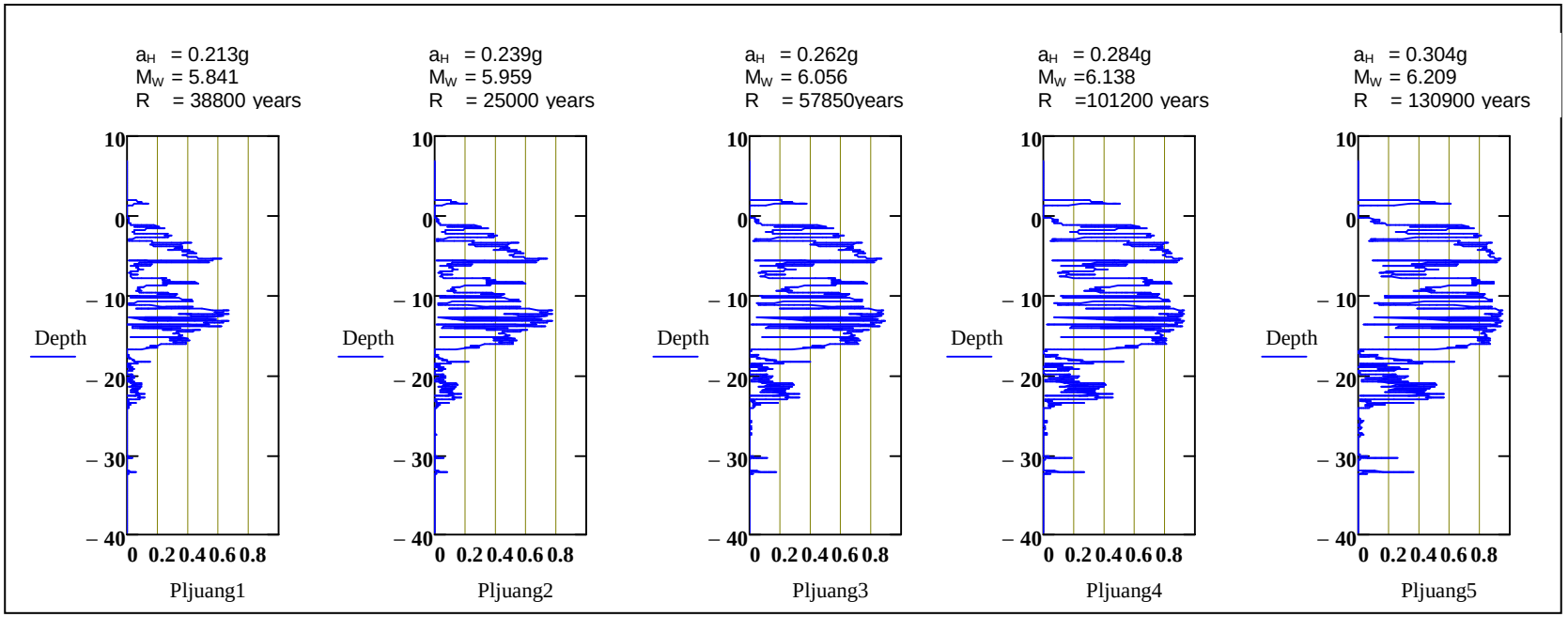

Figure E-15: Probability of liquefaction with different return periods

Methods:
Robertson and Wride (Red)
Juang et al. (Blue)

Location:
240-100

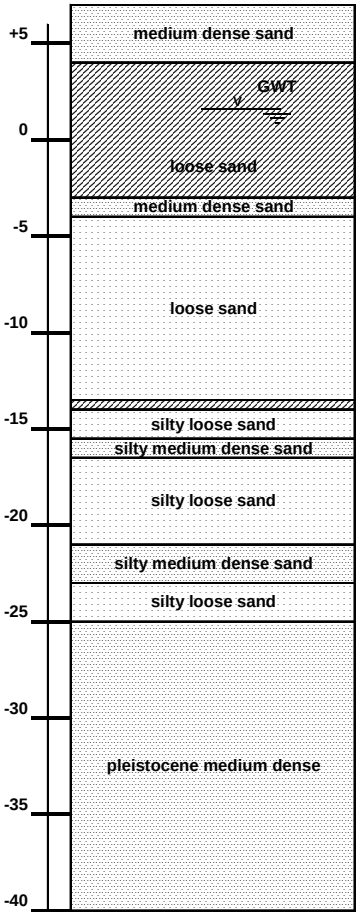

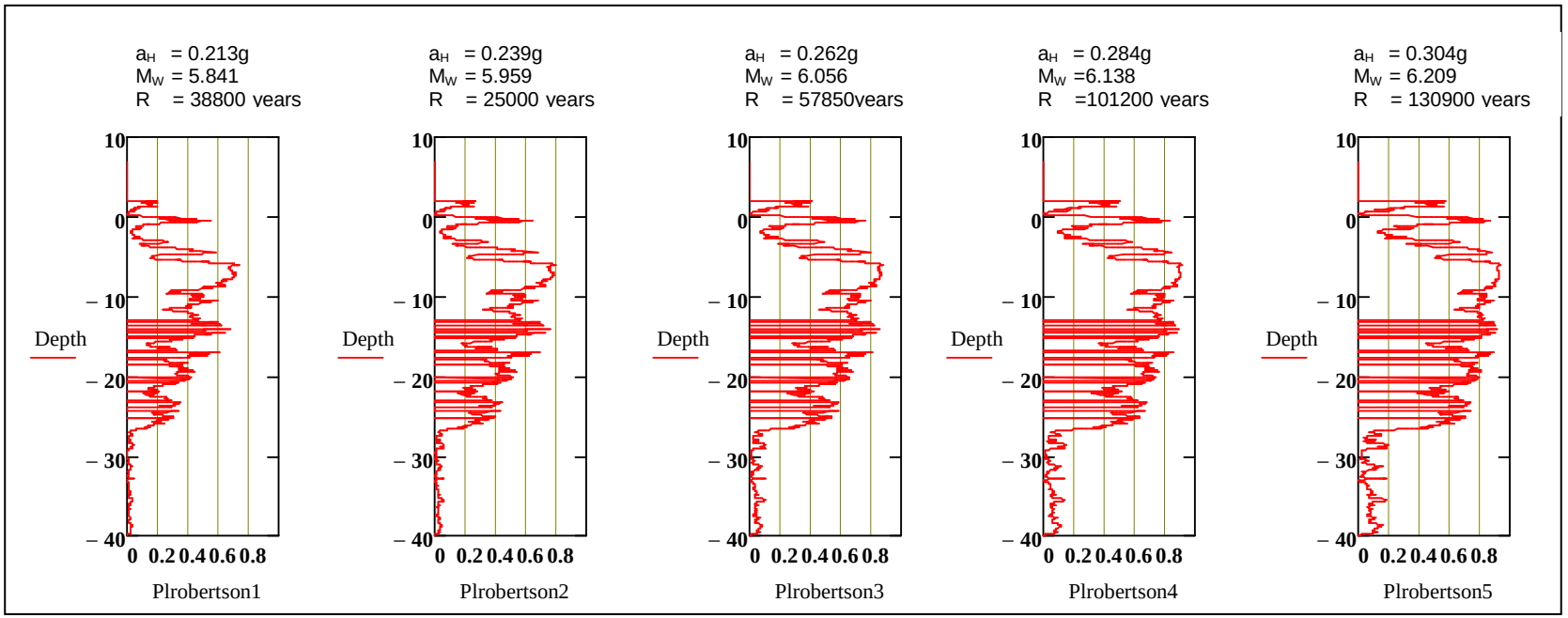

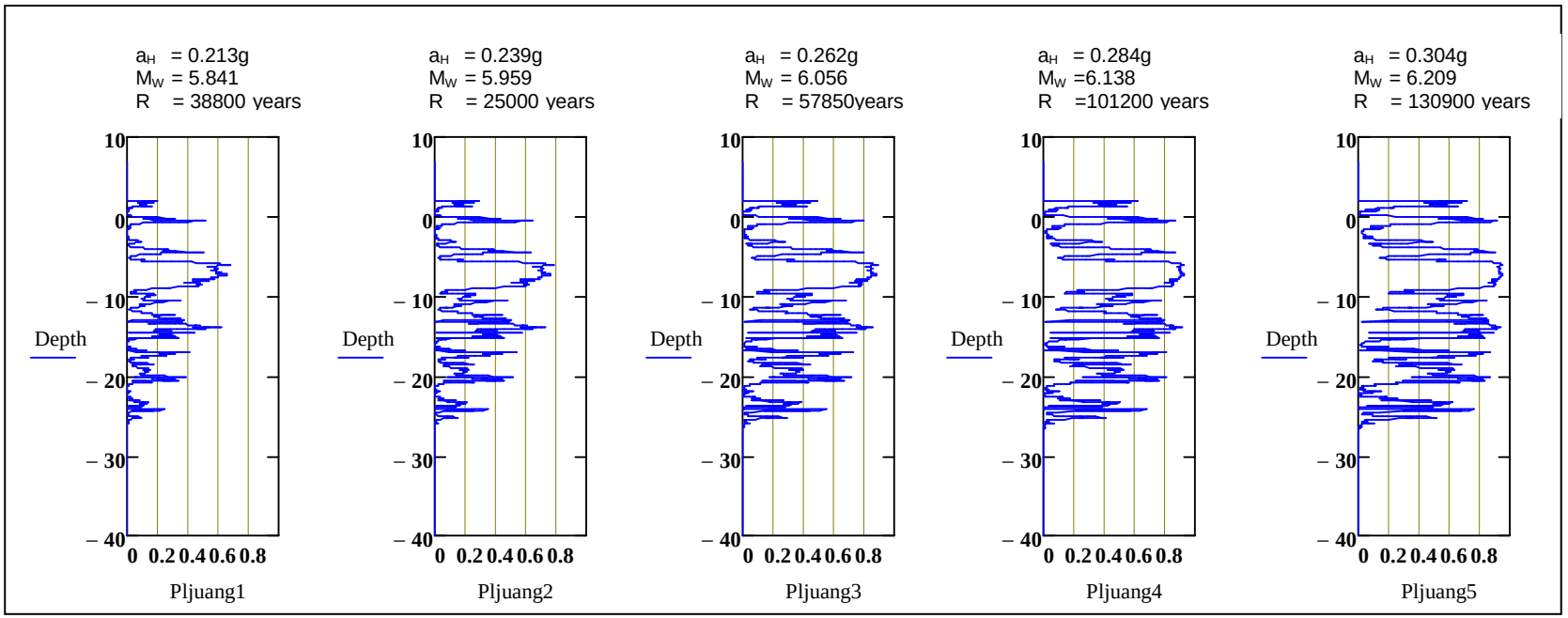

Figure E-16: Probability of liquefaction with different return periods

Methods:
Robertson and Wride (Red)
Juang et al. (Blue)

Location:
100-0

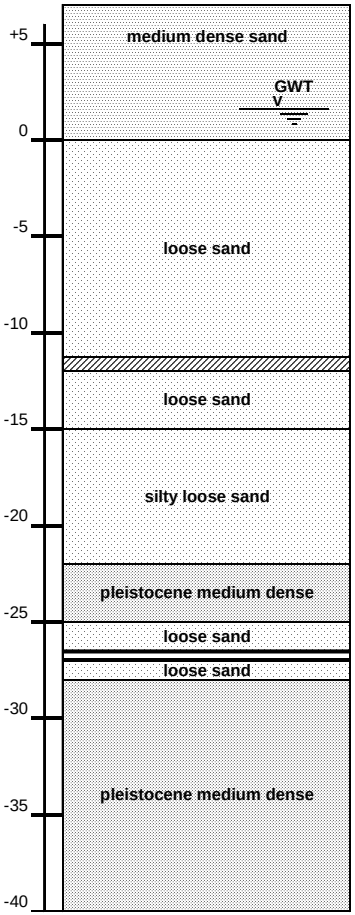

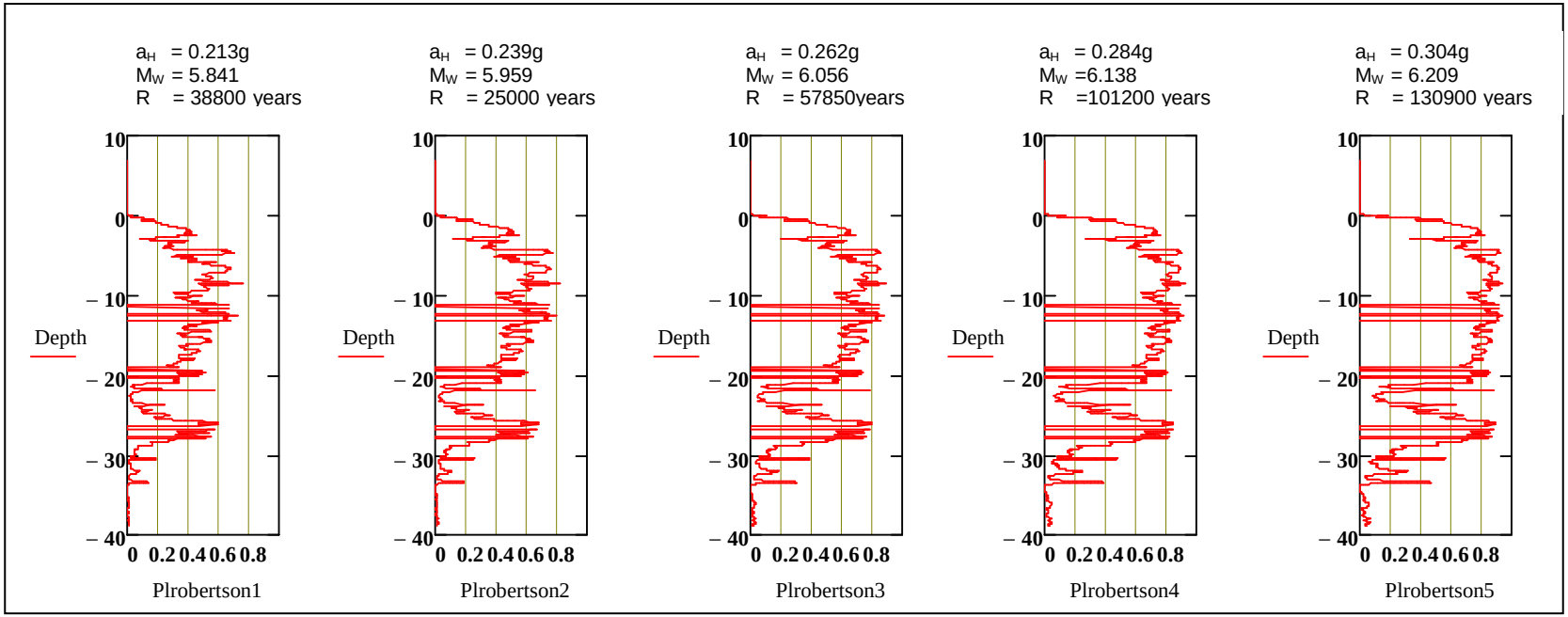

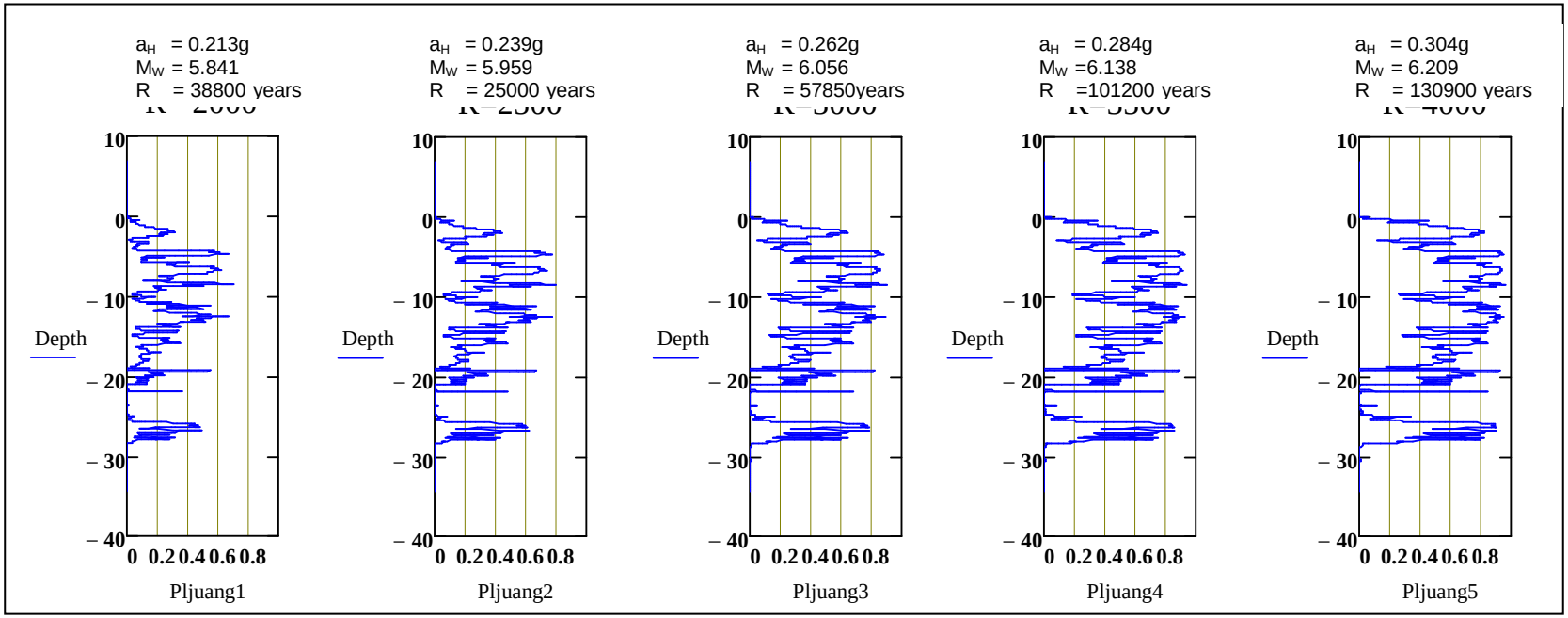

E2 Determining the liquefiable layers

Liquefaction probability functions with different return periods for section 1 have been drawn to determine the liquefiable layers, see Figure E-17 till Figure E-19. This figure illustrates how the soil will react to different return periods of different earthquakes. A higher return period of an earthquake results in more liquefiable soil layers. This is due to a higher horizontal peak ground acceleration and magnitude which comes with a higher return period of earthquakes. During this analysis it was assumed that liquefaction will occur if the probability of liquefaction is higher or equal to 0.6.

The Robertson and Wride method gives a higher liquefaction probability compared the method of Juang et al.. But eventually, when the return periods are very high, both the methods show the same liquefiable layers (loose sand layers). According to the Roberston and Wride method, almost all the loose sand layers will liquefy if an earthquake with return period of 77070 years occurs. For the method of Juang et al. this will be around the 10680 years.

For further calculations, findings achieved from the Robertson and Wride method will be used.

Figure E-17 Liquefiable layers Robertson method P_L>0.6

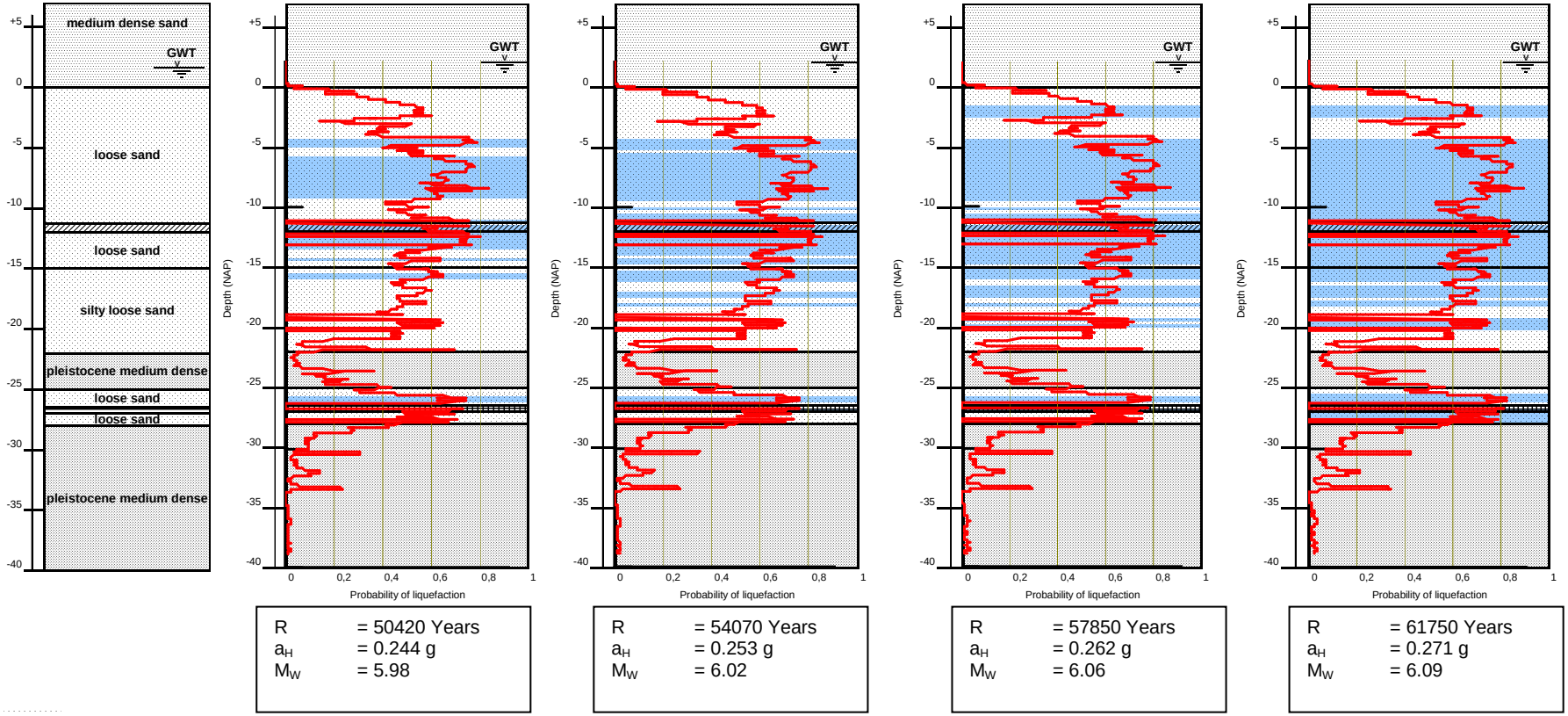

Figure E-18 Liquefiable layers Robertson method P_L>0.6

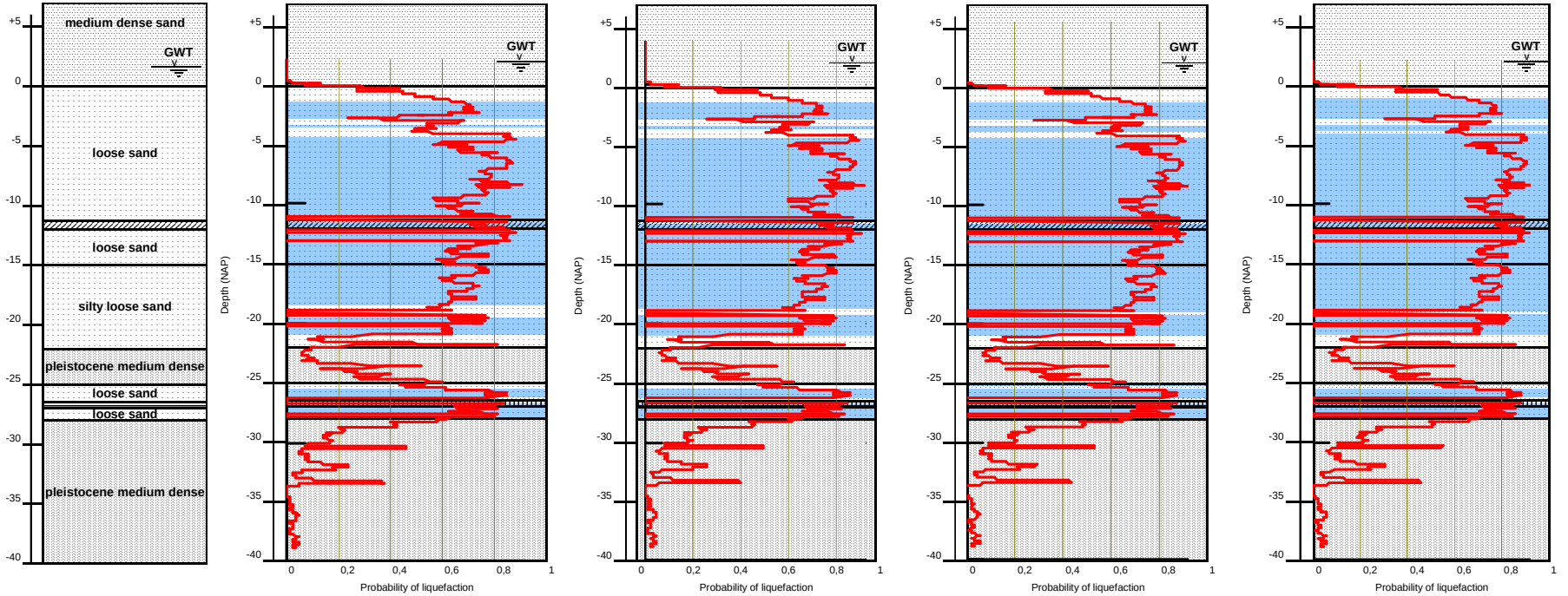

= Loose sand / silty loose sand
= Medium dense sand
= Pleistocene medium dense sand
= Sandy medium/dense loam
= Sandy loam/ clay
= Liquefiable soil layer
= Probability graph of liquefaction

R = **Return period [years]**
a_H = **Horizontal peak ground acceleration**
M_W = **Moment magnitude**

Figure E-19 Liquefiable layers Juang et al. method P_L>0.6

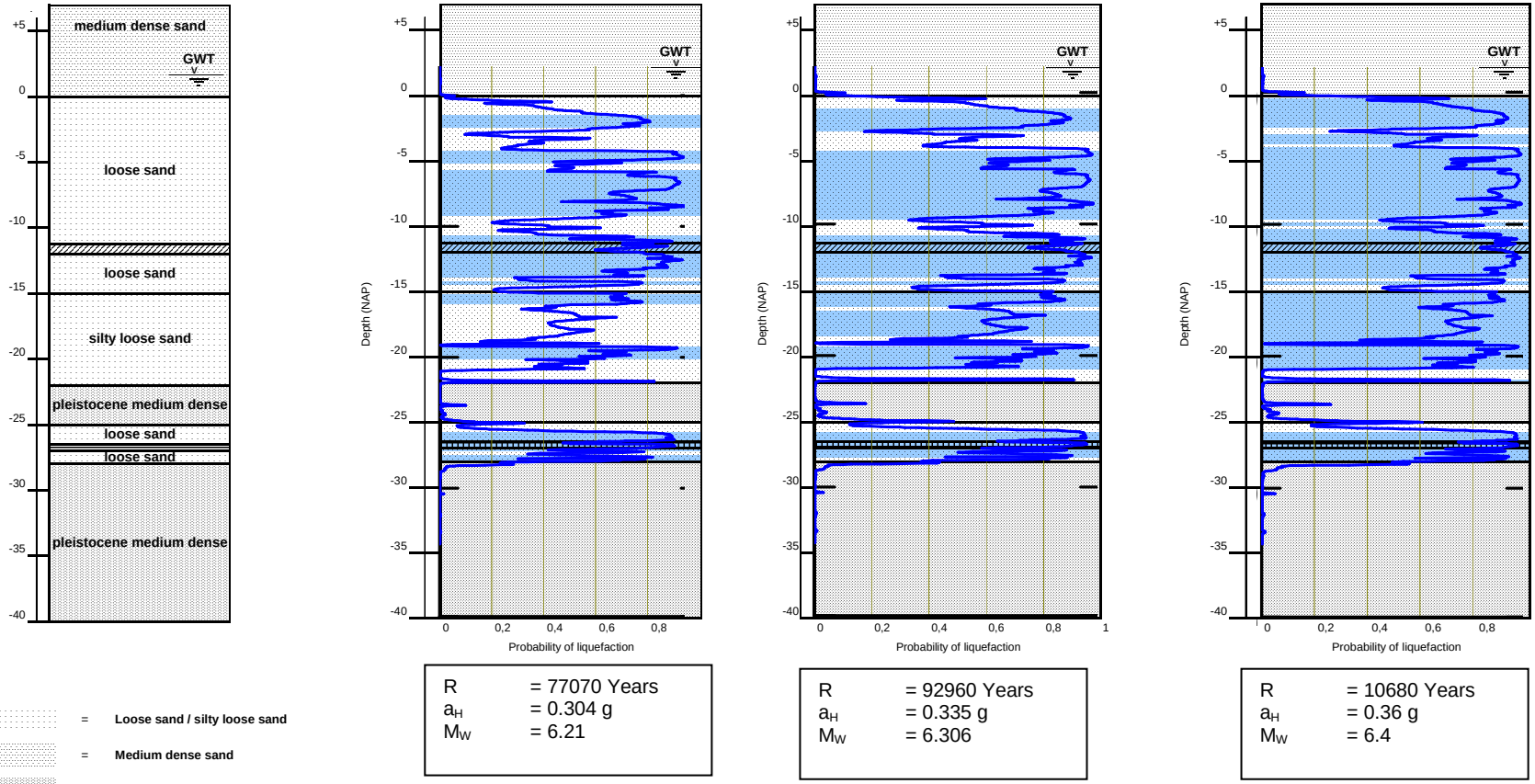

Appendix F Forces on relieving structure

The requirements presented in section 3,3 gave an overview of all the loads that the quay wall structure should be able to resist during its lifetime (note: this does not include seismic loading). In this chapter these loads will be specified in such a way that they can be used in the calculations of the diaphragm wall. Only the loads acting on the relivieng structure are presented. The structure will be analysed per running meter. For this purpose the forces will be determined per running meter.

F1 Static forces on relieving floor

Forces acting on the relieving floor will be handeled seperatly in this section.

Water level

Water levels are needed to determine the water pressure acting on the relieving structure. A distinction is made between the ground water (GWL) at the landside and the water level of the sea (SWL). In the reports from BAM [f-1] several water levels are used. They are summarized in Table F-1. The most normative water levels is used during the seismic analysis of the quay wall. These are high ground water level (NAP +0,52m) and a low sea level (NAP -1,38m).

	Type	Water level (NAP)
1	G.W.L	+0.52
2	G.W.L	-1.12
3	G.W.L	-1.38
4	S.W.L	+1.92
5	S.W.L	+1.67
6	S.W.L	-1.12
7	S.W.L	-1.38

Table F-1 water levels

Ground water pressure (NAP +0,52m)

Hydrostatic water pressure and bouyonce uplifting will act on the relieving structure due to presence of ground water and can be calculated as follows:

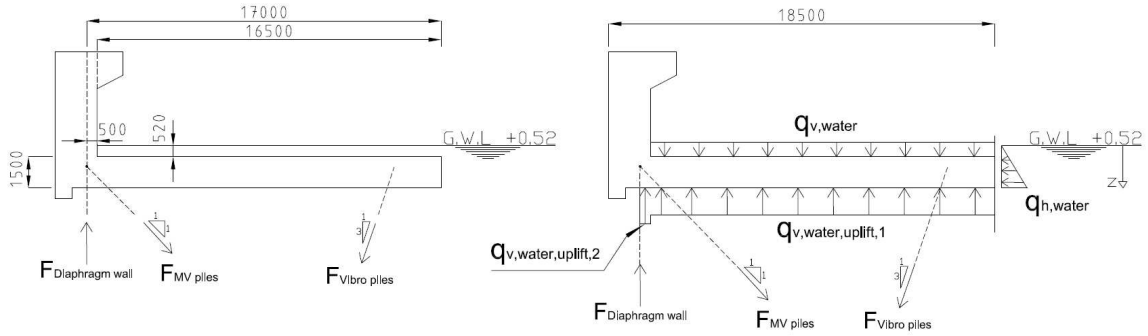

$q_{v,water}$ = $\gamma_w * h_w$ = 10*0.52= 5.2 kN/m/m
$q_{v,water,uplift,1}$ = $\gamma_w * h_{floor}$ = 10*1.5= 15 kN/m/m
$q_{v,water,uplift,2}$ = $\gamma_w * (h_{floor}+h_w$ = 10* (1.5+0.52)= 20.2 kN/m/m
$q_{h,water}$ = 10*z [kN/m/m]

where z is the water depth in meters measured from the referencepoint (G.W.L.)

Sea water pressure (NAP -1,38m)

Horizontal loads due to the seawater are neglected because they are small compared to the other loads and therefore the influence will be small.

$q_{v,seawater,uplift,1}$ = 0,12*γ_w= 1,2 kN/m/m
$q_{v,seawater,uplift,2}$ = 0,62*γ_w= 6,2 kN/m/m

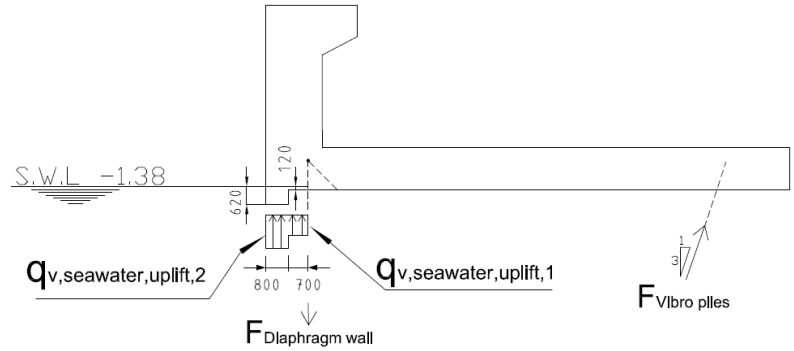

Own weight relieving floor

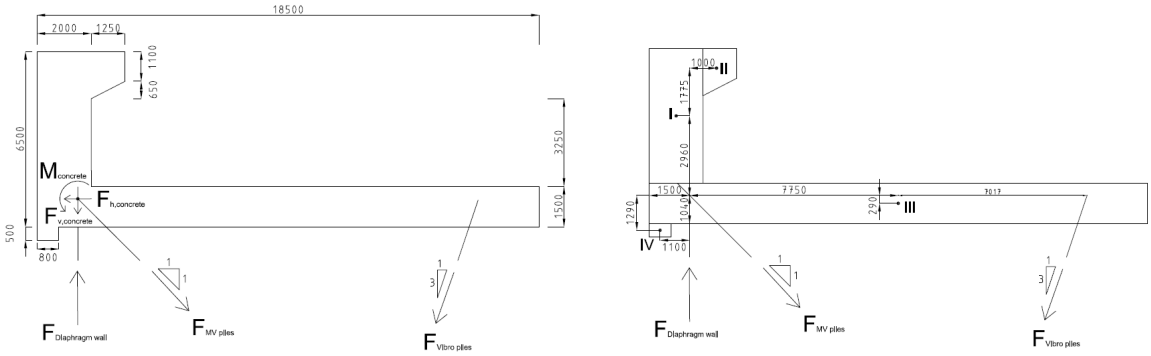

The relieving platform is divided into 4 parts; I, II, III and IV. The mass centre of each individual part has been calculated with Eq. F-1 and is drawn in figure 1 as a dot.

$$R = \frac{m_1 r_1 + m_2 r_2 + ...m_n r_n}{m_1 + m_2 + ...m_n} \qquad \textit{Eq. F-1}$$

where

m_1	=	mass of body number 1
m_2	=	mass of body number 2
m_n	=	mass of body number n
r_1	=	Distance reference point to mass centre of body 1
r_2	=	Distance reference point to mass centre of body 2
r_n	=	Distance reference point to mass centre of body n
R	=	Distance reference point to mass centre of all the bodies

$H * b * \gamma_{concrete}$

I	:	5 * 2 * 25 = 250 kN/m
II	:	1.1 * 1.25 * 25 + 0.65 * 1.25 * 0.5 * 25 = 37 kN/m
III	:	1.5 * 18.5 * 25 = 695 kN/m
IV	:	0.5 * 0.8 * 25 = 10 kN/m

Total force due to own weight of relieving floor: 250+37+695+10 =992 kN/m

Crane force

The vertical crane load in operation acts as a line load on the wall of the superstructure. This wall is 6,5m high. When these loads are transferred to the concrete they will have spread under 45°. This results in a decrease of the load per running meter. Depending on the configuration of the cranes, the normative crane load can be determined. Spreading of the crane loads is presented in a front view of the quay wall in Figure F-1.

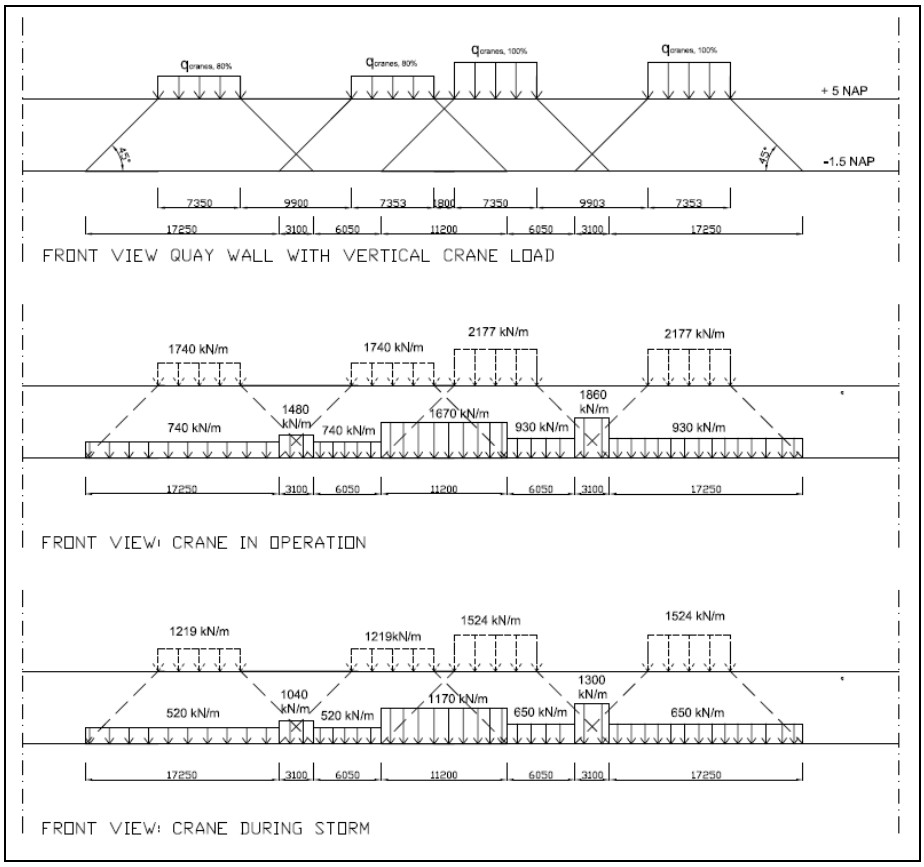

Figure F-1 Spreading of crane loads

Each crane has two legs per crane track with 8 wheels over 7.35m. The distance between the centres of each leg is 17.25m. The c.t.c distance between two different cranes is 26.40m. In the calculation one crane will be fully loaded and the other cranes are loaded for 80%. In Figure F-1 can be seen that the normative load is at the position where the loads of the two legs of the crane that is loaded for 100% overlay. This for the crane in operation and during storm is 1860kN/m and 1300kN/m respectively. This point acts in the crosssection of the structure as a pointload.

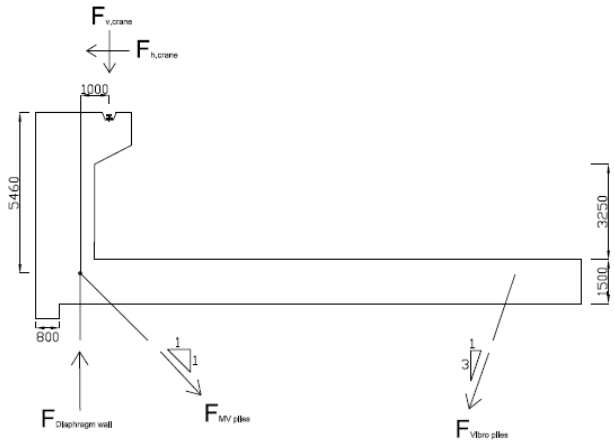

Crane in operation

$F_{v,crane,after\ spreading}$ = 1860 kN/m
$F_{h,crane}$ = 48 kN/m

Crane during storm

$F_{v,crane,after\ spreading}$ = 1300 kN/m
$F_{h,crane}$ = 184 kN/m

Bollard force

The bollards are positioned in couples c.t.c 15.00m. Distance between the two bollards is 2.70m. One bollard is loaded for 100% (2400kN) and the second one for 70% (1680kN).

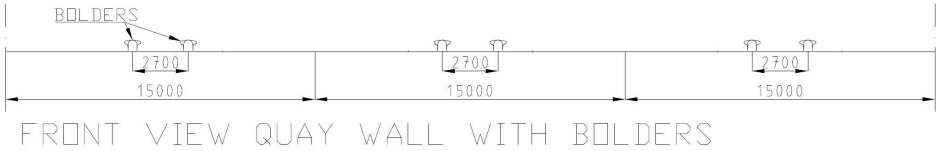

FRONT VIEW QUAY WALL WITH BOLDERS

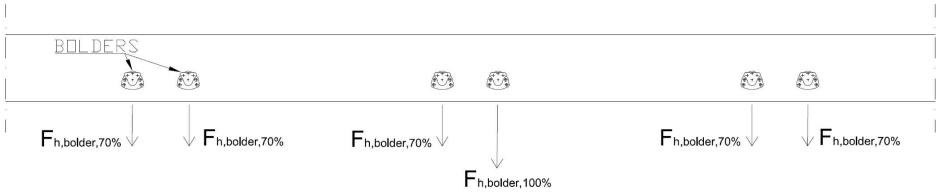

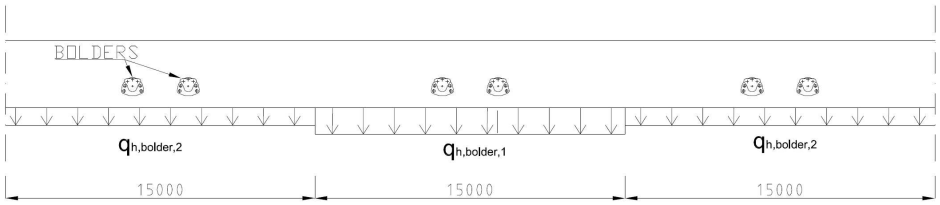

TOP VIEW QUAY WALL WITH BOLDER FORCES WITHOUT AND WITH SPREADING

$q_{h,bolder,1}$ = $(F_{h,bolder,100\%}+F_{h,bolder,70\%})/15$= 272 kN/m
$q_{h,bolder,2}$ = $(F_{h,bolder,70\%}+F_{h,bolder,70\%})/15$= 224 kN/m

Fender force

The fenders have a c.t.c distance of 15.00m. One fender is loaded for 100% (4600kN) and the others for 75% (3450kN).

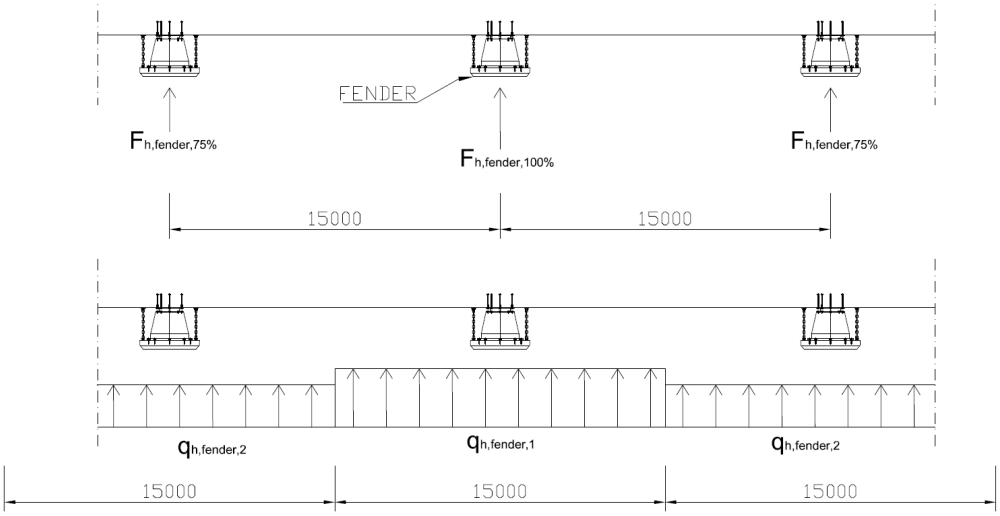

TOP VIEW QUAY WALL WITH FENDER FORCES WITHOUT AND WITH SPREADING

$q_{h,fender,1}$= $F_{h,fender,100\%}$ /15 = 307 kN/m
$q_{h,fender,2}$= $F_{h,fender,75\%}$ /15 = 230 kN/m

Ground pressure on relieving floor

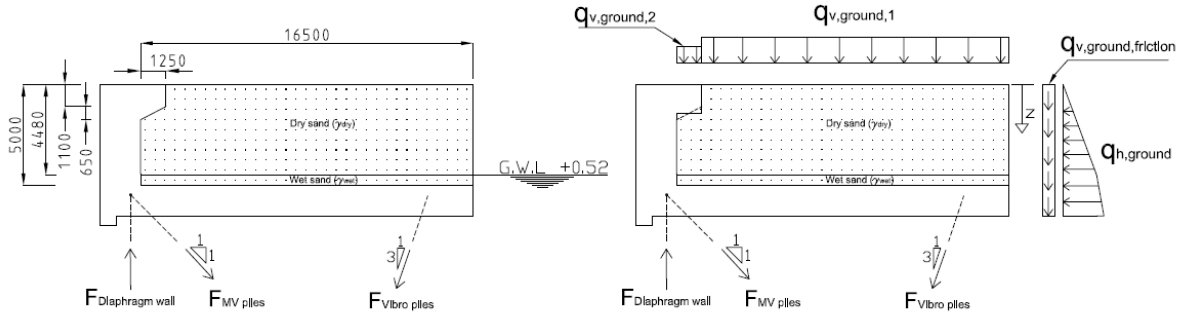

Own weight of sand above the relieving floor act like a vertical force on the floor and is given by:

$q_{v,ground,1}$ = $4.48*\gamma_{dry}+0.52*(\gamma_{wet} - 10)= 4.48*18+0.52*(20-10)= 86$ kN/m/m
$q_{v,ground,2}$ = $(4.48-0.65/2)*\gamma_{dry}+0.52*(\gamma_{wet} - 10)= 80$ kN/m/m

The horizontal effective earth pressure is not distributed linearly due to the presence of dry and saturated soil and is calculated as follows:

$q_{h,ground}$ = $\gamma_{dry}*z*k_a$ for z ≤ 4.48m
= $\gamma_{dry}*4.48*k_a+ (\gamma_{wet}-10)*(z-4.48)*k_a$ for z > 4.48m

where

k_a= active earth pressure coefficient according to Rankine = $k_a = \frac{1-\sin 32.5}{1+\sin 32.5} = 0.3$

The total effective earth pressure can be calculated as follows:
$p_{h,ground,total}$ = $0.5*\gamma_{dry}*4.48^2*k_a+\gamma_{dry}*4.48*k_a*(0.52+1.5) + 0.5*(\gamma_{wet}-10)*(0.52+1.5)^2*k_a= 109$ kN/m

A friction force will occur due to the presence of the relieving floor because the soil above the relieving floor can not move in contrast to the soil behind the relieving sturcture. This friction force is as follows:

$P_{v,ground,friction,total}$ = 109*tanΦ = 109*tan 32.5 = 70 kN/m

Where
φ=internal friction angle = 32,5° (for medium dense sand)

Surcharge load above relieving floor

The surcharge load above the relieving floor follows from the list of requirement mentioned in chapter 3 and is given as 40 kN/m/m.

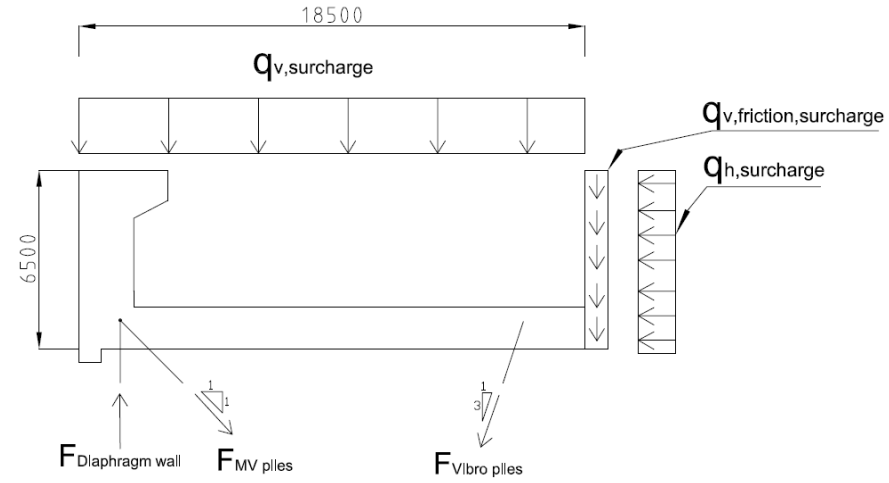

Surcharge load can be seen as an additional layer of soil on top of the exiting soil. It will cause an incremental vertical and horizontal force acting on the wall. These forces can be determined as follows:

$q_{v,surcharge}$ = 40 kN/m/m
$q_{h,surcharge}$ = k_a*$q_{v,surcharge}$ = 0,3*40= 12 kN/m/m
$F_{h,surcharge}$ = 6.5*12= 78 kN/m
$q_{v,friction,surcharge}$ = $F_{h,surcharge}$* tan φ/6.5= 78 tan 32.5/6.5 = 7.7 kN/m/m

where

k_a= active earth pressure coefficient according to Rankine = $k_a = \frac{1-\sin 32.5}{1+\sin 32.5} = 0.3$

φ=internal friction angle = 32,5° (for medium dense sand)

Member forces

The superstructure is modeled as statically determined. The two rows of pressure piles will be schematisized as one support. With hand calculations the stresses in the diaphragm wall, mv - pile and vibro pile are determined for each load case. In this way the normative load combination can be determined easily in a later stadium. First, each load case is shifted to a point above the diaphragm wall which will results in an additional moment force M. The wall and pile forces were determined making use of the moment, vertical and horizontal stress equilibrium.

The bearing stress of diaphragm wall can not be neglected. This stress depends on the total amount of normal stress acting on the MV-pile (load coming from relieving floor and diaphragm wall) and is equal to the horizontal component of the total normal stress of the MV-pille that also influence the forces acting on the diaphragm wall. Interation is neededde in determining the bearing stress of diaphragm wall. Therefore a unit load of 100kN/m will be used.

The relieving floor is supported eccentric to the diaphragm wall (e=0,36m), therefore an additional moment forces is present at the diaphragm given as M_{dw}=F_{dw}*e.

All results are shown in table 2. Notion must be made that the calculated forces are only due to the forces acting on the relieving structure.

Loads	Fv kN/m	Fh kN/m	M kNm/m	Fdw kN/m	Fmv kN/m	Fvp kN/m	Mdw kNm/m
Own weight relieving platform	992	0	5287	-514	-169	-378	-185
Crane load in operation	1860	48	1598	-1764	17	-114	-635
Crane load during storm	1300	184	295	-1457	251	-21	-525
Bolder force	0	272	-1485	-406	432	106	-146
Fender force	0	-307	651	366	-455	-47	132
Groundwater +0,52 NAP	-172	20	-1495	17	76	107	6
Ground pressure +0,52 NAP	1363	103	12523	-334	-254	-895	-120
Seawater -1,38 NAP	-6	0	6	7	0	0	2
Surcharge load above platform	782	73	6292	-286	-98	-450	-103
Bearing stress diaphragm wall*	0	100	0	-100	141	0	-36

*wall and pile forces due to unit bearing stresses diaphragm wall per 100kN/m

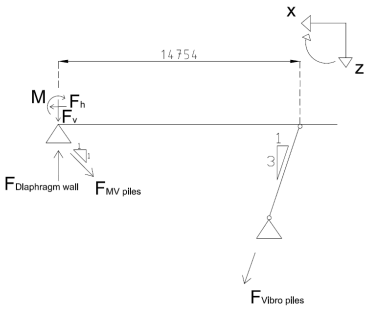

Table F-2 Static forces in structure per load

F2 Seismic forces on relieving structure

For the purpose of the pseudo static analysis, the seismic action is represented by a set of horizontal and vertical static forces equal to the product of the gravity forces and a seismic coefficient. For an earthquake with peak ground acceleration of 0,5 m/s^2 the horizontal and vertical seismic coefficients are k_h=0,067 and k_v=0,022 (section 8.3.1). The most unfavorable direction combination is when the horizontal acceleration (a_h) is directed towards the backfill and the vertical acceleration (a_v) is directed downward and is used in determining the seismic forces on the relieving structure.

By multiplying the gravity force with (1-k_v) for each separate load the dynamic vertical force can be found for that particular loading. For horizontal components, this is (1+k_h). For horizontal earth

pressures, the static earth pressure coefficients (k_a) needs to be replaced by the seismic earth pressure coefficient (k_{ae}).

Member forces can be determined just like the static approach knowing the horizontal and vertical force component for each loading and are listed in Table F-3.

During earthquake

Load combination 2	Fv kN/m	Fh kN/m	M kNm/m	Ndw kN/m	Nmv kN/m	Nvp kN/m	Mdw kNm/m
Own weight relieving platform	969	67	5121	-573	-69	-366	-206
Crane load in operation	1818	51	1538	-1730	23	-110	-623
Crane load during storm	1271	196	198	-1449	271	-14	-522
Bolder force	0	290	1585	-147	359	113	-53
Fender force	0	-286	607	341	-424	-43	123
Groundwater +0,52 NAP	-174	22	-1512	15	79	108	6
Ground pressure +0,52 NAP	1351	134	12527	-353	-211	-895	-127
Seawater -1,38 NAP	-6	0	6	7	0	0	2
Surcharge load above platform	777	93	6314	-299	-70	-451	-108
Bearing stress diaphragm wall*	0	100	0	-100	141	0	-36

*wall and pile forces due to unit bearing stresses diaphragm wall per 100kN/m

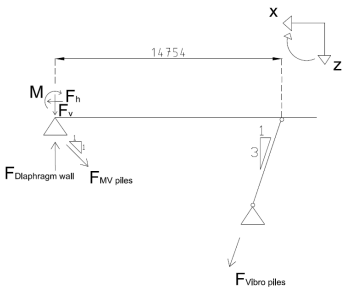

Table F-3 seismic forces in structure per load

Appendix G Static analysis of diaphragm wall with Msheet

G1 Choice of model

Basically two options are available in Msheet: K_a, K_0, K_p model and the C, phi, delta (or Cullmann) model. The former uses a constant earth pressure coefficient per soil layer while the latter allows for a variation over depth within a soil layer. Besides, for modeling non-horizontal surfaces and non-uniform surcharge load, only the Culmann method is valid. For that reason this method is used.

G2 Schematization of the geometry

The geometry of the Msheet model is based on design drawing of the Euromax quay wall (Figure 2-2) and the soundings at quay wall section 1(Figure 7-4). Ground level is founded at NAP+5m and the bed level is NAP-22m. The diaphragm wall reaches a depth of NAP-33m with a thickness of 1,2m. A spring support was placed at NAP-1,5m to simulate the anchor force of the MV-pile. Also a moment load was placed at NAP-1,5m due to the eccentricity between the relieving floor and diaphragm wall. By doing so, the forces coming from the relieving floor are added to the diaphragm wall whereby the relieving floor and it loads can be left out in the geometry. The outside water level is kept at NAP-1,38m while the ground water level is set at NAP+0,52m. These are the normative water levels as mentioned in appendix F. Schematisation of the Msheet geometry is illustrated in Figure G-1.

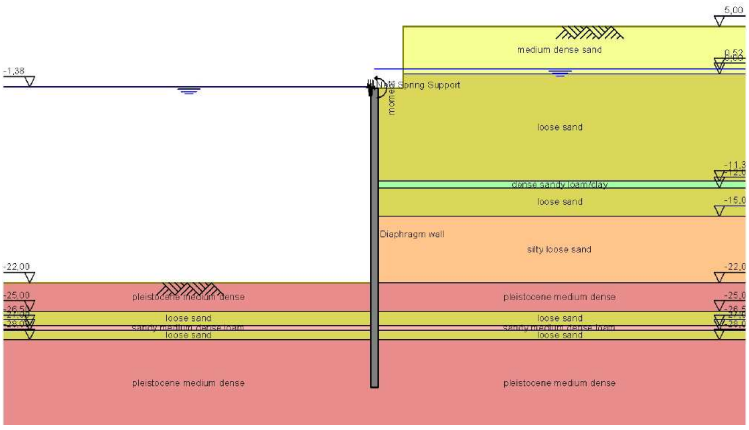

Figure G-1 schematized geometry in Msheet

G3 Soil profile and parameters

The normative soil profile to liquefaction will be used. This soil profile is determined in section 7.3 and is located at the eastern side of the Euromax terminal. Soil parameters for this particular profile are determined by BAM and were used during this analysis [G.1]. The parameters are shown in Table G-1.

G4 Material properties

The flexural rigidity of the diaphragm wall plays an important role in distributing the loads. Delta marine consultants has done a specific analysis in determining the flexural rigidity of the wall by using the method that was described in the VBC based on quasi-linear elasticity theorem [G.2]. By applying MN-Kappa diagrams a more accurate flexural rigidity was found, which is $EI_{diaphragm\ wall} = 1{,}88*10^6\ kNm^2$ [G.3].

The axial spring stiffness was determined using a framework calculation for a cross-section of the quay wall in which horizontal and vertical unit loads were applied. This calculation was also done by Delta marine consultants which results in axial spring stiffness of 27000 kN/m/m [G.3].

Both the flexural rigidity and axial spring stiffness determined by BAM was used during this analysis.

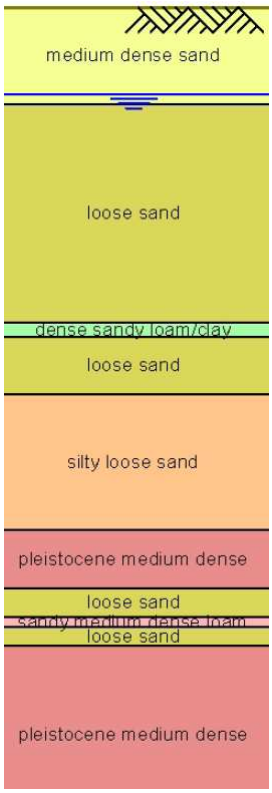

	Level NAP+5,0m	$\gamma_{unsat}/\gamma_{sat}$ [kN/m^3]	φ [deg.]	c [kN/m^2]	δ [deg.]	Modulus of subgrade reaction - tangent K_{h0} [kN/m^3]	K_{h1} [kN/m^3]	K_{h2} [kN/m^3]	K_{h3} [kN/m^3]
Medium dense sand	NAP-0,0m	18 / 20	32,5	0	21,67	32500	32500	8864	2708
Loose sand	NAP-11,3m	17 / 19	30	0	20	19500	19500	5318	1625
dense sandy loam/clay	NAP-12,0m	19,5 / 19,5	28	0	18,6	11000	11000	3634	1042
Loose sand	NAP-15,0m	17 / 19	30	0	20	19500	19500	5318	1625
Silty loose sand	NAP-22,0m	19 / 19	29	0	19,3	12000	12000	3273	1000
Pleistocenen m/d sand	NAP-25,0m	19 / 20	35	0	23,5	32500	32500	8864	2708
Loose sand	NAP-26,5m	17 / 19	30	0	20	19500	19500	5318	1625
Sandy m/d loam	NAP-27,0m	20 / 20	27,5	2	18,3	9750	9750	4179	1083
Loose sand	NAP-28,0m	17 / 19	30	0	20	19500	19500	5318	1625
Pleistocenen m/d sand		19 / 20	35	0	23,5	32500	32500	8864	2708

Table G-1 Soil profile and input parameters for Msheet

G5 Results static analysis Msheet

Three load combinations were analysed as mentioned in section 8.2.1. First the forces acting on the relieving floor will be determined. From this, the normal forces on the piles and wall can be known by making use of Table F-2. The diaphragm wall and relieving floor is not supported eccentricly which result in an eccentric moment on top of the diaphragm wall. By applying the eccentric moment and the loads into the Msheet model, the horizontal spring force can be determined which is equal to the horizontal component of the normal stress of the MV-pile. Notion must be made that the normal pile and wall stresses were determined based on bearing stresses per 100 kN/m. This bearing stress needs to be equal to the spring force. Therefore interation needs to be performed in finding the right bearing stress which corresponds to the horizontal spring force calculated using Msheet. The results are shown in this section.

Load combination 1

							new values			
Load combination 1	**F_{DW}* kN/m**	**F_{MV}* kN/m**	**F_{VP}* kN/m**	**M_{MV}* kNm/m**	**Combi factor**	**Load factor**	**F_{DW} kN/m**	**F_{MV} kN/m**	**F_{VP} kN/m**	**M_{MV} kNm/m**
Own weight relieving platform	-514	-169	-378	-185	1	1	-514	-169	-378	-185
Crane load in operation	-1764	17	-114	-635			0	0	0	0
Crane load during storm	-1457	251	-21	-525			0	0	0	0
Bolder force	-406	432	106	-146			0	0	0	0
Fender force	366	-455	-46	132			0	0	0	0
Groundwater +0,52 NAP	17	76	107	6	1	1	17	76	107	6
Groun pressure +0,52 NAP	-334	-254	-895	-120	1	1	-334	-254	-895	-120
Seawater -1,38 NAP	7	0	0	2	1	1	7	0	0	2
Surcharge load above platform	-286	-98	-450	-103			0	0	0	0
Surcharge load behind platform	0	0	0	0			0	0	0	0
Surcharge load behind landside crane	0	0	0	0			0	0	0	0
Bearing stress diaphragm wall	-100	141	0	-36		4,8	-480	679	0	-173
*Forces due to unit bearing stresses diaphragm wall per 100kN/m					Total		-1305	331	-1166	-470

Table G-2 wall and pile stresses for load combination 1

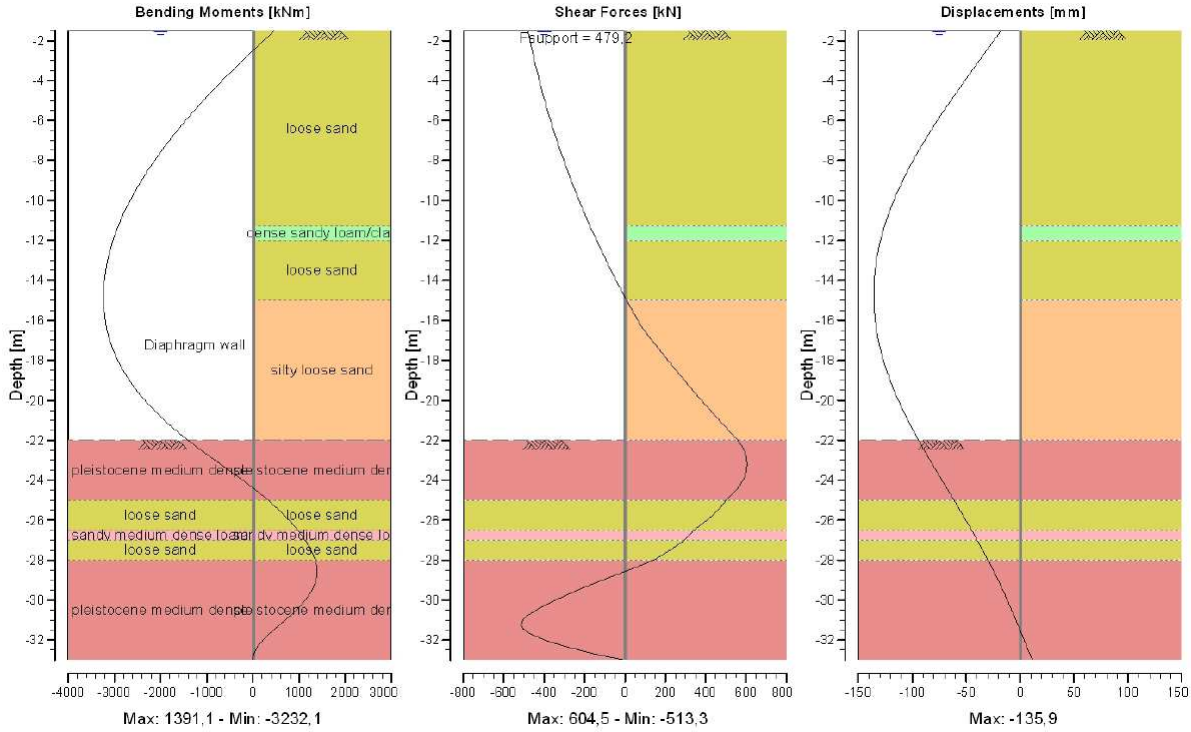

Figure G-2 Msheet results for load combination 1: Bending moment/Shear force/ Displacement ofdiaphragm wall

After a couple of iteration a matching bearing force of 480kN/m was found. Stresses whitin the diaphragm wall due to this bearing force can be found at Table G-2 and Figure G-2 . The most important stresses are listed below:

Maximum normal force	= F_{DW}	= -1305 kN/m
Maximum bending moment	= M_{Msheet}	= -3232 kNm/m

Arching effects

Msheet does not account arching effects during the calculations. For an anchored quay wall, the Msheet approach will lead to incorrect ground pressures. The effects of arching are:

- Decrease of active ground pressure near the maximum deflection of the wall
- Increase of ground pressure near the anchor

According to CUR166 [G.4] a decrease of 33% of the maximum bending moment caused by the ground pressure and an increase of 15% to the spring forces ($F_{support,ground}$) should be applied to include the arching effect. Stresses caused by the ground pressure can be obtained by using equal waterlevels in front and behind the quay wall. By doing so the water pressures will be neutralized and only the stresses due to ground pressures are left. Result of the Msheet calculation with equal water level are shown in Figure G-3.

The moment reduction, M_{arch}, and the spring force addition, F_{arch}, due to arching effects becomes:

$$M_{arch} = M_{Msheet,ground} * 0{,}33 = 1799{,}9 * 0{,}33 = 594 kNm/m$$

$$F_{arch} = F_{\sup port,ground} * 0{,}15 = 244{,}8 * 0{,}15 = 37 kN/m$$

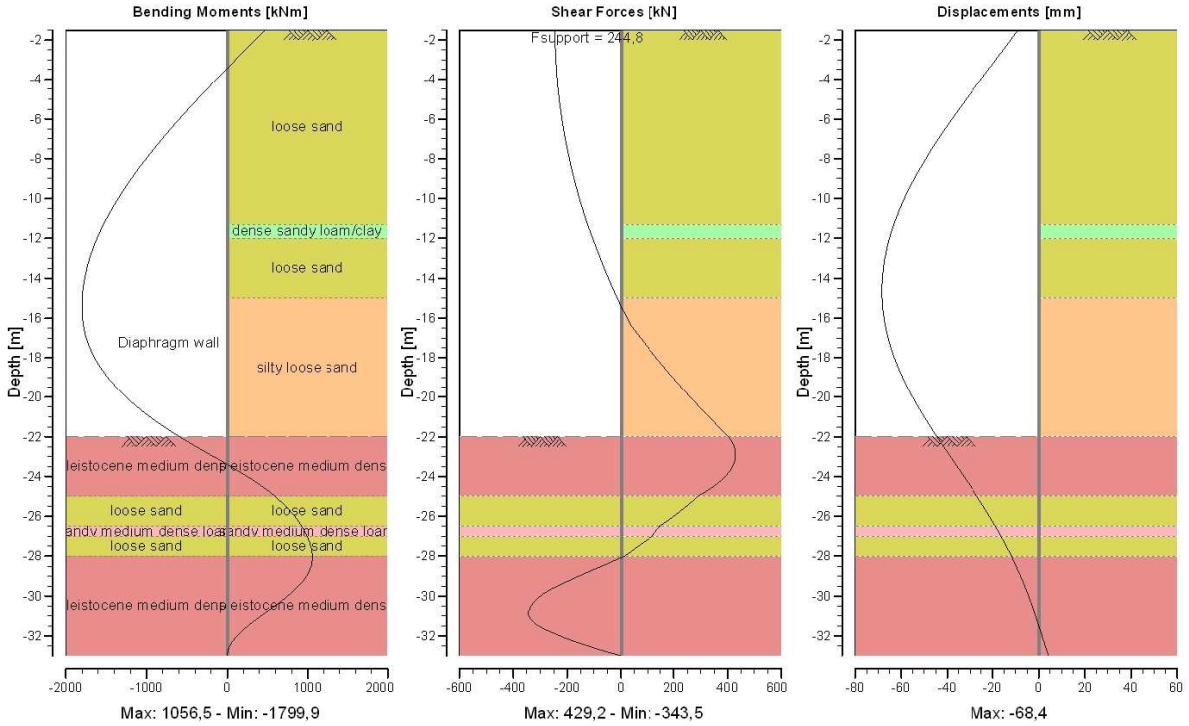

Figure G-3 Msheet results for load combination 1: Bending moment/Shear force/ Displacement ofdiaphragm wall with equal water levels on both side of the quay wall

Second order effect

Another effect Msheet does not account for is the second order effect. As a result of vertical force (F_{DW}) acting on top of the diaphragm wall, second order effect occurs. This will lead to an incremental bending moment, M_{2nd}. This incremental bending moment can be calculated by multiplying the F_{DW} with the eccentricity, e, and the enlargement factor, n/(n-1). The eccentricity, e, is the maximum displacement of the diaphragm wall (δ_{max}) minus the mean displacement between NAP-1,5m (δ_{kop}) and NAP-33m (δ_{ppn}) as shown in Figure G-4. The enlargement factor is calculated by determing the Euler buckling factor, n. Where n is the Euler buckling force, F_{eul} devided by F_{DW}.

$$F_{eul} = \pi^2 EI / l_{eul}^2 = \pi^2 * 1{,}868 * 10^6 / 22^2 = 38100kN$$

$$n = F_{eul} / F_{DW} = 38100 / 1305 = 29$$

$$M_{2nd} = F_{DW} \cdot e \cdot \frac{n}{n-1} = 1305 * 0{,}13 * \frac{29}{29-1} = 176kNm/m$$

Where
F_{DW} = Normal force diaphragm wall = 1305 kN
EI = $EI_{diaphragm\ wall}$ = $1{,}868*10^6$ kN/m^2
L_{eul} = buckling length assumed 22 m
e = 0,13m

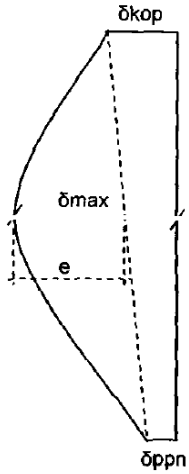

Figure G-4 illustration of eccentricity and displacement of wall

The maximum moment of the diaphragm wall including arching and second order effect for load combination 1 is:

$$M_{\max} = M_{Msheet} - M_{arch} + M_{2nd} = 3232 - 594 + 176 = 2814kNm/m$$

The maximum axial force of the MV-pile include arcing for load combination 1 is:

$$F_{MV,\max} = F_{MV} + F_{arch} = 331 + 37 = 368kN/m$$

Load combination 2

Load combination 2	Fh kN/m	M kNm/m	F_{DW}* kN/m	F_{MV}* kN/m	F_{VP}* kN/m	M_{MV}* kNm/m	Combi factor	Load factor	new values F_{DW} kN/m	new values F_{MV} kN/m	new values F_{VP} kN/m	new values M_{MV} kNm/m
Own weight relieving platform	0	5287	-514	-169	-378	-185	1	1	-514	-169	-378	-185
Crane load in operation	48	1598	-1764	17	-114	-635	0,7	1	-1235	12	-80	-444
Crane load during storm	184	295	-1457	251	-21	-525			0	0	0	0
Bolder force	272	-1485	-406	432	106	-146	0,7	1	-284	302	74	-102
Fender force	-307	651	366	-455	-46	132			0	0	0	0
Groundwater +0,52 NAP	20	-1495	17	76	107	6	1	1	17	76	107	6
Groun pressure +0,52 NAP	103	12523	-334	-254	-895	-120	1	1	-334	-254	-895	-120
Seawater -1,38 NAP	0	6	7	0	0	2	1	1	7	0	0	2
Surcharge load above platform	73	6292	-286	-98	-450	-103	0,7	1	-200	-68	-315	-72
Surcharge load behind platform	0	0	0	0	0	0	0,7	1	0	0	0	0
Surcharge load behind landside crane	0	0	0	0	0	0	0,7	1	0	0	0	0
Bearing stress diaphragm wall	100	0	-100	141	0	-36		5,8	-580	820	0	-209
*Forces due to unit bearing stresses diaphragm wall per 100kN/m							Total		-3124	719	-1486	-1125

Table G-3 wall and pile stresses for load combination 2

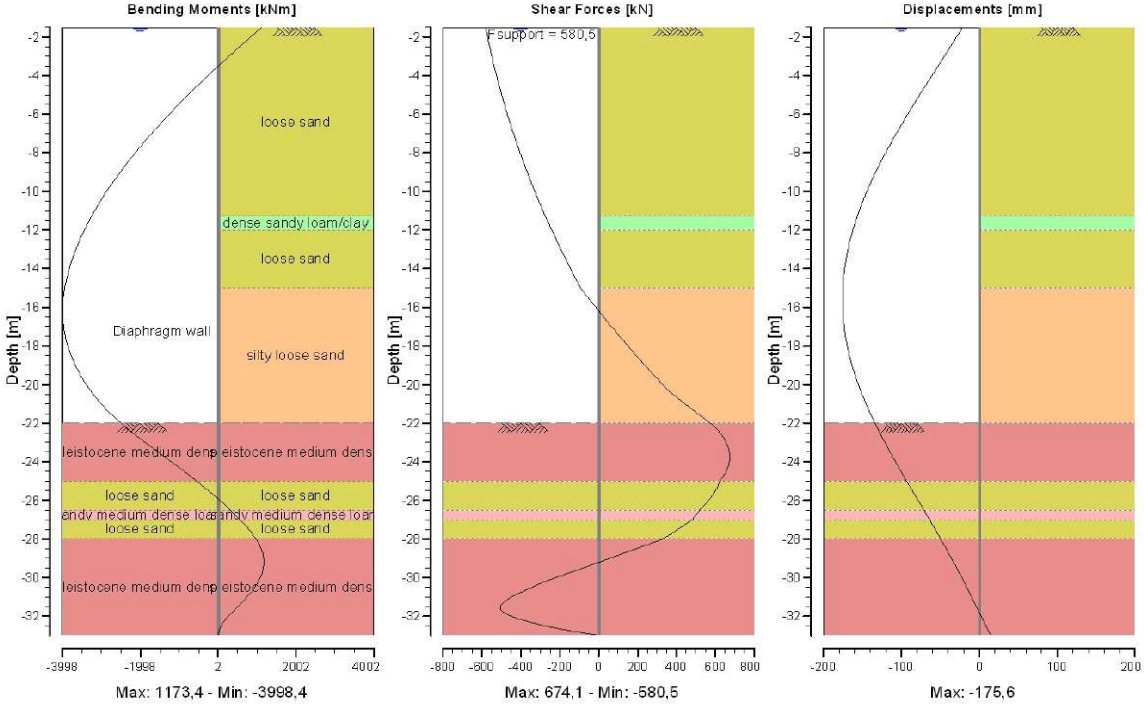

Figure G-5 Msheet results for load combination 2: Bending moment/Shear force/ Displacement ofdiaphragm wall

After a couple of iteration a matching bearing force of 480kN/m was found. Stresses whitin the diaphragm wall due to this bearing force can be found at Table G-3 and Figure G-5. The most important stresses are listed below:

Maximum normal force = F_{DW} = -3124 kN/m
Maximum bending moment = M_{Msheet} = 3998 kNm/m

Arching and second order effects are determined the same way like load combination 1. Result of the Msheet calculation with equal water level for load combination 2 are shown in Figure G-6. Calculations and results of arching and second order effect are as follows:

$$M_{arch} = M_{Msheet} * 0{,}33 = 2385{,}8 * 0{,}33 = 795 kNm/m$$

$$F_{arch} = F_{\sup port,ground} * 0{,}15 = 330{,}7 * 0{,}15 = 50 kN/m$$

$$F_{eul} = \pi^2 EI / l_{eul}^2 = \pi^2 * 1{,}868 * 10^6 / 22^2 = 38100 kN$$

$$n = F_{eul} / F_{DW} = 38100 / 3124 = 12{,}2$$

$$M_{2nd} = F_{DW} \cdot e \cdot \frac{n}{n-1} = 3124 * 0{,}171 * \frac{12{,}2}{12{,}2-1} = 582 kNm/m$$

Where
F_{DW} = Normal force diaphragm wall = 3124 kN
EI = $EI_{diaphragm\ wall}$ = 1,868*10^6 kN/m^2
L_{eul} = buckling length assumed 22 m
e = 0,171m

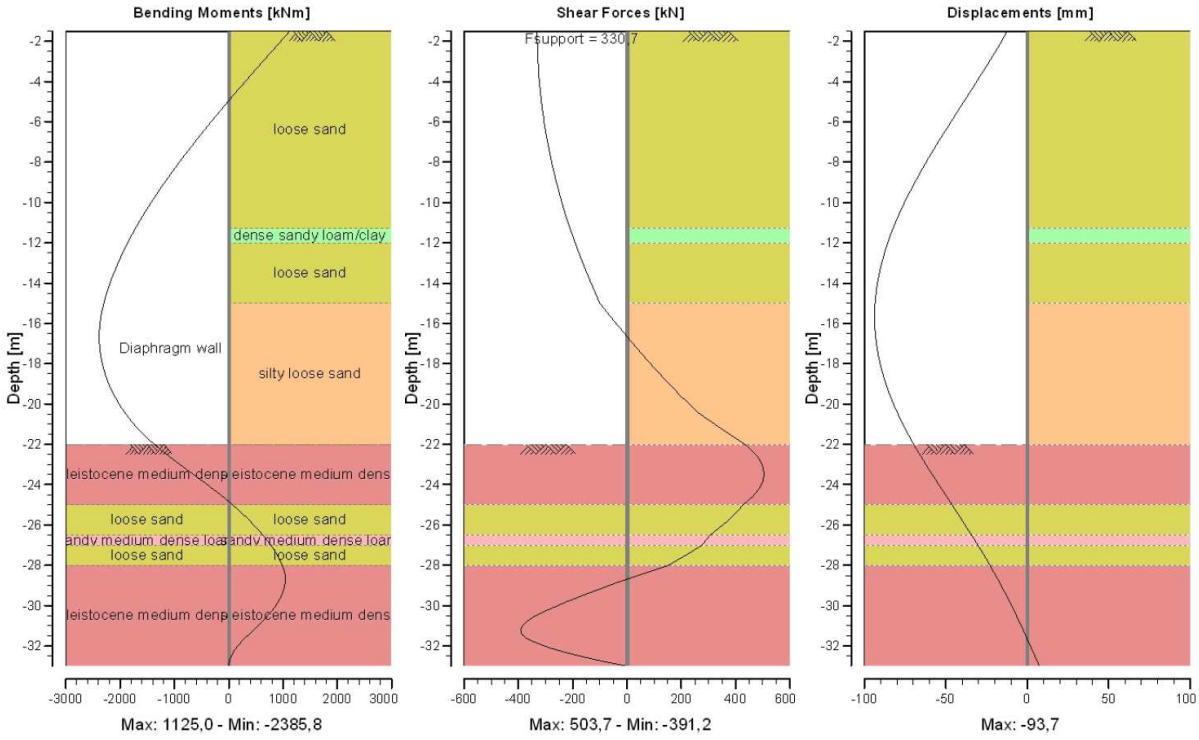

Figure G-6 Msheet results for load combination 2: Bending moment/Shear force/ Displacement ofdiaphragm wall with equal water levels on both side of the quay wall

The maximum moment including arching and second order effect for load combination 2 is:

$$M_{\max} = M_{Msheet} - M_{arch} + M_{2nd} = 3998 - 795 + 582 = 3785 kNm/m$$

The maximum axial force of the MV-pile include arcing for load combination 2 is:

$$F_{MV,\max} = F_{MV} + F_{arch} = 719 + 50 = 769 kN/m$$

Load combination 3
After a couple of iteration a matching bearing force of 480kN/m was found. Stresses whitin the diaphragm wall due to this bearing force can be found at Table G-4 and Figure G-7. The most important stresses are listed below:

Maximum normal force = F_{DW} = -2576 kN/m
Maximum bending moment = M_{Msheet} = 4084 kNm/m

Load combination 3	F_{DW}* kN/m	F_{MV}* kN/m	F_{VP}* kN/m	M_{MV}* kNm/m	Combi factor	Load factor	new values F_{DW} kN/m	F_{MV} kN/m	F_{VP} kN/m	M_{MV} kNm/m
Own weight relieving platform	-514	-169	-378	-185	1	1	-514	-169	-378	-185
Crane load in operation	-1764	17	-114	-635	0,7	1	-1235	12	-80	-444
Crane load during storm	-1457	251	-21	-525			0	0	0	0
Bolder force	-406	432	106	-146			0	0	0	0
Fender force	366	-455	-46	132	0,7	1	256	-318	-33	92
Groundwater +0,52 NAP	17	76	107	6	1	1	17	76	107	6
Groun pressure +0,52 NAP	-334	-254	-895	-120	1	1	-334	-254	-895	-120
Seawater -1,38 NAP	7	0	0	2	1	1	7	0	0	2
Surcharge load above platform	-286	-98	-450	-103	0,7	1	-200	-68	-315	-72
Surcharge load behind platform	0	0	0	0	0,7	1	0	0	0	0
Surcharge load behind landside crane	0	0	0	0	0,7	1	0	0	0	0
Bearing stress diaphragm wall	-100	141	0	-36		5,72	-572	809	0	-206
*Forces due to unit bearing stresses diaphragm wall per 100kN/m					Total		-2576	86	-1593	-927

Table G-4 wall and pile stresses for load combination 3

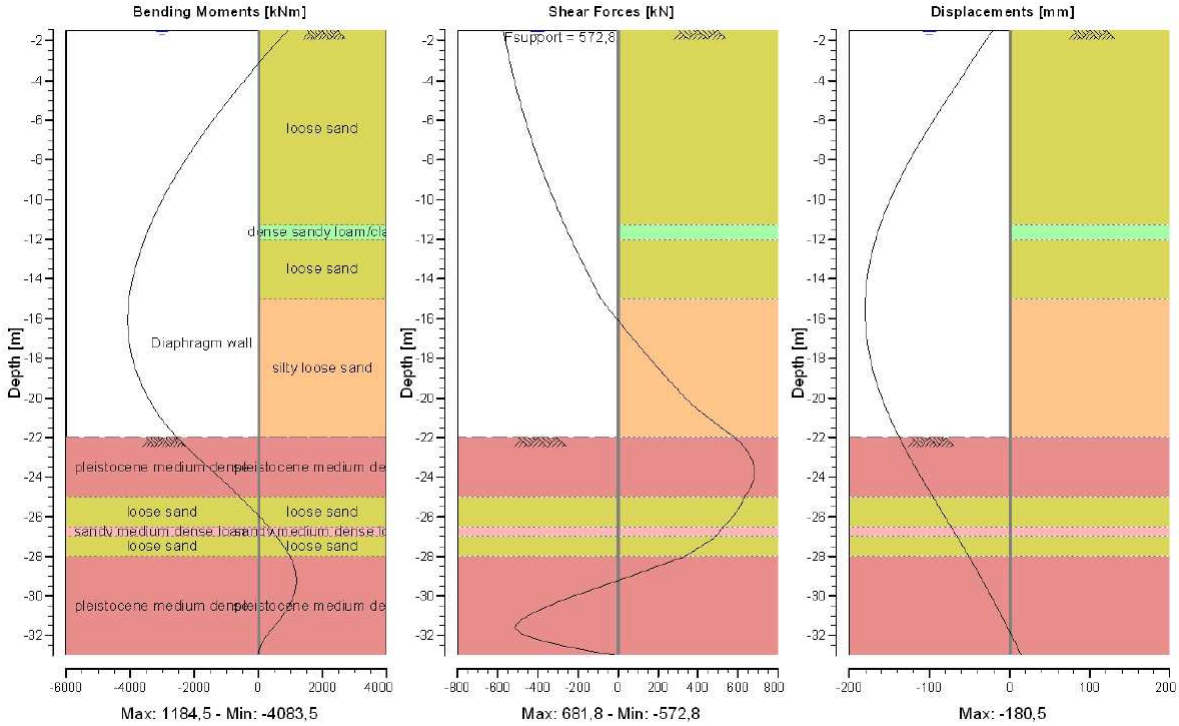

Figure G-7 Msheet results for load combination 3: Bending moment/Shear force/ Displacement ofdiaphragm wall

Arching and second order effects are determined the same way like load combination 1. Result of the Msheet calculation with equal water level for load combination 3 are shown in Figure G-8. Calculations and results of arching and second order effect are as follows:

$$M_{arch} = M_{Msheet,ground} * 0{,}33 = 2454{,}3 * 0{,}33 = 810 kNm/m$$

$$F_{arch} = F_{\sup port,ground} * 0{,}15 = 322{,}1 * 0{,}15 = 48 kN/m$$

$$F_{eul} = \pi^2 EI / l_{eul}^2 = \pi^2 * 1{,}868 * 10^6 / 22^2 = 38100 kN$$

$$n = F_{eul} / F_{DW} = 38100 / 2576 = 14{,}8$$

$$M_{2nd} = F_{DW} \cdot e \cdot \frac{n}{n-1} = 2576 * 0{,}176 * \frac{14{,}8}{14{,}8-1} = 486 kNm/m$$

Where
F_{DW} = Normal force diaphragm wall = 2576 kN
EI = $EI_{diaphragm\ wall}$ = 1,868*10^6 kN/m^2
L_{eul} = buckling length assumed 22 m
e = 0,176m

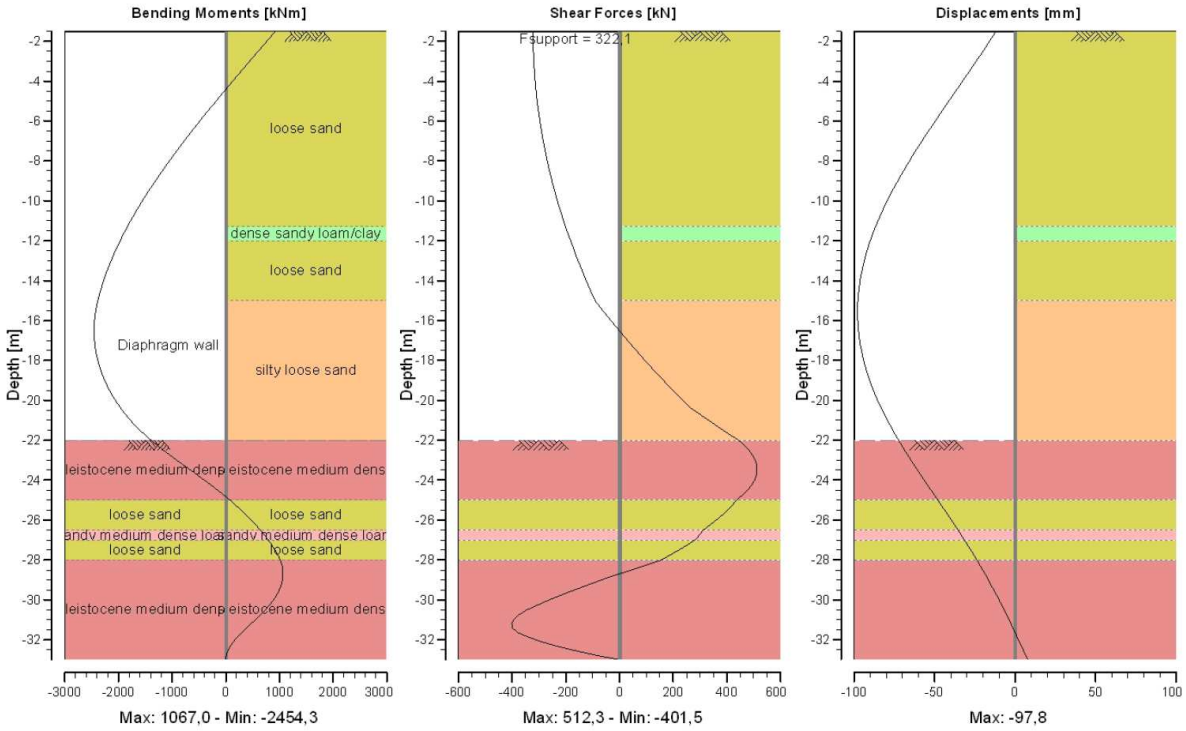

Figure G-8 Msheet results for load combination 3: Bending moment/Shear force/ Displacement ofdiaphragm wall with equal water levels on both side of the quay wall

The maximum moment including arching and second order effect for load combination 3 is:

$$M_{\max} = M_{Msheet} - M_{arch} + M_{2nd} = 4084 - 810 + 486 = 3760 kNm/m$$

The maximum axial force of the MV-pile include arcing for load combination 3 is:

$$F_{MV,\max} = F_{MV} + F_{arch} = 86 + 48 = 134 kN/m$$

An overview of the Msheet results are shown in Table G-5 and Table G-6.

Msheet Stresses	Max. Bending moment diaphragm wall kNm/m	Normal force Diaphragm wall kN/m	Normal force MV-Pile kN/m	Normal force Vibro pile (in total) kN/m
Load combination 1	3232	-1305	331	-1166
Load combination 2	3998	-3124	719	-1486
Load combination 3	4084	-2576	86	-1593

Table G-5 Wall and pile stresses for different load combinations according to Msheet

Msheet Stresses	Max. Bending moment diaphragm wall kNm/m	Normal force Diaphragm wall kN/m	Normal force MV-Pile kN/m	Normal force Vibro pile (in total) kN/m
Load combination 1	2814	-1305	368	-1166
Load combination 2	3785	-3124	769	-1486
Load combination 3	3760	-2576	134	-1593

Table G-6 Wall and pile stresses for different load combinations according to Msheet with arching and second order effects included

G6 References

[G.1] Delta marine consultants, kadeconstructie Euromax – ontwerp, report O-R-013 rev B, 06-2005
[G.2] NEN 6720, Voorschriften beton constructieve eisen en rekenmethoden (VBC), 1995
[G.3] Delta marine consultants, Berekening kadeconstructie aanbieding 2, 022518-rap-u-0008 rev B 03-2005
[G.4] CUR 166, Damwandconstructies, 4e druk, 2005

Appendix H Static analysis Diaphragm wall with Plaxis

H1 Static model Plaxis

H.1.1 Schematization of the geometry

The geometry of the Plaxis model is based on design drawing of the Euromax quay wall (Figure 2-2) and the soundings at quay wall section 1(Figure 7-4). Ground level is founded at NAP+5m and the bed level is located at NAP-22m. Water levels vary during each construction phase of the quay wall. After the construction is finished the outside water level is kept at NAP-1,38m while the ground water level is set at NAP+0,52m. These are the normative water levels as mentioned in appendix F. The elements which where used in the Plaxis model are:

- Relieving platform: is drawn as a cluster with connected geometry lines. The material is modelled like a linear elastic non-porous soil with the stiffness and the properties of concrete. The interaction between relieving platform and the soil layers is modelled with interface elements.
- Diaphragm wall: it reaches a depth of NAP-33m and is modelled as a plate. The interaction between the soil layers is modelled with interface elements. The weight of the wall is the actual weight minus the weight of the soil, due the fact that Plaxis superimposes a plate over the soil layer. A strut is placed on their footing to induce the footing stiffness of the structure.
- Virtual beam: in order to model the support between the relieving platform and the diaphragm wall with a hinge, an additional virtual beam in the form of a plate is required. To minimize the influence of the virtual beam in the model, a low flexural and axial stiffness and a small width was assumed.
- MV piles: are tension piles that induce the axial force with friction. No contribution of friction resistance occurs within the sliding soil wedge due to the movement of the soil wedge. Through this, the MV pile can be modelled using two elements; node to node anchor (above failure surface) and plate with interface elements (below failure surface).
- Vibro piles: they are modeled with node to node anchors with a strut on the footing.
- Landside beam: is drawn as a cluster with connected geomety lines. The material is moedelled like a linear elastic non-porous soil with the properties of concrete. Again interface elemetns are used.

Schematisation of the Plaxis geometry is illustrated in Figure H-1.

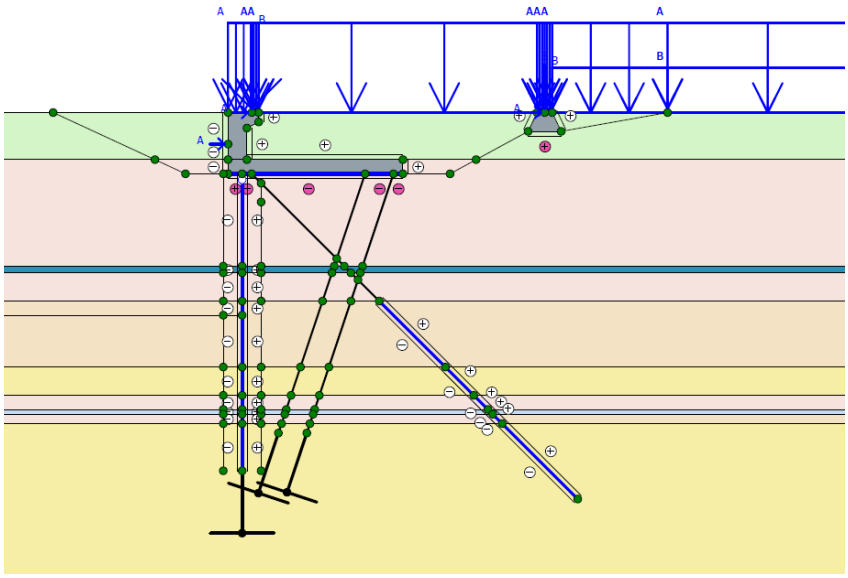

Figure H-1 Schematization of the Plaxis geometry

H.1.2 Boundary conditions

The vertical boundaries are taken at about 4 times the retaining height resulting in 100 meter seaward and 100 meter land inward. These boundaries are far enough not to affect the area of interest between diaphragm wall, tension and bearing piles. The vertical edges have fixed displacements in horizontal direction and are closed, to allow excess pore pressure to be present. The boundary at the base of the geometry is located in the Pleistocene sand layer at NAP-70m and is set at full fixity, since settlements may be assumed to be very small here. Special boundary conditions have to be defined to account for the fact that in reality the soil is a semi-infinite medium. Without these special boundary conditions the waves would be reflected on the model boundaries, causing perturbations. To avoid these spurious reflections, absorbent boundaries are specified at the vertical boundaries. The above described boundary conditions are known in Plaxis as “standard earthquake boundaries”.

H.1.3 Choice of the material model

Many material models are available in Plaxis. But only three material models are suited for this analysis based on soil strata of the Euromax terminal. For a fist estimation and fast calculation, Mohr Coulomb model could be used. This model does not implement stress dependency of the stiffness. It uses a linear constitutive relation for elastic (reversible) strains and a fixed yield surface for plastic (irreversible) strains.

However, stresses will change when applying load on the soil. The development of the reaction of the soil, the stiffness, is highly dependent on theses stresses. Thus, for analyzing the influence of large loading conditions, a model should be chosen that accounts for the stress dependency of the stiffness. This soil model is referred to as the Hardening Soil model (HS model). This model uses two types of hardening for plastic straining; compression hardening and deviatoric hardening. In the HS model the relation between stress and strain is assumed to be linear for unloading and reloading. It has proven that this model can be applied for either soft soils or stiff soils.

At small strains, soil seems to react much stiffer than at larger strains. The Hardening Soil model with small-strain stiffness (HSsmall model), is an extension of the HS model in which this higher stiffness for smaller strains is accounted for. In contrast to the HS model, in the HSsmall model hysteretic behaviour of soil at loading and unloading can be modeled. Due to a higher initial stiffness, smaller settlements at ground level are often calculated when applying the HSsmall model. A limitation of the HSsmall material model, like every other model in Plaxis, is that gradual softening of the soil during cyclic loading is not incorporated. In fact, just as in the HS model, softening due to soil dilatancy and debonding effects are not taken into account. Moreover, the HSsmall model does not incorporate the accumulation of irreversible volumetric straining nor liquefaction behaviour with cyclic loading. Knowing the limitations of the Hssmall model, this model is still preffered and will be used.

H.1.4 Soil parameters

Soil parameters determined by Delta Marine Consultants were used for this analysis with Plaxis [H.1]. These parameters were determined based on soundings and traxial tests of soil samples. The parameters needed for the Hssmall model are given in Table H-1. Notice that the average clayey soils located between NAP-11,3m and NAP-12m contains a lot sand particles and are expected to have some sandy properties, low cohesion and a higher unit weight compaired to clayey soils. This also accounts for the layers between NAP-16,5m and NAP-17m. Hence, drained calculation is performed for this static analysis.

Soil properties

Level	name	Material model	Material type	γ_{unsat} / γ_{sat} [kN/m^3]	φ [deg.]	ν [-]	c [kN/m^2]	ψ [deg.]	k_x [m/day]	k_y [m/day]	E_{ref} [kN/m^2]	E_{50}^{ref} [kN/m^2]	E_{oed}^{ref} [kN/m^2]	E_{ur}^{ref} [kN/m^2]	G_0^{ref} [kN/m^2]	$\gamma_{0,7}$ [-]	m [-]	R_{inter} [-]
	Relieving platform	Linear Elastic	Non-porous	25	-	0,15	-	-	-	-	1,30E+07	-	-	-	-	-	-	0,67
	Landside foundation	Linear Elastic	Non-porous	25	-	0,15	-	-	-	-	1,30E+07	-	-	-	-	-	-	0,67
NAP+5,0m																		
NAP-0,0m	Medium dense sand	HS small	Drained	18 / 20	32,5	-	0,1	3	8	8	-	3,00E+04	3,00E+04	1,50E+05	1,50E+05	2,00E-05	0,5	0,7
NAP-11,3m	Loose sand	HS small	Drained	17 / 19	30	-	0,1	2	8	8	-	1,80E+04	1,80E+04	9,00E+04	9,00E+04	3,80E-04	0,5	0,7
NAP-12,0m	dense sandy loam/clay	HS small	Drained	19,5 / 19,5	28	-	0,1	0	0,002	0,002	-	1,00E+04	5,00E+03	5,00E+04	5,00E+04	2,00E-05	0,5	0,6
NAP-15,0m	Loose sand	HS small	Drained	17 / 19	30	-	0,1	2	8	8	-	1,80E+04	1,80E+04	9,00E+04	9,00E+04	3,80E-04	0,5	0,7
NAP-22,0m	Silty loose sand	HS small	Drained	19 / 19	29	-	1	0	1	1	-	1,15E+04	1,15E+04	5,75E+04	1,75E+05	2,00E-05	0,5	0,7
NAP-25,0m	Pleistocenen m/d sand	HS small	Drained	19 / 20	35	-	0,1	3	20	20	-	3,50E+04	3,50E+04	1,75E+05	1,75E+05	2,00E-05	0,5	0,7
NAP-26,5m	Loose sand	HS small	Drained	17 / 19	30	-	0,1	2	8	8	-	1,80E+04	1,80E+04	9,00E+04	9,00E+04	3,80E-04	0,5	0,7
NAP-27,0m	Sandy m/d loam	HS small	Drained	20 / 20	27,5	-	0,1	0	0,002	0,002	-	1,00E+04	5,00E+03	5,00E+04	5,00E+04	2,00E-05	0,5	0,6
NAP-28,0m	Loose sand	HS small	Drained	17 / 19	30	-	0,1	2	8	8	-	1,80E+04	1,80E+04	9,00E+04	9,00E+04	3,80E-04	0,5	0,7
	Pleistocenen m/d sand	HS small	Drained	19 / 20	35	-	0,1	3	20	20	-	3,50E+04	3,50E+04	1,75E+05	1,75E+05	2,00E-05	0,5	0,7

Table H-1 Input soil properties for Plaxis

H.1.5 Material properties

In the geometry, seven different material datasets have been used. The diaphragm wall, virtual beam and lower part of the MV pile are modelled as plate while the upper part of the MV pile and vibro piles are modeled as node to node anchors. Struts have been placed on the footing of both the vibro piles and the diaphragm wall. These struts have the same axial rigidity as the diaphragm wall and vibro pile. To determine the flexural and axial rigidity of the MV pile on the lower part (modeled as plate), the EI and EA of the pile is devided by the center to center distance in order to equally spread out the flexural and axial rigidity over the plate. To minimize the influence of the virtual beam in the model, a low flexural and axial rigidity was assumed.

$$EI_{MV,low,plaxis} = \frac{EI_{MVpile}}{c.t.c} = \frac{2{,}10 \cdot 10^{8} * 1{,}353 \cdot 10^{-4}}{5{,}6} = 5073 kNm^2/m$$

$$EA_{MV,low,plaxis} = \frac{EA_{MVpile}}{c.t.c} = \frac{2{,}10 \cdot 10^{8} * 2{,}7 \cdot 10^{-2}}{5{,}6} = 1{,}01 \cdot 10^{6} kN/m/m$$

$$EA_{MV,up,plaxis} = EA_{MVpile} = 2{,}10 \cdot 10^{8} * 2{,}7 \cdot 10^{-2} = 5{,}67 \cdot 10^{6} kN/m/m$$

$$EI_{DW,plaxis} = EI_{DW} = 1{,}87 \cdot 10^{6} kNm^2/m$$

$$E_{DW} = \frac{EI_{DW}}{I_{DW}} = \frac{1{,}87 \cdot 10^{6}}{\frac{1}{12} * 1 * 1{,}2^{3}} = 1{,}30 \cdot 10^{7}$$

$$EA_{DW,plaxis} = EA_{DW} = 1{,}30 \cdot 10^{7} * 1{,}2 = 1{,}56 \cdot 10^{7} kN/m/m$$

$$EA_{VP,plaxis} = EA_{VP} = EA_{VP,steel} + EA_{VP,concrete}$$
$$= 2{,}1 \cdot 10^{8} * 1{,}61 \cdot 10^{-3} + 3{,}40 \cdot 10^{7} * 0{,}245 = 8{,}66 \cdot 10^{6} kN/m/m$$

Where

$EI_{MV,low,plaxis}$	:Flexural rigidity of the lower part of the MV pile modelled in Plaxis
$EA_{MV,low,plaxis}$	:Axial rigidity of the lower part of the MV pile modelled in Plaxis
$EA_{MV,up,plaxis}$	:Axial rigidity of the upper part of the MV pile modelled in Plaxis
EI_{DW}	:Flexual rigidity of diaphragm wall = $1{,}87*10^{6}$ kNm^2/m (see appendix G4)
I_{MVpile}	:Moment of inertia of MV pile with profile HE600B ≈ $1{,}353\ 10^{6}$ m^4
A_{MVpile}	:Surface area of MV pile with profile HE600B ≈ $2{,}7\ 10^{-2}$ m^2
$EA_{VP,steel}$	:Axial rigidity of vibro pile due to steel = $3{,}381\ 10^{5}$ kN/m [H.2]
$EA_{VP,Concrete}$	:Axial rigidity of vibro pile due to concrete = $8{,}32\ 10^{6}$ kN/m [H.2]

The wall and piles that are modeled as plates have zero thickness. The volume of materials of these elements that is present in reality is now replaced by soil. Through here, the input weight of these elements becomes less than the real weight of the elements. The input unit weight for Plaxis is the real unit weight of the element minus the unit weight of the soil. For the unit weight an average weigth over depth of 19 kN/m is used.

$$w_{input,plaxis} = w_{element} - w_{soil}$$

Poisson ratio for croncrete according to NEN6720 [H.3] should be between $\nu = 0{,}1$ and $\nu = 0{,}2$. For concrete elements a poisson ration of $\nu = 0{,}15$ is chosen. For steel elements poisson ratio is $\nu = 0{,}3$.

The material properties for the different material sets of the quay wall are shown in *Table H-2*.

Material properties

name	Material type	Normal stiffness [kN/m/m]	Flexural rigidity [kNm²/m]	weight [kN/m]	poisson's ratio [-]	Spacing out of plane [m]
		EA	EI	w	v	$L_{spacing}$
PLATES						
Diaphragm wall	Elastic	1,56E+07	1,87E+06	6	0,15	-
MV Piles	Elastic	1,01E+06	5,07E+03	0,2	0,3	-
Virtual beam	Elastic	1,00E+00	1,00E-04	0	0,15	-
NODE TO NODE ANCHORS						
Vibro piles	Elastic	8,66E+06	-	-	-	2,8
MV Piles	Elasitic	5,67E+06	-	-	-	5,6
ANCHORS/STRUTS						
Diaphragm wall	Elastic	1,56E+07	-	-	-	1
Vibro piles	Elastic	8,66E+06	-	-	-	2,8

Table H-2 Input material properties for Plaxis

H.1.6 Mesh generation

After completing the geometry and dataset, the mesh is generated. For the first approach, the global coarseness is set to “medium” since this is supposed to be sufficient for analyzing different influences and not to loose too much time for calculation. This means a global mesh of about 506 elements. In addition, around the diaphragm wall a cluster refinement is applied because here stress concentrations might be expected. Eventually this results in a mesh with 706 elements. There is chosen to use the 15 noded elements instead of the 6 noded elements because close to failure behaviour this element type give a 10% higher accuracy according to Watermann [H.4].

H.1.7 Soil-structure interaction

If a plate element is introduced in Plaxis, it is always fully permeable. Interface elements can be given in between soil and plate elements to make the plate impermeable and to simulate soil-structure behaviour , which is intermediate between smooth and fully rough. The roughness of the interaction is modeled by choosing a suitable value for the strength reduction factor in the interface, R_{inter}. This factor relates the interface strength (wall friction and adhesion) to the soil strength (friction angle and cohesion). Values for R_{inter} = 0,6 or 0,7 are used for clay-steel/concrete or sand-steel/concrete interfaces respectively. The application of interfaces is done for the diaphragm wall, lower part of the MV pile and the virtual beam. For the virtual beam R_{inter} = 0,1 is chosen because no attachment is present between the virtual beam and the soil below for the reason that the virtual beam is supported on piles.

H2 Static model calculation Plaxis

H.2.1 Construction method

The quay wall has been built in a certain way. To take the building sequence into account in Plaxis the option “staged construction” can be used. This option allows users to (de)activate weight, strength, stiffness and to change material properties or water pressures. The Diaphragm quay wall is created in nine phases. The function “update mesh” will not be used. This function allows the mesh to update after each phase calculation, which will lead to a more accurate second order effect. Since the deformations are very small which result in small second order effects this effect is negligible.

The nine different faces are presented to you in the figures on the next page. On the left figure you can see the the constructions elemements and material which are installed or will be installed. Elements which are not activated yet are not installed yet. On the right figure you can see the water level of the model during the construction.

Phase 0: initial phase

State of the soil before construction. Ground and water level located at NAP+5m and NAP+0,52m respectivily. Notion must be made that the quay wall elements are not activated and therefore they are not installed yet.

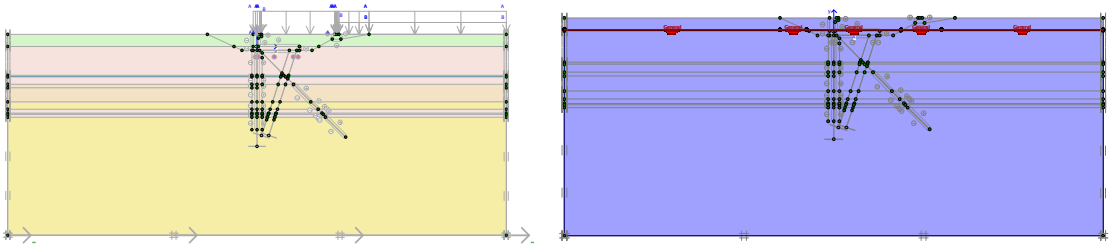

Phase 1: excavation

Preparation for installing the quay wall element by creating a building pit till NAP-1,5m. Drainage till NAP-2m is performed to keep the building pit dry.

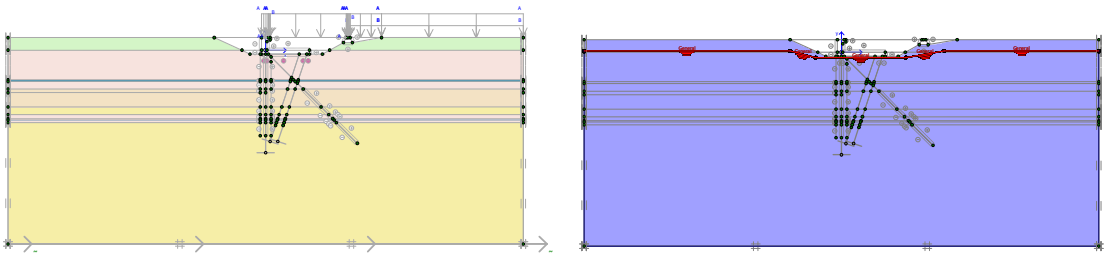

Phase 2: intallation of quay wall elements

Diaphragm wall, MV pile, vibro piles, relieving platform and landside crane foundation are installed.

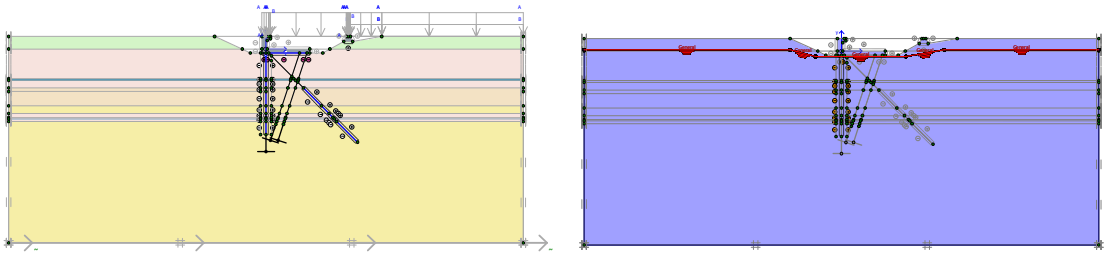

Phase 3: backfill behind wall

Soil behind the relieving floor are placed back in this phase. Displacement is set to zero starting from this phase.

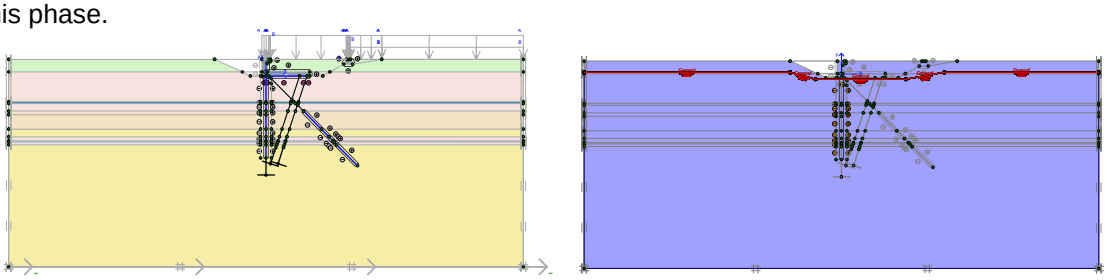

Phase 4: excavation seaside till NAP-16,5m

Excavation of soil on the seaside till NAP-16,5m. Groundwater level and Seawater level are kept constant (NAP+0,52m).

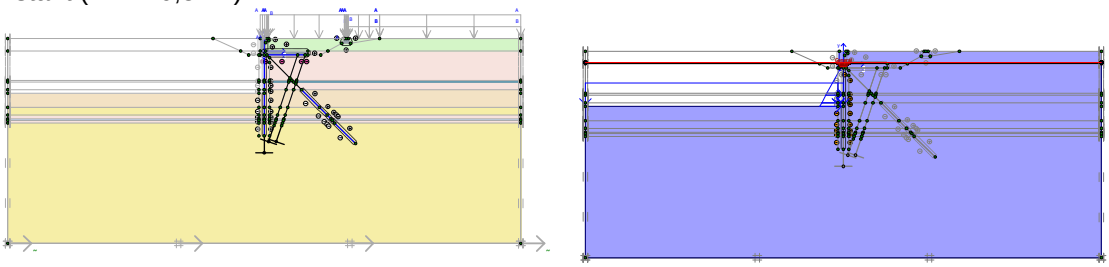

Phase 5: applying surcharge load behind landside crane rail
Surcharge load of 14 kPa is applied behind the landside crane rail.

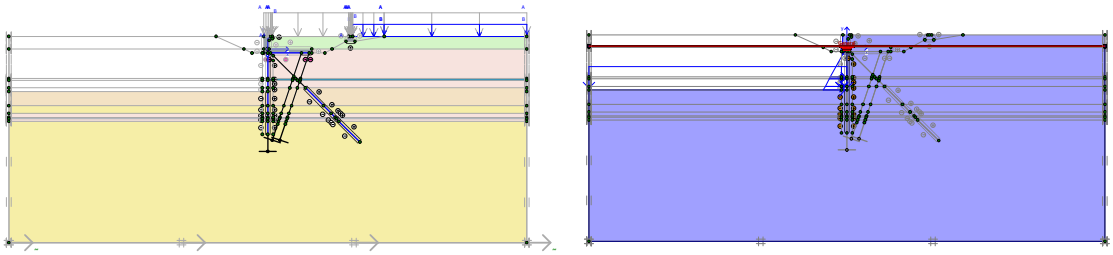

Phase 6: excavation seaside till NAP-22m
Further deepening of seabed by excavting soil till NAP-22m.

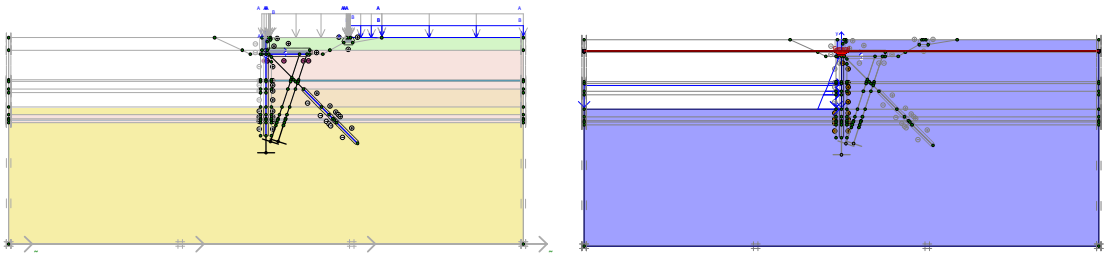

Phase 7:applying fender/bolder load and surcharge load
Fender load (215 kN) or Bolder load (190 kN) is applied depending on the load combination. Also surcharge load of 28 kPa is aplied above and behind the qauy wall. Further more, seawater level is set to NAP-1,38m.

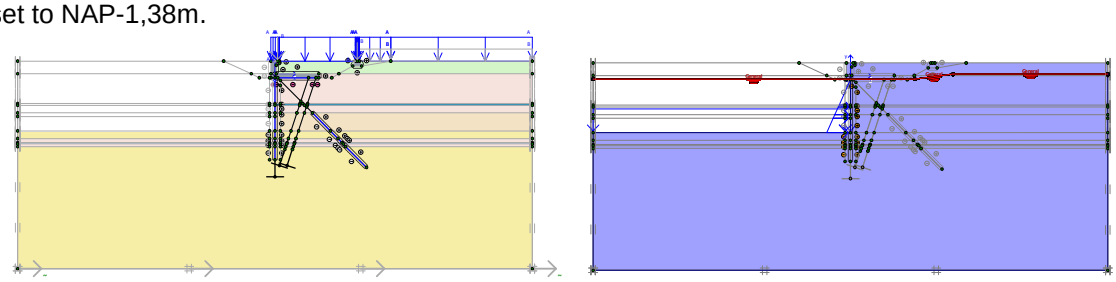

Phase 8: applying crane load
Horizontal and vertical crane loads is applied, 34 kN and 1302kN respectivily.

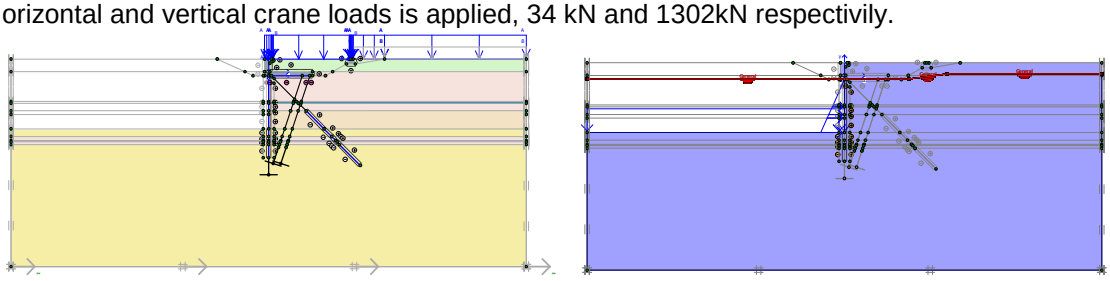

Phase 9:increase load behind landside rail
Surcharge load behind the landside crane rail is increased to 42 kPa.

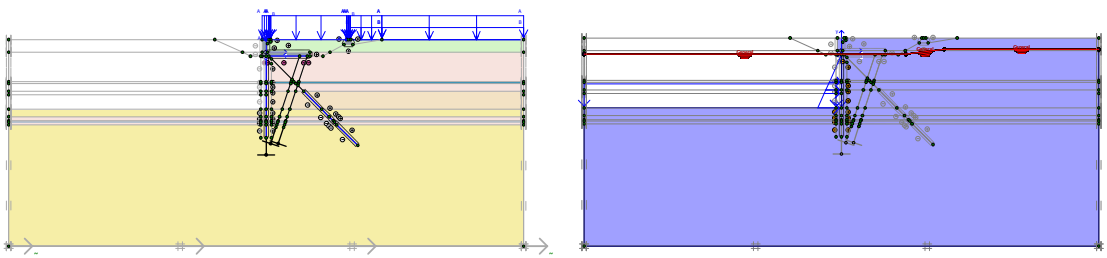

H3 Static model output Plaxis

Load combination 1

Displacements

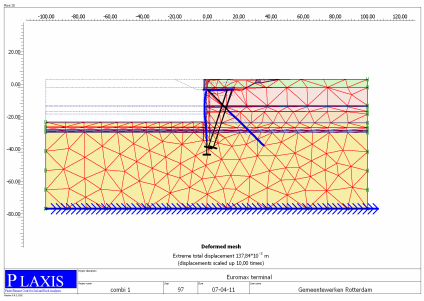

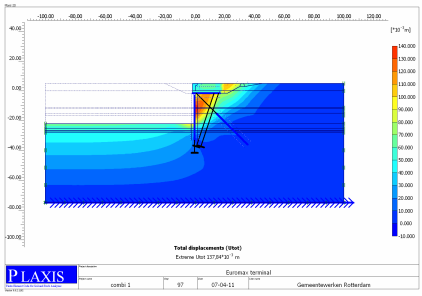

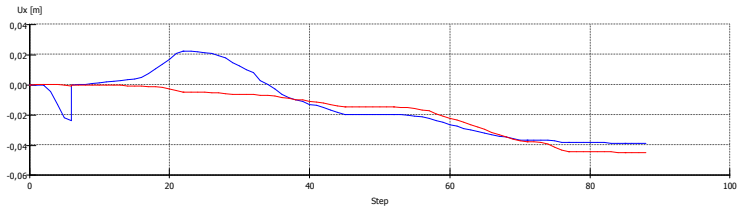

Horizontal displacement

Seaside crane rail

Landside crane rail

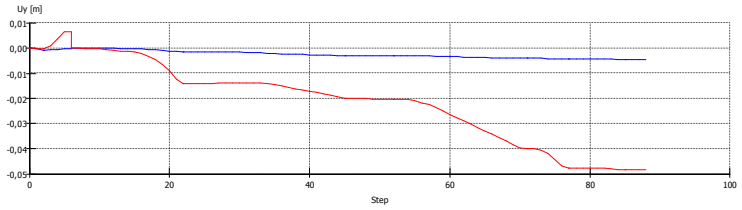

Vertical displacement

Seaside crane rail

Landside crane rail

Plaxis Displacement	Hor. displacement After last phase	Vert. displacement After last phase
Seaside crane rail	-0,039 m	-0,005 m
Landside crane rail	-0,045 m	-0,048 m

Stresses

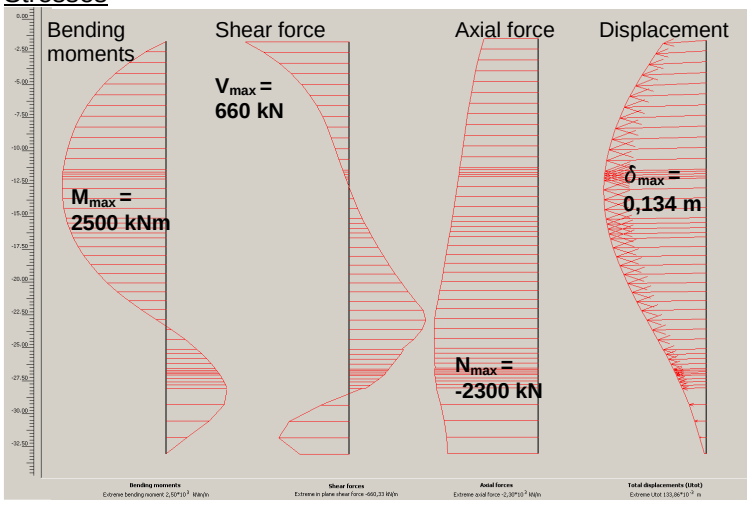

The maximum bending moment of the diaphragm wall is 2500 kNm/m and is located at NAP-12,75m. The corresponding axial force at this depth is 1792 kN/m.

Plaxis Stresses	Depth Max. bending moment	Max. Bending moment kNm/m	Axial force kN/m
Diaphragm wall	NAP-12,75m	2500	-1792
MV pile	-	-	836
Vibro pile 1	-	-	-822
Vibro pile 2	-	-	-247

Load combination 2

Displacements

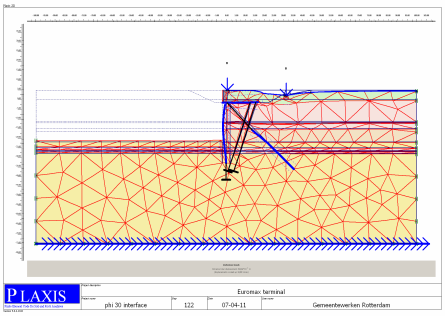

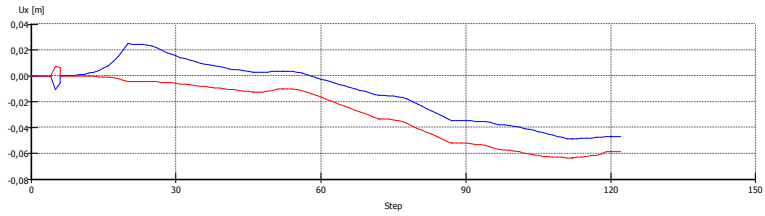

Horizontal displacement

Seaside crane rail

Landside crane rail

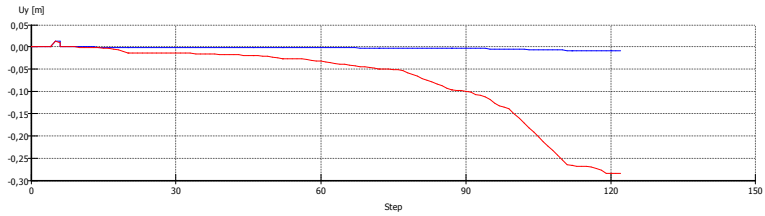

Vertical displacement

Seaside crane rail

Landside crane rail

Plaxis Displacement	Hor. displacement After last phase	Vert. displacement After last phase
Seaside crane rail	-0,047 m	-0,008 m
Landside crane rail	-0,060 m	-0,285 m

Stresses

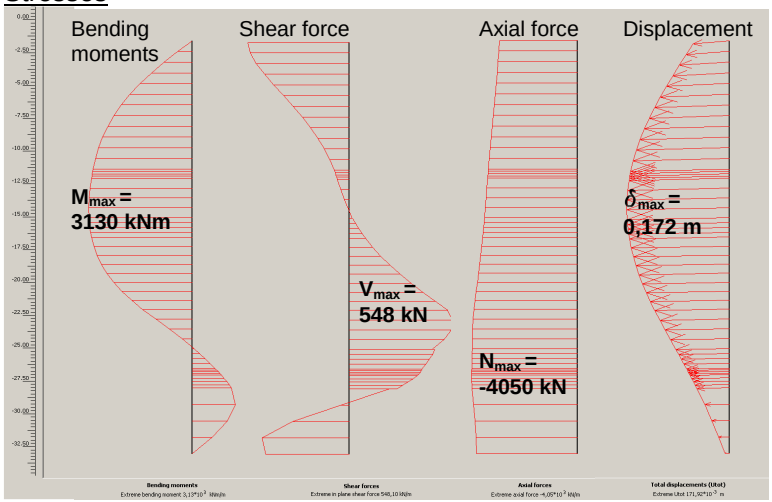

The maximum bending moment of the diaphragm wall is 3130 kNm/m and is located at NAP-14,25m. The corresponding axial force at this depth is 3527 kN/m.

Plaxis Stresses	Depth Max. bending moment	Max. Bending moment kNm/m	Axial force kN/m
Diaphragm wall	NAP-14,25m	3130	-3527
MV pile	-	-	851
Vibro pile 1	-	-	-1601
Vibro pile 2	-	-	-545

Load combination 3

Displacements

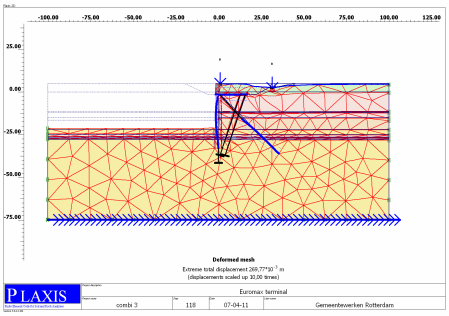

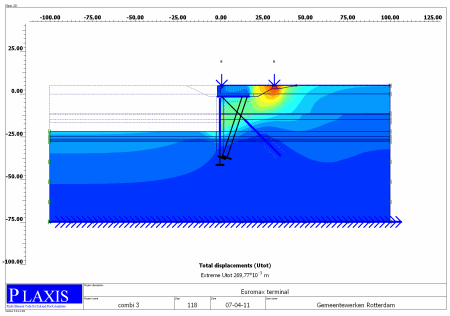

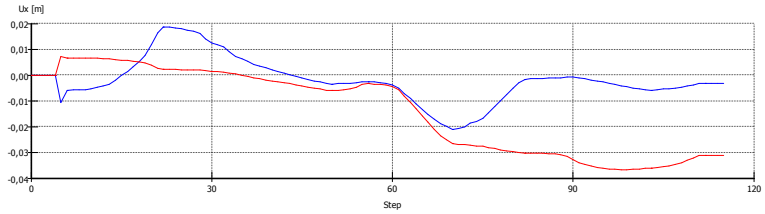

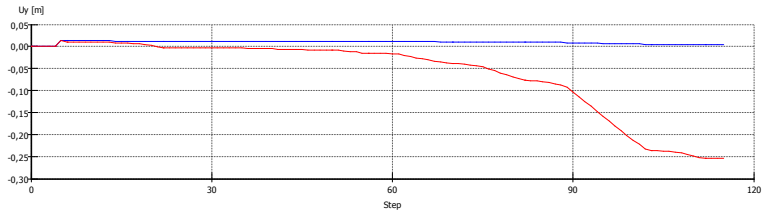

PLAXIS Displacement	Hor. displacement After last phase	Vert. displacement After last phase
Seaside crane rail	-0,003 m	0,005 m
Landside crane rail	-0,031 m	-0,254 m

Stresses

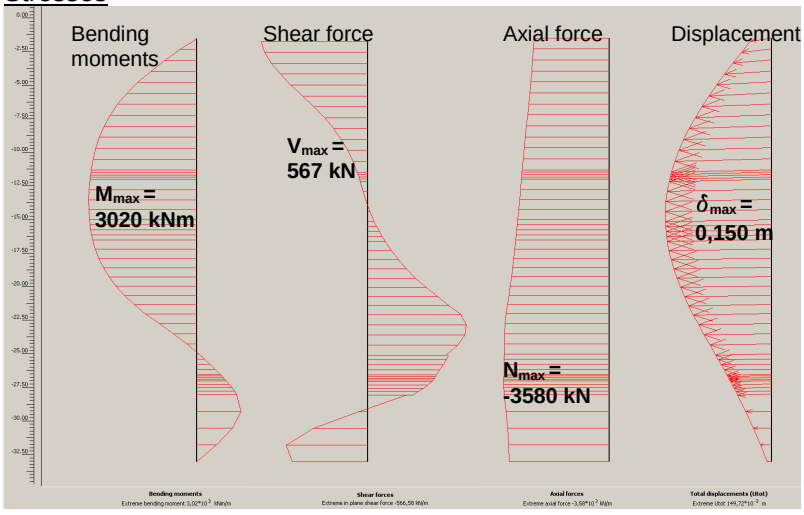

The maximum bending moment of the diaphragm wall is 3020 kNm/m and is located at NAP-13,5m. The corresponding axial force at this depth is 3039 kN/m.

PLAXIS Stresses	Depth Max. bending moment	Max. Bending moment M kNm/m	Axial force N kN/m
Diaphragm wall	NAP-13,5m	3020	-3039
MV pile	-	-	428
Vibro pile 1	-	-	-1670
Vibro pile 2	-	-	-611

An overview of the Plaxis results are shown in Table H-3 and Table H-4.

PLAXIS Displacements	Displacement seaside crane rail		Displacement landside crane rail	
	Horizontal	Vertical	Horizontal	Vertical
Load combination 1	-0,039 m	-0,005 m	-0,045 m	-0,048 m
Load combination 2	**-0,047 m**	**-0,008 m**	**-0,060 m**	**-0,285 m**
Load combination 3	-0,003 m	0,005 m	-0,031 m	-0,254 m

Table H-3 Displacements of crane rails according to Plaxis

PLAXIS Stresses	Max. M diaphragm wall kNm/m	N diaphragm wall kN/m	Max. N MV pile kN/m	Max. N Vibro pile 1 kN/m	Max. N Vibro pile 2 kN/m
Load combination 1	2500	-1792	836	-822	-247
Load combination 2	**3130**	**-3527**	**851**	-1601	-545
Load combination 3	3020	-3039	428	**-1670**	**-611**

Table H-4 Wall stresses for different load combinations according to Plaxis

H4 References

[H.1] Delta marine consultants, Berekening kadeconstructie aanbieding 2, 022518-rap-u-0008 rev B 03-2005
[H.2] Pichler Lukas, Additional graduation work : Earthquake analysis of quay wall, Delft, 04-2010
[H.3] NEN 6720, Voorschriften beton constructieve eisen en rekenmethoden (VBC), 1995
[H.4] Waterman D., Plaxis presentation, Computational Geotechnics 1: Meshing-Output-Curves, Chile, 05-2006

Appendix I Pseudo static calculation diaphragm wall

In this chapter a pseudo static analysis is made for the diaphragm wall. A simplified soil profile was used shown in Figure I-1. Earthquake acceleration of 0,5 m/s^2 is used during this analysis to see whether or not the diaphragm wall can resist this magnitude of earthquake. The corresponding seismic coefficients for this earthquake acceleration is k_h=0,067 and k_v=0,022. Three different Cases are analyzed depending upon the magnitude of excess pore water pressure generated during the earthquake. By doing this the influence of excess pore water pressure can be shown.

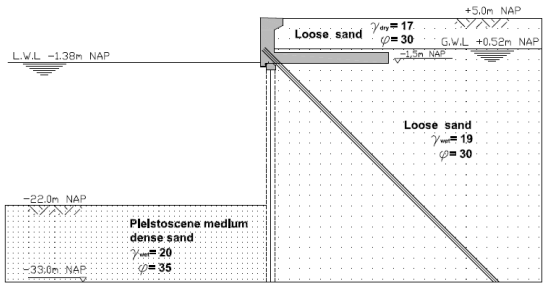

Figure I-1 Simplified soil model

Case 1: no excess pore water pressure
Case 2: excess pore water pressure is 50 percent of the initial vertical effective stress
Case 3: Complete liquefaction of backfill

By determining the static and dynamic forces acting on the diaphragm wall caused by the earthquake, the maximum bending moment of the wall and axial pile force of the MV pile can be calculated using the horizontal and moment equilibrium.

I1 Case 1 (no excess pore water pressure)

The presence of water within the backfill and in front of the sheet pile wall results in additional static and dynamic forces acting on the wall and alters the distribution of forces within the active and passive soil wedges developing behind and in front of the sheet pile wall. This section describes the calculations that are made to determine the anchor force and the maximum bending moment of the wall. This analysis, described as case 1, assumes that no excess pore pressures are generated within the submerged portion of the backfill or within the foundation during earthquake shaking.

I.1.1 Loads

The static and additional seismic forces during an earthquake are determined in this section for case 1. The structure will be calculated per running meter.

Static water pressure
Static water pressures are determined using Eq. 5-3. Point of application of these forces are determined using Eq. F-1 and are shown in Figure I-2.

$$U_{stat,sea,front} = \frac{1}{2}\gamma_w h_1^{\,2} = \frac{1}{2} * 10 * (22 - 1{,}38)^2 = 2126 kN/m$$

$$U_{stat,ground,front} = \frac{1}{2}\gamma_w h_2^{\,2} - U_{stat,ground,front} = \frac{1}{2} * 10 * (22 - 1{,}38)^2 - 2126 = 2873 kN/m$$

$$U_{stat,ground,back} = \frac{1}{2}\gamma_w h_3^{\,2} - \frac{1}{2}\gamma_w h_4^{\,2} = \frac{1}{2} * 10 * (33 + 0{,}52)^2 - \frac{1}{2} * 10 * (0{,}52 + 1{,}5)^2 = 5598 kN/m$$

Dynamic water pressure
Distinction is made for free standing water outboard of the wall and water in backfill. These water pressures are determined using the Westergaard solution mentioned in chapter 5.4. For water located at the backfill of the wall Matsuo and Ohara (1965) suggested the hydrodynamic pressure to be around 70% of that of the free standing water. This suggestion was used during the calculation. Resultant thrust is determined for the dynamic water pressures and are shown below and in
Figure I-3. They are acting at an elevation equal to 0,4 times the total water depth h_{total} above the base of the wall.

$$U_{dyn,sea,front} = \int_0^{20,62}\left(\frac{7}{8}k_h\gamma_w\sqrt{y*31,62}\right)dy = \frac{7}{8}*0,067*10*\sqrt{31,62}*\frac{1}{1,5}*20,62^{1,5} = 207kN/m$$

$$U_{dyn,ground,fromt} = \left(\frac{7}{12}k_h\gamma_w h_{total}{}^2 - U_{dyn,sea,fromt}\right)*0,7$$

$$= \left(\frac{7}{12}*0,067*10*31,62^2 - 207\right)*0,7 = 131kN/m$$

$$U_{dyn,ground,back} = \left(\frac{7}{12}k_h\gamma_w h_{total}{}^2\right)*0,7 = \left(\frac{7}{12}*0,067*10*33,52^2\right)*0,7 = 310kN/m$$

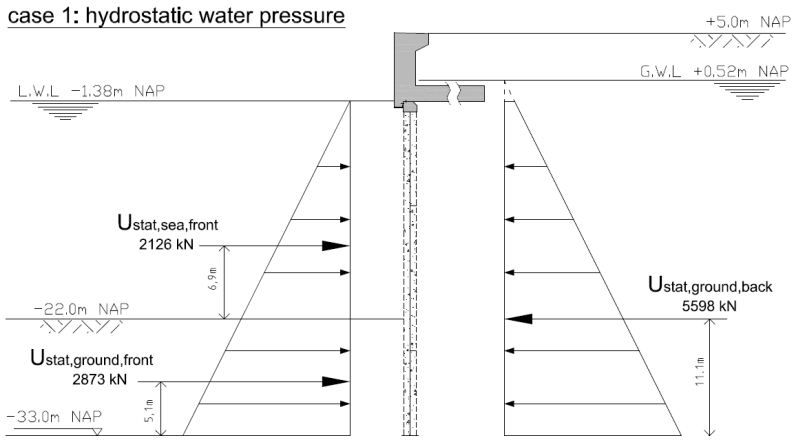

Figure I-2 Hydrostatic water pressure for case 1

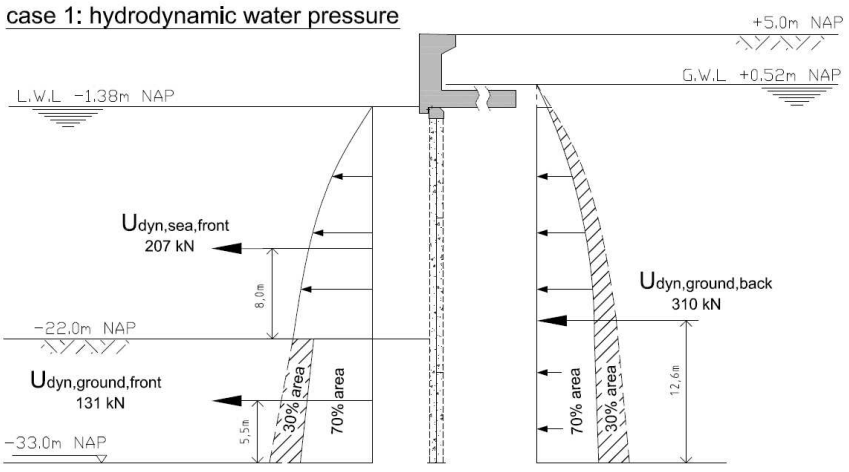

Figure I-3 Hydrodynamic water pressure for case 1

Dynamic ground pressure

Dynamic earth pressure is determined using the M-O method mentioned in Appendix C . The M-O method assumes that the wall movements are sufficient to fully mobilize the shear resistance along the backfill wedge, as is the case for Coulomb's active and passive earth pressure theories. To develop the dynamic active earth pressure force, P_{ae}, the wall movements are away from the backfill, and for the passive dynamic earth pressure force, P_{pe}, the wall movements are towards the backfill. The most unfavorable direction combination is used during this analysis. This is when the horizontal acceleration (a_h) is directed towards the backfill and the vertical acceleration (a_v) is directed

downward, causing the incremental dynamic earth pressure forces ($\Delta P_{AE/PE}$) acting away from the backfill. This has the normative effect of increasing the driving force behind the sheet pile and decreasing the stabilizing force in front of the sheet pile.

The dynamic active earth pressure coefficient k_{ae} and seismic inertia angle ψ_a for case 1 is determines using Eq. C-2 and Eq. C-3.

$$\psi_a = \tan^{-1}\left(\frac{k_h}{1-k_v}\frac{\gamma_d}{\gamma-\gamma_w}\right) = \tan^{-1}\left(\frac{0{,}067}{1-0{,}022}\frac{17}{19-10}\right) = 7{,}43$$

$$k_{ae} = \frac{\cos^2(\varphi-\beta-\psi)}{\cos\psi\cos^2\beta\cos(\delta+\beta+\psi)\left[1+\sqrt{\frac{\sin(\delta+\varphi)\sin(\varphi-\alpha-\psi)}{\cos(\delta+\beta+\psi)\cos(\alpha-\beta)}}\right]^2}$$

$$= \frac{\cos^2(30-0-7{,}43)}{\cos 7{,}43\cos^2 0\cos(20+0+7{,}43)\left[1+\sqrt{\frac{\sin(20+30)\sin(30-0-7{,}43)}{\cos(20+0+7{,}43)\cos(0-0)}}\right]^2} = 0{,}39$$

Hence the dynamic active pressure thrust P_{ae} is calculated using Eq. C-1

$$P_{ae} = \frac{1}{2}k_{ae}\gamma_{eff}H^2(1-k_v) = \frac{1}{2}*0{,}39*(19-10)(33-1{,}5)^2(1-0{,}022) = 1702kN/m$$

P_{ae}, can be divided into a static component, P_a, and a dynamic component, ΔP_{ae}. The static component can be calculated using Eq. B-7 and Eq. B-8 which is based on the Coulomb Theorem.

$$k_a = \frac{\cos^2(\varphi-\beta)}{\cos^2\beta\cos(\delta+\beta)\left[1+\sqrt{\frac{\sin(\delta+\varphi)\sin(\varphi-\alpha)}{\cos(\delta+\beta)\cos(\alpha-\beta)}}\right]^2} = 0{,}29$$

$$P_a = \frac{1}{2}k_a\gamma_{eff}H^2 = \frac{1}{2}*0{,}29*9*31{,}5^2 = 1296kN/m$$

The dynamic component ΔP_{ae} is

$$\Delta P_{ae} = P_{ae} - P_a = 1702 - 1296 = 406kN/m$$

The static component is known to act at H/3 above the base of the wall. Seed & Whitman (1970) recommended that the dynamic component be taken to act at approximately 0.6 H. On this basis, the total dynamic active thrust P_{ae} will act at a height h from the base of the wall.

$$h = \frac{P_a\cdot H/3 + \Delta P_{ae}(0.6H)}{P_{ae}} = \frac{1296*31.5/3 + 406*(0.6H)}{1702} = 12{,}5m$$

The dynamic passive earth pressure coefficient k_{pe} and seismic inertia angle ψ_p for case 1 is determines the same way like for the active case. But know loose sand is replaced by pleistocene sand, which results in the following dynamic earth pressures:

$$\psi_a = \tan^{-1}\left(\frac{k_h}{1-k_v}\frac{\gamma_d}{\gamma-\gamma_w}\right) = \tan^{-1}\left(\frac{0{,}067}{1-0{,}022}\frac{20}{20-10}\right) = 7{,}86$$

$$k_{pe} = \frac{\cos^2(\varphi+\beta-\psi)}{\cos\psi\cos^2\beta\cos(\delta-\beta+\psi)\left[1+\sqrt{\frac{\sin(\delta+\varphi)\sin(\varphi+\alpha-\psi)}{\cos(\delta-\beta+\psi)\cos(\alpha-\beta)}}\right]^2} = 8{,}78$$

$$P_{pe} = \frac{1}{2}k_{pe}\gamma_{eff}H^2(1-k_v) = 5192kN/m$$

P_{pe} is acting at 1/3H above the base of the wall. Figure I-4 shows a illustration of the dynamic earth pressure forces and its point of application.

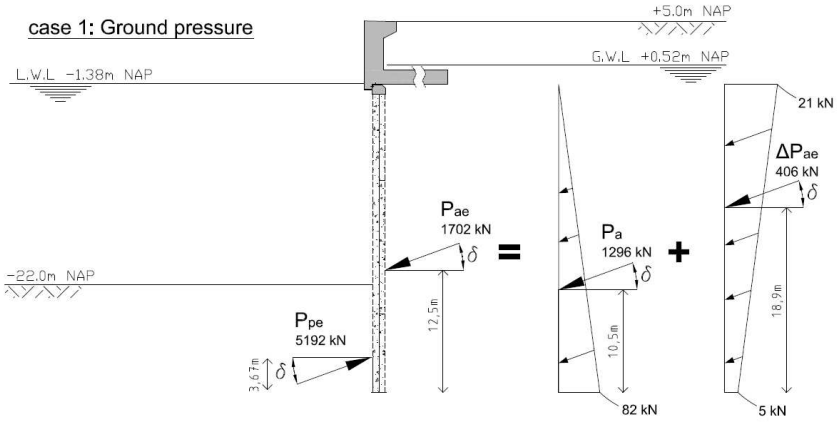

Figure I-4 Dynamic earth pressures for case 1

Surcharge load

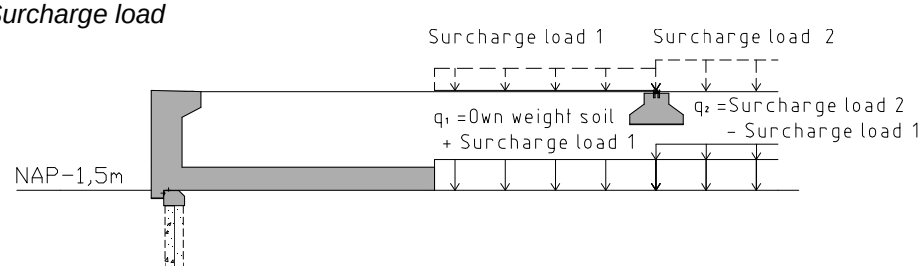

Figure I-5 schematization of surcharge load and own weight behind relieving structure

Backfill behind the relieving platform and above NAP-1,5m can be schematized as surcharge load as shown in Figure I-5. The impact of this one-sided limited surcharge load on the wall can be estimate using the method created by Ohde **Error! Reference source not found.** which is illustrated in Figure I-6. The area of influence begins where the line at angle φ cuts the axis of the sheet pile. The full influence is valid when the line at angle ϑ_a cuts the axis. The angle of the sliding plane angle ϑ_a depends on the angle of internal friction φ, the slope of the ground surface β and the inclination of the sheet pile α.

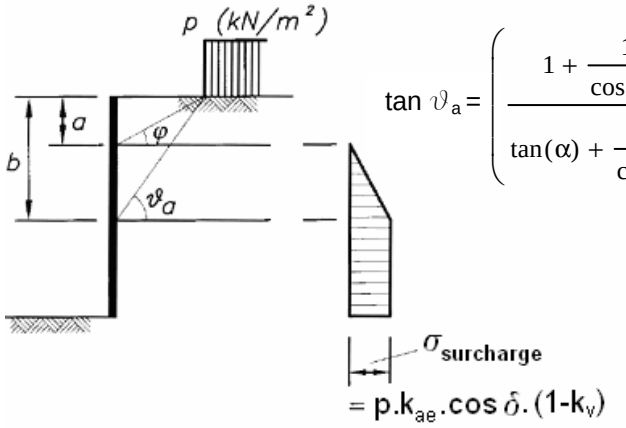

$$\tan\vartheta_a = \left(\frac{1+\frac{1}{\cos(\alpha)}\cdot\sqrt{\frac{\sin(\varphi+\delta)\cdot\cos(\alpha+\beta)}{\cos(\delta-\alpha)\cdot\sin(\varphi-\beta)}}\cdot\sin(\varphi)}{\tan(\alpha)+\frac{1}{\cos(\alpha)}\cdot\sqrt{\frac{\sin(\varphi+\delta)\cdot\cos(\alpha+\beta)}{\cos(\delta-\alpha)\cdot\sin(\varphi-\beta)}}\cdot\cos(\varphi)}\right)$$

Figure I-6 Horizontal ground pressure for one- sided limited surcharge load

Forces acting on the wall due to of surcharge load and own weight behind the relieving structure are shown in Figure I-7.

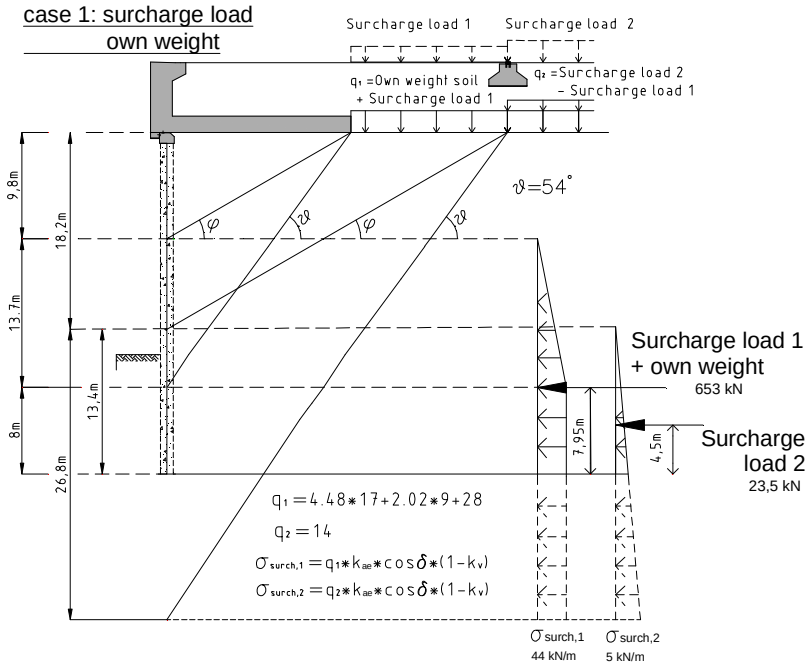

Figure I-7 Horizontal ground pressure as result of surcharge load and own weight behind relieving structure

Crane load

The landside crane load is schematized as a two-sided limited distributed load with a width of the crane rail foundation of 3,5m and a loading of the crane load divided by the width. The total extra horizontal thrust on the wall due the presence of the two-sided limited distributed crane load can be determined using the method shown in Figure I-8 **Error! Reference source not found.**.

Thrust acting on the wall due to the landside crane load is shown in Figure I-9.

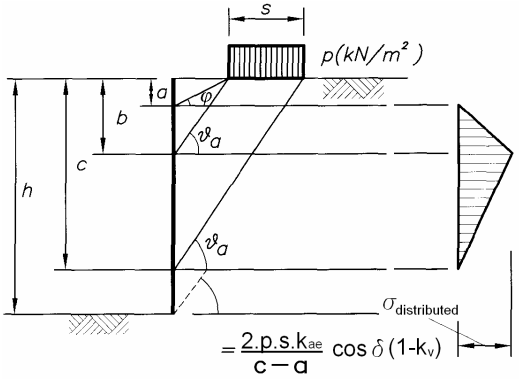

Figure I-8 Horizontal ground pressure for two - sided limited distribution load

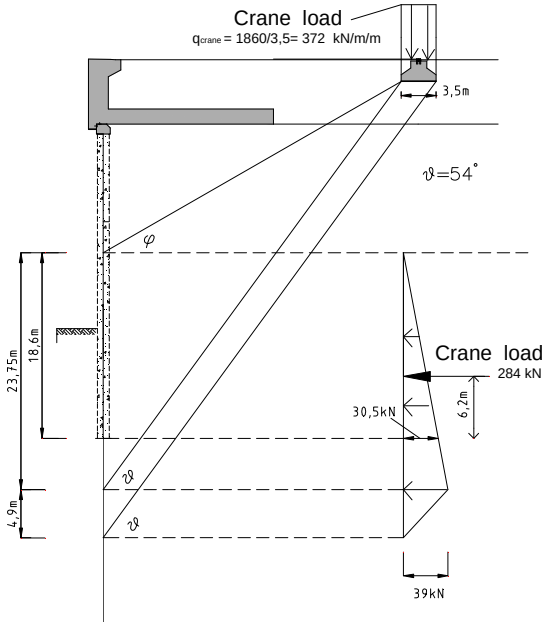

Figure I-9 Horizontal ground pressure for two - sided limited distribution load

I.1.2 Calculation case 1

Force equilibrium
By making use of the horizontal force equilibrium the anchor force (MV pile) can be determined. This is done by summing up the horizontal forces determined in section I.1.1.

$$\begin{aligned} F_{MVpile} &= -U_{stat,sea,front} - U_{stat,ground,front} + U_{stat,ground,back} + U_{dyn,sea,front} + U_{dyn,ground,front} + U_{dyn,ground,back} \\ &\quad - P_{pe} + P_{ae} + F_{surcharge,1} + F_{surcharge,2} + F_{crane} \\ &= -2126 - 2873 + 5598 + 207 + 131 + 310 - 5192\cos\delta + 1702\cos\delta + 653 + 23{,}5 + 284 \\ &= -1072 kN/m \end{aligned}$$

The result of this first estimation shows that the MV pile becomes a bearing pile instead of the tension pile. The reason for this is that the passive earth pressure is overestimated. In reality, ground will not always be fully mobilized which result in less passive earth pressure and more active pressure. When the wall is deep enough into the ground it can be assumed as an inclined wall. In this situation, passive ground will even turn into active ground and vice versa.

To get a more accurate estimation another calculation was made by hand. For this calculation the minimum required depth of the sheet pile penetration is determined. By summing up the driving forces and the resisting forces at the point where the MV pile is connecting the diaphragm wall and equalling it to zero, the minimum required depth penetration of the wall can be determined. Table I-1 summarizes the horizontal force components acting on the diaphragm wall as shown in Figure I-10 and are expressed in terms of the generalized dimensions D_1 and D_2, which is respectively the distance between the connection of the MV pile to the seabed and the distance from the seabed to the penetration depth of the wall.

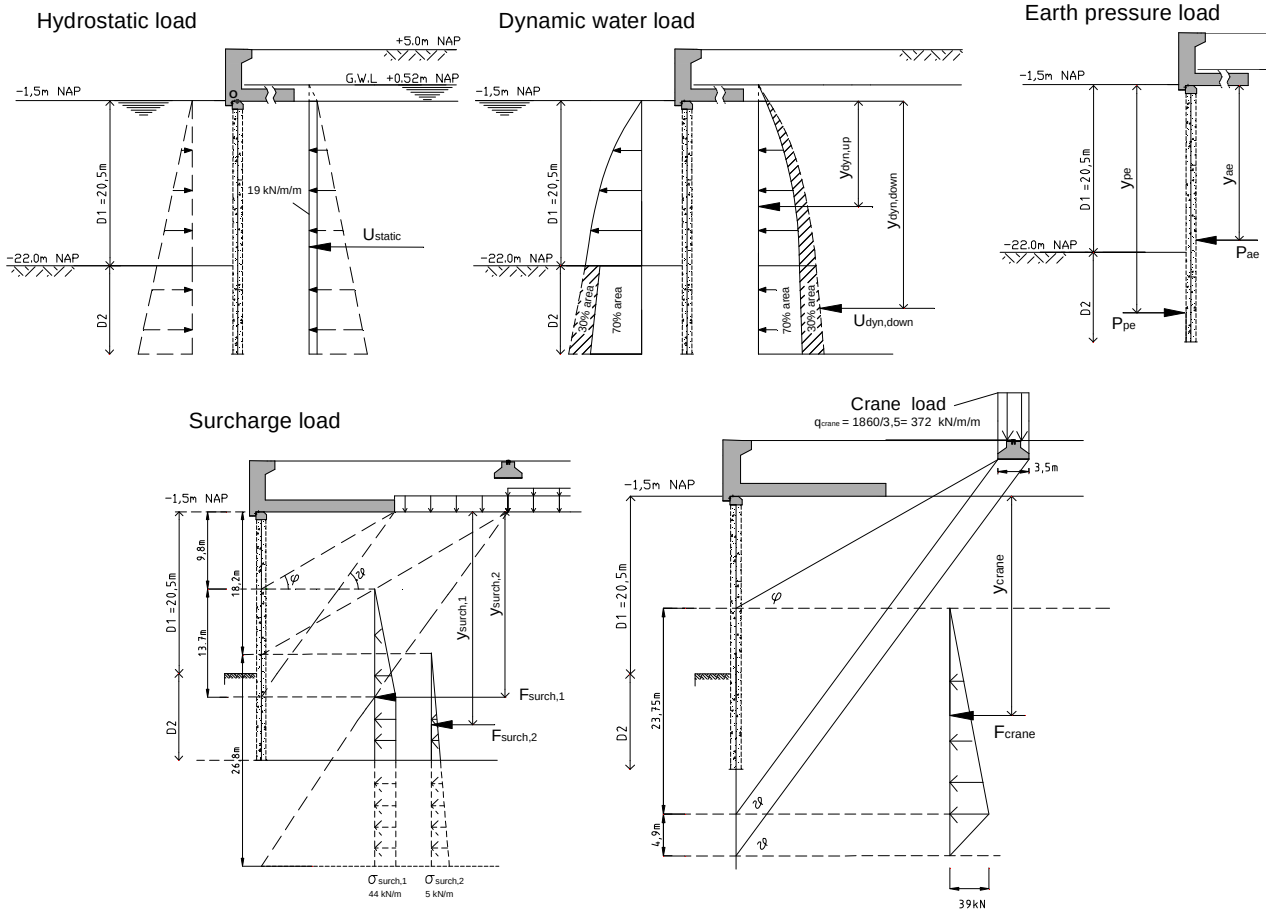

Figure I-10 Horizontal force components on diaphragm wall with unknown penetration depth

Type of loading	Horizontal force [kN/m]	Distance to MV Pile (y_n) [m]
U_{static}	$(0.52 + 1.38)\cdot 10\cdot(D_1 + D_2)$	$0.5(D_1 + D_2)$
$U_{dyn,up}$	$(1 + 0.7)\cdot\int_0^{20.5} \frac{7}{8}k_h\gamma_w\cdot\sqrt{y\cdot(D_1 + \lvert D_2\rvert)}\,dy$	$0.4(D_2)$
$U_{dyn,down}$	$\frac{7}{12}\cdot k_h\cdot\gamma_w\cdot(D_1 + \lvert D_2\rvert)^2\cdot 1.4 - 1.4\cdot\int_0^{D_1}\frac{7}{8}k_h\gamma_w\cdot\sqrt{y\cdot(D_1 + \lvert D_2\rvert)}\,dy$	$\frac{[(D_1 + \lvert D_2\rvert) - 20.5]}{2} + 20.5$
P_{pe}	$\frac{1}{2}k_{pe}\cdot\gamma_{eff1}\cdot(\lvert D_2\rvert)^2\cdot(1 - k_v)\cdot\cos(\delta)$	$\frac{2}{3}(\lvert D_2\rvert) + 20.5$
P_{ae}	$\frac{1}{2}k_{ae}\cdot\gamma_{eff2}\cdot(D_1 + \lvert D_2\rvert)^2\cdot(1 - k_v)\cdot\cos(\delta)$	$\frac{P_a\cdot\frac{2}{3}(D_1 + \lvert D_2\rvert) + \Delta P_{ae}\cdot 0.6\cdot(D_1 + \lvert D_2\rvert)}{P_{ae}}$
$F_{surch,1}$	$\frac{1}{2}\cdot 48\cdot 13.7 + (D_2 - 3)\cdot 48$	$\frac{\left(\frac{2}{3}\cdot 13.7 + 9.8\right)\cdot\left(\frac{1}{2}\cdot 48\cdot 13.7\right) + \left(\frac{D_2 - 3}{2} + D_1 + 3\right)\cdot(D_2 - 3)\cdot 48}{F_{surch.1}}$
$F_{surch,2}$	$\frac{(D_2 + 2.4)^2\cdot 7}{31.5}\frac{1}{2}$	$(D_2 + 2.4)\cdot\frac{2}{3} + 20.5 - 2.4$
F_{crane}	$\frac{1}{2}\cdot\frac{(D_2 + 7.6)^2\cdot 39}{23.75}$	$(D_2 + 7.6)\cdot\frac{2}{3} + 20.5 - 7.6$

Table I-1 Horizontal force components and distance to MV pile

Equilibrium of moments about the elevation of the MV pile is required to find needed penetration depth. By multiplying the horizontal force and its distance to the MV pile the bending moment for each separate force component can be determined. By summing up these separate bending moments and equal it to zero the equilibrium of moment is achieved.

$$\sum M_{MV\ pile} = 0 =$$
$$U_{static}\cdot y_{static} + U_{dyn.up}\cdot y_{dyn.up} + U_{dyn.down}\cdot y_{dyn.down} + P_{ae}\cdot y_{ae} + F_{surch.1}\cdot y_{surch.1} + F_{surch.2}\cdot y_{surch.2} - P_{pe}\cdot y_{pe}$$

From this it follows that the minimum wall penetration needs to be D_2 = 7,21m. The existing penetration depth is larger than the required penetration depth. This indicates that some part of the ground will not be fully mobilized and that the above calculated anchor force is not correct.

The horizontal forces acting on the diaphragm wall and the bending moment about the elevation of the MV pile for the minimum required penetration depth are listed in Table I-2.

Type of loading	Horizontal force [kN/m]	Moment about MV pile [kNm/m]
U_{static}	526	7295
$U_{dyn,up}$	325	4058
$U_{dyn,down}$	153	3684
P_{pe}	-2097	-53080
P_{ae}	1238	22290
$F_{surch,1}$	531	11400
$F_{surch,2}$	10	252
F_{crane}	180	4101
		+
Total:	866	0

Table I-2 Moment about MV pile due to horizontal force components for D_2=7,21m

Once the required depth of wall penetration is determined the equilibrium horizontal component of the anchor force per running meter width of the wall, $F_{MV\ pile,h}$, is computed using the equations for horizontal force equilibrium. The minimum required penetration depth of the wall is 7.21m where the real penetration depth is 11m. Earth and water pressures forces will also act on the wall below the required penetration depth. Below this depth the resultant horizontal forces are assumed to be zero which means it can be neglected. This assumption is allowed because between the required penetration depth and the real penetration depth ground will not be fully mobilized and at a certain moment it active ground will even turn to passive ground and vice versa, hence the resultant horizontal force on both side of the wall will neutralize each other.

$$F_{MV\ pile,h} = U_{static} + U_{dyn.up} + U_{dyn.down} - P_{pe} + P_{ae} + F_{surch.1} + F_{surch.2} + F_{crane} = 866$$

Hence the anchor force becomes:

$$F_{MV\ pile} = 866 * \sqrt{2} = 1221 kN/m$$

The distribution of the bending moments within the wall is computed from the external earth pressure along the front and back of the sheet pile, the anchor force, water pressure, surcharge load and crane load. First, the elevation of zero stress is determined. To accomplish this, the earth pressure forces must be converted to equivalent earth pressure distribution. One approach for doing this is to separate P_{ae} into its static and incremental dynamic components and corresponding point of action as mentioned in Appendix C and illustrated in Figure I-11. **Figure I-12** is used to define the variation in horizontal stress with depth for the different loadings. At a given elevation, an imaginary section is made through the diaphragm wall, as shown in **Figure I-12**, and the internal shear force V and internal bending moment M are represented. The internal shear force V is equal to the sum of earth pressure, water pressure , surcharge loading, crane loading and anchor force acting on the free body of the diaphragm wall above the imaginary section. The internal bending moment M is equal to moment of the different forces at the elevation of the imaginary section. The maximum bending moment within the diaphragm wall is denoted as $M_{diaph,max}$. The value for $M_{diaph,max}$ is determined by calculating the internal bending moment at the elevation at which the shear is equal to zero.

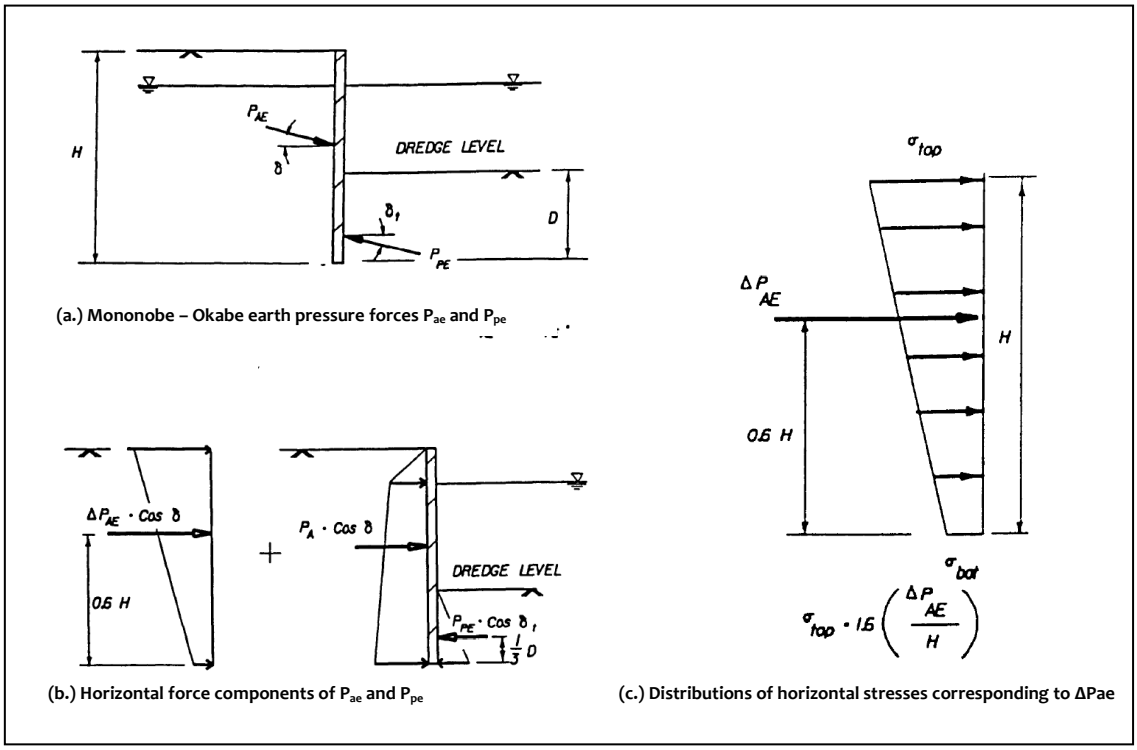

Figure I-11 Horizontal force components on diaphragm wall with unknown penetration depth Error! Reference source not found.

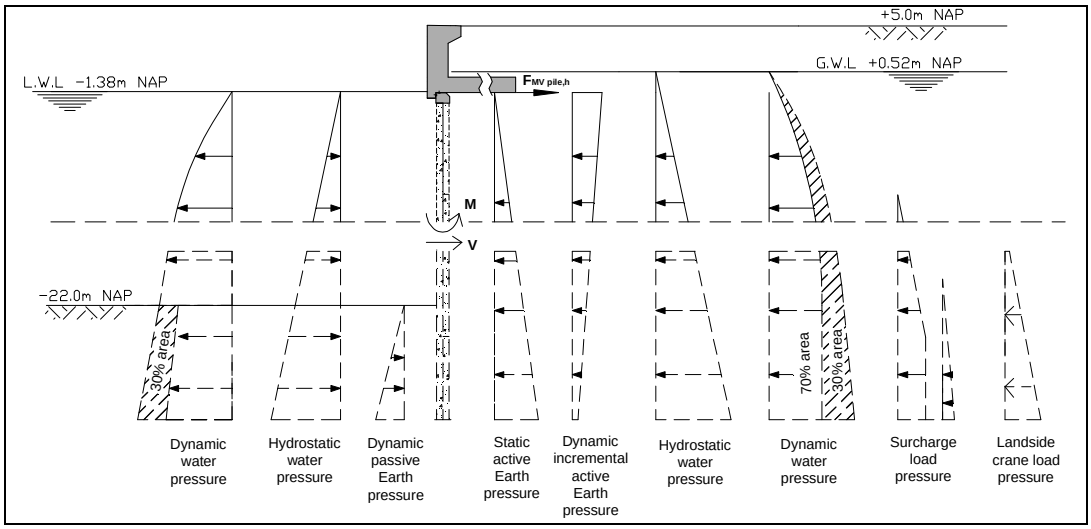

Figure I-12 Horizontal pressure components and anchor force acting on the diaphragm wall

Table I-3 summarizes the resulting horizontal force per component acting on the diaphragm wall and are expressed in terms of y_0, which is the distance between the top of the diaphragm wall (NAP-1,5m) and the elevation where zero shear is located.

Type of loading	Horizontal force [kN/m]		
U_{static}	$(0.52 + 1.38)\cdot 10\cdot y_0$		
U_{dyn}	$\left(\int_0^{y_0} \frac{7}{8}\cdot k_h\cdot\gamma_w\sqrt{y_0\cdot 31.5}\,dy_0\right)\cdot(1 + 0.7)$		
P_a	$\frac{1}{2}k_a\cdot\gamma_{eff2}\cdot(y_0)^2\cdot(1 - k_v)\cdot\cos(\delta)$		
ΔP_{ae}	$\sigma_{top}\cdot y_0 - \frac{(\sigma_{top} - \sigma_{bot})\cdot y_0^2}{(7.21 + 20.5)\cdot 2}$	=	$18.336\cdot y_0 - \frac{(18.336 - 4.584)\cdot y_0^2}{(7.21 + 20.5)\cdot 2}$
$F_{surch,1}$	$\frac{(y_0 - 9.8)^2.44}{13.7\cdot 2}$		
$F_{MV\ pile,h}$	866		

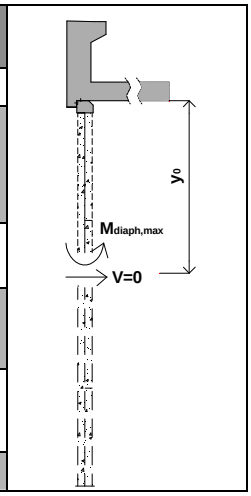

Table I-3 Horizontal force components expressed in terms of y_0

$$\sum F_{MV\ pile,h} = U_{static} + U_{dyn} + P_a + \Delta P_{ae} + F_{surch,1}$$

After a couple of iterations the elevation of zero shear has been found which is located at NAP-14,8m (y_0 = 13.3m). Hence, the maximum bending moment of the diaphragm wall at NAP-14,8m can be calculated by taken the moment of forces at this point as shown in Table I-4.

Type of loading	Horizontal force [kN/m]	Lever arm [m]	Moment at NAP-14,8 [kNm/m]
U_{static}	-253	6,65	-1682
U_{dyn}	-181	5,32	-963
P_a	-212	4,43	-840
ΔP_{ae}	-200	8	-1600
$F_{surch,1}$	-20	1,17	-23
$F_{MV\ pile,h}$	866	13,3	11518
			+
Total:	0		6409

Table I-4 Bending moment of diaphragm wall at NAP-14,8m

According to the pseudo static calculation for case 1 the maximum bending moment is located at NAP-14,8m and reaches a value of 6409kNm/m. The anchor force of the MV pile is 1221 kN.

I2 Case 2 (50% excess pore water pressure)

This analysis, describes as case 2, assumes that the excess pore water pressure is 50% of the initial vertical effective stress. Just like case 1, an earthquake acceleration of 0,5 m/s^2 is chosen.

I.2.1 Loads case 2

The static and additional seismic forces during an earthquake are determined in this section for case 2. The structure will be calculated per running meter.

Static water pressure
Static water pressures stays the same like case 1 and are shown in Figure I-13.

Dynamic water pressure
Dynamic water pressure results from the dynamic response of a body of water. Distinction is made for free standing water outboard of the wall and water in backfill. These water pressures are determined using the Westergaard solution mentioned in chapter 5.4. For saturated backfill, development of dynamic pore water pressure only occurs for free pore water conditions. Water in the pores cannot escape quickly enough to accommodate instantaneously compaction which results in excess pore water pressure build up. Therefore, no free pore water conditions are present during the presence of excess pore water build up which results in no dynamic water pressure.

The dynamic water pressure for the free standing water outboard is the same as calculated for case 1 while for the saturated backfill soil it becomes zero as shown in Figure I-13.

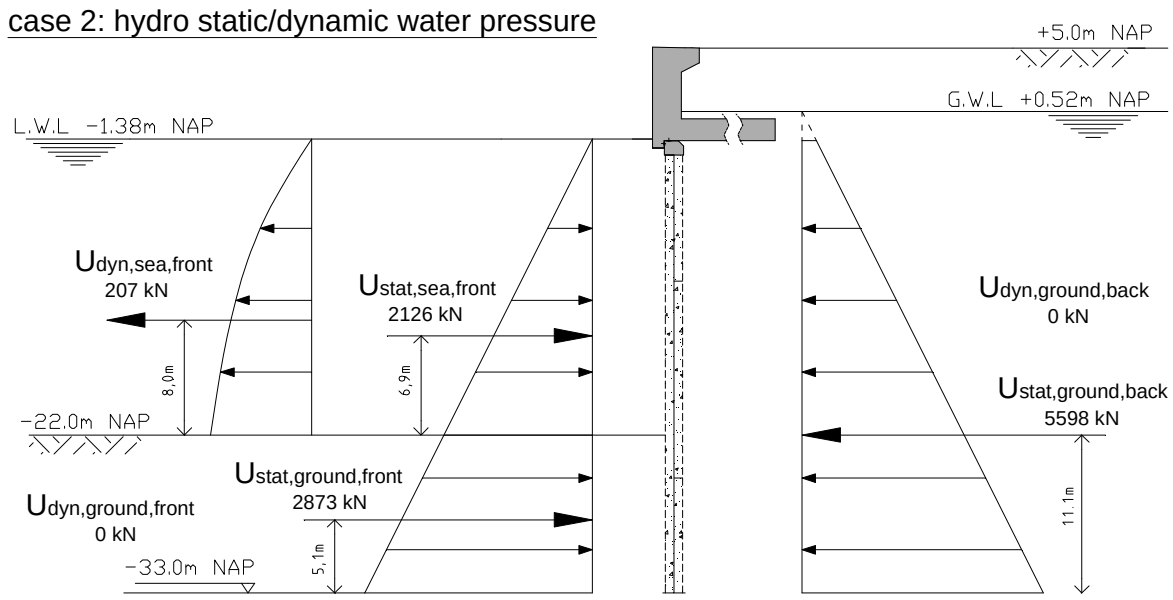

Figure I-13 Hydrostatic and dynamic water pressure for case 2

Dynamic ground pressure
For restrained pore water conditions, the M-O method can be modified to account for the presence of excess pore water within the backfill by replacing γ_{eff} and ψ by $\gamma_{eff,1}$ and ψ_1 respectively (chapter 5.4.1).

$$\gamma_{eff,1} = (\gamma - \gamma_w)(1 - r_u)$$

$$\psi_1 = \tan^{-1}\left[\frac{\gamma \cdot k_h}{\gamma_{eff,1}(1-k_v)}\right]$$

where
$\gamma_{eff,1}$ effective unit weight of soil with excess pore pressure
ψ_1 seismic inertia angle with excess pore pressure
r_u excess pore ratio = 0,5 (for 50% excess pore build up)

The dynamic active earth pressure coefficient k_{ae} and seismic inertia angle ψ_1 for case 2 is determines using Eq. C-2 and Eq. C-3.

$$\psi_1 = \tan^{-1}\left(\frac{k_h}{1-k_v}\frac{\gamma_d}{\gamma_{eff,1}}\right) = \tan^{-1}\left(\frac{0{,}067}{1-0{,}022}\frac{17}{(19-10)(1-0{,}5)}\right) = 14{,}6$$

$$k_{ae} = \frac{\cos^2(\varphi-\beta-\psi)}{\cos\psi\cos^2\beta\cos(\delta+\beta+\psi)\left[1+\sqrt{\frac{\sin(\delta+\varphi)\sin(\varphi-\alpha-\psi)}{\cos(\delta+\beta+\psi)\cos(\alpha-\beta)}}\right]^2}$$

$$= \frac{\cos^2(30-0-14{,}5)}{\cos 14{,}5\cos^2 0\cos(20+0+14{,}5)\left[1+\sqrt{\frac{\sin(20+30)\sin(30-0-14{,}5)}{\cos(20+0+14{,}5)\cos(0-0)}}\right]^2} = 0{,}52$$

Hence the dynamic active pressure thrust P_{ae} is calculated using Eq. C-1

$$P_{ae} = \frac{1}{2}k_{ae}\gamma_{eff,1}H^2(1-k_v) = \frac{1}{2}*0{,}52*(19-10)(1-0{,}5)(33-1{,}5)^2(1-0{,}022) = 1135kN/m$$

P_{ae}, can be divided into a static component, P_a, and a dynamic component, ΔP_{ae}. The static component can be calculated using Eq. B-7 and Eq. B-8 which is based on the Coulomb Theorem.

$$k_a = \frac{\cos^2(\varphi-\beta)}{\cos^2\beta\cos(\delta+\beta)\left[1+\sqrt{\frac{\sin(\delta+\varphi)\sin(\varphi-\alpha)}{\cos(\delta+\beta)\cos(\alpha-\beta)}}\right]^2} = 0{,}29$$

$$P_a = \frac{1}{2}k_a\gamma_{eff}H^2 = \frac{1}{2}*0{,}29*9*31{,}5^2 = 1296kN/m$$

The dynamic component ΔP_{ae} is

$$\Delta P_{ae} = P_{ae} - P_a = 1135 - 1296 = -161kN/m$$

The static component is known to act at H/3 above the base of the wall. Seed & Whitman (1970) recommended that the dynamic component be taken to act at approximately 0.6 H. On this basis, the total dynamic active thrust P_{ae} will act at a height h from the base of the wall.

$$h = \frac{P_a\cdot H/3 + \Delta P_{ae}(0.6H)}{P_{ae}} = \frac{1296*31.5/3 - 161*(0.6*31.5)}{1135} = 9{,}3m$$

The dynamic passive earth pressure coefficient k_{pe} and seismic inertia angle ψ_p for case 2 is determines the same way like for the active case. But know loose sand is replaced by pleistocene sand, which results in the following dynamic earth pressures:

$$\psi_1 = \tan^{-1}\left(\frac{k_h}{1-k_v}\frac{\gamma_d}{\gamma_{eff,1}}\right) = \tan^{-1}\left(\frac{0{,}067}{1-0{,}022}\frac{20}{(20-10)(1-0{,}5)}\right) = 15{,}3$$

$$k_{pe} = \frac{\cos^2(\varphi+\beta-\psi)}{\cos\psi\cos^2\beta\cos(\delta-\beta+\psi)\left[1+\sqrt{\frac{\sin(\delta+\varphi)\sin(\varphi+\alpha-\psi)}{\cos(\delta-\beta+\psi)\cos(\alpha-\beta)}}\right]^2} = 7{,}6$$

$$P_{pe} = \frac{1}{2}k_{pe}\gamma_{eff,1}H^2(1-k_v) = 2248kN/m$$

P_{pe} is acting at 1/3H above the base of the wall.

An equivalent hydrostatic thrust based on a fluid of unit weight $\gamma_{eq}=\gamma_w+r_u(\gamma-\gamma_w)$ must be added to the soil thrust. The fluid weight in front of the wall is $\gamma_{eq,front}$ = 5 kN/m^2 and behind the wall it is $\gamma_{eq,back}$= 4,5 kN/m^2. The hydrostatic thrusts cause by the excess pore water pressure can be calculated as follows:

$$U_{dyn,epwp,front} = \frac{1}{2}\gamma_{eq,front}H^2 = \frac{1}{2}*5*(11)^2 = 303kN/m$$

$$U_{dyn,epwp,back} = \frac{1}{2}\gamma_{eq,back}H^2 = \frac{1}{2}*4{,}5*(33{,}52)^2 - \frac{1}{2}*4{,}5*(0{,}52+1{,}5)^2 = 2519kN/m$$

Figure I-14 shows an illustration of the dynamic earth pressure thrusts and the equivalent hydrostatic thrust due to excess pore pressure and its point of application.

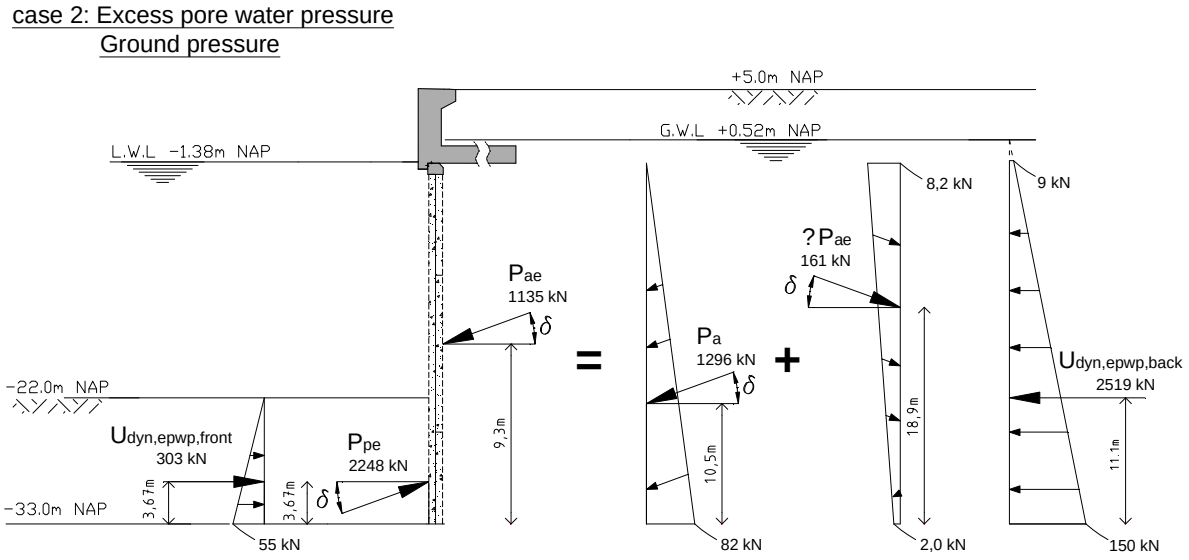

Figure I-14 Ground pressure and excess pore water pressure for case 2

Surcharge load

Just like case 1, the backfill behind the relieving platform and above NAP-1,5m can be schematized as surcharge load as shown in Figure I-5. The impact of this one-sided limited surcharge load on the wall is estimated using the method created by Ohde **Error! Reference source not found.** which is illustrated in Figure I-6. Forces acting on the wall due to of surcharge load and own weight behind the relieving structure are shown in Figure I-15

Crane load

The landside crane load is schematized as a two-sided limited distributed load with a width of the crane rail foundation of 3,5m and a loading of the crane load divided by the width. The total extra horizontal thrust on the wall due the presence of the two-sided limited distributed crane load can be determined using the method shown in Figure I-8 **Error! Reference source not found.**.

Thrust acting on the wall due to the landside crane load is shown in Figure I-16.

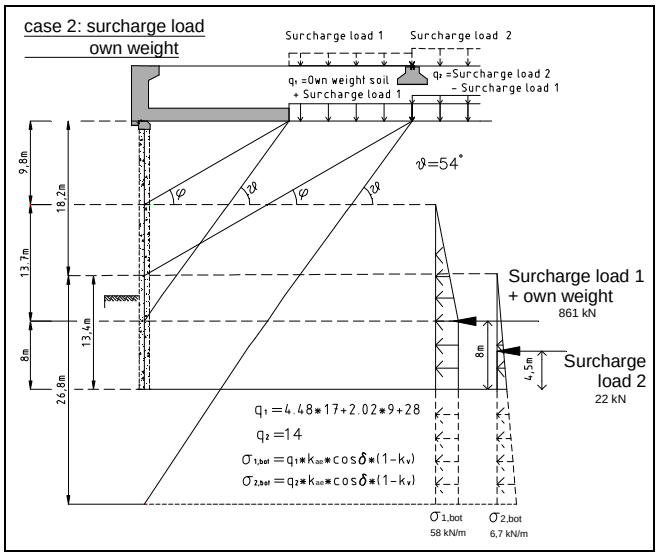

Figure I-15 Horizontal ground pressure as result of surcharge load and own weight behind relieving structure case 2

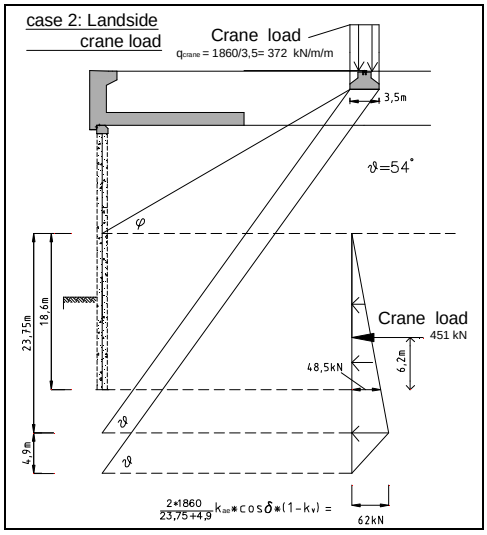

Figure I-16 Horizontal ground pressure as result of landside crane case 2

I.2.2 Calculation case 2

Force equilibrium

By making use of the horizontal force equilibrium the anchor force (MV pile) can be determined. This is done by summing up the horizontal forces determined in section I.2.1. Forces coming from the relieving platform are neglected during this pseudo static analysis.

$$\begin{aligned} F_{MVpile} &= -U_{stat,sea,front} - U_{stat,ground,front} + U_{stat,ground,back} + U_{dyn,sea,front} + U_{dyn,ground,front} + U_{dyn,ground,back} \\ &\quad - P_{pe} + P_{ae} - U_{dyn,epwp,front} + U_{dyn,epwp,back} + F_{surch\,arg\,e,1} + F_{surch\,arg\,e,2} + F_{crane} \\ &= -2126 - 2873 + 5598 + 207 + 0 + 0 - 2248\cos\delta + 1135\cos\delta - 303 + 2519 + 861 + 22 + 451 \\ &= 3310 kN/m \end{aligned}$$

The result of this first estimation shows that the MV pile has a tension force of 3310kN/m. When the wall is penetrated deep enough into the ground it can be assumed as an inclined wall. In this situation, ground will not be fully mobilized which result in less passive earth pressure and more active pressure. Passive ground may even turn into active ground and vice versa.

To see if the diaphragm wall is deep enough the minimum required depth of the sheet pile penetration is determined. By summing up the driving forces and the resisting forces at the point where the MV pile is connecting the diaphragm wall and equalling it to zero, the minimum required depth penetration of the wall can be determined. Table I-5 summarizes the horizontal force components acting on the diaphragm wall as shown in Figure I-17 and are expressed in terms of the generalized dimensions D_1 and D_2, which is respectively the distance between the connection of the MV pile to the seabed and the distance from the seabed to the penetration depth of the wall.

Equilibrium of moments about the elevation of the MV pile is required to find the needed penetration depth. By multiplying the horizontal force and its distance to the MV pile the bending moment for each separate force component can be determined. By summing up these separate bending moments and equal it to zero the equilibrium of moment is achieved.

$$\sum M_{MV\,pile} = 0 =$$
$$U_{static} \cdot y_{static} - U_{dyn.epwp.front} \cdot y_{dyn.epwp.front} + U_{dyn.epwp.back} \cdot y_{dyn.epwp.back} +$$
$$U_{dyn.sea.front} \cdot y_{dyn.sea.front} + P_{ae} \cdot y_{ae} - P_{pe} \cdot y_{pe} + F_{surch.1} \cdot y_{surch.1} + F_{surch.2} \cdot y_{surch.2} + F_{crane} \cdot y_{crane}$$

From this equilibrium it follows that the minimum required wall penetration needs to be D_2 = 17,6m which is larger than the existing penetration depth of 11m. The diaphragm wall will slip away from

below resulting in an unstable situation. The quay wall cannot function anymore and no further calculation where performed any further.

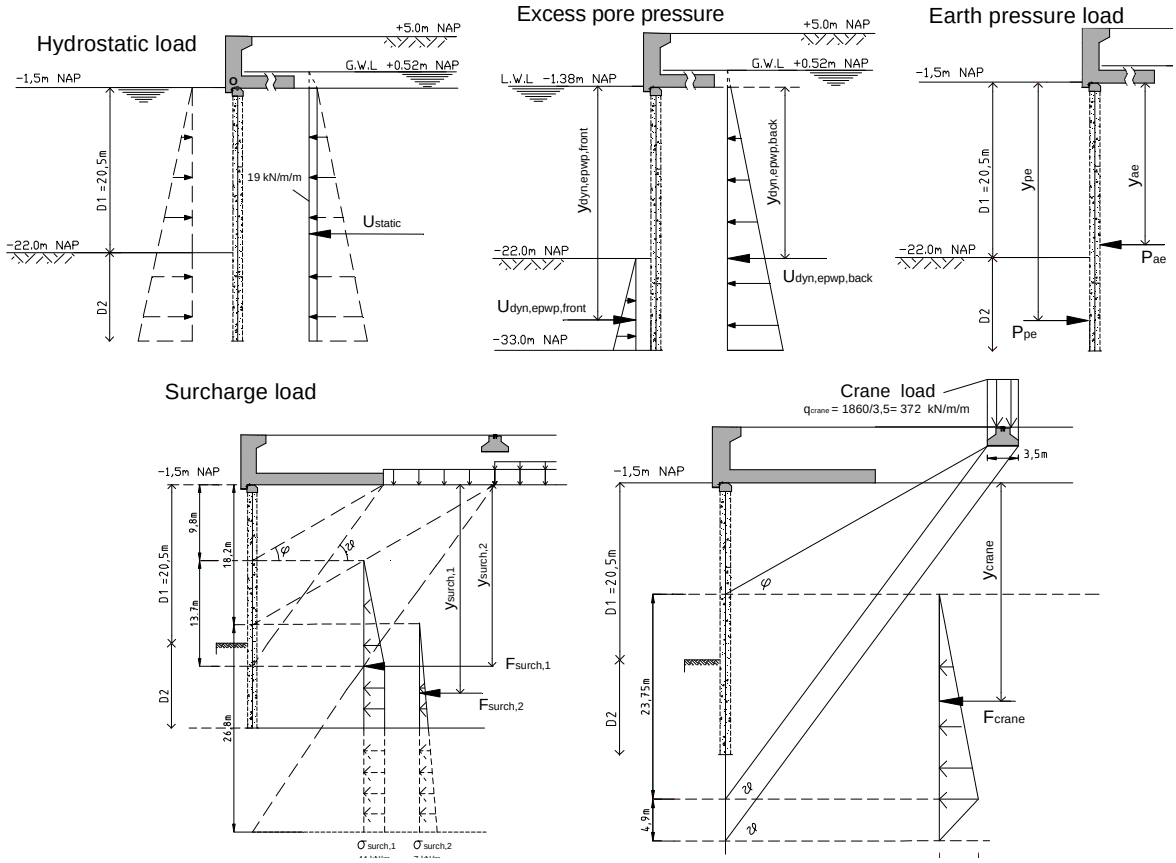

Figure I-17 Horizontal force components on diaphragm wall with unknown penetration depth case 2

Type of loading	Horizontal force [kN/m]	Distance to MV Pile (y_n) [m]
U_{static}	$(0.52 + 1.38)\cdot 10\cdot(D_1 + D_2)$	$0.5(D_1 + D_2)$
$U_{dyn,epwp,front}$	$\frac{1}{2}(D_2^2)\cdot y_{eq.front}$	$\frac{2}{3}D_2 + D_1$
$U_{dyn,epwp,back}$	$\frac{1}{2}y_{eq.back}\cdot(D_1 + D_2 + 2.02)^2 - \frac{1}{2}y_{eq.back}\cdot 2.02^2$	$\frac{2}{3}\cdot(D_1 + D_2)$
P_{pe}	$\frac{1}{2}k_{pe}\cdot\gamma_{eff1.p}\cdot(\lvert D_2\rvert)^2\cdot(1 - k_v)\cdot\cos(\delta)$	$\frac{2}{3}D_2 + D_1$
P_{ae}	$\frac{1}{2}k_{ae}\cdot\gamma_{eff1.a}\cdot(D_1 + \lvert D_2\rvert)^2\cdot(1 - k_v)\cdot\cos(\delta)$	$\frac{P_a\cdot\frac{2}{3}(D_1 + \lvert D_2\rvert) + \Delta P_{ae}\cdot 0.6\cdot(D_1 + \lvert D_2\rvert)}{P_{ae}}$
$F_{surch,1}$	$\frac{1}{2}\cdot 58\cdot 13.7 + (D_2 - 3)\cdot 58$	$\frac{\left(\frac{2}{3}\cdot 13.7 + 9.8\right)\cdot\left(\frac{1}{2}\cdot 58\cdot 13.7\right) + \left(\frac{D_2 - 3}{2} + D_1 + 3\right)\cdot(D_2 - 3)\cdot 58}{F_{surch.1}}$
$F_{surch,2}$	$\frac{(D_2 + 2.4)^2\cdot 6.7}{31.5}\frac{1}{2}$	$(D_2 + 2.4)\cdot\frac{2}{3} + 20.5 - 2.4$
F_{crane}	$\frac{1}{2}\cdot\frac{(D_2 + 7.6)^2\cdot 62}{23.75}$	$(D_2 + 7.6)\cdot\frac{2}{3} + 20.5 - 7.6$

Table I-5 Horizontal force components and distance to MV pile for case 2

I3 Case 3 (Liquefied backfill)

This analysis, describes as case 3, assumes a fully liquefied backfill. Just like case 1 and case 2, an earthquake acceleration of 0,5 m/s^2 is chosen. Assumed was that no liquefaction occurs in front of the wall. Here, a generation of 50% excess pore water is generated just like case 2. Therefore, the forces acting in front of the wall are the same as case 2.

I.3.1 Loads case 3

The static and additional seismic forces during an earthquake are determined in this section for case 3. The structure will be calculated per running meter. In the case of a liquefied backfill, soil behaves like a heavy fluid with an equivalent unit weight of $\gamma_{LF} = \gamma_{saturated\ sand}$.

Static water pressure
No liquefaction was assumed in front of the diaphragm wall. The static water pressure in front of the quay wall stays the same as case 2. On the contrary, saturated soils behind the quay wall are assumed to be liquefied. This means that they behave like a heavy fluid. An equivalent hydrostatic thrust based on a fluid of unit weight γ_{LF} is replacing the ground pressure thrust and is determined as follows:

$$LF_{hydrostatic} = \frac{1}{2}\gamma_{LF} H^2 = \frac{1}{2} * 19 * (33{,}52)^2 = 10674 kN/m$$

Dynamic water pressure
The dynamic water pressure for the free standing water outboard is the same as calculated for case 1 and case 2 while for the saturated backfill soil in front of the wall it becomes zero just like case 2. Behind the quay wall, soil behaves like a free standing heavy fluid. Dynamic response of this free standing heavy fluid can be determined using the Westergaard's solution mentioned in section 5.4.1.

$$LF_{hydrodynamic} = \frac{7}{12} k_h \gamma_{LF} H^2 = \frac{7}{12} * 0{,}067 * 19 * (33{,}52)^2 = 834 kN/m$$

Dynamic ground pressure
Passive earth pressure is the same like case 2. No active earth thrust will act on the wall because the soil behind the wall is fully liquefied.

Surcharge load and crane load
No cranes or surcharge load is present due to the liquefied backfill. Objects on the surface behind the quay wall will sink into the heavy fluid or just float on top of it.

The horizontal force components acting on the diaphragm wall due to water and earth pressure for case 3 is shown in ***Figure I-18***

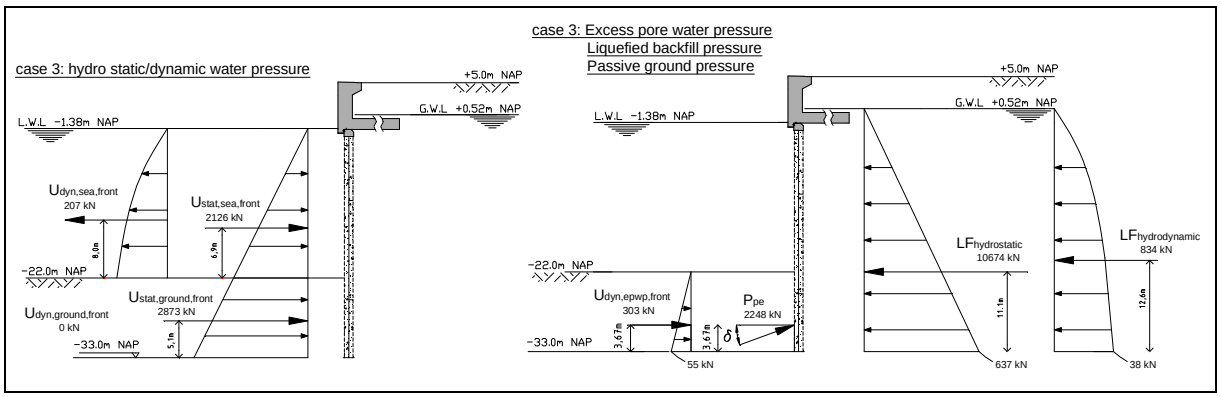

Figure I-18 Horizontal force components on diaphragm wall for case 3

I.3.2 Calculation case 3

Force equilibrium
By making use of the horizontal force equilibrium the anchor force (MV pile) can be determined. This is done by summing up the horizontal forces determined in section I.2.1. Forces coming from the relieving platform are neglected during this pseudo static analysis.

$$F_{MVpile} = -U_{stat,sea,front} - U_{stat,ground,front} + U_{dyn,sea,front} + U_{dyn,ground,front} - P_{pe} - U_{dyn,epwp,front} + LF_{hydrostatic} + LF_{hydrodynamic}$$
$$= -2126 - 2873 + 207 + 0 - 2248\cos\delta - 303 + 10674 + 840 = 4306 kN/m$$

The result of this first estimation shows that the MV pile has a tension force of 4306kN/m. When the wall is penetrated deep enough into the ground it can be assumed as an inclined wall. In this situation, Ground will not be fully mobilized which means that the passive earth pressure thrust becomes even less. Passive ground will even turn into active ground and vice versa.

To see if the diaphragm wall is deep enough the minimum required depth of the sheet pile penetration is determined. By summing up the driving forces and the resisting forces at the point where the MV pile is connecting the diaphragm wall and equalling it to zero, the minimum required depth penetration of the wall is determined. Table I-5 summarizes the horizontal force components acting on the diaphragm wall as shown in Figure I-19 and are expressed in terms of the generalized dimensions D_1 and D_2, which is respectively the distance between the connection of the MV pile to the seabed and the distance from the seabed to the penetration depth of the wall.

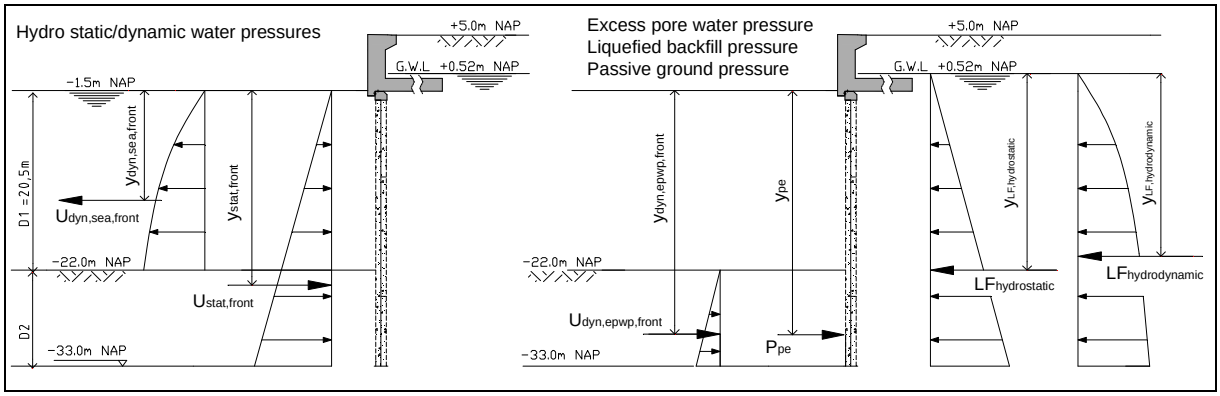

Figure I-19 Horizontal force components on diaphragm wall with unknown penetration depth case 3

Type of loading	Horizontal force [kN/m]	Distance to MV Pile (y_n) [m]
$U_{static,front}$	$\frac{1}{2}\gamma_w\left(D_1 + D_2\right)^2$	$\frac{2}{3}\left(D_1 + D_2\right)$
$U_{dyn.sea.front}$	$\int_0^{20.5} \frac{7}{8} k_h \gamma_w \cdot \sqrt{y \cdot \left(D_1 + \lvert D_2 \rvert\right)}\, dy$	12,5
$U_{dyn,epwp,front}$	$\frac{1}{2}\left(D_2^2\right) \cdot y_{eq.front}$	$\frac{2}{3}D_2 + D_1$
P_{pe}	$\frac{1}{2}k_{pe} \cdot \gamma_{eff1.p} \cdot \left(\lvert D_2 \rvert\right)^2 \cdot \left(1 - k_v\right) \cdot \cos(\delta)$	$\frac{2}{3}D_2 + D_1$
$LF_{hydrostatic}$	$\frac{1}{2} \cdot \gamma_{LF} \cdot \left(D_1 + D_2 + 2.02\right)^2$	$\frac{2}{3}\left(D_1 + D_2 + 2.02\right) - 2.02$
$LF_{hydrodynamic}$	$\frac{7}{12} \cdot k_h \gamma_{LF} \cdot \left(D_1 + D_2 + 2.02\right)^2$	$0.6 \cdot \left(D_1 + D_2 + 2.02\right) - 2.02$

Table I-6 Horizontal force components and distance to MV pile for case 3

Equilibrium of moments about the elevation of the MV pile is required to find the needed penetration depth. By multiplying the horizontal force and its distance to the MV pile the bending moment for each separate force component can be determined. By summing up these separate bending moments and equal it to zero the equilibrium of moment is achieved.

$$\sum M_{MV\ pile} = 0 =$$
$$-U_{static.front} \cdot y_{static.front} - U_{dyn.epwp.front} \cdot y_{dyn.epwp.front} + U_{dyn.sea.front} \cdot y_{dyn.sea.front} - P_{pe} \cdot y_{pe} +$$
$$LF_{hydrostatic} \cdot y_{LFhydrostatic} + LF_{hydrodynamic} \cdot y_{LFhydrodynamic}$$

From this equilibrium it follows that the minimum required wall penetration needs to be D_2 = 19.6m which is larger than the existing penetration depth of 11m. The diaphragm wall will slip away from below resulting in an unstable situation. Notion must be made that when the backfill is liquefied, the MV pile will not work properly. Hence, the quay wall will fall over. The quay wall cannot function anymore and no further calculation where performed any further.

Appendix J dynamic calculation Diaphragm wall Msheet

J1 Choice of model

Basically two options are available in Msheet: K_a, K_0, K_p model and the C, phi, delta (or Cullmann) model. Both models do not have a seismic module which implement earthquake loadings. Hence, seismic loadings should be added manually in Msheet. The K_a, K_0, K_p model in Msheet allows manual changing of the earth pressure coefficient while for the C, phi, delta model static earth pressure coefficient is calculated and can not be changed. For that reason is the K_a, K_0, K_p model preferred over the C, phi, delta model and is used for this seismic analysis to replace the Static earth pressure coefficients (k_a, k_p) by the seismic earth pressure coefficient (k_{ae}, k_{pe}) determined using the (modified) M-O method.

J2 Schematization of the geometry

The geometry of the Msheet model is based on design drawing of the Euromax quay wall (Figure 2-3) and the soundings at quay wall section 1(Figure 7-4). Ground level is founded at NAP+5m and the bed level is NAP-22m. The diaphragm wall reaches a depth of NAP-33m with a thickness of 1,2m. A spring support was placed at NAP-1,5m to simulate the anchor force of the MV-pile. Also a moment load was placed at NAP-1,5m due to the eccentricity between the relieving floor and diaphragm wall. By doing so, the forces coming from the relieving floor are added to the diaphragm wall whereby the relieving floor and it loads can be leaved out in the geometry. The outside water level is kept at NAP-1,38m while the ground water level is set at NAP+0,52m. These are the normative water levels as mentioned in appendix F. The surface is kept flat and horizontal at a level of NAP-1,5m. This is needed to be able to make use of the K_a, K_0, K_p model. Schematisation of the Msheet geometry is illustrated in Figure J-1.

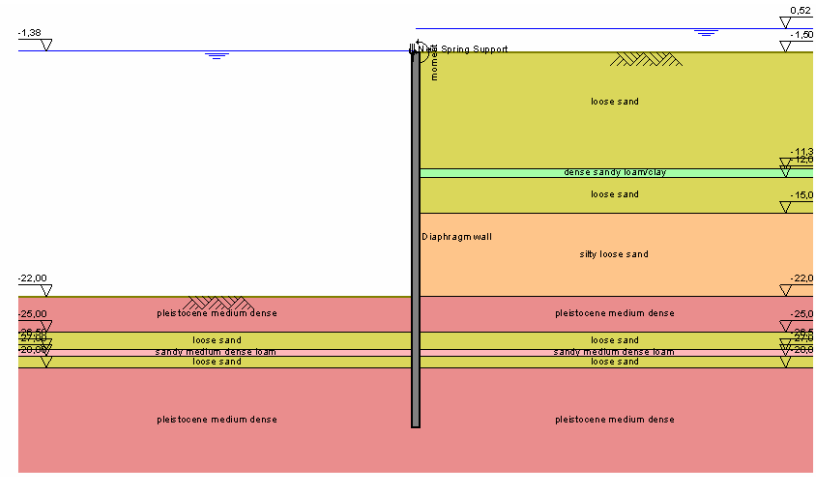

Figure J-1 schematized geometry in Msheet

J3 Soil profile and parameters

The normative soil profile to liquefaction will be used. This soil profile is determined in section 7.3 and is located at the eastern side of the Euromax terminal. Soil parameters for this particular profile are determined by BAM and were used during this analysis [G.1]. The parameters are shown in Table G-1.

J4 Material properties

The flexural rigidity of the diaphragm wall plays an important role in distributing the loads. Delta marine consultants has done a specific analysis in determining the flexural rigidity of the wall by using the method that was described in the VBC based on quasi-linear elasticity theorem [G.2]. By applying MN-Kappa diagrams a more accurate flexural rigidity was found, which is $EI_{diaphragm\ wall} = 1{,}88*10^6$ kNm^2 [G.3]. The axial spring stiffness was determined using a framework calculation for a cross-section of the quay wall in which horizontal and vertical unit loads were applied. This calculation was also done by Delta marine consultants which results in axial spring stiffness of 27000 kN/m/m [G.3]. Both the flexural rigidity and axial spring stiffness determined by BAM was used during this analysis.

J5 Calculation

Case 1

Earth pressure coefficients are determined using the M-O method and are listed in Table J-1. Seismic point loads applied in Msheet are determined Appendix I and listed in Table J-2.

Soil type	k_{ae}	k_{pe}
medium dense sand	0,35	6,85
loose sand	0,39	5,38
dense sandy loam/clay	0,43	4,47
silty loose sand	0,42	4,84
pleistoscene medium dense	0,33	8,78
sandy medium dense loam	0,43	4,30

Table J-1 Earth pressure coefficients for case 1 per soil layer

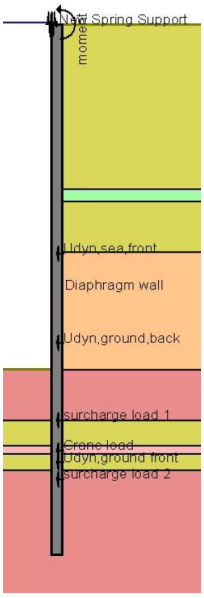

Type of loading	Horizontal force [kN/m]	Elevation NAP [m]
$U_{dyn,sea,front}$	207	-15,1
$U_{dyn,ground,front}$	131	-27,5
$U_{dysn,ground,back}$	310	-20,4
$F_{surch,1}$	653	-25
$F_{surch,2}$	23,5	-28,5
F_{crane}	284	-26,8

Table J-2 Seismic point loads for case 1

The seismic forces acting on the relieving floor are determined Appendix F2. From this, the normal forces on the piles and wall can be known by making use of Table F-3. The diaphragm wall and relieving floor is not supported eccentricly which result in an eccentric moment on top of the diaphragm wall. By applying the eccentric moment and the loads into the Msheet model, the horizontal spring force can be determined which is equal to the horizontal component of the normal stress of the MV-pile. Notion must be made that the normal pile and wall stresses were determined based on bearing stresses per 100 kN/m. This bearing stress needs to be equal to the spring force. Therefore interation needs to be performed in finding the right bearing stress which corresponds to the horizontal spring force calculated using Msheet.

After a couple of iteration a matching bearing force of 934kN/m was found. Stresses within the diaphragm wall due to this bearing force can be found at Table J-3 and Figure J-2. The most important stresses are listed below:

Maximum axial force MV-pile = F_{MV} = 1339 kN/m
Maximum bending moment = M_{Msheet} = -8424 kNm/m

During earthquake							**new values**			
Loads case 1	F_{DW}* kN/m	F_{MV}* kN/m	F_{VP}* kN/m	M_{MV}* kNm/m	Combi factor	Load factor	F_{DW} kN/m	F_{MV} kN/m	F_{VP} kN/m	M_{MV} kNm/m
Own weight relieving platform	-574	-69	-366	-207	1	1	-574	-69	-366	-207
Crane load in operation	-1731	23	-110	-623	0,7	1	-1212	16	-77	-436
Crane load during storm	-1449	271	-14	-522			0	0	0	0
Bolder force	-147	359	113	-53	0,7	1	-103	252	79	-37
Fender force	341	-424	-43	123			0	0	0	0
Groundwater +0,52 NAP	9	79	108	3	1	1	9	79	108	3
Ground pressure +0,52 NAP	-335	-211	-895	-121	1	1	-335	-211	-895	-121
Seawater -1,38 NAP	7	0	0	2	1	1	7	0	0	2
Surcharge load above platform	-287	-70	-451	-103	0,7	1	-201	-49	-316	-72
Bearing stress diaphragm wall*	-100	141	0	-36	9,34		-934	1321	0	-336
*wall and pile forces due to unit bearing stresses diaphragm wall per 1					Total		-3343	1339	-1467	-1203

Table J-3 Wall and pile forces for load case 1

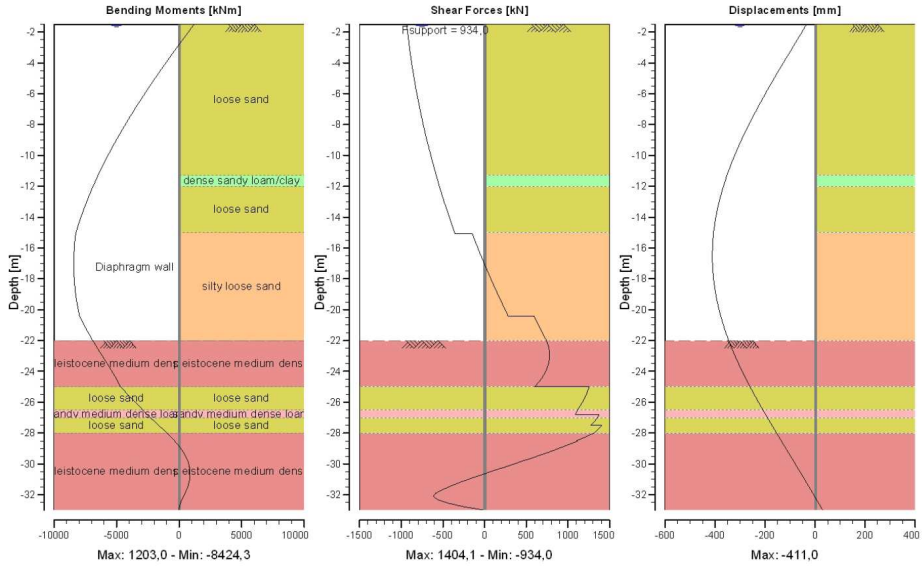

Figure J-2 Msheet results for load case 1: Bending moment/Shear force/ Displacement of diaphragm wall

Arching effects

Msheet does not account arching effects during the calculations. For an anchored quay wall, the Msheet approach will lead to incorrect ground pressures. The effects of arching are:

- Decrease of active ground pressure near the maximum deflection of the wall
- Increase of ground pressure near the anchor

According to CUR166 [G.4] a decrease of 33% of the maximum bending moment caused by the ground pressure and an increase of 15% to the spring forces ($F_{support,ground}$) should be applied to include the arching effect. Stresses caused by the ground pressure can be obtained by using equal waterlevels in front and behind the quay wall. By doing so the water pressures will be neutralized and only the stresses due to ground pressures are left. Result of the Msheet calculation with equal water level are shown in Figure J-3.

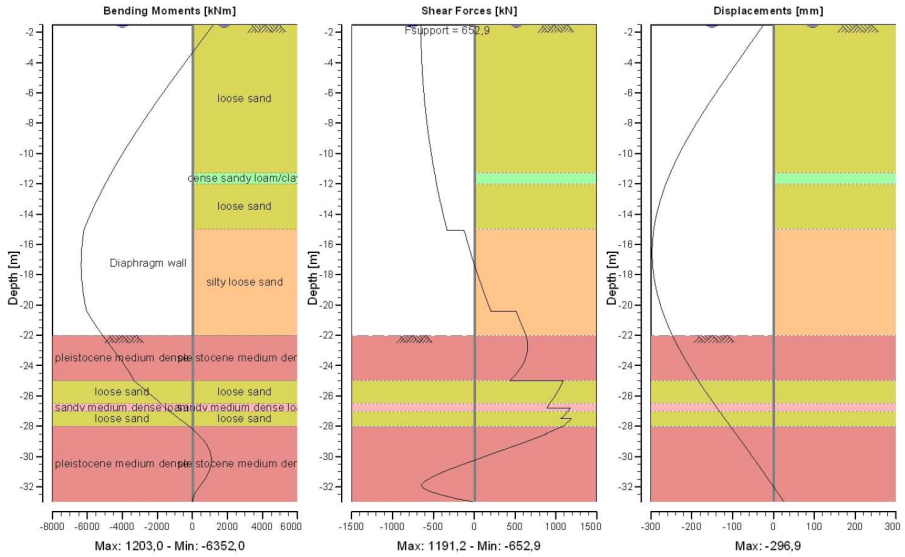

Figure J-3 Msheet results for load case 1: Bending moment/Shear force/ Displacement ofdiaphragm wall with equal water levels on both side of the quay wall

The moment reduction, M_{arch}, and the spring force addition, F_{arch}, due to arching effects becomes:

$$M_{arch} = M_{Msheet,ground} * 0{,}33 = 6352 * 0{,}33 = 2096 kNm/m$$

$$F_{arch} = F_{\sup port,ground} * 0{,}15 = 652{,}9 * 0{,}15 = 98 kN/m$$

Second order effect

Another effect Msheet does not account for is the second order effect. As a result of vertical force (F_{DW}) acting on top of the diaphragm wall, second order effect occurs. This will lead to an incremental bending moment, M_{2nd}. This incremental bending moment can be calculated by multiplying the F_{DW} with the eccentricity, e, and the enlargement factor, n/(n-1). The eccentricity, e, is the maximum displacement of the diaphragm wall (δ_{max}) minus the mean displacement between NAP-1,5m (δ_{kop}) and NAP-33m (δ_{ppn}) as shown in Figure G-4. The enlargement factor is calculated by determing the Euler buckling factor, n. Where n is the Euler buckling force, F_{eul} devided by F_{DW}.

$$F_{eul} = \pi^2 EI / l_{eul}^2 = \pi^2 * 1{,}868 * 10^6 / 22^2 = 38100 kN$$

$$n = F_{eul} / F_{DW} = 38100 / 3343 = 11{,}4$$

$$M_{2nd} = F_{DW} \cdot e \cdot \frac{n}{n-1} = 3343 * 0{,}4 * \frac{11{,}4}{11{,}4-1} = 1466 kNm/m$$

Where

F_{DW} = Normal force diaphragm wall = 3343 kN
EI = $EI_{diaphragm\ wall}$ = $1{,}868*10^6$ kN/m^2
L_{eul} = buckling length assumed 22 m
e = 0,4m

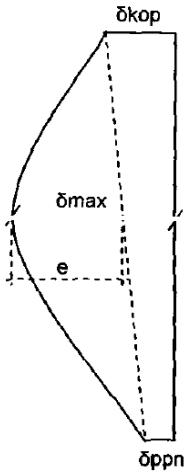

Figure J-4 illustration of eccentricity and displacement of wall

The maximum moment of the diaphragm wall including arching and second order effect for load combination 1 is :

$$M_{\max} = M_{Msheet} - M_{arch} + M_{2nd} = 8424 - 2096 + 1466 = 7794 kNm/m$$

This is located at an elevation of NAP-1643m.

The maximum axial force of the MV-pile include arcing for load combination 1 is:

$$F_{MV,\max} = F_{MV} + F_{arch} = 1339 + 98 = 1437 kN/m$$

Case 2

Earth pressure are determined using the M-O method and are listed in Table J-4. Seismic point loads applied in Msheet are determined Appendix I and listed in Table J-5.

Soil type	k_{ae}	k_{pe}
medium dense sand	0,47	5,97
loose sand	0,52	4,61
dense sandy loam/clay	0,59	3,73
silty loose sand	0,58	4,03
pleistoscene medium dense	0,46	7,56
sandy medium dense loam	0,59	3,61

Table J-4 Earth pressure coefficients for case 2 per soil layer

Type of loading	Horizontal force [kN/m]	Elevation NAP [m]
$U_{dyn,sea,front}$	207	-15,1
$U_{dyn,epwp,front}$	-303	-29,3
$U_{dysn,epwp,back}$	2519	-21,9
$F_{surch,1}$	861	-25
$F_{surch,2}$	22	-28,5
F_{crane}	451	-26,8

Table J-5 Seismic point loads for case 2

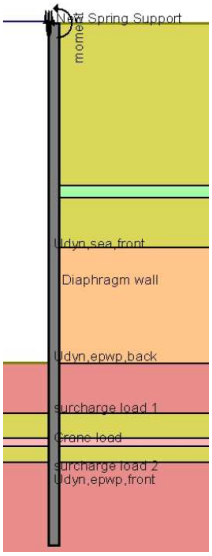

The total pressure (earth + water pressure) needs to stay equal. Increase of 50% excess pore water pressure results in a 50% decrease of effective ground pressure. Therefore, the saturated unit weight has been decreased by 50% of the effective unit weight.

After adding the seismic point loads and decreasing of the saturated unit weight Msheet gives an error. This indicates that the diaphragm wall becomes unstable which corresponds to failure of the quay wall.

Case 3

Earth pressure are determined using the M-O method and are listed in Table J-6. Seismic point loads applied in Msheet are determined Appendix I and listed in Table J-7.

Soil type	k_{ae}	k_{pe}
medium dense sand	0,35	6,85
loose sand	0,39	5,38
dense sandy loam/clay	0,43	4,47
silty loose sand	0,42	4,84
pleistoscene medium dense	0,33	8,78
sandy medium dense loam	0,43	4,30

Table J-6 Earth pressure coefficients for case 3 per soil layer

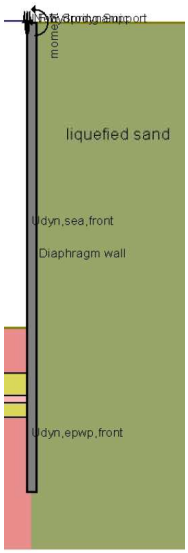

Type of loading	Horizontal force [kN/m]	Elevation NAP [m]
$U_{dyn,sea,front}$	207	-15,1
$U_{dyn,epwp,front}$	-303	-29,3
$U_{dysn,epwp,back}$	2519	-21,9
$LF_{hydrodynamic}$	834	-20,4

Table J-7 Seismic point loads for case 3

To simulate liquefaction, groundwater level behind the wall is leaved out and the active, passive and neutral earth pressure coefficient is set to 1. Msheet gives an error during the calculation. This indicates that the diaphragm wall becomes unstable which corresponds to failure of the quay wall.

Appendix K Dynamic calculation Plaxis diaphragm wall

The procedure to perform a dynamic analysis with Plaxis is somehow similar to that for a static analysis. This entails creation of a geometry model, mesh generation, initial stress generation, defining and executing calculation and evaluation of results. In addition to the static model, the dynamic model makes use of the Plaxis dynamic analysis module to analyze the vibration of soil. In modeling the dynamic response of a soil structure, the inertia of the subsoil and the time dependence of the load are considered. Also, damping due to material and geometry is taken into account. Initially the HSsmall model is utilized for the simulation of the dynamic effects.

K1 Dynamic model Plaxis

The same Plaxis model like the static Plaxis calculation is used during this dynamic calculation, see section section H1.

K2 Dynamic loading

The earthquake is modeled by imposing a prescribed acceleration at the bottom boundary resulting to shear waves that propagate upwards. The vertical component of the prescribed displacement is kept zero which, according to the Eurocode 8, can be neglected for sheet pile walls. The vertical edges have fixed displacements in horizontal direction and are closed, to allow excess pore pressure to be present. The boundary at the base of the geometry is located in the Pleistocene sand layer at NAP-70m and is set at full fixity, since settlements may be assumed to be very small here. Special boundary conditions have to be defined to account for the fact that in reality the soil is a semi-infinite medium. Without these special boundary conditions the waves would be reflected on the model boundaries, causing perturbations. To avoid these reflections, absorbent boundaries are specified at the vertical boundaries. Plaxis has a convenient default setting to generate standard boundary conditions for earthquake loadings. In this way the boundary conditions as described above are automatically generated, see Figure K-1.

The above described boundary conditions are known in Plaxis as “standard earthquake boundaries”.

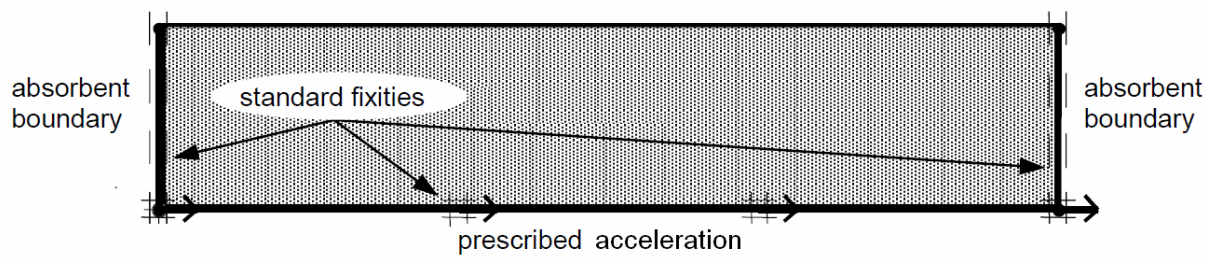

Figure K-1 Model with standard earthquake boundary conditions

Besides harmonic loading there is also the possibility to read data from digitized load signal. Variations of different real accelerograms of earthquakes are used for this analysis. These accelerograms varies in magnitude caused by different earthquakes and are recorded at different stations over the United States by the United States Geological Survey [K.1]. Inputted accelerograms are listed below.

Earthquake 1: ($a_{max} \approx 0{,}01g$) Earthquake 2: ($a_{max} \approx 0{,}02g$)

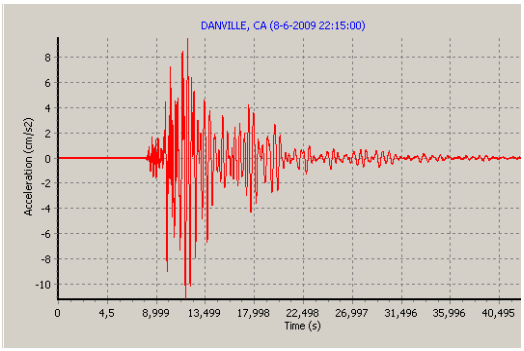

Earthquake 3: (a_{max} ≈ 0,03g)

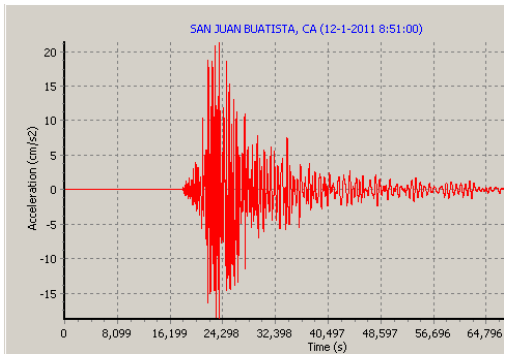

Earthquake 4: (a_{max} ≈ 0,04g)

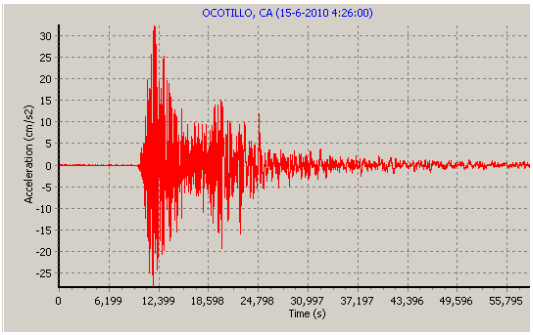

Earthquake 5: (a_{max} ≈ 0,05g)

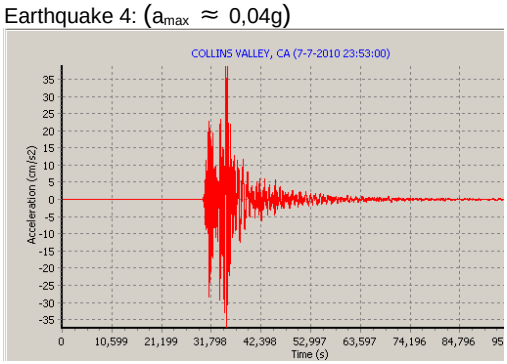

Earthquake 6: (a_{max} ≈ 0,06g)

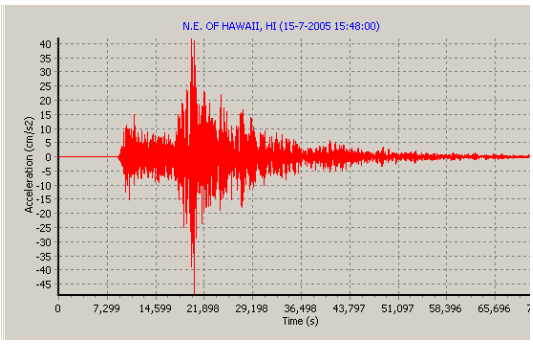

Earthquake 7: (a_{max} ≈ 0,07g)

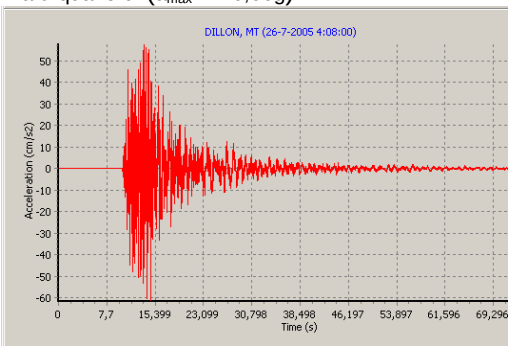

Earthquake 8: (a_{max} ≈ 0,08g)

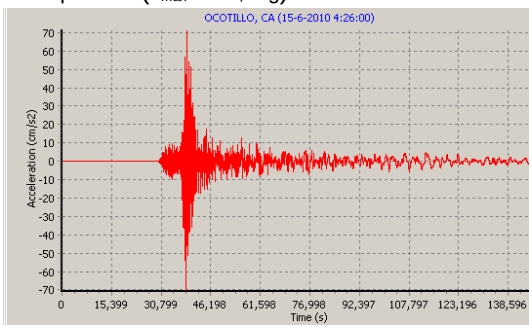

Earthquake 9: (a_{max} ≈ 0,09g)

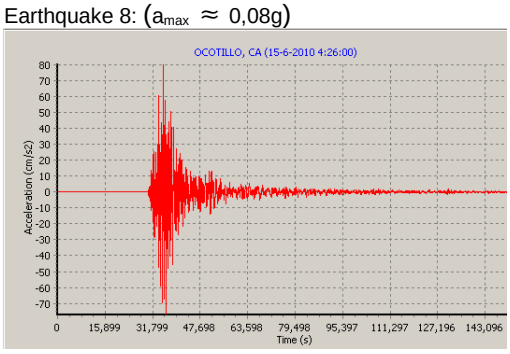

Earthquake 10: (a_{max} ≈ 0,10g)

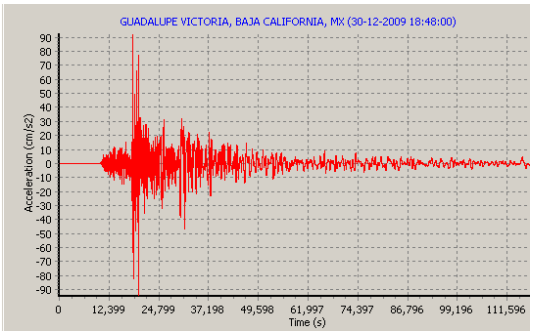

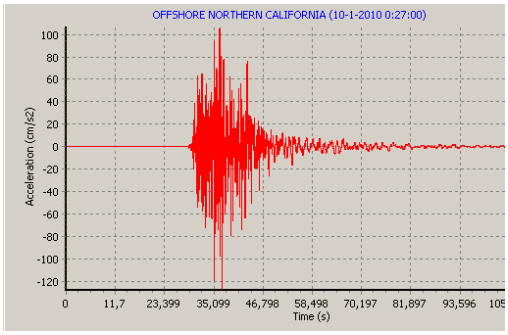

K3 Dynamic damping

It is well known fact that damping in a soil structure influence significantly the magnitude and shape of its response. However and despite the considerable amount of research work in this field, little have yet been achieved for the development of a commonly accepted procedure for damping parameter identification. Instead, for engineering purpose, some measures are made to account for the material and geometrical damping. A commonly used engineering parameter is the damping ratio ξ. This ratio is a dimensionless measure describing how oscillations in a system decay after a disturbance and is given as:

$$\xi = \frac{C}{C_{critical}} = \frac{C}{2\sqrt{KM}}$$

where:

ξ : damping ratio
C : damping of the system
K : stiffness of the system
M : mass of the system
$C_{critical}$: critical damping of the system $C_{critical} = 2\sqrt{KM}$

The value of the damping ratio ξ determines the behaviour of the system. A damped harmonic oscillator can be:

- Overdamped (ξ>1): the system returns to equilibrium without oscillating. Larger values of the damping ratio ξ return to equilibrium slower.
- Critically damped (ξ=1):the system returns to equilibrium as quickly as possible without oscillating.
- Underdamped (0< ξ <1): the system oscillates with the amplitude gradually decreasing to zero.
- Undamped (ξ=0): the system oscillates at its natural resonant frequency ω_0

The nature of soil damping in soils can be linked to the following phenomena:

- Non-linearity which governs the so called hysteretic damping controlled by the current shear strain level. This kind of material damping is absent or negligible at very small strains
- Viscosity of the soil skeleton (creep) which is relevant at very small strain rates

Hysteretic damping

Although the HSsmall model has not been designed specifically for dynamic applications, it does have capabilities to describe dynamic soil behaviour to some extend. The small-strain-stiffness formulation involves the degradation of the shear stiffness with the shear strain, and it takes into account that the high small-strain stiffness is regained upon load reversal. When subjected to cyclic shear loading, the HSsmall model will show typical hysteretic behaviour as shown in Figure K-2. This feature provides

damping in dynamic applications [K.2]. It should be noted that this damping is independent from the loading frequency, since this damping is purely based on the stress-strain relationship, which is time-independent.

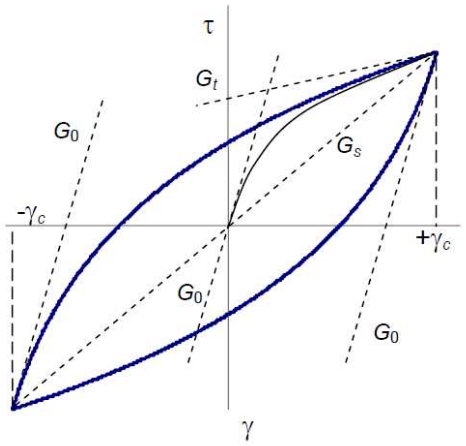

Figure K-2 Hysteretic behaviour in the HSsmall model of Plaxis

Viscosity of the soil skeleton/ Rayleigh damping

Material damping in soil is generally caused by its viscous properties, friction and the development of plasticity. However, In Plaxis the soil models do not include viscosity as such. Instead, a damping term is assumed, which is proportional to the mass and the stiffness of the system (Rayleigh damping), such that:

$$C = \alpha M + \beta K \qquad \text{Eq. K-1}$$

where:
α , β : Rayleigh coefficients

Rayleigh coefficient α is the parameter that determines the influence of the mass in the damping of the system. The higher the α value, the more the lower frequencies are damped. Rayleigh coefficient β is the parameter that determines the influence of the stiffness in the damping of the system. The higher the β value, the more the higher frequencies are damped.

The Rayleigh damping coefficients α and β can be determined from at least two given damping ratios ξ_i that correspond to two frequencies of vibration, $\omega_i = \sqrt{K/M}$. *Eq. K-2*

After substitution of Eq. K-1 into Eq. K-2, the relationship between α , β , ξ_i and ω_i can be presented as:

$$\alpha + \beta\omega_i^2 = 2\omega_i\xi_i \qquad \text{Eq. K-3}$$

With two damping ratio's known together with its frequencies of vibration, the Rayleigh damping coefficient α and β can be determined using the following equation:

$$\alpha = \frac{2\omega_1\omega_2\left(\xi_1\omega_2 - \xi_2\omega_1\right)}{\omega_2^{\,2} - \omega_1^{\,2}} \qquad \beta = \frac{2\left(\xi_2\omega_2 - \xi_1\omega_1\right)}{\omega_2^{\,2} - \omega_1^{\,2}} \qquad \text{Eq. K-4}$$

For the frequencies of vibration the upper and lower frequencies of earthquakes are used which varies between 1Hz and 10Hz. At the end of the earthquake the frequency can be lower (0,5 Hz), but the

acceleration are low and so not leading. Damping ratios corresponding to the above mentioned frequencies are assumed to be 5% (ξ_i =0,05) for the whole soil strata. Hence the following Rayleigh coefficients are computed.

$\alpha = 0{,}5712$

$\beta = 0{,}0014$

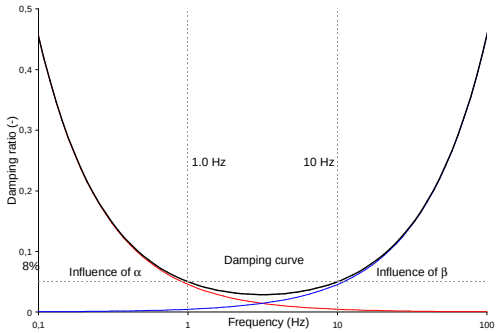

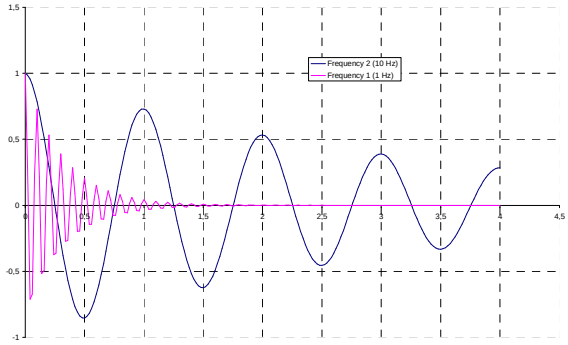

Rayleigh damping is frequency dependant and is only relevant at very small strains. Hysteretic damping in combination with Rayleigh damping gives a more realistic result compared to using hysteretic damping only, because now damping at very small strain is included.

K4 Simulating excess pore water and liquefaction in Plaxis

As the HSsmall model incorporates the loading history of the soil and a strain-dependent stiffness, it can, to some extent, be used to model cyclic loading. However, it does not incorporate a gradual softening during cyclic loading, so is not suitable for cyclic loading problems in which softening plays a role. Moreover, the HSsmall model does not incorporate the accumulation of irreversible volumetric straining nor liquefaction behaviour with cyclic loading.

By reducing the internal friction angle φ excess pore water and even liquefaction are simulated in Plaxis. Earth pressure coefficients are related to φ. Reduction of φ results in increase and decrease of active and passive earth pressure coefficient respectively. Active pressure behind the wall will increase by reducing φ which simulates the pressure increase due excess pore water generation and the heavy water during liquefaction.

Another important notice is that by reducing φ shear friction between grains is also decreasing and having a more liquid like behaviour which simulated the shear strain loss during excess pore water generation and/or liquefaction.

Assumption is made for the amount of excess pore water generation. No decrease in φ means no excess pore water pressure is generated. On the other hand when φ reach zero, it is assumed that the soil is fully liquefied. The development from no excess pore pressure to totally full liquefaction is assumed to be linear. From early calculations it is known that soil will liquefy at an earthquake acceleration of 0,3g. This results in the following expressions as shown in Table K-1.

Percentage of excess pore pressure	φ after reduction	Earthquake acceleration [m/s^2]
0 %	30	0,00g
16,7%	25	0,05g
33,3%	20	0,10g
50%	15	0,15g
66,7%	10	0,20g
83,3	5	0,25g
100%	0	0,30g

Table K-1 Assumed excess pore pressure generation and the corresponding phi reduction

K5 Construction method

The quay wall has been built in a certain way. To take the building sequence into account in Plaxis the option “staged construction” can be used. This option allows users to (de)activate weight, strength, stiffness and to change material properties or water pressures. Just like the static analysis, the diaphragm quay wall is created in 9 phases, see section H.2.1. For the purpose of dynamic analysis, a dynamic calculation phase is added. The function “update mesh” will not be used. This function allows the mesh to update after each phase calculation, which will lead to a more accurate second order effect. Since the deformations are very small which result in small second order effects this effect is negligible.

K6 Dynamic model output Plaxis

K.6.1 No excess pore water generation

Earthquake 1 (a=0,1 m/s^2):

Displacements

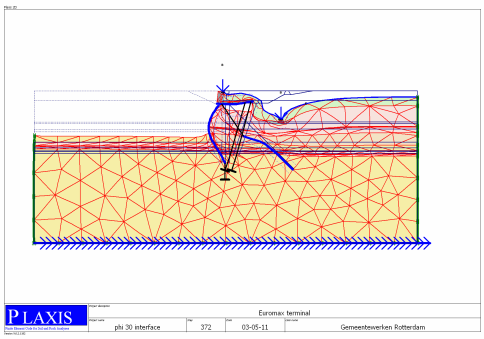

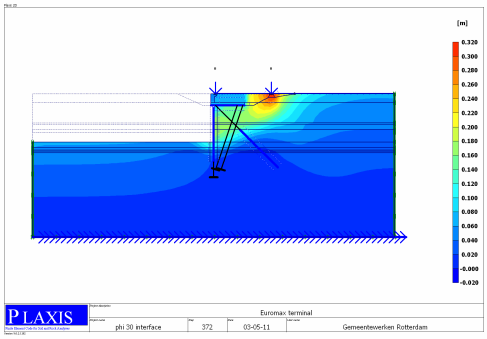

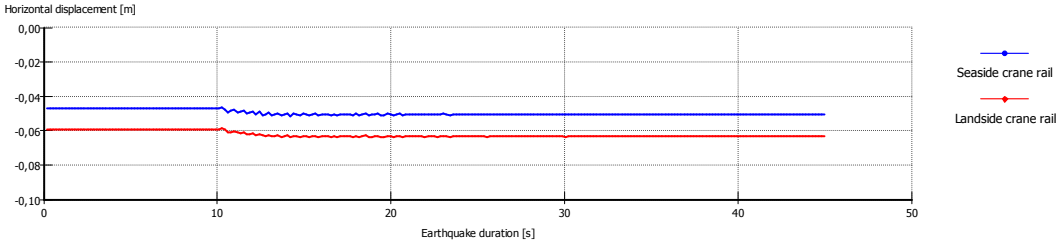

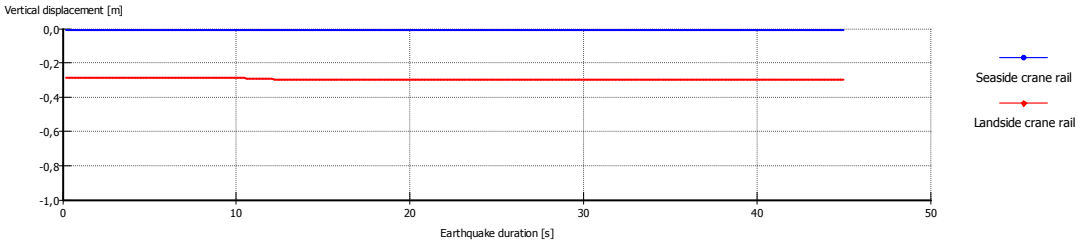

Plaxis Displacement	Hor. displacement After last phase	Vert. displacement After last phase
Seaside crane rail	-0,051 m	-0,007 m
Landside crane rail	-0,063 m	-0,298 m

Stresses

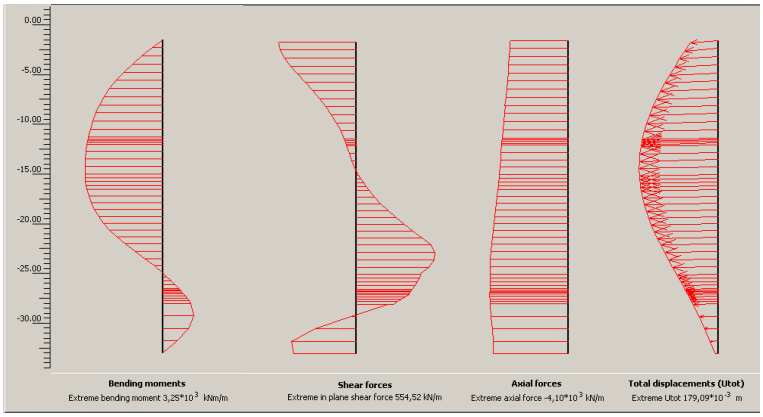

Plaxis Stresses	**Max. Axial force [kN/m]**	**Max. Bending moment [kNm/m]**
Diaphragm wall	-4100	3250
MV-pile	906	-

Earthquake 2 (a=0,2 m/s^2):

Displacements

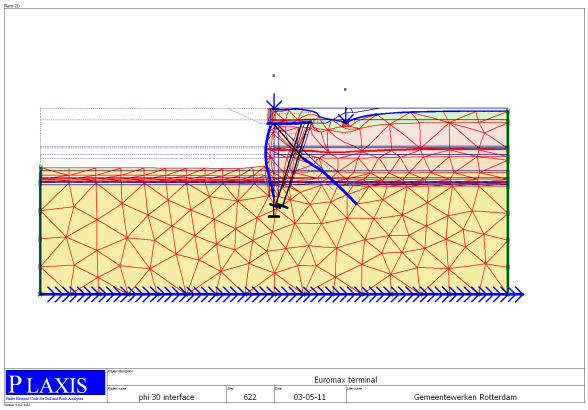

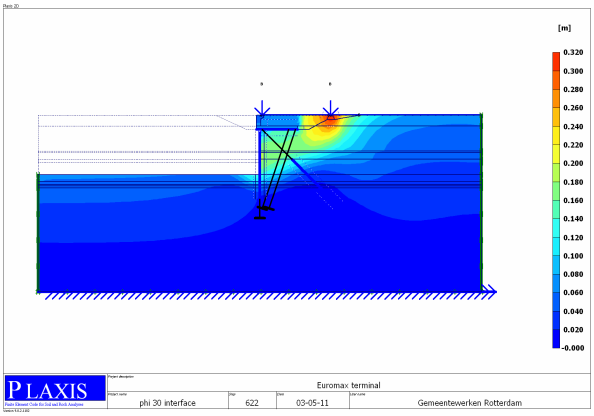

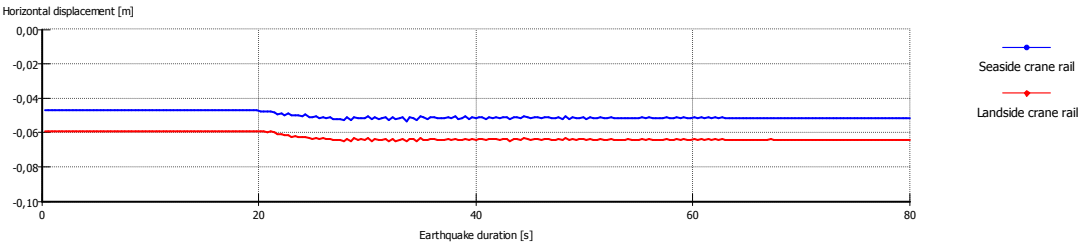

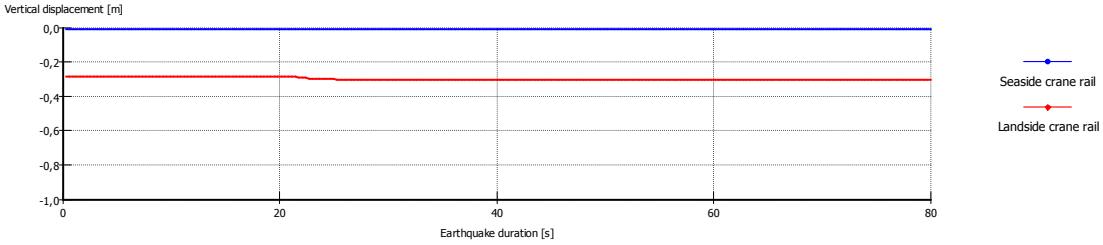

Plaxis Displacement	Hor. displacement After last phase	Vert. displacement After last phase
Seaside crane rail	-0,052 m	-0,008 m
Landside crane rail	-0,065 m	-0,304 m

Stresses

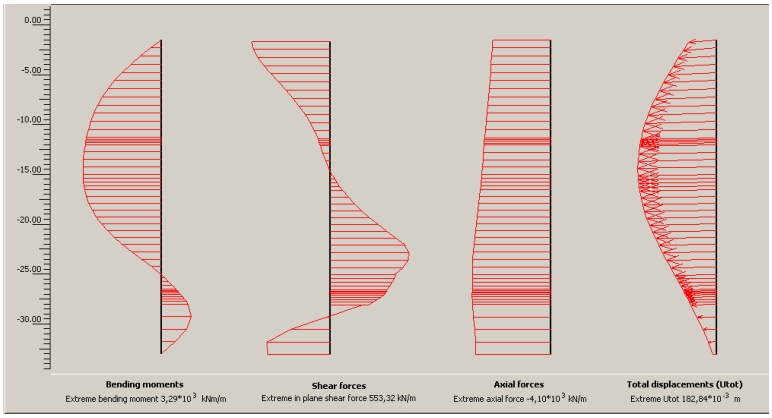

Plaxis Stresses	**Max. Axial force [kN/m]**	**Max. Bending moment [kNm/m]**
Diaphragm wall	-4100	3290
MV-pile	913	-

Earthquake 3 (a=0,2 m/s^2):

Displacements

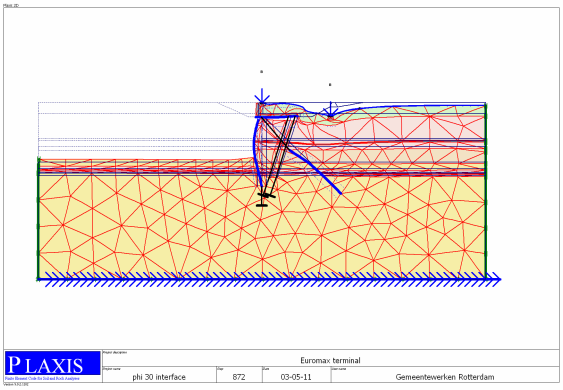

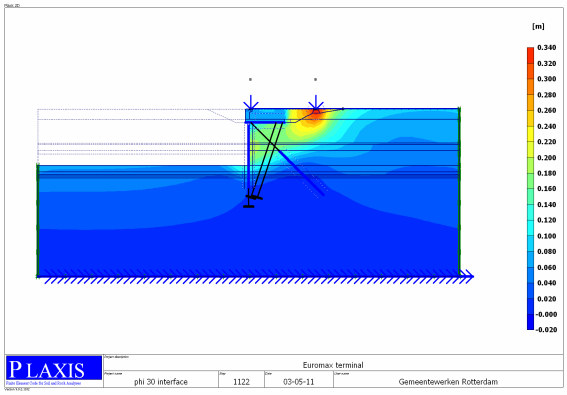

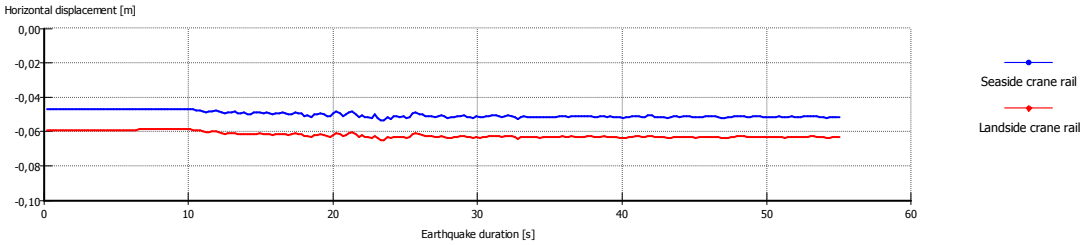

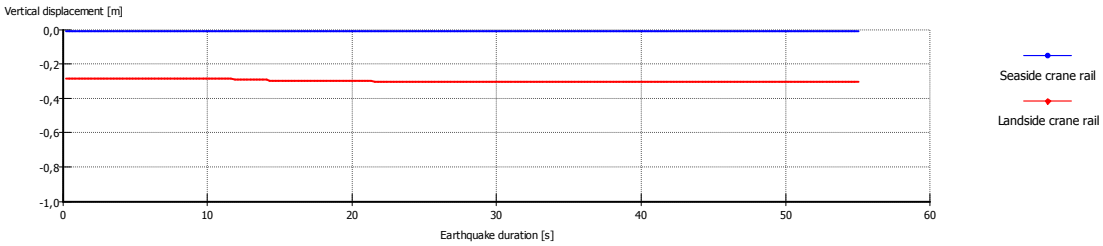

Plaxis Displacement	Hor. displacement After last phase	Vert. displacement After last phase
Seaside crane rail	-0,052 m	-0,008 m
Landside crane rail	-0,064 m	-0,303 m

Stresses

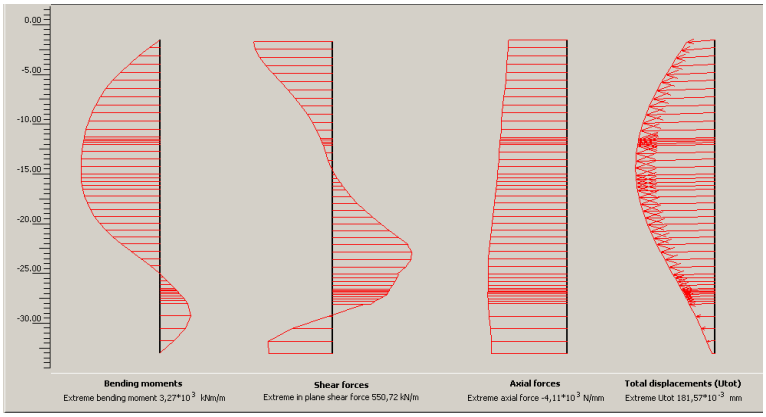

Plaxis Stresses	**Max. Axial force [kN/m]**	**Max. Bending moment [kNm/m]**
Diaphragm wall	-4110	3270
MV-pile	919	-

Earthquake 4 (a=0,4 m/s^2):

Displacements

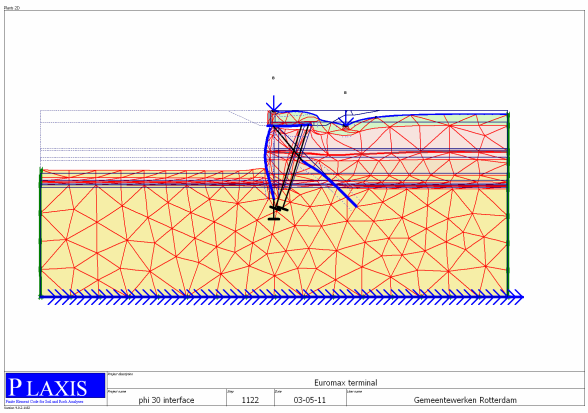

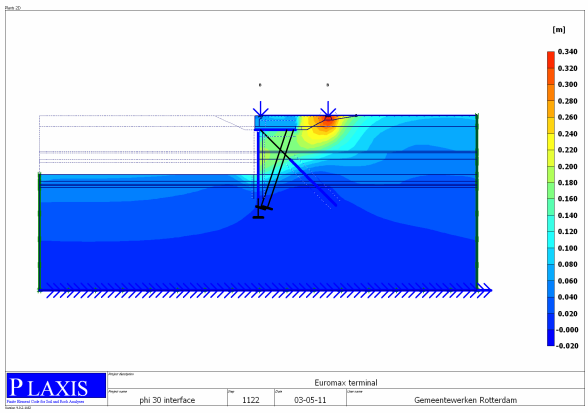

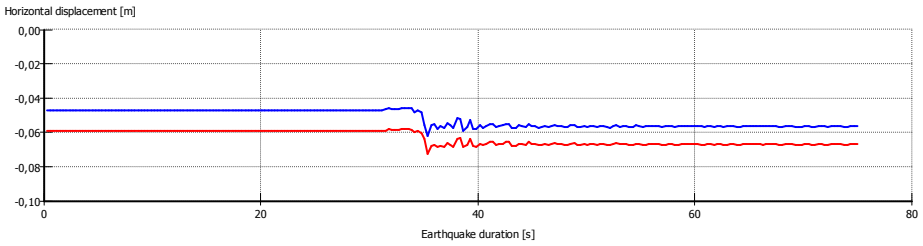

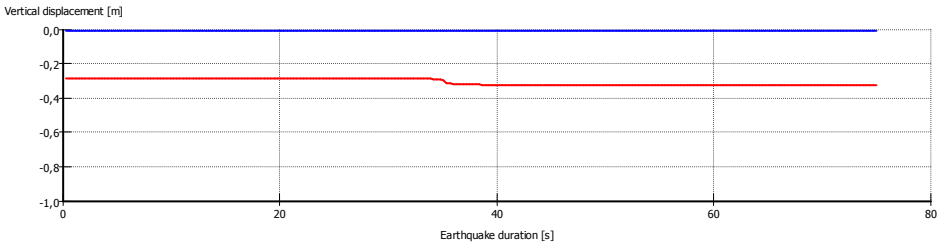

Plaxis Displacement	Hor. displacement After last phase	Vert. displacement After last phase
Seaside crane rail	-0,057 m	-0,008 m
Landside crane rail	-0,067 m	-0,324 m

Stresses

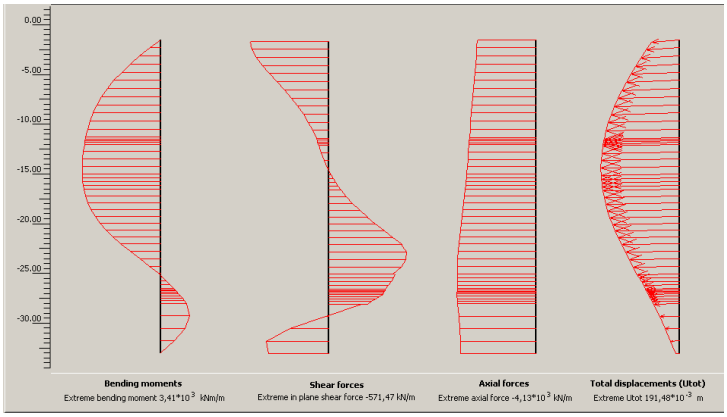

Plaxis Stresses	**Max. Axial force [kN/m]**	**Max. Bending moment [kNm/m]**
Diaphragm wall	-4130	3410
MV-pile	963	-

Earthquake 5 (a=0,5 m/s^2):

Displacements

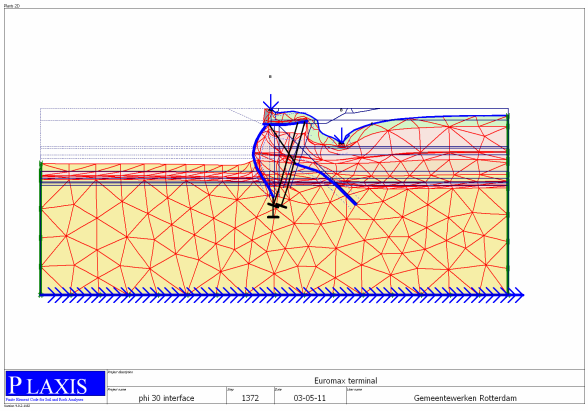

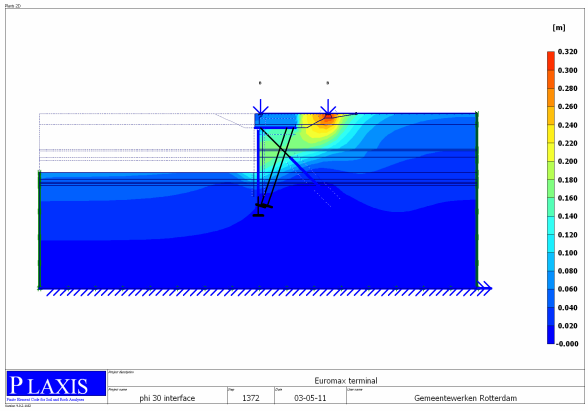

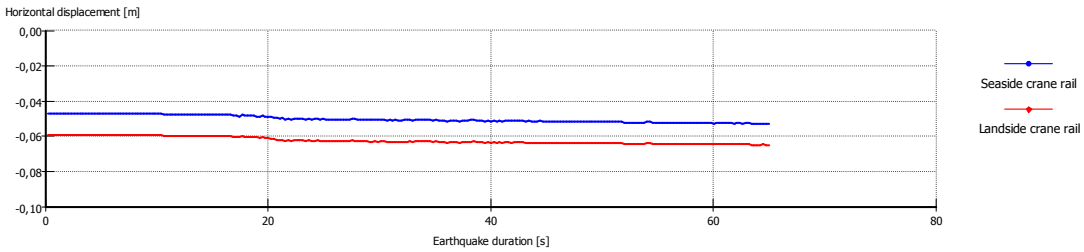

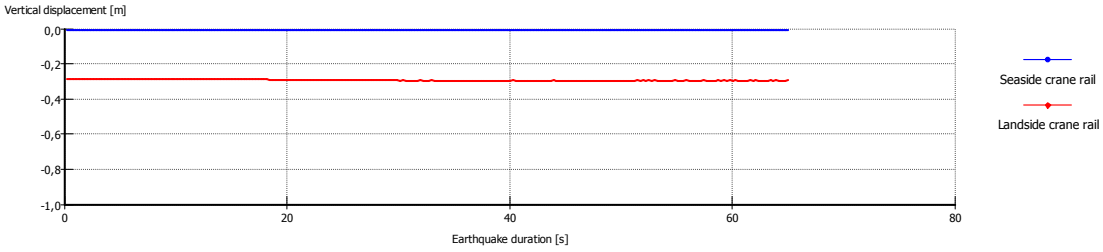

Plaxis Displacement	Hor. displacement After last phase	Vert. displacement After last phase
Seaside crane rail	-0,053 m	-0,008 m
Landside crane rail	-0,065 m	-0,295 m

Stresses

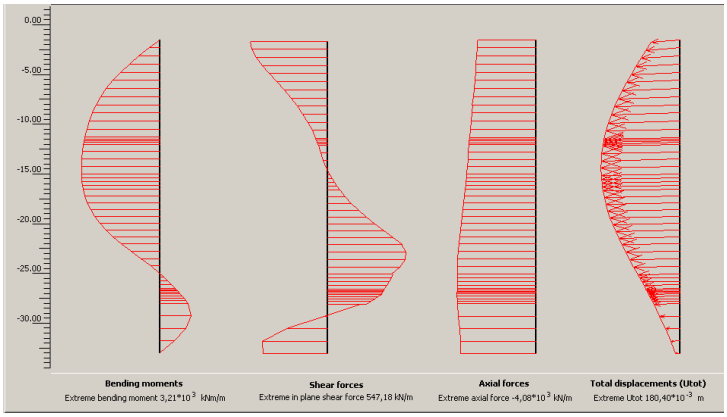

Plaxis Stresses	**Max. Axial force [kN/m]**	**Max. Bending moment [kNm/m]**
Diaphragm wall	-4080	3210
MV-pile	896	-

Earthquake 6 (a=0,6 m/s^2):

Displacements

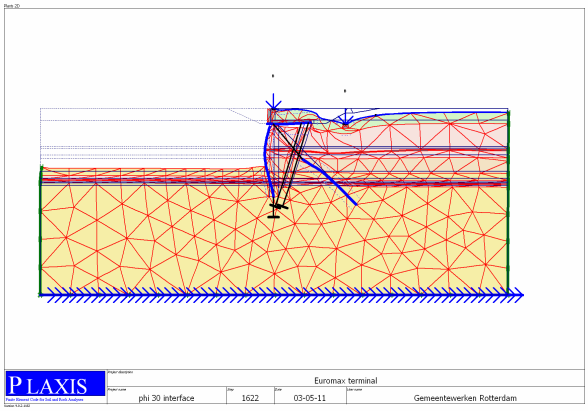

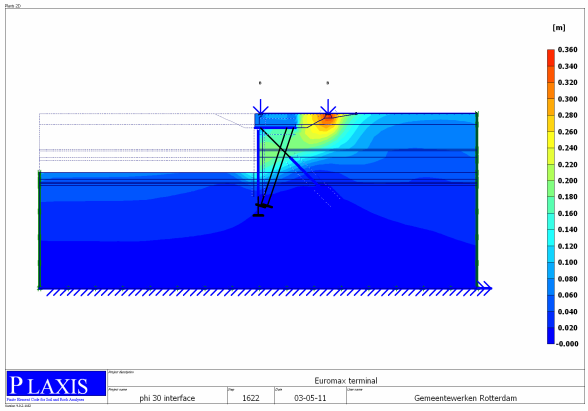

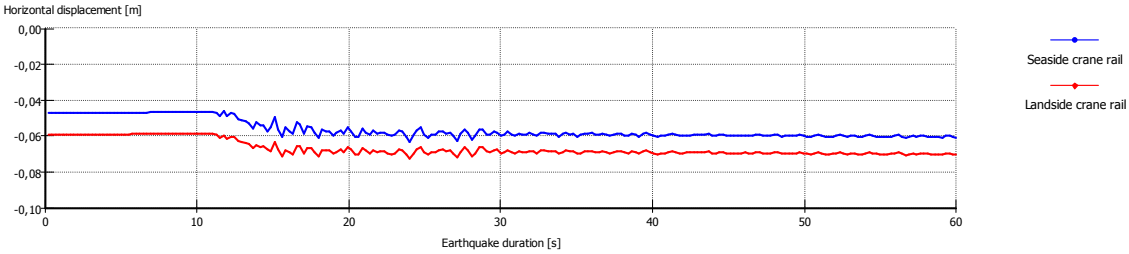

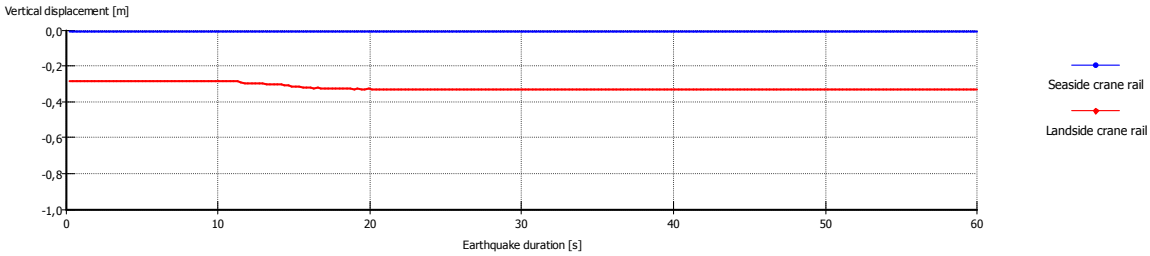

Plaxis Displacement	Hor. displacement After last phase	Vert. displacement After last phase
Seaside crane rail	-0,061 m	-0,005 m
Landside crane rail	-0,071 m	-0,333 m

Stresses

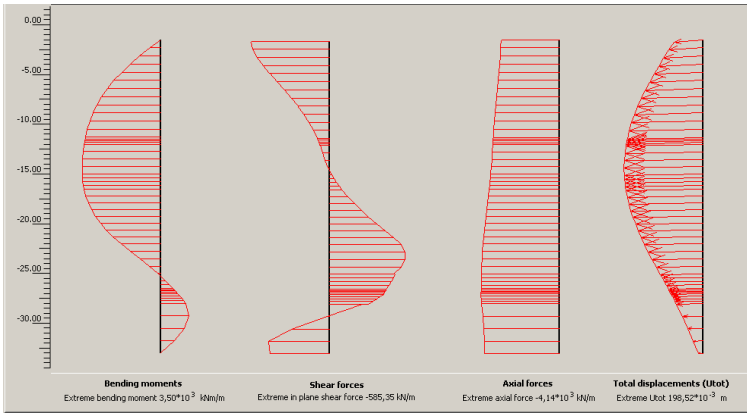

Plaxis Stresses	**Max. Axial force [kN/m]**	**Max. Bending moment [kNm/m]**
Diaphragm wall	-4140	3500
MV-pile	1002	-

Earthquake 7 (a=0,7 m/s^2):

Displacements

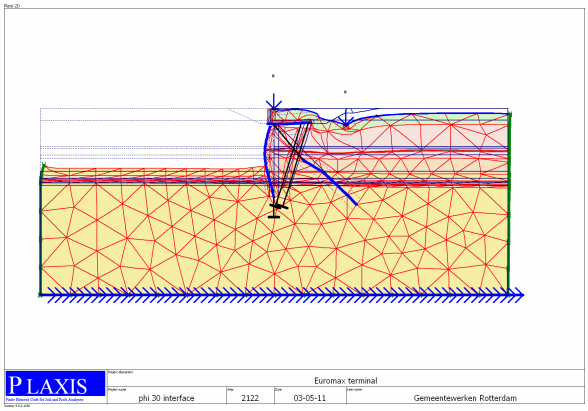

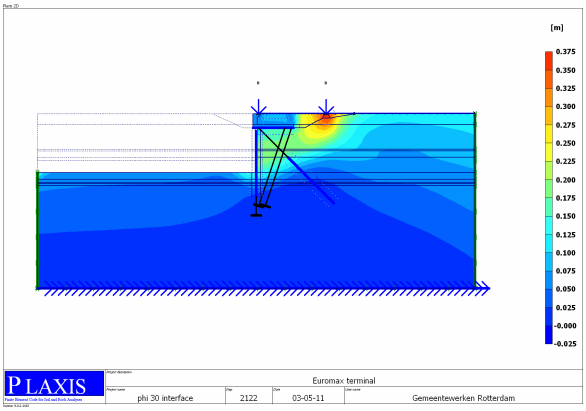

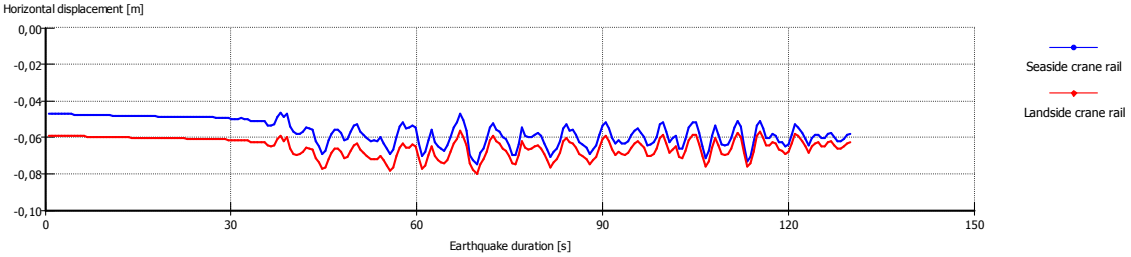

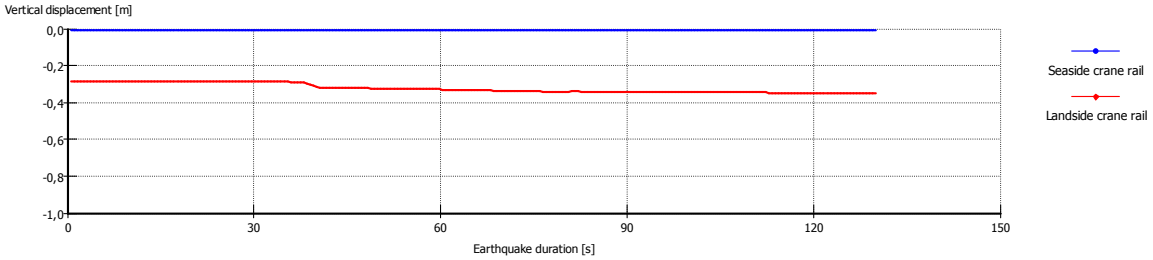

Plaxis Displacement	Hor. displacement After last phase	Vert. displacement After last phase
Seaside crane rail	-0,062 m	-0,008 m
Landside crane rail	-0,066 m	-0,350 m

Stresses

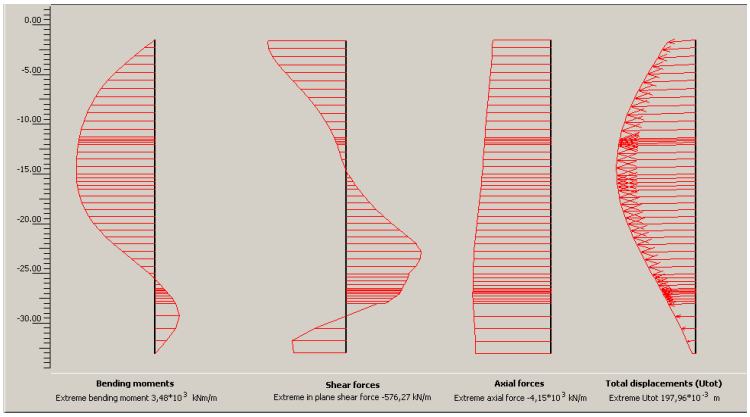

Plaxis Stresses	**Max. Axial force [kN/m]**	**Max. Bending moment [kNm/m]**
Diaphragm wall	-4150	3480
MV-pile	996	-

Earthquake 8 (a=0,8 m/s^2):

Displacements

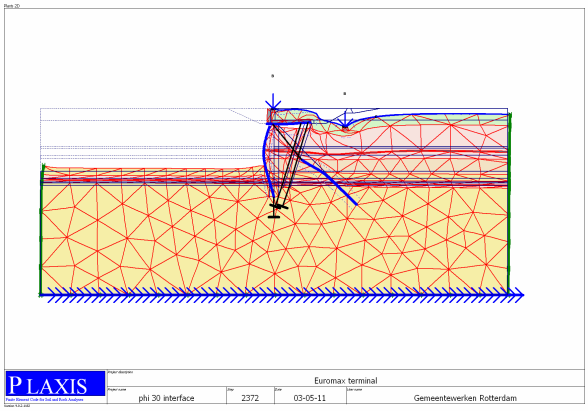

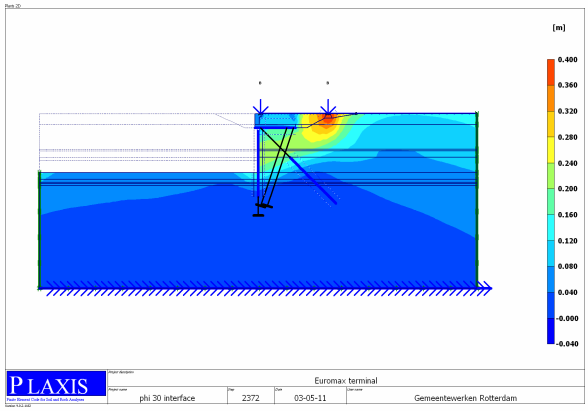

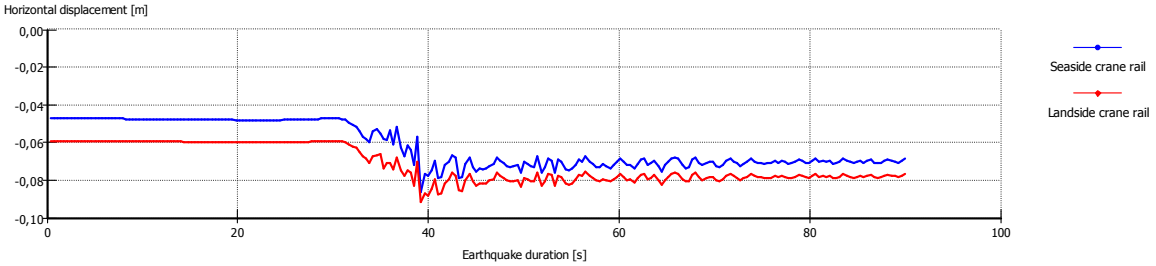

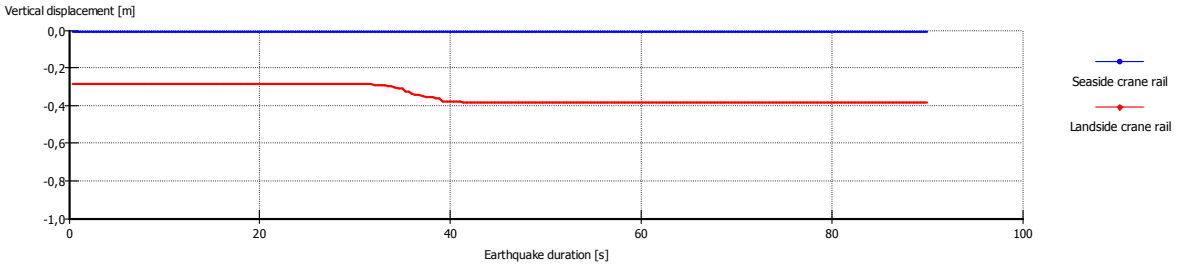

Plaxis Displacement	Hor. displacement After last phase	Vert. displacement After last phase
Seaside crane rail	-0,069 m	-0,005 m
Landside crane rail	-0,079 m	-0,386 m

Stresses

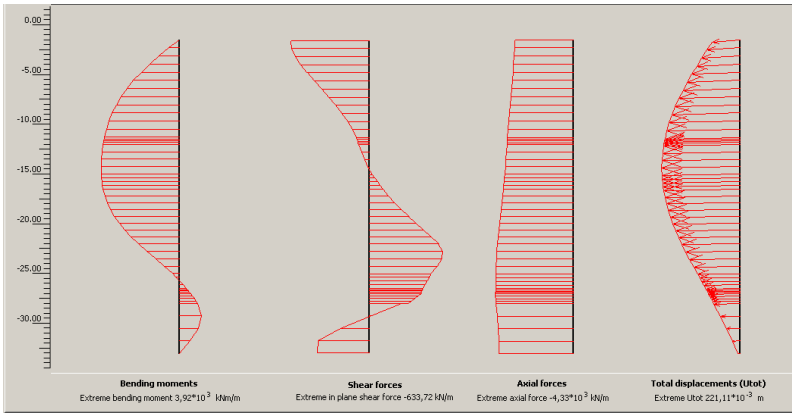

Plaxis Stresses	**Max. Axial force [kN/m]**	**Max. Bending moment [kNm/m]**
Diaphragm wall	-4330	3920
MV-pile	1190	-

Earthquake 9 (a=0,9 m/s^2):

Displacements

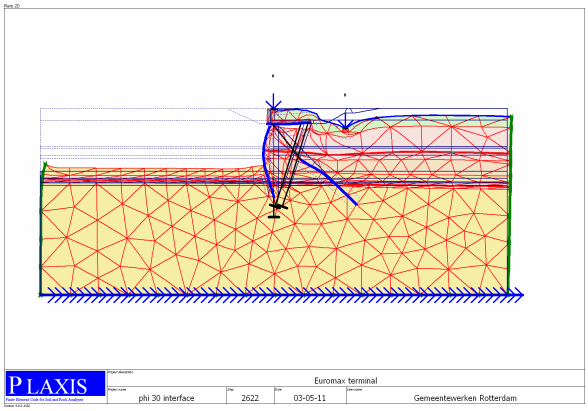

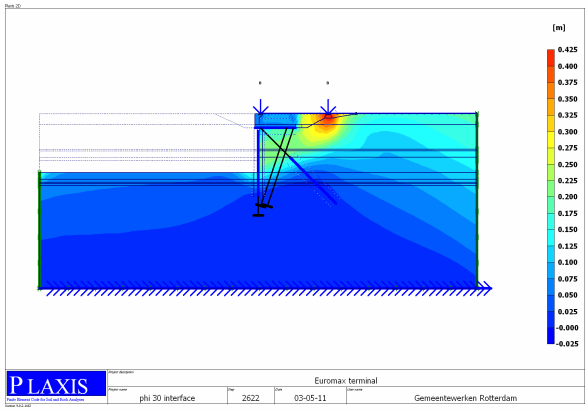

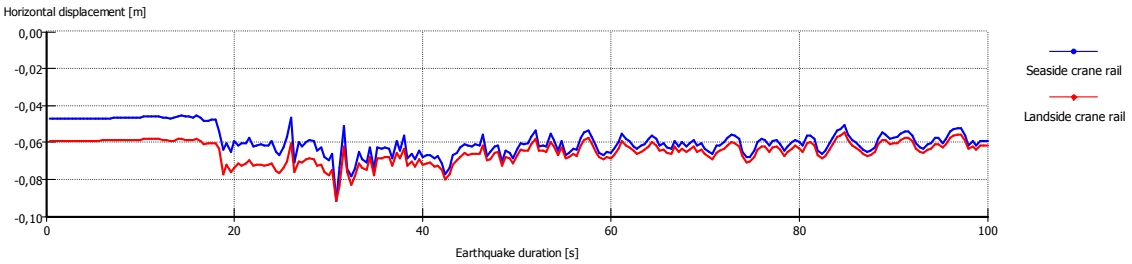

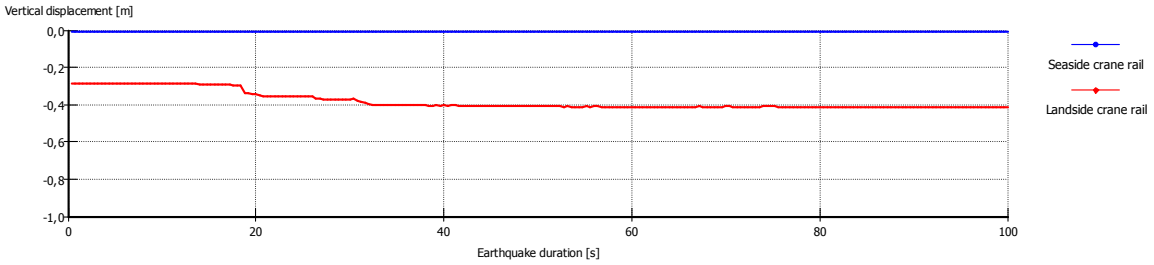

Plaxis Displacement	Hor. displacement After last phase	Vert. displacement After last phase
Seaside crane rail	-0,062 m	-0,008 m
Landside crane rail	-0,064 m	-0,413 m

Stresses

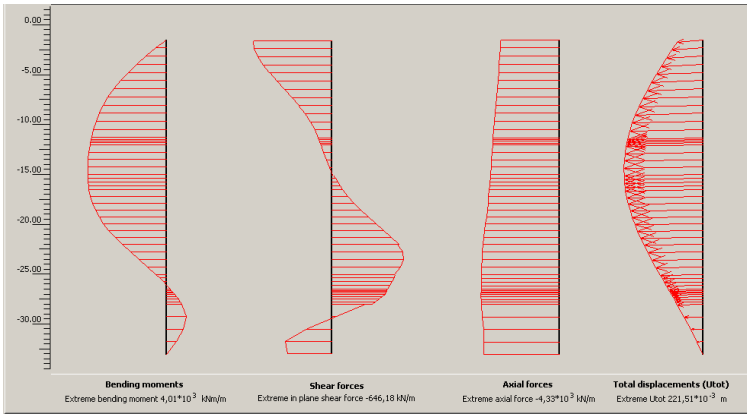

Plaxis Stresses	**Max. Axial force [kN/m]**	**Max. Bending moment [kNm/m]**
Diaphragm wall	-4330	4010
MV-pile	1220	-

Earthquake 10 (a=1,0 m/s^2):

Displacements

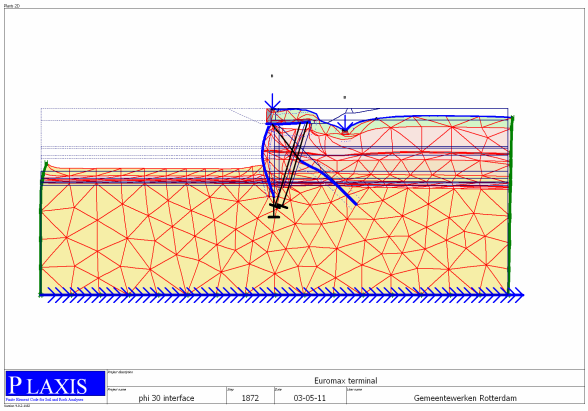

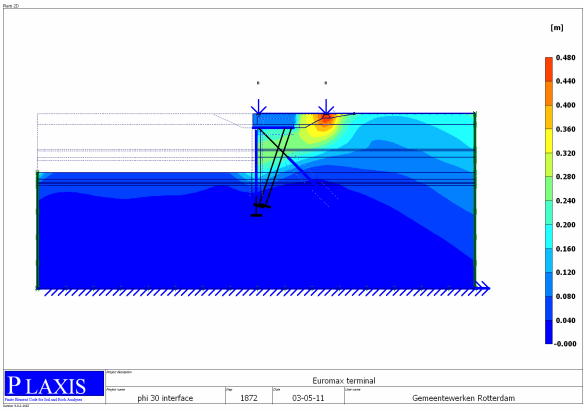

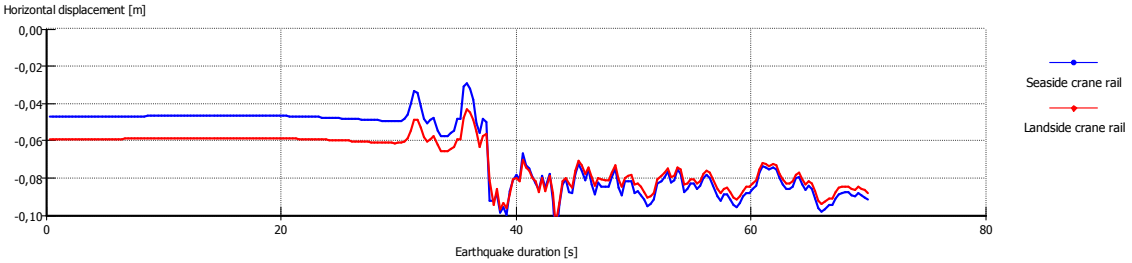

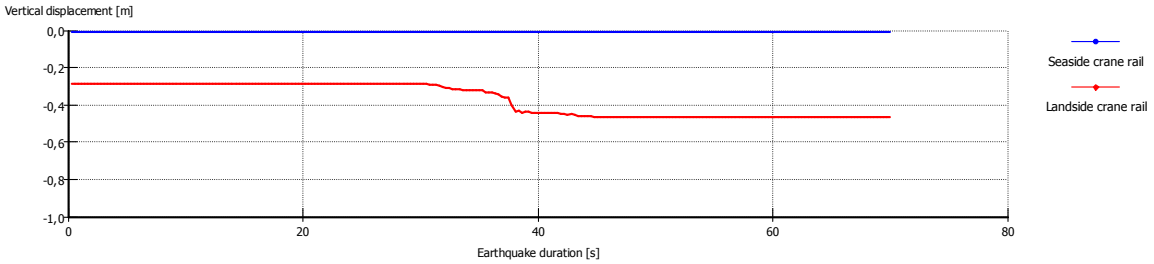

Plaxis Displacement	Hor. displacement After last phase	Vert. displacement After last phase
Seaside crane rail	-0,092 m	-0,008 m
Landside crane rail	-0,088 m	-0,463 m

Stresses

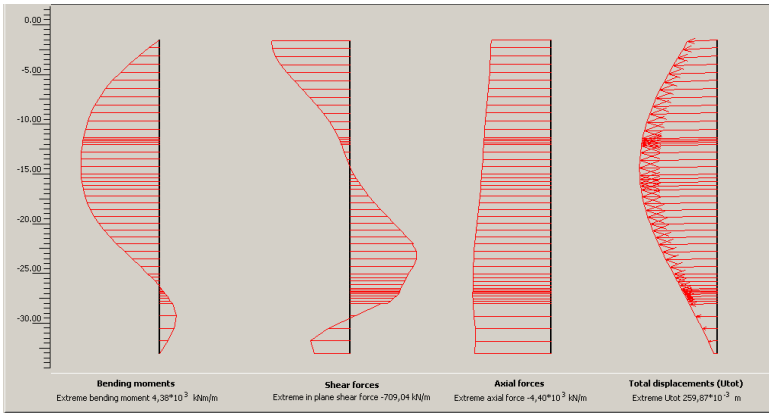

Plaxis Stresses	**Max. Axial force [kN/m]**	**Max. Bending moment [kNm/m]**
Diaphragm wall	-4400	4380
MV-pile	1390	-

K.6.2 With excess pore water generation/liquefaction

Percentage of excess pore pressure	φ after reduction	Earthquake acceleration [m/s^2]
0 %	30	0,00g
3,3%	29	0,01g
6,7%	28	0,02g
10%	27	0,03g
13,3%	26	0,04g
16,7%	25	0,05g
20%	24	0,06g
23,3%	23	0,07g
26,7%	22	0,08g
30%	21	0,09g
33,3%	20	0,1g

Table K-2 Assumed excess pore pressure generation and the corresponding phi reduction (smaller range)

The result of the Plaxis calculation with 0%, 16,7%, 20%, 23,3%, 26,7% and 30% excess pore water pressure are shown in this section.

0% excess pore water pressure

No excess pore water generation is assumed when there is no earthquake. Hence, φ is set to 30 which correspond with no excess pore water pressure and no earthquake according to Table K-2. The results are the same as the static calculation of Plaxis shown in section H3.

16,7% excess pore water pressure

16,7% excess pore water generation is assumed. This is simulated in Plaxis by reducing φ to 25 and implementing an earthquake acceleration of 0,05g into Plaxis (see Table K-2).

Displacement

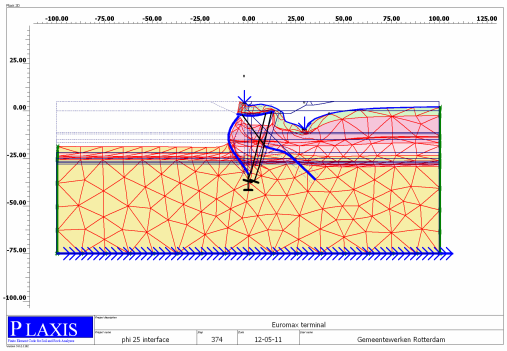

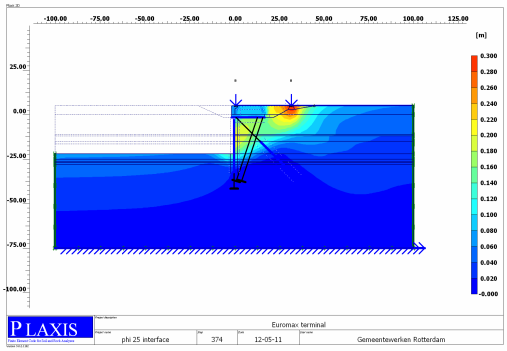

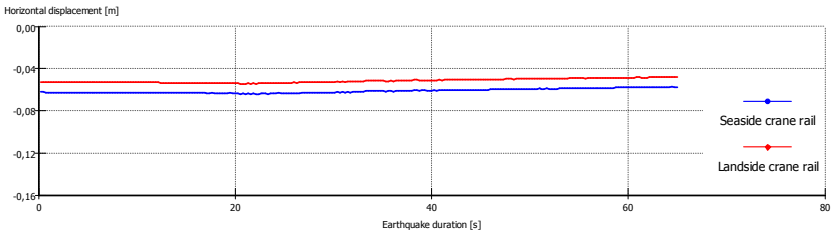

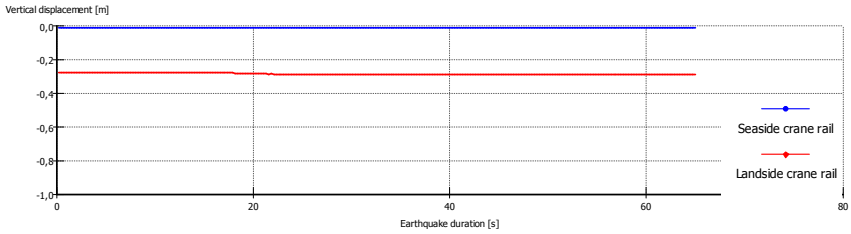

Plaxis Displacement	Hor. displacement After last phase	Vert. displacement After last phase
Seaside crane rail	-0,057 m	-0,013 m
Landside crane rail	-0,048 m	-0,290 m

Stresses

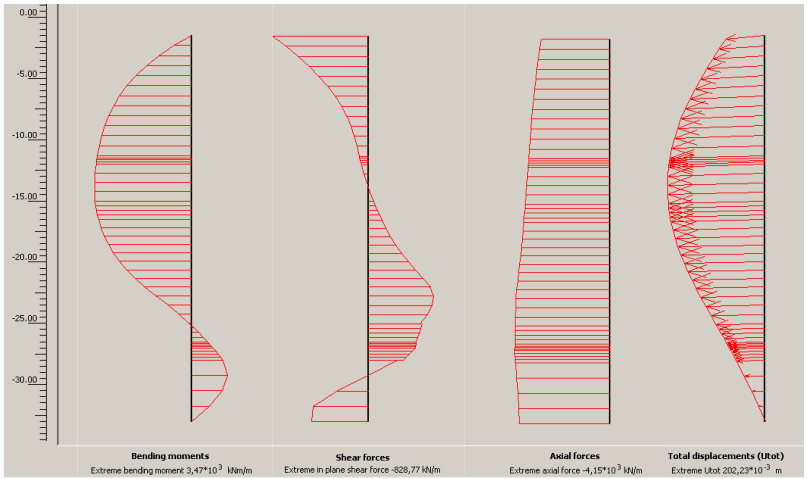

Plaxis Stresses	**Max. Axial force [kN/m]**	**Max. Bending moment [kNm/m]**
Diaphragm wall	-4150	3470
MV-pile	1270	-

20% excess pore water pressure

20% excess pore water generation is assumed. This is simulated in Plaxis by reducing φ to 24 and implementing an earthquake acceleration of 0,06g into Plaxis (see Table K-2).

Displacement

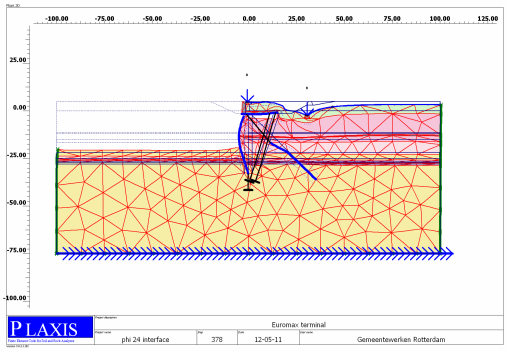

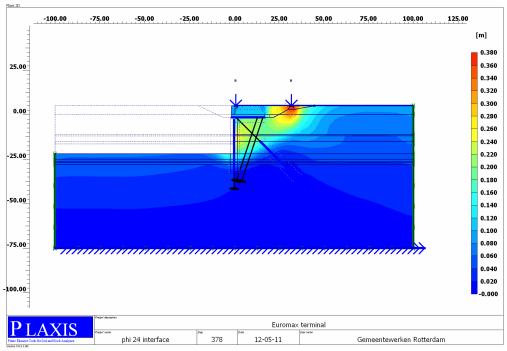

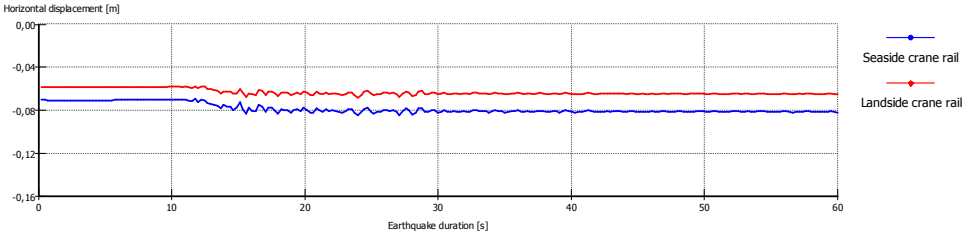

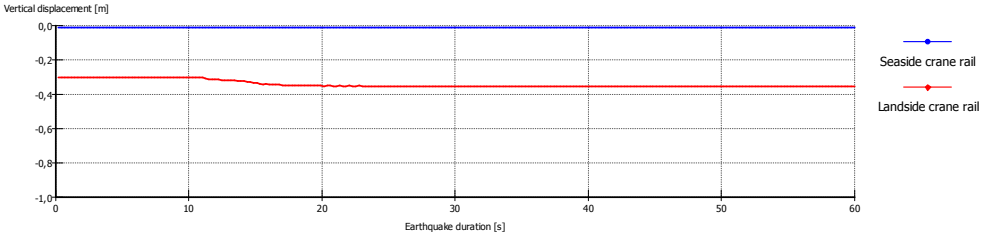

Plaxis Displacement	Hor. displacement After last phase	Vert. displacement After last phase
Seaside crane rail	-0,082 m	-0,013 m
Landside crane rail	-0,065 m	-0,357 m

Stresses

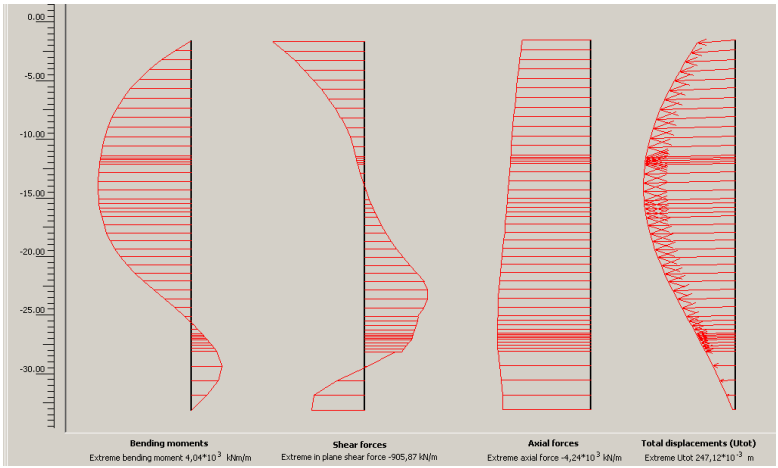

Plaxis Stresses	**Max. Axial force [kN/m]**	**Max. Bending moment [kNm/m]**
Diaphragm wall	-4240	4040
MV-pile	1500	-

23,3% excess pore water pressure

23,3% excess pore water generation is assumed. This is simulated in Plaxis by reducing φ to 23 and implementing an earthquake acceleration of 0,07g into Plaxis (see Table K-2).

Displacement

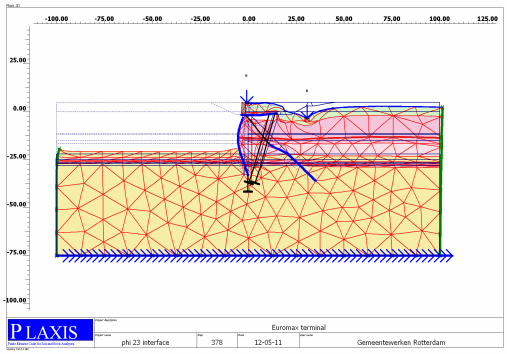

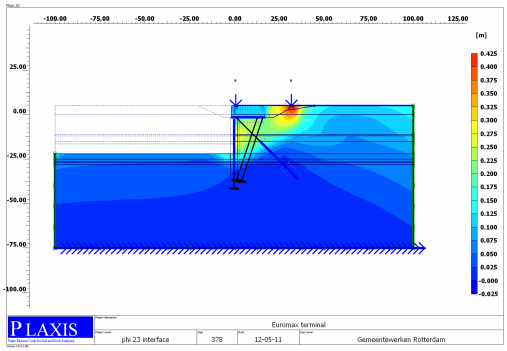

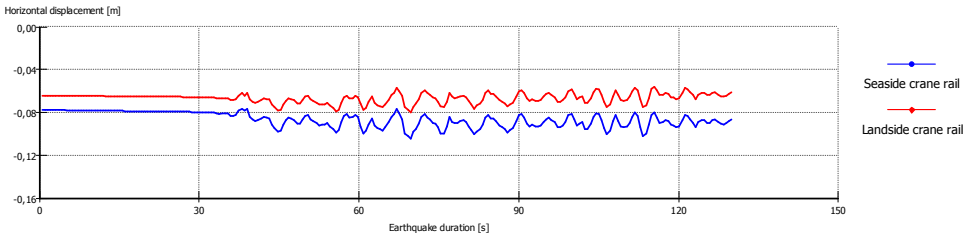

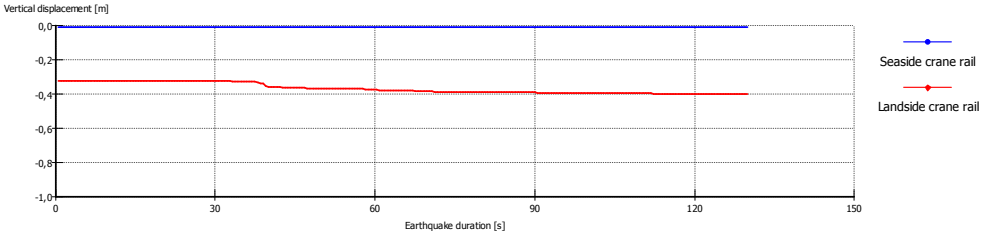

Plaxis Displacement	Hor. displacement After last phase	Vert. displacement After last phase
Seaside crane rail	-0,087 m	-0,013 m
Landside crane rail	-0,061 m	-0,404 m

Stresses

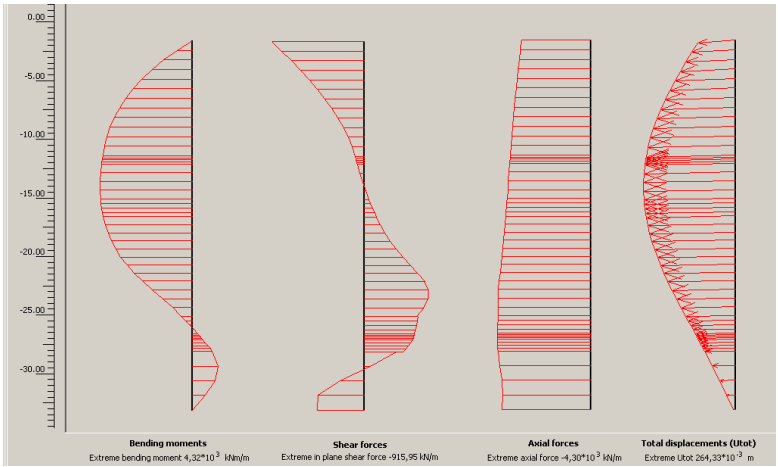

Plaxis Stresses	**Max. Axial force [kN/m]**	**Max. Bending moment [kNm/m]**
Diaphragm wall	-4300	4320
MV-pile	1580	-

26,7% excess pore water pressure

26,7% excess pore water generation is assumed. This is simulated in Plaxis by reducing φ to 22 and implementing an earthquake acceleration of 0,08g into Plaxis (see Table K-2).

Displacement

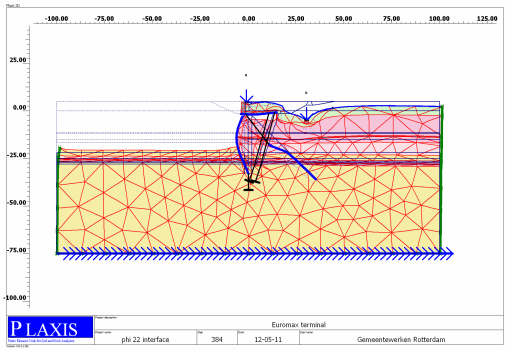

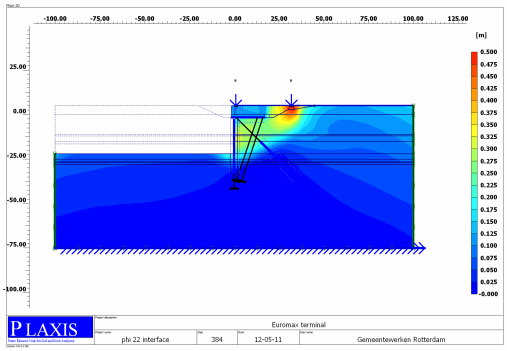

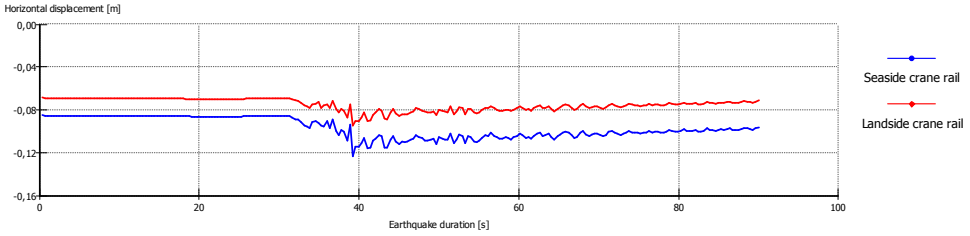

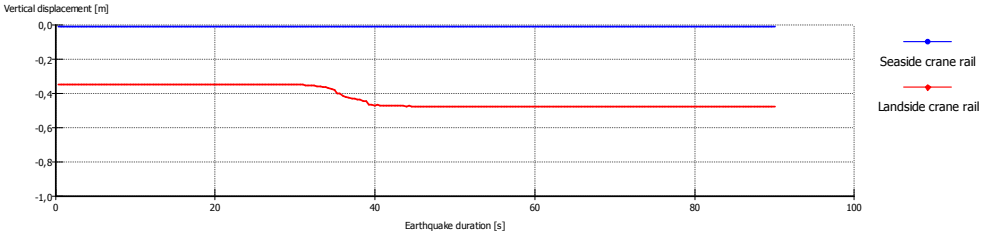

Plaxis Displacement	Hor. displacement After last phase	Vert. displacement After last phase
Seaside crane rail	-0,096 m	-0,014 m
Landside crane rail	-0,071 m	-0,480 m

Stresses

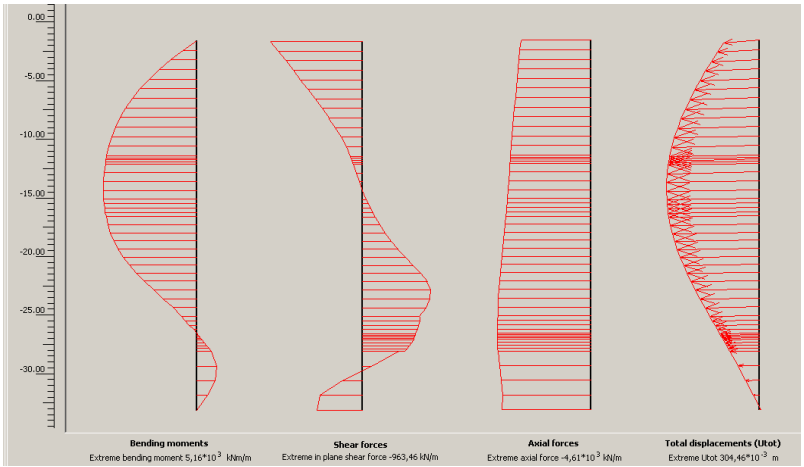

Plaxis Stresses	**Max. Axial force [kN/m]**	**Max. Bending moment [kNm/m]**
Diaphragm wall	-4610	5160
MV-pile	1870	-

30% excess pore water pressure

30% excess pore water generation is assumed. This is simulated in Plaxis by reducing φ to 21 and implementing an earthquake acceleration of 0,09g into Plaxis (see Table K-2).

Displacement

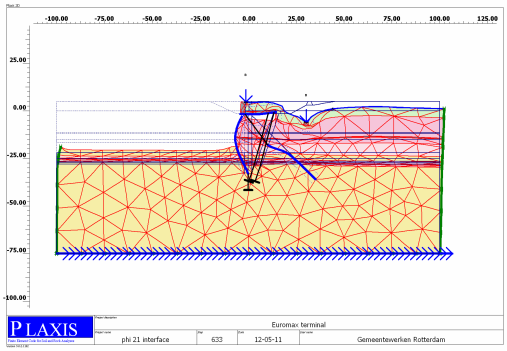

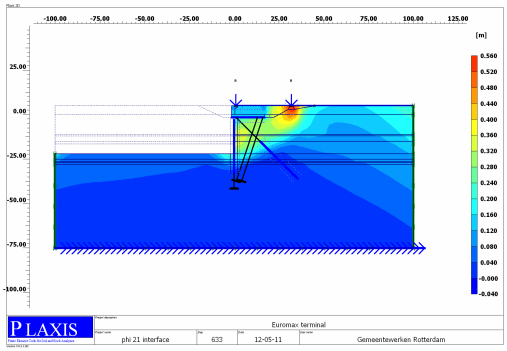

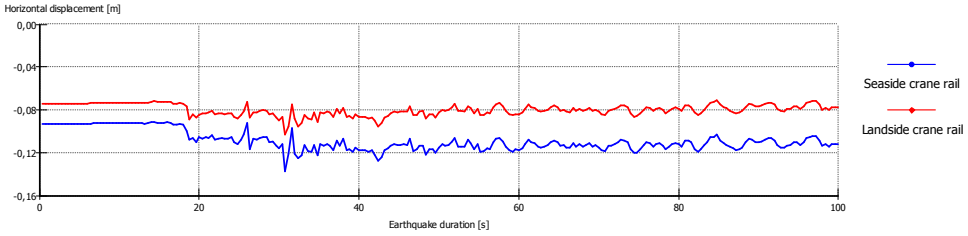

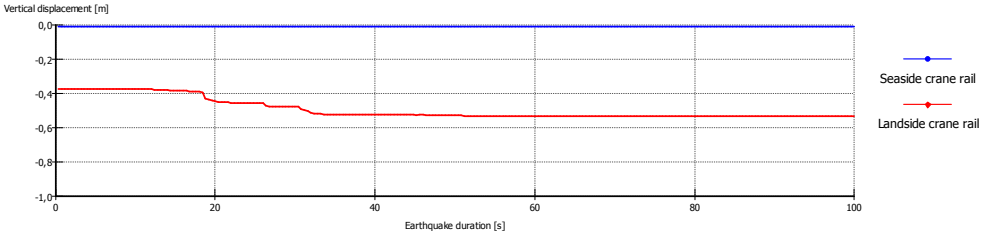

Plaxis Displacement	Hor. displacement After last phase	Vert. displacement After last phase
Seaside crane rail	-0,112 m	-0,013 m
Landside crane rail	-0,078 m	-0,538 m

Stresses

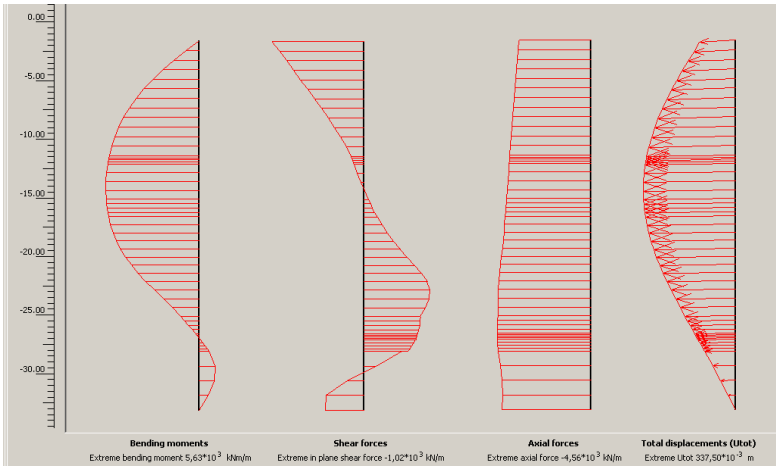

Plaxis Stresses	**Max. Axial force [kN/m]**	**Max. Bending moment [kNm/m]**
Diaphragm wall	-4560	5630
MV-pile	2010	-

K7 References

[K.1] http://nsmp.wr.usgs.gov/data.html
[K.2] Brinkgreve R., Kappert M.H., Bonnier P.G., Hysteretic damping in a small-strain stiffness model, 2007

Appendix L Moment capacity concrete diaphragm wall

L1 Current situation

The concrete diaphragm wall consists of different reinforcement bars spread all over the diaphragm wall. More reinforcements are placed at location were the forces supposed to be large. For the diaphragm wall the moment forces acting on the diaphragm wall is normative. Therefore, the amount of reinforcement is larger at places where the moment forces are large. The as-build drawing of the diaphragm wall and the placement of the reinforcement are shown in Figure L-2.

To make sure the whole quay wall will not collapse the diaphragm wall must withstand the forces caused by the earthquake. The maximum bending moment capacity of the diaphragm wall is determined. Moment capacity will be the largest were the reinforcement is maximal. The reinforcement drawing in Figure L-2 shows that most of the reinforcement is located between NAP-8,0m and NAP-19,0m. This depth correspondents to the depth in which the maximum moment was found during the design calculation. This section with maximum reinforcement will be used in determining the maximal moment capacity for the diaphragm wall. Upper cross-section for this section can be found in Figure L-1.

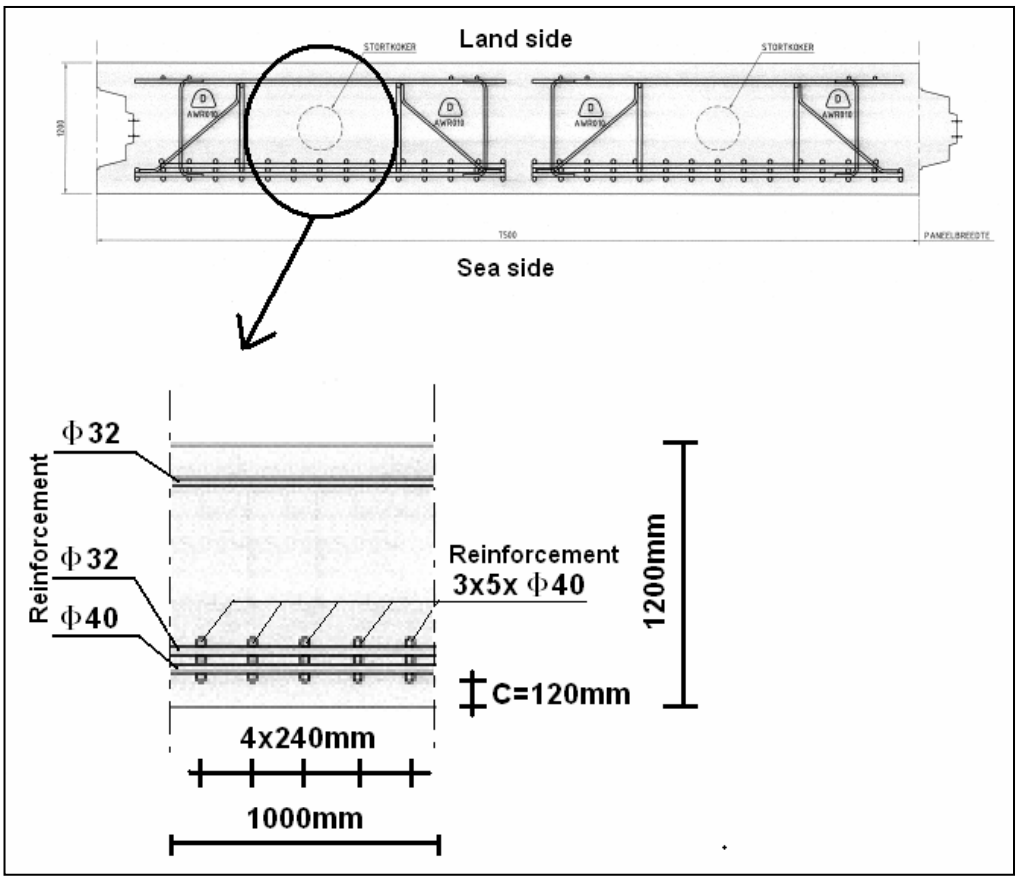

Figure L-1 Upper cross-section of diaphragm wall and the location of the reinforcement bars

The diaphragm wall was build in-situ and in sections of 7,5m length. Concrete class C28/35 and steel class FeB 500 HwL was used for the diaphragm wall and its reinforcement. Three layers of reinforcement bars places next to each other alongside the wall to provide the necessary moment capacity to withstand the forces. The diameter and center to center distance of these reinforcement bars are 40mm and 240mm respectively.

Figure L-2 Reinforcement drawing of diaphragm wall

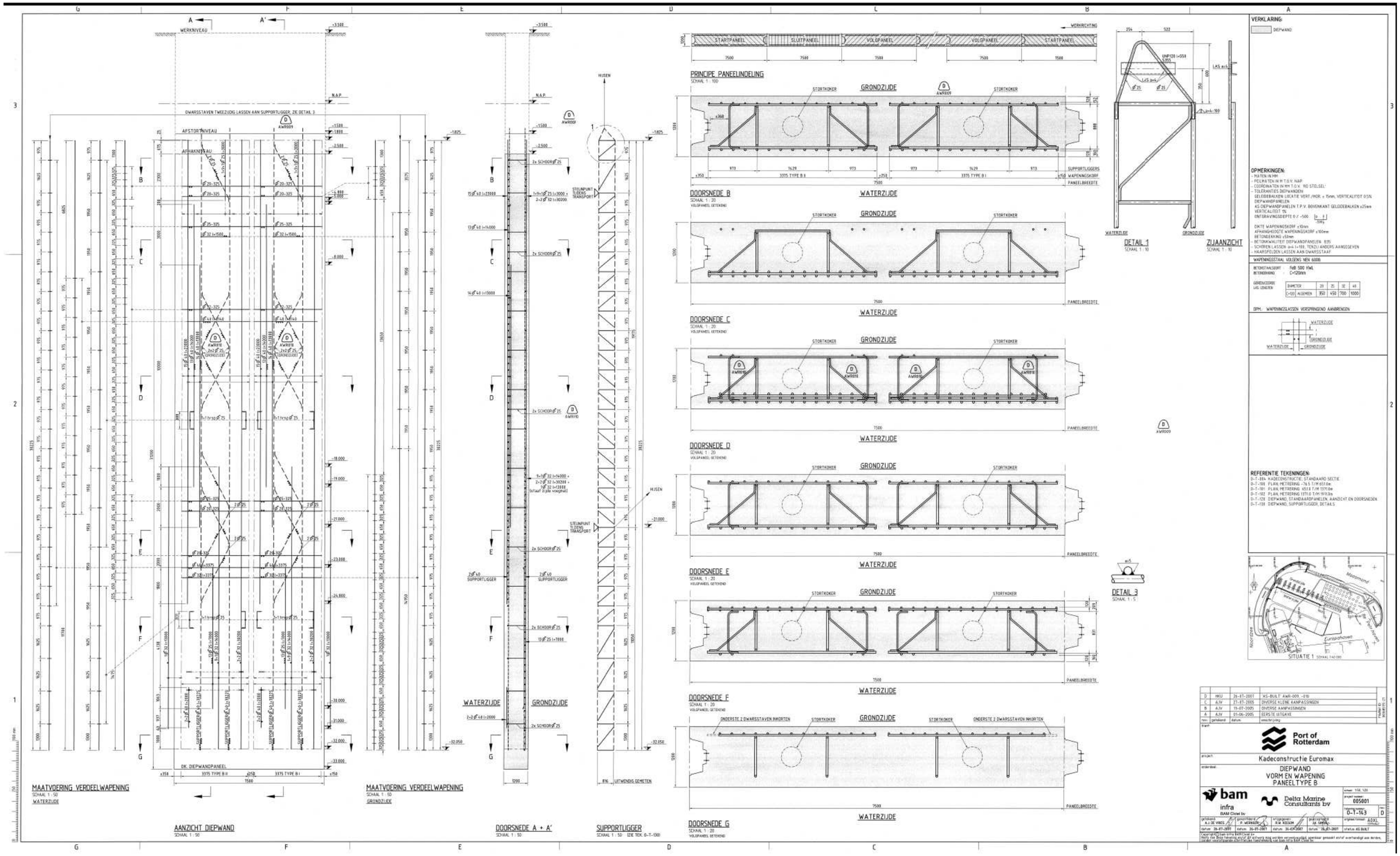

L2 Determining the maximum moment capacity

Some material properties of the diaphragm wall that are relevant for this calculation are listed below in Table L-1 and Table L-2

Concrete	
f'_{ck}	35 N/mm^2
f'_b	21 N/mm^2
f_b	1,4 N/mm^2
f_{bm}	2,74 N/mm^2
E'_b	31000 N/mm^2
ε'_b	3,5%
ε'_{bpl}	1,75%

Table L-1 Concrete properties of diaphragm wall

Reinforcement bars	FeB 500 HwL
f_{rep}	500 N/mm^2
f_s	435 N/mm^2
E_s	200000 N/mm^2
ε_s	3,25 %

Table L-2 Properties of reinforcement bars of diaphragm wall

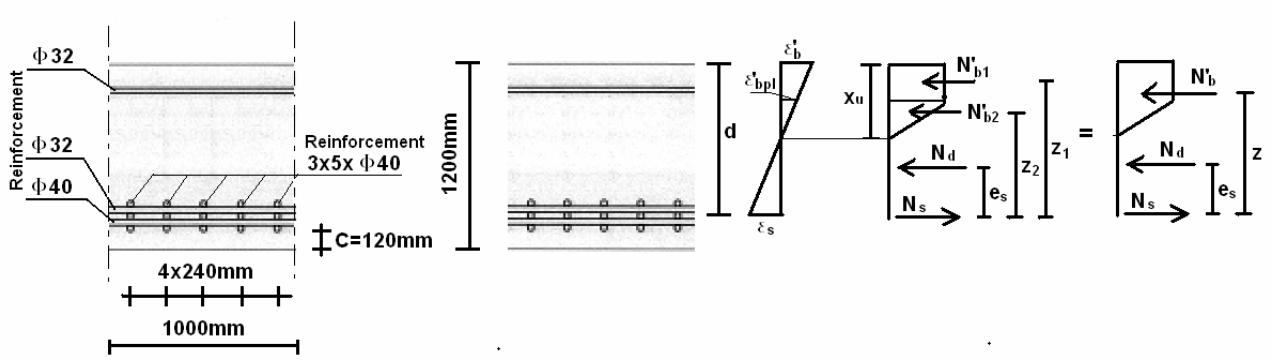

Figure L-3 Determination of moment capacity of diaphragm wall

First the effective distance from the top of a reinforced concrete wall to the mass centre of the steel is determined.

$$d = 1200 - 120 - 40 - 40 - 20 = 980mm$$

The distance of the normal force to the mass centre of the steel becomes:

$$e_s = d - 960 = 980 - 960 = 20mm$$

Then the height of the compressive zone, x_u, needs to be determined. For that purpose the compressive forces N'_b are determined.

$$N'_{b1} = \frac{\varepsilon'_{bpl}}{\varepsilon'_b} \cdot x_u \cdot b \cdot f'_b = \frac{1,75}{3,5} \cdot x_u \cdot 1000 \cdot *21 = 10500 x_u$$

$$N'_{b2} = 0,5 \cdot \frac{\varepsilon'_{bpl}}{\varepsilon'_b} \cdot x_u \cdot b \cdot f'_b = 0,5 \cdot \frac{1,75}{3,5} \cdot x_u \cdot 1000 \cdot *21 = 5250 x_u$$

$$N'_b = N'_{b1} + N'_{b2} = 15750 x_u$$

When the reinforcing steel yields, the total force in this steel equals $A_s f_s$.

$$N_s = A_s \cdot f_s = 0,25 \cdot 40^2 \cdot \pi \cdot 15 \cdot 435 = 82 \cdot 10^5 N$$

The sum of N'_b , N_s and the normal force within the wall N_d needs to be in equilibrium. Resulting in the following formulation of x_u.

$$N_d + N'_b = N_s \qquad N_d + 15750 x_u = 82 \cdot 10^5 N$$

$$x_u = \frac{82 \cdot 10^5 - N_d}{15750}$$

Depending on the earthquake magnitude N_d is calculated using the finite element program Plaxis. x_u can be determined when N_d is known. With the correct height x_u of the concrete compression zone, the moment capacity of the diaphragm wall can be determined. This follows from (see also Figure L-3):

$$Z_1 = d - x_u / 4$$
$$Z_2 = d - x_u / 2$$
$$Z = \frac{N'_{b1} \cdot Z_1 + N'_{b2} \cdot Z_2}{N'_{b1} + N'_{b2}}$$
$$M_{cap} = N'_b \cdot Z + N_d \cdot e_s$$

N_d [kN/m]	N'_b [kN/m]	Z [m]	M_{cap} [kNm/m]
1000	7200	0,828	5979
2000	6200	0,849	5302
3000	5200	0,870	4584
4000	4200	0,891	3823

No excess pore pressure	N_d [kN/m]	M_{cap} [kNm/m]
Earthquake 1	-4100	3744
Earthquake 2	-4100	3744
Earthquake 3	-4110	3736
Earthquake 4	-4130	3721
Earthquake 5	-4080	3760
Earthquake 6	-4140	3713
Earthquake 7	-4150	3705
Earthquake 8	-4330	3562
Earthquake 9	-4330	3562
Earthquake 10	-4400	3506

With excess pore pressure	N_d [kN/m]	M_{cap} [kNm/m]
0% (a=0,00g)	-4050	3784
16,7% (a=0,05g)	-4150	3705
20% (a=0,06g)	-4240	3634
23,3% (a=0,07g)	-4300	3586
26,7% (a=0,08g)	-4610	3338
30% (a=0,09g)	-4560	3378

Appendix M Static analysis caisson by hand

The width of the caisson is an important parameter. Not only does the width of the caisson have influence on the amount of sand and concrete that is needed but it directly determine the stability of the structure. Two factors play an important role in determining the width:

- Sliding
- Overturning

The longer the width the more downward forces (own weight) which results in more friction resistance against sliding. The moment capacity against overturning will also increase due to the increase of the moment arm.

To check if the caisson quay wall has enough width, sliding and overturning stability has been checked and presented in this appendix.

Global amount of reinforcement within the concrete walls that is needed to withstand the occurring static stresses and prevent failure of the wall are also determined in this appendix. No calculation are performed concerning the concrete floor and roof because the stresses occurring in the walls are higher and is therefore assumed to be the normative construction element.

M1 Geometry of caisson

A preliminary design of Public Works of Rotterdam was used []. An estimation of dimensions for the caisson was made in this preliminary design. The width of the caisson was not determined yet and is assumed to be 27m for the first calculation. The assumed geometry is shown below:

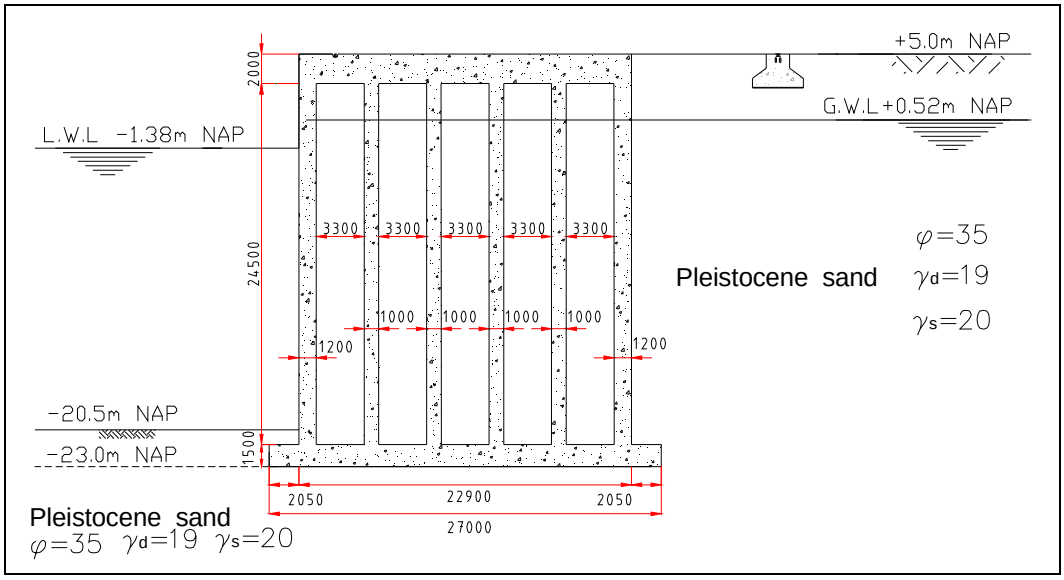

The caisson quay wall reaches a depth of NAP – 23,0m, is 27m wide and consists:

- A concrete front and a back wall with a thickness of 1,2m
- A concrete floor with a thickness of 1,5m
- 5 partition walls with a thickness of 1,0m
- A concrete roof with a thickness of 2,0m
- Landside rail foundation behind caisson structure

M2 Static forces acting on caisson

Own weight
This include the own weight of the concrete and the Sand filling on top and within the structure. This can be determined by multiplying the surface area with the specific weight of the material as shown below:

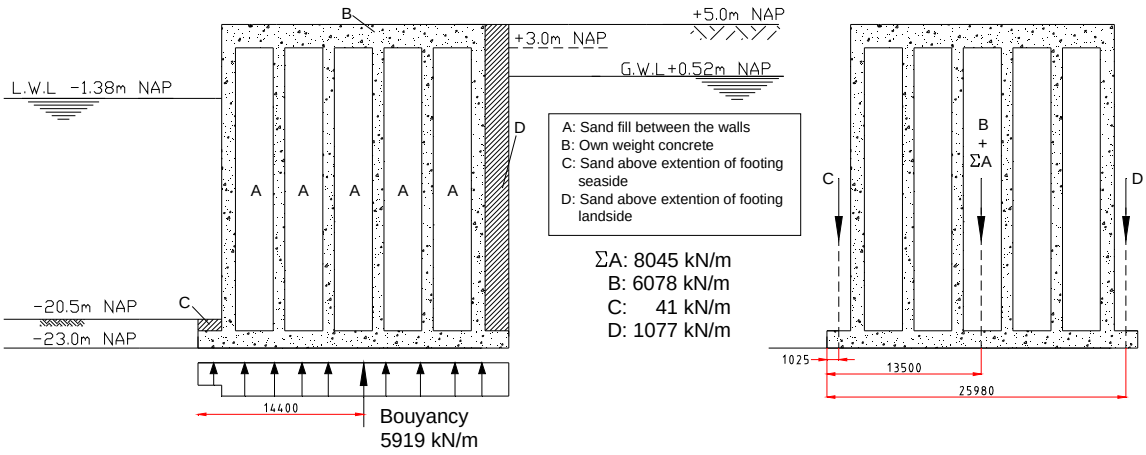

A= $A_{A,sand,dry}*\gamma_d + A_{A,sand,wet}*\gamma_s$ = (3,3*2,48)*19+(3,3*22,02)*20 = 1609 kN/m
B= $A_{concrete}*\gamma_{concrete}$ = (22,9*2+27*1,5+2*1,2*24,5+4*1*24,5)*25 = 6078 kN/m
C= $A_{E,sand}*\gamma_s$ = 1*2,05*20 = 41 kN/m
D= $A_{F,sand,dry}*\gamma_d + A_{F,sand,wet}*\gamma_s$ = (4,48*2,05)*19+(22,02*2,05)*20 = 1077 kN/m

Bouyancy
Bouyancy is an upward acting force exerted by a fluid, that opposes an object's weight. Any object, wholly or partially imeersed in a fluid, is buoyed up by a force equal to the weight of the fluid displaced by the object.

Bouyancy = $A_{below\ water}* \gamma_w$ = (24,95*23,52+2,5*2,05)*10 = 5919 kN/m

Whithout movement (neutral earth pressure coefficient k_0=0,5)

Earth- and water pressure

First, earth pressures will be determined assuming no movement of the wall. Neutral earth pressure coefficient k_0=0,5 will be used.

Water pressure is determined using equation 5-3 while the earth pressure is calculated using equation B-3 by replacing k_a by k_0. The resultant thrust due too earth and water pressure are shown in the figure below.

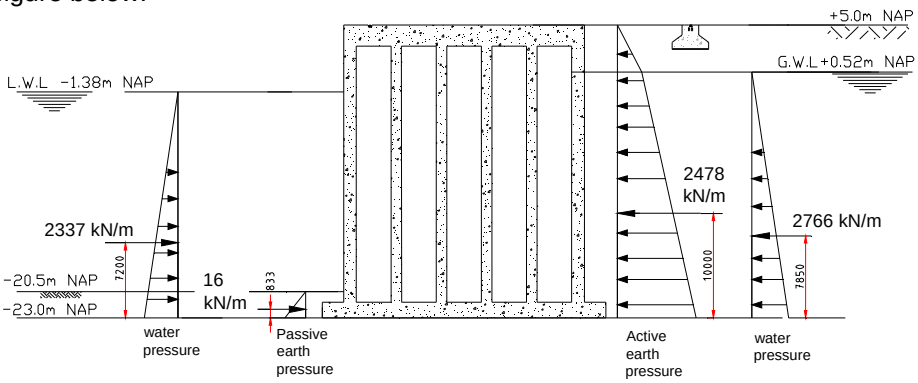

Surcharge load, Crane load and Bolder force

Surcharge load, crane load and bolder force acting on the caisson are the same as for the diaphragm wall and can be found in Appendix F Surcharge and crane loads behind the quay wall can be schematized as horizontal forces acting on the wall as shown below using the method shown in Figure I-6 and Figure I-8[CUR 166].

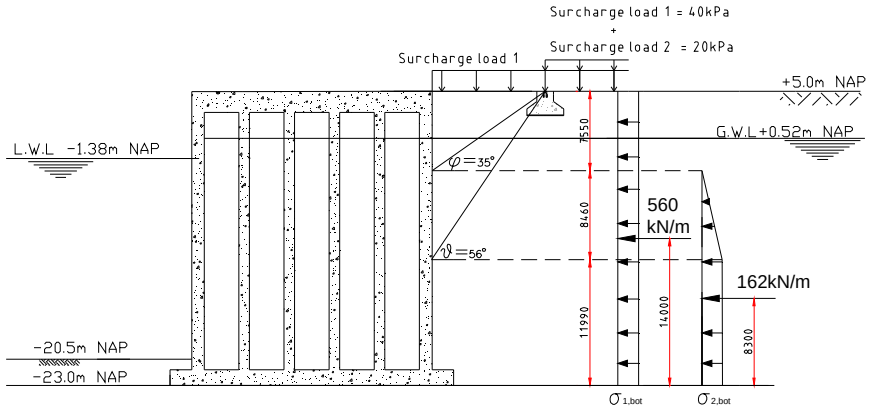

$\sigma_{1,bot}$ =40*k_a= 40*0,5 = 20 kPa

$\sigma_{2,bot}$ =20*k_a= 20*0,5 = 10 kPa

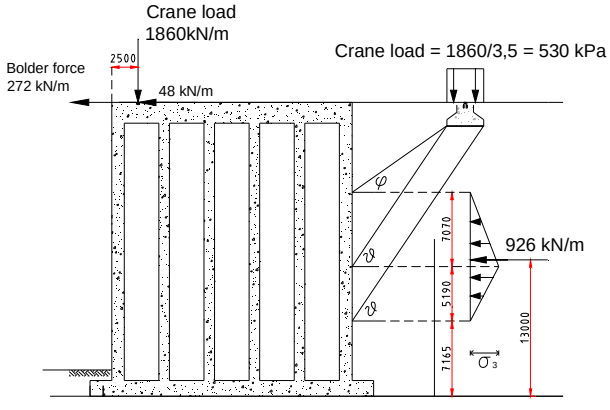

σ_3 =2*530*3.5*0.5/(7.07+5.19)=151 kN/m

With movement (active/passive earth pressure coefficient k_a=0,224 and k_p=9,96)

Earth- and water pressure

When the quay wall starts to move for a little bit, soil will get mobilized and the backfill become active and soil in front of the quay wall becomes passive. Active and passive earth pressure coefficients determined by the method of Coulomb will be used and are k_a=0,244 and k_p=9,96 respectively. This will result in less earth pressure behind the wall and more in front of the wall. Quay wall will eventually stop moving due to the decrease of forces.

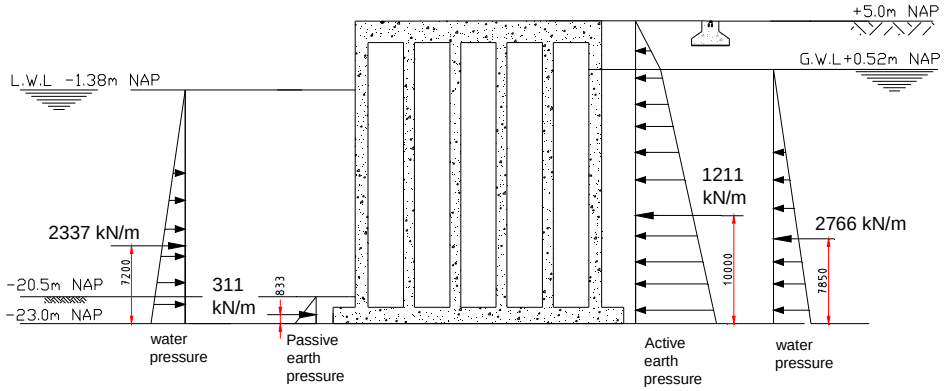

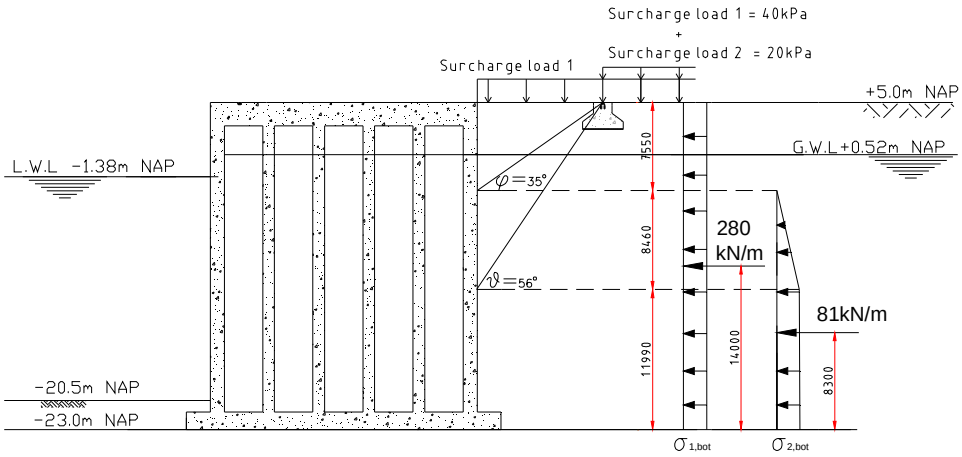

$\sigma_{1,bot}$ =40*k_a= 40*0,244 = 10 kPa

$\sigma_{2,bot}$ =20*k_a= 20*0,244 = 5 kPa

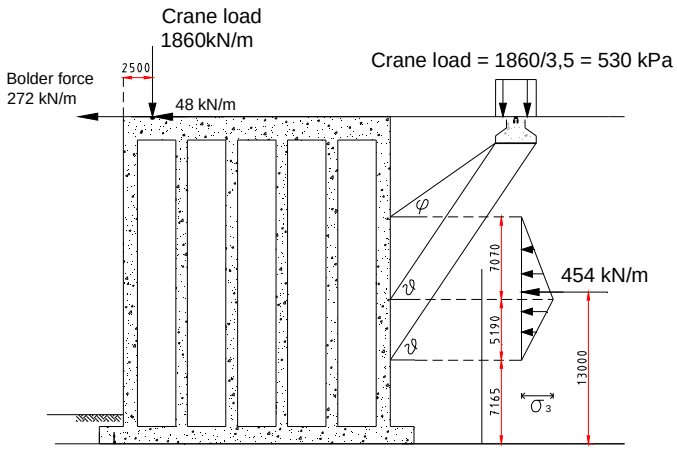

σ_3 =2*530*3.5*0.244/(7.07+5.19)=74 kN/m

M3 Static calculations of caisson

Safety factors
Safety factors γ_{sf} are used according to the Eurocode 7 and are listed in Table 9-1.

Load combinations and combination factors
Two load combinations are checked for the caisson quay wall and are listed in Table 9-2. Combination factors Ψ for separate loads are also listed in Table 9-2.

Sliding stability
The friction force must withstand the horizontal forces acting on the caisson otherwise the caisson will start to move. Calculations have been made to check whether the width of caisson is sufficient enough. Safety factors shown in Table 9-1 are used during the calculations for load combination 4 and 5.

$\sum(F_h * \gamma_{sf} * \Psi) \leq F_{friction}$
$F_{friction} = (\mu/\gamma_{\varphi'}) * \sum(F_v * \gamma_{sf} * \Psi)$

$\sum F_h$: Sum of horizontal forces acting on caisson
$F_{friction}$: Frictional force between caisson floor and the sand beneath with safety coefficient included
γ_{sf} : Safety factor
$\gamma_{\varphi'}$: Coefficient of shearing resistance (tanφ')
Ψ : Combination factor
μ : Dynamic friction coefficient (tan φ)
F_v : Vertical forces acting on the caisson

Load combination 4: no movement caisson

$\sum F_h$ = -2337*0,9 - 16*0,9 + 2478*1,35 + 2766*1,35 + 560*1,5*0,7 + 162*1,5*0,7 + 926*1,5*0,7 + 272*1,5 + 48*1,5*0,7 = 7151 kN/m
$F_{friction}$ = tan 35 * 0,8*((8045+6078+41+1077)*0,9-5919*1,35+1860*0,9*0.7) = 5356 kN/m

Factor of safety against sliding: $\frac{5356kN/m}{7151kN/m} = 0.75 < 1$ ➔ Caisson will slide

Caisson will move towards the sea and ground will be mobilized resulting in active and passive ground pressures.

Load combination 4: with movement of the caisson

$\sum F_h$ = -2337-0,9-311*0.9 + 1211*1,35 + 2766*1,35 + 280*1,5*0,7 + 81*1,5*0,7 + 454*1,5*0,7 + 272*1,5 + 48*1,5*0,7= 4300 kN/m
$F_{friction}$ = tan 35 * 0,8*((8045+6078+41+1077)*0,9-5919*0,9+1860*0,9*0,7) = 5356 kN/m

Factor of safety against sliding: $\frac{5356kN/m}{4300kN/m} = 1{,}25 > 1$ ➔ Caisson will not slide

After some mobilization of ground, the caisson will stop sliding towards the sea.

Load combination 5: no movement caisson

$\sum F_h$ = -2337*0,9-16*0,9 + 2478*1,35 + 2766*1,35 + 560*1,5*0,7 + 162*1,5*0,7 + 272*1,5= 6128 kN/m
$F_{friction}$ = tan 35 * 0,8*((8045+6078+41+1077)*0,9-5919*0,9) = 4700 kN/m

Factor of safety against sliding: $\frac{4700kN/m}{6128kN/m} = 0.77 < 1$ ➔ Caisson will slide
Caisson will move towards the sea and ground will be mobilized resulting in active and passive ground pressures.

Load combination 5: with movement of the caisson

$\sum F_h$ = -2337-0,9-311*0.9 + 1211*1,35 + 2766*1,35 + 280*1,5*0,7 + 81*1,5*0,7 + 272*1,5= 3773 kN/m
$F_{friction}$ = tan 35 * 0,8*((8045+6078+41+1077)*0,9-5919*0,9) = 4700 kN/m

Factor of safety against sliding: $\frac{4700kN/m}{3773kN/m} = 1{,}25 > 1$ ➔ Caisson will not slide

After some mobilization of ground, the caisson will stop sliding towards the sea.

Overturning stability
Overturning failure occurs when moment equilibrium is not satisfied. Overturning stability is checked by taking the moment around point M.

Load combination 4

bouyancy	-5919*14,40*1.35	= -115065 kNm/m
own weight	8045*13,5*0,9	= 97747 kNm/m
	6078*13,5*0,9	= 73848 kNm/m
	41*1,025*0,9	= 38 kNm/m
	1077*25,98*0,9	= 25182 kNm/m
		----------+
		81750 kNm/m
water pressure	2337*7,2*0,9	= 15144 kNm/m
	-2766*7,85*1,35	= -29313 kNm/m
earth pressure	311*0,833*1,35	= 350 kNm/m
	-1211*10*1,35	= -16349 kNm/m
surcharge load	-280*14*1,5*0,7	= -4116 kNm/m
	-81*8,3*1,5*0,7	= -706 kNm/m
crane load	1860*6,05*0,9*0,7	= 7090 kNm/m
	-454*13*1,5*0,7	= -6197 kNm/m
	-48*28*1,5*0,7	= -1411 kNm/m
bolder load	-272*28*1,5	= -11424 kNm/m
		----------+
		-46932 kNm/m

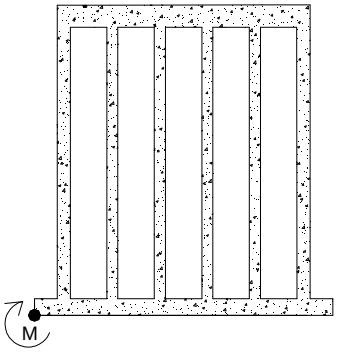

Factor of safety against overturning: $\frac{81750kN/m}{46932kN/m} = 1{,}74 > 1$ ➔ Caisson won't overturn

The Caisson quay wall is stable for the chosen dimensions. The presented caisson design will therefore be used for the earthquake analysis.

Load combination 5

bouyancy	-5919*14,40*1.35	= -115065 kNm/m
own weight	8045*13,5*0,9	= 97747 kNm/m
	6078*13,5*0,9	= 73848 kNm/m
	41*1,025*0,9	= 38 kNm/m
	1077*25,98*0,9	= 25182 kNm/m
		----------+
		81750 kNm/m
water pressure	2337*7,2*0,9	= 15144 kNm/m
	-2766*7,85*1,35	= -29313 kNm/m
earth pressure	311*0,833*1,35	= 350 kNm/m
	-1211*10*1,35	= -16349 kNm/m
surcharge load	-280*14*1,5*0,7	= -4116 kNm/m
	-81*8,3*1,5*0,7	= -706 kNm/m
bolder load	-272*28*1,5	= -11424 kNm/m
		----------+
		-46414 kNm/m

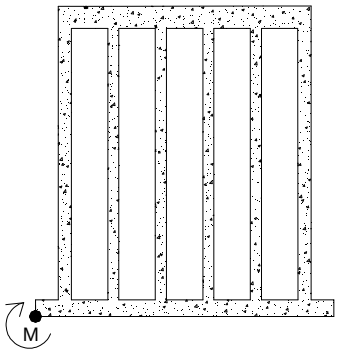

Factor of safety against overturning: $\frac{81750kN/m}{46414kN/m} = 1{,}76 > 1$ ➔ Caisson won't overturn

The Caisson quay wall is stable for the chosen dimensions. The presented caisson design will therefore be used for the earthquake analysis.

Bearing capacity of soil

The ultimate bearing capacity for the general shear mode of failure can be estimated from the traditional Buisman-Terzaghi (Terzaghi 1943) bearing capacity expression:

$q_{ult} = cN_c + \gamma_{eff} DN_q + 0.5\ \gamma_{eff} BN_\gamma$

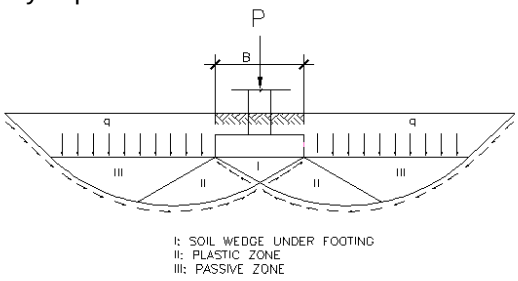

where

q_{ult} = the ultimate bearing capacity [kPa]
γ_{eff} = effective unit weight [kN/m^3]
B = width of foundation [m]
D = depth of foundation below ground surface [m]
c = the cohesion intercepts for the rock mass [kN/m^2]

The terms N_c, N_γ, and N_q are bearing capacity factors given by the following equations:

$N_c = (N_q\text{-}1)/\tan \varphi$
$N_q = k_p\, e^{(\pi \tan \varphi)}$
$N_\gamma = 2(N_q\text{-}1)\tan \varphi$

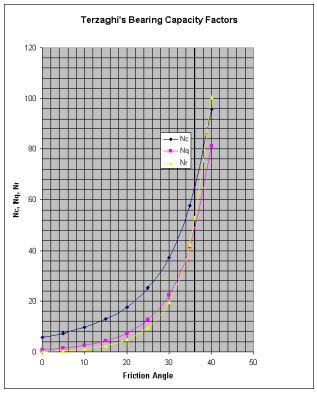

where

φ = angle of internal friction for the rock mass [-]
k_p = passive earth pressure coefficient [-]

Based on Terzaghi's bearing capacity theory, column load P is resisted by shear stresses at edges of three zones under the footing and the overburden pressure, q (=γD) above the footing. The first term in the equation is related to cohesion of the soil. The second term is related to the depth of the footing and overburden pressure. The third term is related to the width of the footing and the length of shear stress area. The bearing capacity factors, Nc, Nq, Nγ, are function of internal friction angle, φ. This equation is valid for long continuous foundations with length to width ratios in excess of ten.

For φ=35 ➔ N_c = 57,8 N_q = 41,4 N_γ = 42,4

The bearing capacity of the soil beneath the caisson structure according to the Terzaghi expression becomes for γ_{eff}=10 kN/m^3, c=0 kN/m^2, B=27m, D=2,5m, φ=35 ➔ q_{ult}= 5410 kPa. Including safety and over the total width of the caisson this becomes $q_{ult,r}$ = 5410*27/1,4= 104335 kN/m. The reason that D=2,5m was chosen and not the height of the caisson D=28m is due to the fact that the sand in front of the caisson is located at NAP-20,5m which results in less overburden pressure. By taking D=2,5m, the most unfavourable situation is created in determining the bearing capacity.

The down force due to the weight of the caisson and the vertical crane load (load combination 4) including safety factors is q_d= 9322*1,35+1302*1,5=14538 kN/m.

The bearing capacity of the soil is much higher than the down force (104335> 14538) and therefore no failure due to bearing beneath the caisson will occur.

The same was done to determine the bearing capacity of the landside crane foundation using γ_{eff}=19 kN/m^3, c=0 kN/m^2, B=27m, D=2,5m, φ=35. The bearing capacity including safety factors becomes 6750 kN/m whilst the down force acting on the caisson due to crane and surcharge load becomes 2163 kN/m. Failure due to insufficient bearing capacity will not occur for the landside crane foundation.

The downward force becomes less without crane load (load combination 5) and therefore it is not needed to determine.

Strength of caisson walls

The concrete caisson consists of six concrete walls which need reinforcement to resist the bending moment stresses due to static loading. Stresses within each wall are determined using the finite element program Plaxis which can be found in Appendix N Stresses within the walls according to Plaxis for load combination 4 and 5 are shown in tables below.

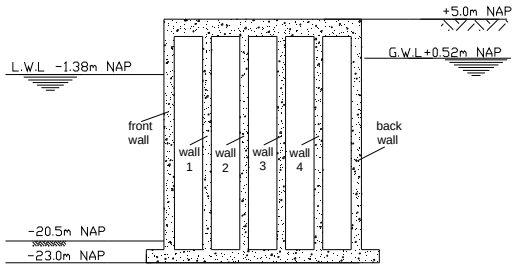

Plaxis Stresses Load Combi. 4	M_{max} kNm/m	Max. axial force kN/m
Front wall	-3490	-1920
Wall 1	-2480	-1680
Wall 2	-2910	-1270
Wall 3	-3260	-1080
Wall 4	-3140	-860
Back wall	-3150	-819

Plaxis Stresses Load Combi. 5	M_{max} kNm/m	Max. axial force kN/m
Front wall	-3420	-1140
Wall 1	-2560	-1210
Wall 2	-2610	-1050
Wall 3	-2540	-983
Wall 4	-2200	-836
Back wall	-1910	-929

The limit state design of reinforced concrete flexural members is based on the principles of strain compatibility and force equilibrium. The balanced flexural strength of a member is reached when the strain in the extreme compression fiber reaches the ultimate strain of concrete at the time the tension reinforcement reaches yield strain. It is essential to design a reinforced concrete member with sufficient ductility to avoid brittle failure in flexure. Therefore, maximum and minimum reinforcement ratio are introduces in national standards. A limitation of maximum reinforcement ensure that failure of reinforced concrete beams is initiated and proceeded by yielding of tensile steel. The minimum reinforcement ratio is essential to prevent early brittle failure of reinforced concrete beams by steel rupture. It ensures that nominal flexural strength exceeds the cracking moment. According to the Dutch standards an minimum and maximum reinforcement ratio of ω_{min}=0,18% and ω_{max}=1,93% is required for Concrete class B35 and steel class FeB500 [M.1]. This result in the following surface area of reinforcement:

$A_{min,steel,wall\ front/back} = 2160\ mm^2$ $A_{min,steel,wall\ 1/2/3/4} = 1800\ mm^2$
$A_{max,steel,wall\ front/back} = 23160\ mm^2$ $A_{max,steel,wall\ 1/2/3/4} = 19300\ mm^2$

For the first approximation 12 reinforcement bars with diameter of 40mm (A_s=15079 mm^2) are used for all the six caisson walls. Configuration of the reinforcement bars for the most critical section (highest bending moment) of the walls are shown in the figure below.

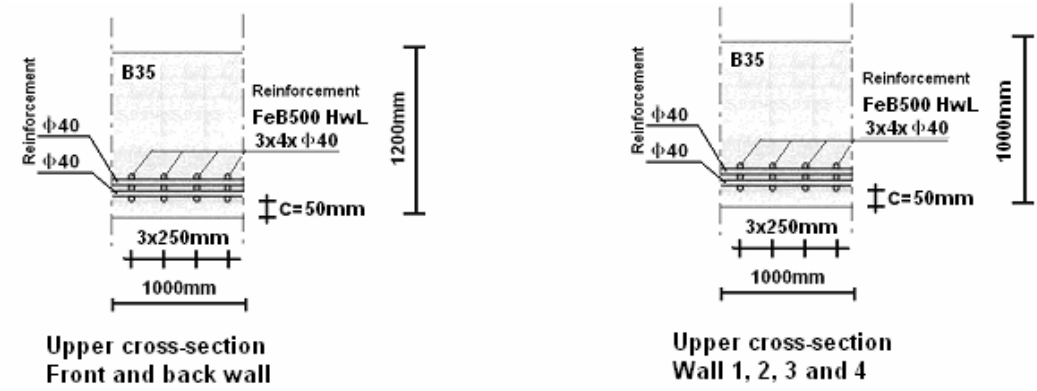

The bending moment capacity of the walls can be determined by knowing the amount of reinforcement steel placed in the walls. Some material properties of the caisson quay wall that are relevant in determining the moment capacity is listed in the tables below.

Concrete		B35
f'_{ck}		35 N/mm^2
f'_b		21 N/mm^2
f_b		1,4 N/mm^2
f_{bm}		2,74 N/mm^2
E'_b		31000 N/mm^2
ε'_b		3,5%
ε'_{bpl}		1,75%

Reinforcement bars		FeB 500 HwL
f_{rep}		500 N/mm^2
f_s		435 N/mm^2
E_s		200000 N/mm^2
ε_s		3,25 %

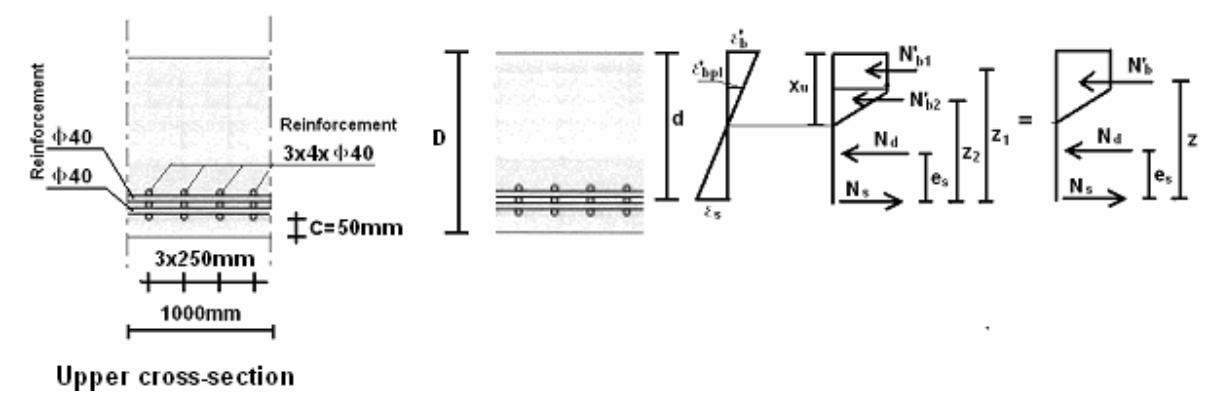

First the effective distance from the top of a reinforced concrete wall to the mass centre of the steel is determined.

$$d = D - c - 40 - 40 - 20$$

The distance of the normal force to the mass centre of the steel becomes:

$$e_s = D/2 - c - 40 - 40 - 20$$

Then the height of the compressive zone, x_u, needs to be determined. For that purpose the compressive forces N'_b are determined.

$$N'_{b1} = \frac{\varepsilon'_{bpl}}{\varepsilon'_b} \cdot x_u \cdot b \cdot f'_b = \frac{1{,}75}{3{,}5} \cdot x_u \cdot 1000 \cdot *21 = 10500 x_u$$

$$N'_{b2} = 0{,}5 \cdot \frac{\varepsilon'_{bpl}}{\varepsilon'_b} \cdot x_u \cdot b \cdot f'_b = 0{,}5 \cdot \frac{1{,}75}{3{,}5} \cdot x_u \cdot 1000 \cdot *21 = 5250 x_u$$

$$N'_b = N'_{b1} + N'_{b2} = 15750 x_u$$

When the reinforcing steel yields, the total force in this steel equals $A_s f_s$.

$$N_s = A_s \cdot f_s = 0{,}25 \cdot 40^2 \cdot \pi \cdot 15 \cdot 435 = 6{,}56 \cdot 10^6 N$$

The sum of N'_b, N_s and the normal force within the wall N_d needs to be in equilibrium. Resulting in the following formulation of x_u.

$$N_d + N'_b = N_s \qquad N_d + 15750 x_u = 6{,}56 \cdot 10^6 N$$

$$x_u = \frac{5{,}56 \cdot 10^6 - N_d}{15750}$$

N_d is determined using the finite element program Plaxis for each separate wall, see section N3. Hence, x_u can be determined when N_d is known. With the correct height x_u of the concrete compression zone, the moment capacity of the diaphragm wall can be determined by making use of the moment equilibrium.

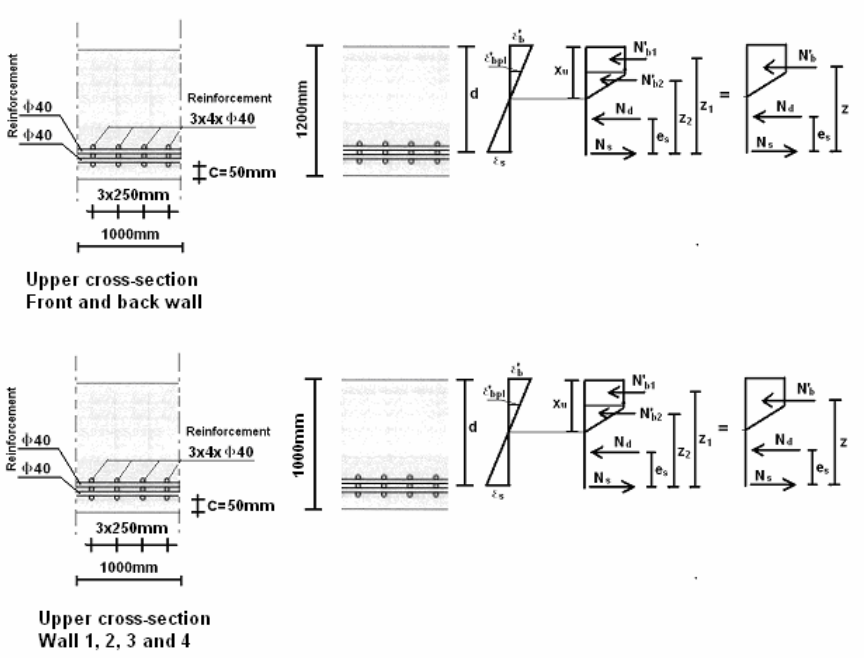

$$Z_1 = d - x_u / 4$$

$$Z_2 = d - x_u / 2$$

$$Z = \frac{N'_{b1} \cdot Z_1 + N'_{b2} \cdot Z_2}{N'_{b1} + N'_{b2}}$$

$$M_{cap} = N'_b \cdot Z + N_d \cdot e_s$$

Extra safety will be included by multiplying the stresses occurring in the wall elements of the caisson structure with a global safety factor. According to CURR 211[M.2], a global safety factor Ψ=1,3 needs to be taken for an quay wall structure. This results in the following design bending moments, M_d, and design axial forces ,N_d, and bending moment capacities, M_{cap}, as shown in the table below:

Plaxis Stresses Load Combi. 4	N_d kN/m	M_d kNm/m	M_{cap} kNm/m
Front wall	-2496	-4537	-4982
Wall 1	-2184	-3224	-4011
Wall 2	-1651	-3783	-4155
Wall 3	-1404	-4238	-4240
Wall 4	-1118	-4082	-4285
Back wall	-1065	-4095	-5503

Plaxis Stresses Load Combi. 5	N_d kN/m	M_d kNm/m	M_{cap} kNm/m
Front wall	-1482	-4446	-5503
Wall 1	-1573	-3328	-4175
Wall 2	-1365	-3393	-4227
Wall 3	-1278	-3302	-4248
Wall 4	-1087	-2860	-4293
Back wall	-1208	-2483	-5455

The chosen amount of reinforcement is sufficient to resist the maximum occurring bending moments due to static loading. This amount of reinforcement bars will be used at places where the bending moments are high. At places where the occurring bending moments are not that high, less reinforcement can be used. Determination of this lower amount of reinforcement is not included in this analysis because the stresses are not normative within these sections.

M4 References

[M.1] NEN 672,Voorschriften beton – Constructieve eisen en rekenmethode (VBC 1995),09-1995
[M.2] CURR 211

Appendix N Satic analysis Caisson with Plaxis

N1 Static caisson model Plaxis

N.1.1 Schematization of the geometry

The geometry of the Plaxis model is based on the early disapproved quay wall concept design of the Euromax quay wall (Figure 9-1). The caisson is prefabricated and sunk into position. Excavation is needed during the construction of the caisson. Hence, an assumption is made that good compressed/densified soil with properties listed in Table N-1 is put back during the backfill. Ground level is founded at NAP+5m and the seabed level is located at NAP-20,5m. The bottom of the caisson is located at a depth of NAP-23,0m. Outside water level is kept at NAP-1,38m while the ground water level is set at NAP+0,52m. These are the normative water levels as mentioned in Appendix F . The elements which where used in the Plaxis model are:

- Roof of the concrete caisson: is drawn as a cluster with connected geometry lines. The material is modelled like a linear elastic non-porous soil with the stiffness and the properties of concrete. It has a width and thickness of 22,9m and 2,0m respectively. The interaction between the soil layers is modelled with interface elements.
- Floor of the concrete caisson: is drawn as a cluster with connected geometry lines. The material is modelled like a linear elastic non-porous soil with the stiffness and the properties of concrete. It has a width and thickness of 27,0m and 1,5m respectively. The interaction between the soil layers is modelled with interface elements.
- Front and back wall of the concrete caisson: is modelled as plate with a length of 24,5m and a thickness of 1,2m. The interaction between the soil layers is modelled with interface elements. The weight of the wall is the actual weight minus the weight of the soil, due the fact that Plaxis superimposes a plate over the soil layer.
- Walls within the concrete caisson: is modelled as plate with a length of 24,5m and a thickness of 1,0m. The interaction between the soil layers is modelled with interface elements. The weight of the wall is the actual weight minus the weight of the soil, due the fact that Plaxis superimposes a plate over the soil layer.
- Landside beam: is drawn as a cluster with connected geomety lines. The material is moedelled like a linear elastic non-porous soil with the properties of concrete. Again interface elemetns are used.

Schematisation of the Plaxis geometry is illustrated in Figure N-1.

Soil properties

name	Material model	Material type	$\gamma_{unsat}/\gamma_{sat}$ [kN/m^3]	φ [deg.]	ν [-]	c [kN/m^2]	ψ [deg.]
Good compressed/densified soil	HS small	Drained	19 / 20	35	-	0,1	5

k_x [m/day]	k_y [m/day]	E_{ref} [kN/m^2]	E_{50}^{ref} [kN/m^2]	E_{oed}^{ref} [kN/m^2]	E_{ur}^{ref} [kN/m^2]	G_0^{ref} [kN/m^2]	$\gamma_{0,7}$ [-]	m [-]	R_{inter} [-]
20	20	-	1,00E+05	1,00E+05	2,20E+05	1,50E+05	3,50E-04	0,5	0,7

Table N-1 Soil properties of caisson backfill needed for Plaxis calculation

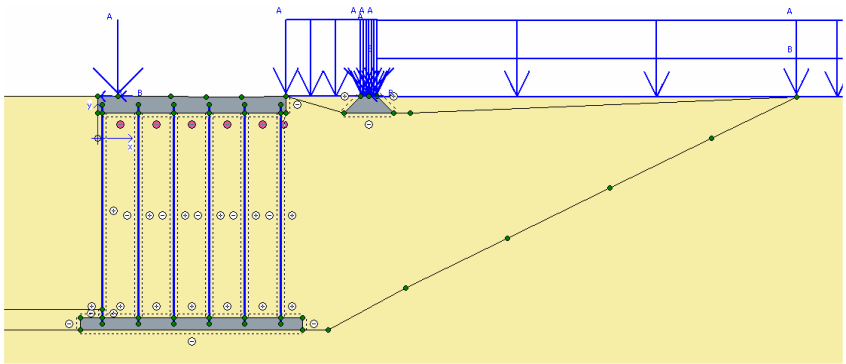

Figure N-1 Caisson schematization of the Plaxis geometry

N.1.2 Boundary conditions

The vertical boundaries are taken at about 4 times the retaining height resulting in 100 meter seaward and 100 meter land inward. These boundaries are far enough not to affect the area of interest. The vertical edges have fixed displacements in horizontal direction and are closed, to allow excess pore pressure to be present. The boundary at the base of the geometry is located at NAP-70m and is set at full fixity, since settlements may be assumed to be very small here. Special boundary conditions have to be defined to account for the fact that in reality the soil is a semi-infinite medium. Without these special boundary conditions the waves would be reflected on the model boundaries, causing perturbations. To avoid these spurious reflections, absorbent boundaries are specified at the vertical boundaries. The above described boundary conditions are known in Plaxis as “standard earthquake boundaries”.

N.1.3 Choice of the material model

The hardening soil model with small-strain stiffness is used with the same reason it was chosen during the static analysis of the diaphragm wall (section H.1.3)

N.1.4 Soil parameters

Soil behind the caisson is assumed compacted well enough just like the Pleistocene medium dense sand located at large depth during the backfill. Hence, only this soil type is used during the Plaxis analysis of the caisson. Soil parameters of Pleistocene medium dense sand can be found in section H.1.4.

N.1.5 Material properties

In the geometry, two different material datasets have been used for the Front/back wall and the walls in between. The flexural and axial rigidity of these walls are determined as follows assuming that reinforced concrete has the same young’s modulus as the diaphragm wall of $1{,}30 \cdot 10^7\, kPa$ (section H.1.5):

$$EI_{wall,\,front/back} = E_{concrete} \cdot \frac{1}{12} bh^3 = 1{,}3 \cdot 10^7 \frac{1}{12} \cdot 1 \cdot 1{,}2^3 = 1{,}872 \cdot 10^6\, kNm^2/m$$

$$EA_{wall,\,front/back} = E_{concrete} \cdot bh = 1{,}3 \cdot 10^7 \cdot 1 \cdot 1{,}2 = 1{,}56 \cdot 10^7\, kN/m/m$$

$$EI_{wall,between} = E_{concrete} \cdot \frac{1}{12} bh^3 = 1{,}3 \cdot 10^7 \frac{1}{12} \cdot 1 \cdot 1{,}0^3 = 1{,}083 \cdot 10^6\, kNm^2/m$$

$$EA_{wall,between} = E_{concrete} \cdot bh = 1{,}3 \cdot 10^7 \cdot 1 \cdot 1{,}0 = 1{,}3 \cdot 10^7\, kN/m/m$$

The side walls of the caisson also influence the flexural rigidity of the whole caisson and needs to be included in the Plaxis model. By dividing the flexural rigidity of the side walls by the caisson length of 22m, the flexural rigidity of the sidewalls per quay length is determined. Distribute this flexural rigidity evenly to the front/back wall and the wall in between. By doing so, the flexural rigidity of the side walls is included.

The flexural rigidity of the side wall is determined as follows:

$$EI_{wall,side} = E_{concrete} \cdot \frac{1}{12} tb^3 = 1{,}3 \cdot 10^7 \frac{\frac{1}{12} \cdot 1{,}0 \cdot (5 \cdot 3{,}3)^3}{22} = 2{,}219 \cdot 10^8\, kNm^2/m$$

After distribution of the flexural rigidity of the two side wall evenly the Flexural rigidity of the front/back and the wall in between implemented in Plaxis becomes :

$$EI_{plaxis,wall,front/back} = EI_{wall,front/back} + \frac{2EI_{wall,side}}{10} = 4{,}7 \cdot 10^7\, kNm^2/m$$

$$EI_{plaxis,wall,between} = EI_{wall,between} + \frac{2EI_{wall,side}}{5} = 9{,}0 \cdot 10^7\, kNm^2/m$$

The walls that are modeled as plates have zero thickness. The volume of materials of these elements that is present in reality is now replaced by soil. Through here, the input weight of these elements becomes less than the real weight of the elements. The input unit weight for Plaxis is the real unit weight of the element minus the unit weight of the soil. For the unit weight an average weight over depth of 20 kN/m is used.

$$w_{input,plaxis} = w_{element} - w_{soil}$$

Poisson ratio for croncrete according to NEN6720 [H.3] should be between ν=0,1 and ν=0,2. For concrete elements a poisson ration of ν=0,15 is chosen. For steel elements poisson ratio is ν=0,3.

The material properties for the different material sets of the quay wall are shown in *Table N-2*.

Material properties

name	Material type	Normal stiffness [kN/m/m]	Flexural rigidity [kNm²/m]	weight [kN/m]	poisson's ratio [-]	Spacing out of plane [m]	Damping coefficient [-]	
		EA	EI	w	v	$L_{spacing}$	Rayleigh α	Rayleigh β
PLATES								
Caisson front/back wall	Elastic	1,56E+07	4,70E+07	6	0,15	-	-	-
Caisson wall in between	Elastic	1,30E+07	9,00E+07	5	0,15	-	-	-

Table N-2 Input material properties for Plaxis

N.1.6 Mesh generation

After completing the geometry and dataset, the mesh is generated. The global coarseness is set to “fine” since this is supposed to be sufficient for analyzing different influences and not to loose too much time for calculation. This means a global mesh of about 630 elements. There is chosen to use the 15 noded elements instead of the 6 noded elements because close to failure behaviour this element type give a 10% higher accuracy according to Watermann [H.4].

N.1.7 Soil-structure interaction

If a plate element is introduced in Plaxis, it is always fully permeable. Interface elements can be given in between soil and plate elements to make the plate impermeable and to simulate soil-structure behaviour, which is intermediate between smooth and fully rough. The roughness of the interaction is modeled by choosing a suitable value for the strength reduction factor in the interface, R_{inter}. This factor relates the interface strength (wall friction and adhesion) to the soil strength (friction angle and cohesion). Values for R_{inter} = 0,6 or 0,7 are used for clay-steel/concrete or sand-steel/concrete interfaces respectively. The application of interfaces is done for the caisson quay wall. Below the roof of the caisson R_{inter} = 0,1 is chosen because no attachment is present between the virtual beam and the soil below for the reason that the roof is supported by the walls.

N2 Static caisson model calculation Plaxis

N.2.1 Construction method

The quay wall has been built in a certain way. To take the building sequence into account in Plaxis the option “staged construction” can be used. This option allows users to (de)activate weight, strength, stiffness and to change material properties or water pressures. The caisson quay wall is created in 9 phases. The function “update mesh” will not be used. This function allows the mesh to update after each phase calculation, which will lead to a more accurate second order effect. Since the deformations are very small which result in small second order effects this effect is negligible.

Loads which is applied during the different phases includes combinations factors shown in Table 9-2. A global safety factor will be included in a later stadium replacing the partial safety factors mentioned in section 9.3 by multiplying the stresses occurring in the elements of the caisson structure with the global safety factor. According to CURR 211[N.1], a global safety factor Ψ=1,3 needs to be taken for an quay wall structure.

Phase 0: initial phase
State of the soil before construction. Ground and water level located at NAP+5m and NAP+0,52m respectivily.

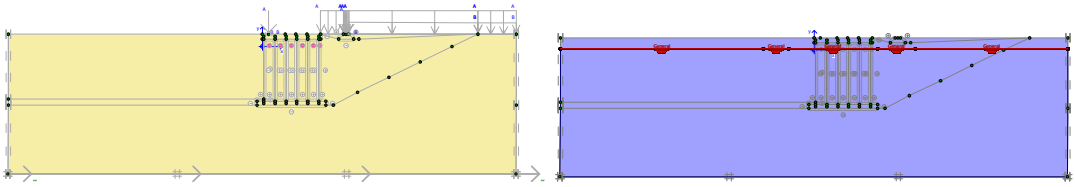

Phase 1: excavation
Preparation for placing the caisson quay wall by excavating the ground till NAP -23m.

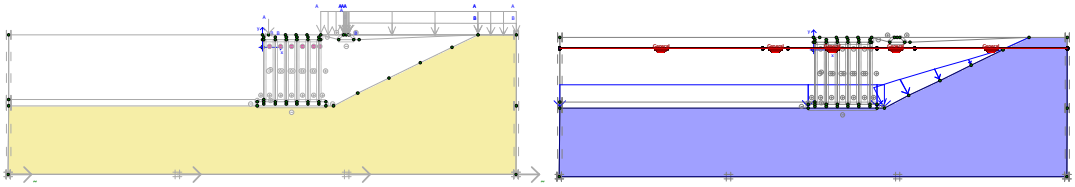

Phase 2: placing the caisson
The prefab caisson is sunk into location and put on top of the excavated seabed level of NAP-23m.

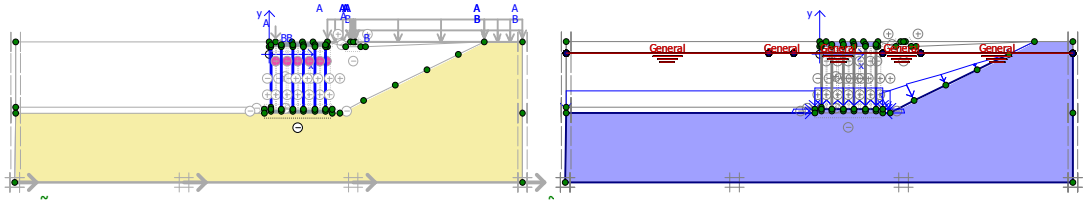

Phase 3: backfill 1
The caisson is filled with sand. In front of the caisson quay wall the soil is filled back till NAP-20,5m. Behind the caisson quay wall soil has been filled till NAP+3m.

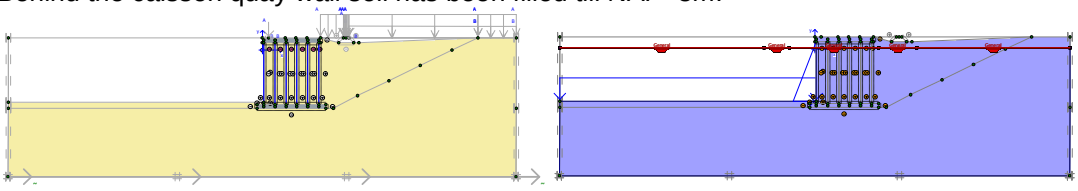

Phase 4: Installation landside crane foundation and final backfill
Landside crane foundation is being installed behind the caisson quay wall. Behind the caisson quay wall soil is filled back till NAP+5m.

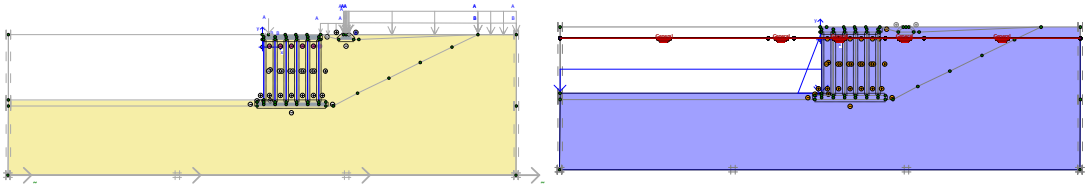

Phase 5: applying surcharge load behind landside crane rail
Surcharge load of 14 kPa is applied behind the landside crane rail. Displacement is set to zero starting from this phase.

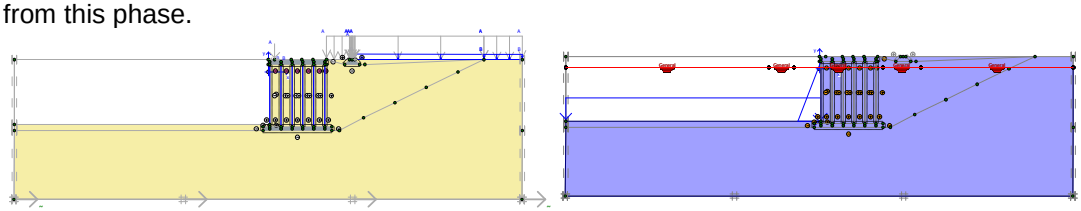

Phase 6:increase surcharge load
Surcharge load behind the caisson quay wall is increased to 28 kPa.

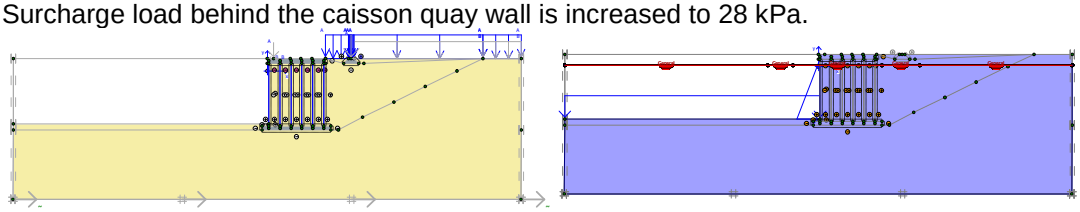

Phase 7: applying bolder and crane load
272 kPa bolder load is applied and horizontal and vertical crane loads of 34 kN and 1302kN respectively is applied depending on the load combination.

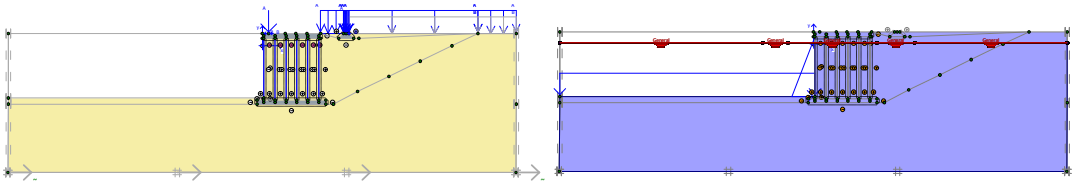

Phase 8:increase surcharge load behind landside rail
Surcharge load behind the landside crane rail is increased to 42 kPa.

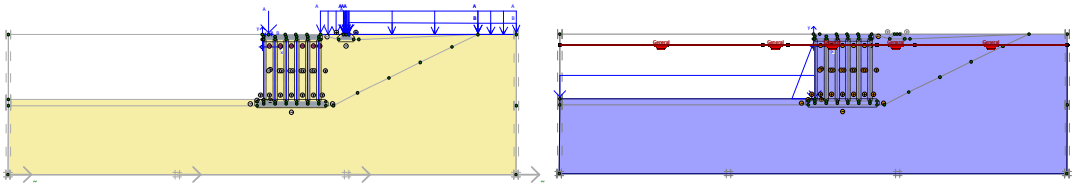

Phase 9: Change seawater level
Seaside water level is set to NAP-1,38m while the ground water level stays at NAP+0,52m

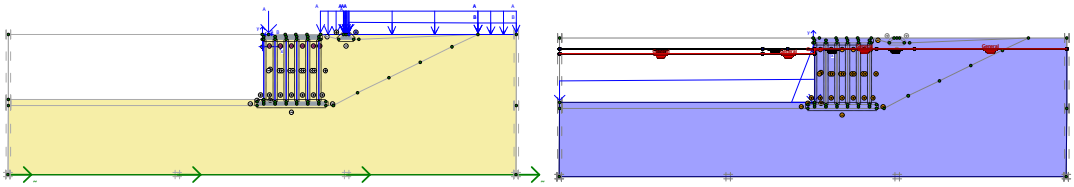

N3 Static model output Plaxis

Load combination 4

Displacements

The final horizontal and vertical displacements after the last phase (phase 9) are shown in the figure and table below.

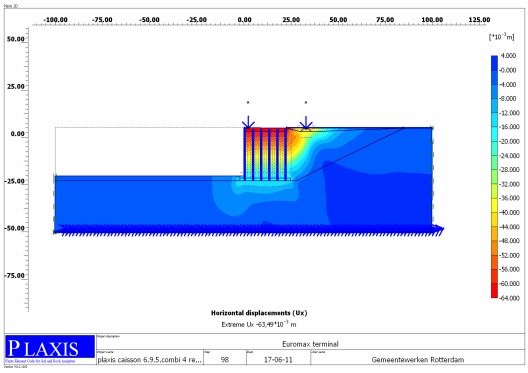

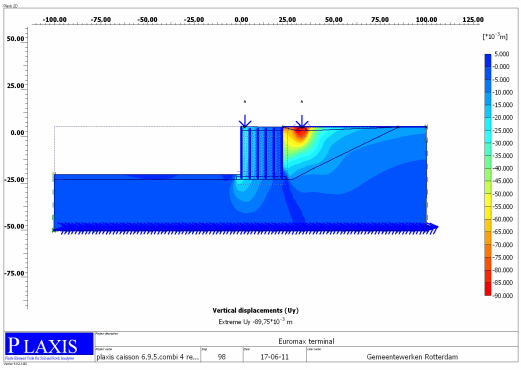

Plaxis Displacement	Hor. displacement After last phase	Vert. displacement After last phase
Seaside crane rail	-0,064 m	-0,022 m
Landside crane rail	-0,042 m	-0,086 m

The development of displacements due to the different phases is shown in the graphs below, where:

Step 1 till step 8 corresponds to phase 1
Step 9 till step 10 corresponds to phase 2
Step 11 till step 62 corresponds to phase 3
Step 63 till step 68 corresponds to phase 4
Step 69 till step 72 corresponds to phase 5
Step 73 till step 77 corresponds to phase 6
Step 78 till step 87 corresponds to phase 7
Step 88 till step 91 corresponds to phase 8
Step 92 till step 98 corresponds to phase 9

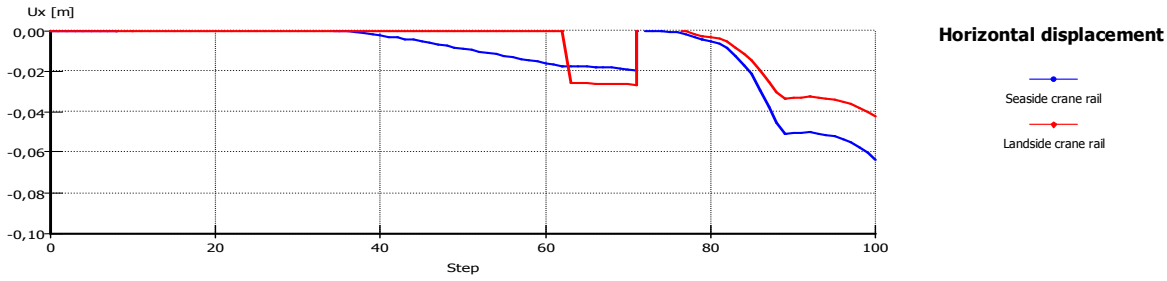

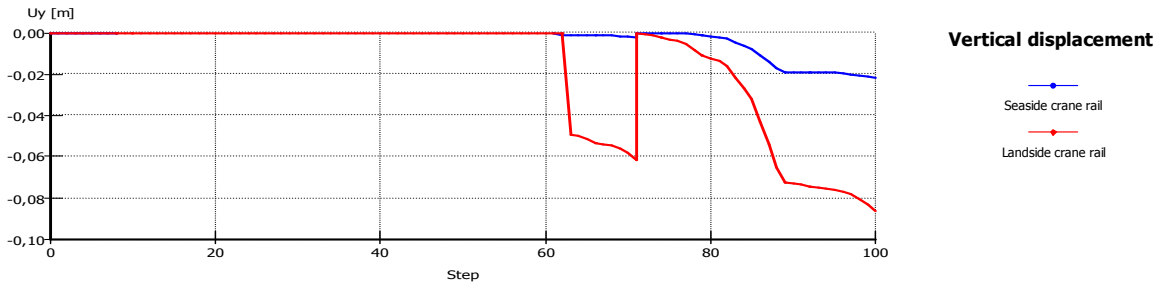

Stresses

Static bending moments and axial stresses of the caisson walls for load combination 4 can be found in the figures and tables below.

Plaxis Stresses	Depth M_{max} m NAP	M_{max} kNm/m	Max. axial force kN/m
Front wall	-7,8	-3330	-1900
Wall 1	3	-2330	-1170
Wall 2	3	-2650	-1270
Wall 3	3	-2870	-987
Wall 4	3	-2680	-821
Back wall	-5,75	-2380	-746

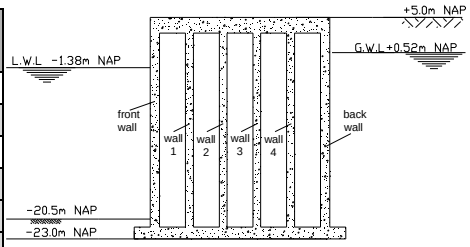

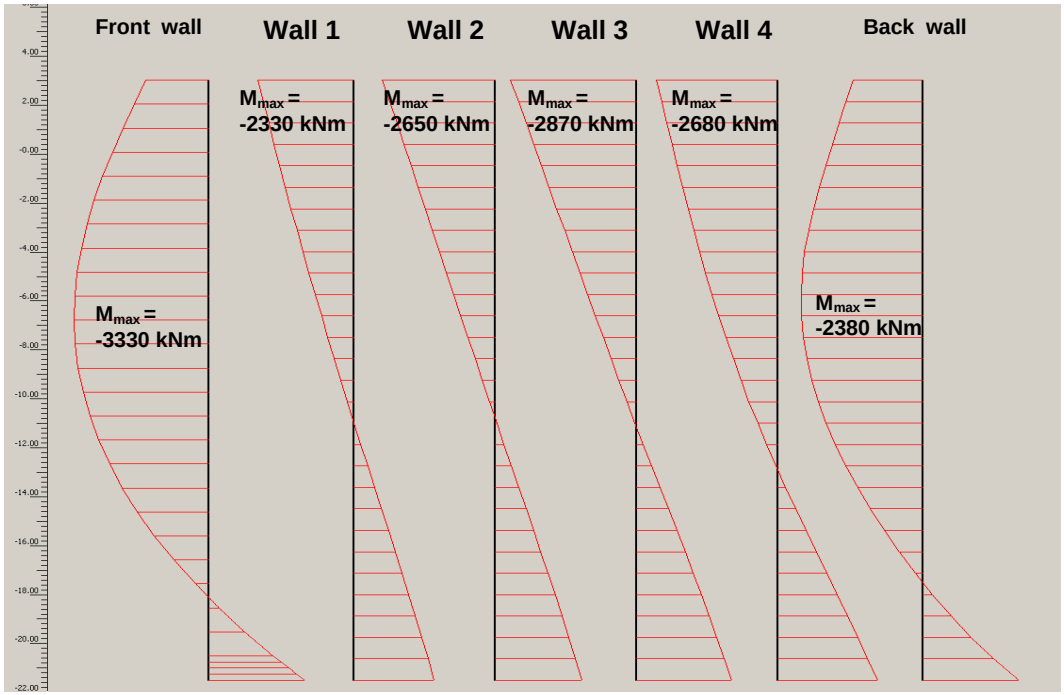

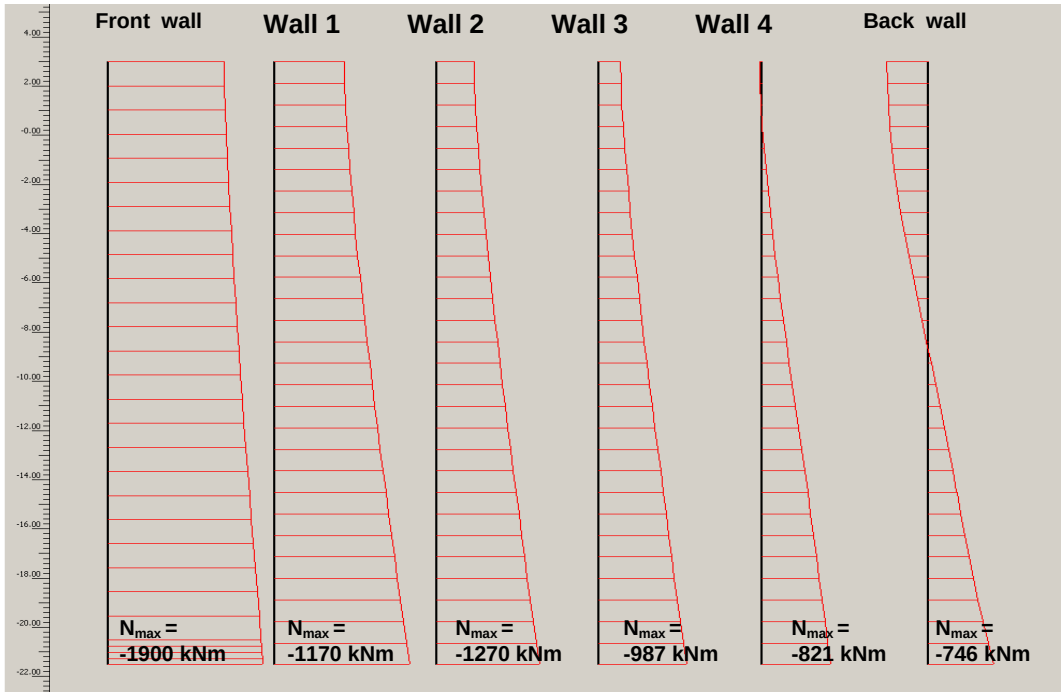

Load combination 5

Displacements

The final horizontal and vertical displacements after the final phase 9 are shown in the figure and table below.

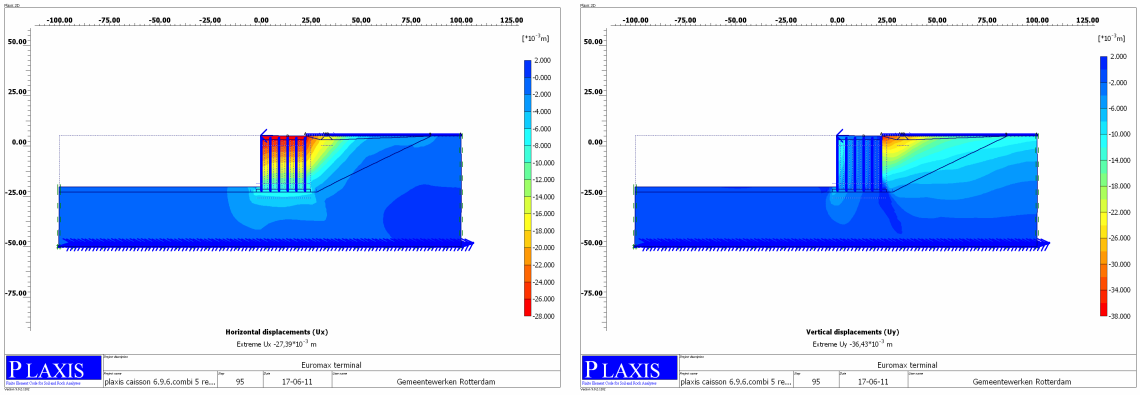

The development of displacements due to the different phases are shown in the graphs below, where:

Step 1 till step 8 corresponds to phase 1
Step 9 till step 20 corresponds to phase 2
Step 11 till step 66 corresponds to phase 3
Step 67 till step 71 corresponds to phase 4
Step 72 till step 74 corresponds to phase 5
Step 75 till step 79 corresponds to phase 6
Step 80 till step 84 corresponds to phase 7
Step 85 till step 88 corresponds to phase 8
Step 89 till step 95 corresponds to phase 9

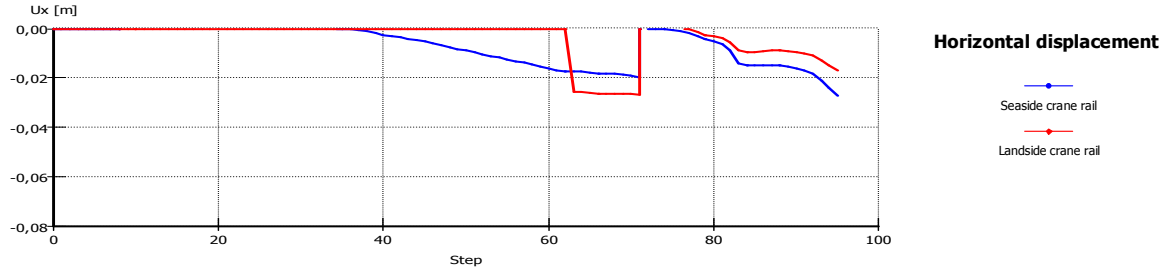

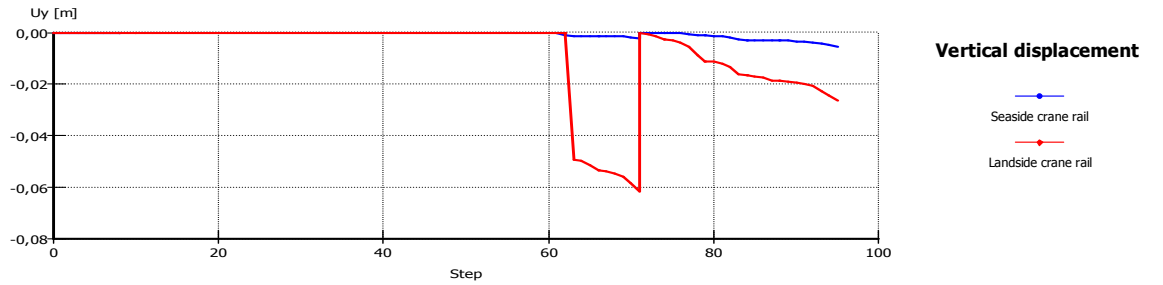

Plaxis Displacement	Hor. displacement After last phase	Vert. displacement After last phase
Seaside crane rail	-0,027 m	-0,005 m
Landside crane rail	-0,017 m	-0,026 m

Stresses

Static bending moments and axial stresses of the caisson walls for load combination 5 can be found in the figures and tables below.

Plaxis Stresses	Depth M_{max} m NAP	M_{max} kNm/m	Max. axial force kN/m
Front wall	-6,8	-3240	-1110
Wall 1	3	-2390	-1120
Wall 2	3	-2380	-974
Wall 3	3	-2230	-920
Wall 4	3	-1890	-820
Back wall	-4,9	-1370	-860

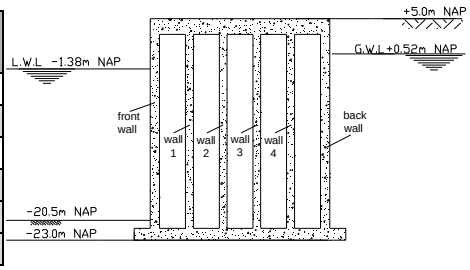

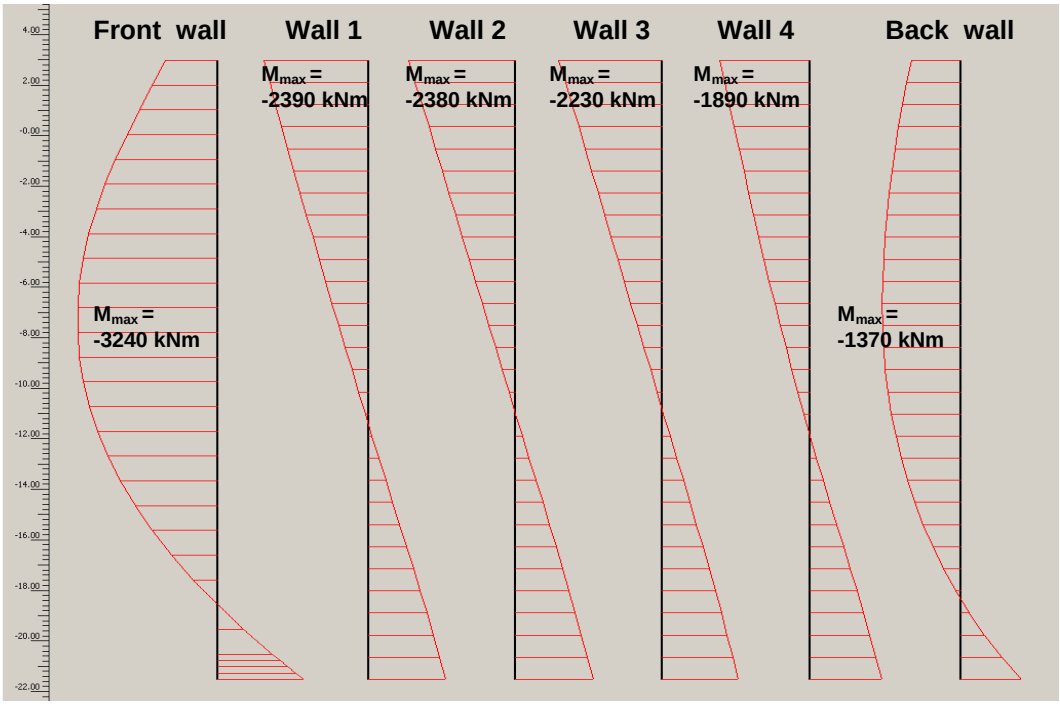

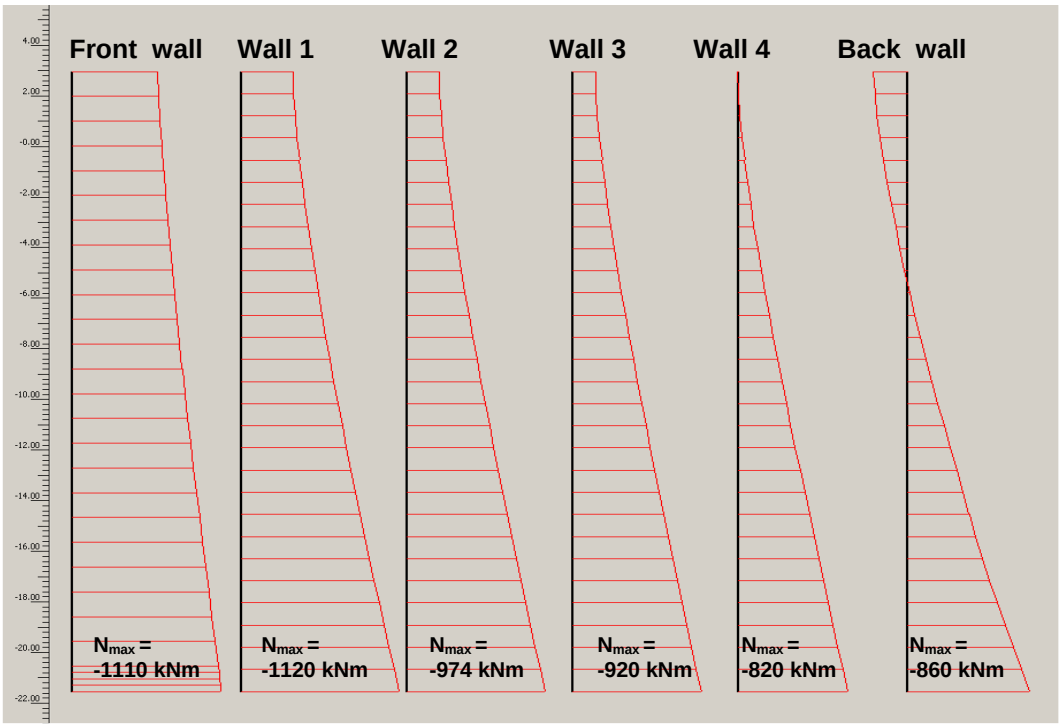

N4 References

[N.1] CUR 211, Handbook quay wall, 2005

Appendix O Pseudo static analysis Caisson quay wall

In this appendix a pseudo static analysis is performed for the caisson quay wall. Soil profile shown in Figure I-19-1 and a earthquake acceleration of 0,5 m/s^2 is used during this analysis to see whether or not the diaphragm wall can resist this magnitude of earthquake. The corresponding seismic coefficients for this earthquake acceleration is k_h=0,067 and k_v=0,022. It should be noted that the forces arise due to the inertia of the caisson is considered in this pseudo seismic analysis.

Three different Cases are analyzed depending upon the magnitude of excess pore water pressure generated during the earthquake. By doing this the influence of excess pore water pressure can be shown.

Case 1: no excess pore water pressure
Case 2: excess pore water pressure is 50 percent of the initial vertical effective stress
Case 3: Complete liquefaction of backfill

By determining the static and dynamic forces acting on the caisson quay wall caused by the earthquake, the stability of the caisson can be checked using the horizontal and moment equilibrium.

O1 Caisson Case 1 (no excess pore water pressure)

The presence of water within the backfill and in front of the caisson quay wall results in additional static and dynamic forces acting on the wall and alters the distribution of forces within the active and passive soil wedges developing behind and in front of the caisson. This section describes the calculations that are made to determine the stability of the caisson wall. This analysis, described as case 1, assumes that no excess pore pressures are generated within the submerged portion of the backfill or within the foundation during earthquake shaking.

O.1.1 Loads

The static and additional seismic forces during an earthquake are determined in this section for case 1. The structure will be calculated per running meter.

Static water pressure
Static water pressures are determined using Eq. 5-3. Point of application of these forces are determined using Eq. F-1 and are shown in Figure I-2Figure O-1.

$$U_{stat,front} = \frac{1}{2}\gamma_w h_1^{\,2} = \frac{1}{2} * 10 * (23 - 1{,}38)^2 = 2337 kN/m$$

$$U_{stat,ground,back} = \frac{1}{2}\gamma_w h_2^{\,2} = \frac{1}{2} * 10 * (23 + 0{,}52)^2 = 2766 kN/m$$

Dynamic water pressure
Distinction is made for free standing water seaside of the wall and water in backfill. These water pressures are determined using the Westergaard solution mentioned in chapter 5.4. For water located at the backfill of the wall Matsuo and Ohara (1965) suggested the hydrodynamic pressure to be around 70% of that of the free standing water. This suggestion was used during the calculation. Resultant thrust is determined for the dynamic water pressures and are shown below and in Figure O-2. They are acting at an elevation equal to 0,4 times the total water depth h_{total} above the base of the wall.

$$U_{dyn,front} = \int_0^{21{,}62} \left(\frac{7}{8} k_h \gamma_w \sqrt{y * 21{,}62} \right) dy = \frac{7}{8} * 0{,}067 * 10 * \sqrt{21{,}62} * \frac{1}{1{,}5} * 21{,}62^{1{,}5} = 183 kN/m$$

$$U_{dyn,ground,back} = \left(\frac{7}{12} k_h \gamma_w h_{total}^{\,2} \right) * 0{,}7 = \left(\frac{7}{12} * 0{,}067 * 10 * 23{,}52^2 \right) * 0{,}7 = 151 kN/m$$

Case 1: hydrostatic water pressure

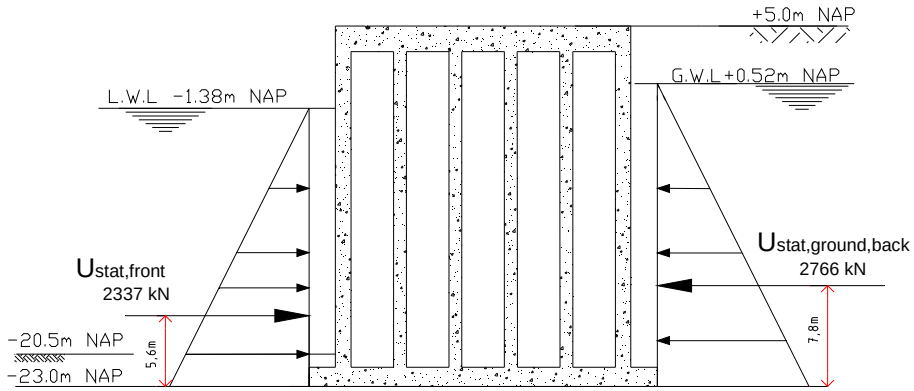

Figure O-1 Hydrostatic water pressure for case 1

case 1: hydrodynamic water pressure

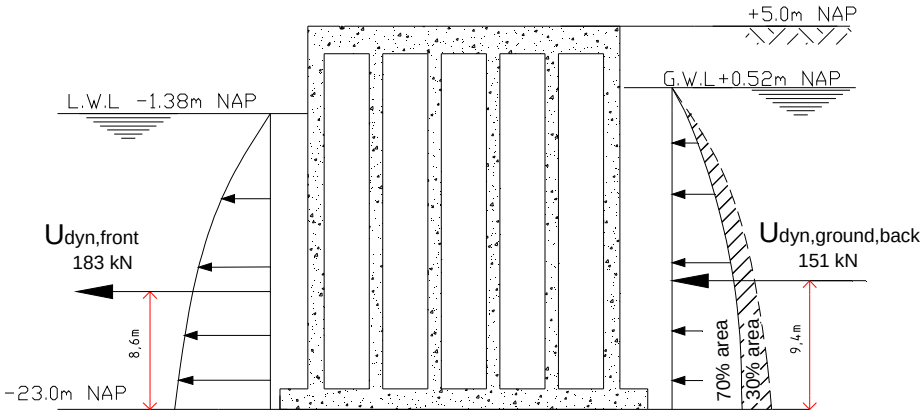

Figure O-2 Hydrodynamic water pressure for case 1

Dynamic ground pressure

Dynamic earth pressure is determined using the M-O method mentioned in Appendix C . The M-O method assumes that the wall movements are sufficient to fully mobilize the shear resistance along the backfill wedge, as is the case for Coulomb's active and passive earth pressure theories. To develop the dynamic active earth pressure force, P_{ae}, the wall movements are away from the backfill, and for the passive dynamic earth pressure force, P_{pe}, the wall movements are towards the backfill. The most unfavorable direction combination is used during this analysis. This is when the horizontal acceleration (α_h) is directed towards the backfill and the vertical acceleration (α_v) is directed downward, causing the incremental dynamic earth pressure forces ($\Delta P_{AE/PE}$) acting away from the backfill. This has the normative effect of increasing the driving force behind the quay wall and decreasing the stabilizing force.

The dynamic active earth pressure coefficient k_{ae} and seismic inertia angle ψ_a for case 1 is determines using Eq. C-2 and Eq. C-3.

$$\psi_a = \tan^{-1}\left(\frac{k_h}{1-k_v}\frac{\gamma_d}{\gamma-\gamma_w}\right) = \tan^{-1}\left(\frac{0{,}067}{1-0{,}022}\frac{19}{20-10}\right) = 7{,}42$$

$$k_{ae} = \frac{\cos^2(\varphi-\beta-\psi)}{\cos\psi\cos^2\beta\cos(\delta+\beta+\psi)\left[1+\sqrt{\frac{\sin(\delta+\varphi)\sin(\varphi-\alpha-\psi)}{\cos(\delta+\beta+\psi)\cos(\alpha-\beta)}}\right]^2}$$

$$= \frac{\cos^2(35-0-7{,}42)}{\cos 7{,}42\cos^2 0\cos(23+0+7{,}42)\left[1+\sqrt{\frac{\sin(23+35)\sin(35-0-7{,}42)}{\cos(23+0+7{,}42)\cos(0-0)}}\right]^2} = 0{,}334$$

Hence the dynamic active pressure thrust P_{ae} is:

$$P_{ae} = \frac{1}{2}k_{ae}\gamma_{dry}H_1^{\,2}(1-k_v) + k_{ae}\gamma_{dry}H_1H_2(1-k_v) + \frac{1}{2}k_{ae}\gamma_{eff}H_2^{\,2}(1-k_v)$$

$$= \frac{1}{2}*0{,}334*19*4{,}48^2*(1-0{,}022) + 0{,}334*19*4{,}48*23{,}52*(1-0{,}022) +$$

$$\frac{1}{2}*0{,}334*(20-10)(23{,}52)^2*(1-0{,}022) = 1620kN/m$$

P_{ae}, can be divided into a static component, P_a, and a dynamic component, ΔP_{ae}. The static component can be calculated using Eq. B-7 and Eq. B-8 which is based on the Coulomb Theorem.

$$k_a = \frac{\cos^2(\varphi-\beta)}{\cos^2\beta\cos(\delta+\beta)\left[1+\sqrt{\frac{\sin(\delta+\varphi)\sin(\varphi-\alpha)}{\cos(\delta+\beta)\cos(\alpha-\beta)}}\right]^2} = 0{,}244$$

$$P_a = \frac{1}{2}k_a\gamma_{dry}H_1^{\,2}(1-k_v) + k_a\gamma_{dry}H_1H_2(1-k_v) + \frac{1}{2}k_a\gamma_{eff}H_2^{\,2}(1-k_v) = 1170kN/m$$

The dynamic component ΔP_{ae} is

$$\Delta P_{ae} = P_{ae} - P_a = 1620 - 1170 = 450kN/m$$

The static component is known to act at H/3 above the base of the wall. Seed & Whitman (1970) recommended that the dynamic component be taken to act at approximately 0.6 H. On this basis, the total dynamic active thrust P_{ae} will act at a height h from the base of the wall.

$$h = \frac{P_a\cdot 9{,}6 + \Delta P_{ae}(0.6H)}{P_{ae}} = \frac{1170*9{,}6 + 450*(0.6*28)}{1620} = 11{,}6m$$

The dynamic passive earth pressure coefficient k_{pe} and seismic inertia angle ψ_p for case 1 is determines the same way like for the active case which results in the following dynamic earth pressures:

$$\psi_p = \tan^{-1}\left(\frac{k_h}{1-k_v}\frac{\gamma_d}{\gamma-\gamma_w}\right) = \tan^{-1}\left(\frac{0{,}067}{1-0{,}022}\frac{19}{20-10}\right) = 7{,}42$$

$$k_{pe} = \frac{\cos^2(\varphi+\beta-\psi)}{\cos\psi\cos^2\beta\cos(\delta-\beta+\psi)\left[1+\sqrt{\frac{\sin(\delta+\varphi)\sin(\varphi+\alpha-\psi)}{\cos(\delta-\beta+\psi)\cos(\alpha-\beta)}}\right]^2} = 8{,}84$$

$$P_{pe} = \frac{1}{2}k_{pe}\gamma_{eff}H^2(1-k_v) = 270kN/m$$

P_{pe} is acting at 1/3H above the base of the wall. Figure O-3 shows an illustration of the dynamic earth pressure forces and its point of application.

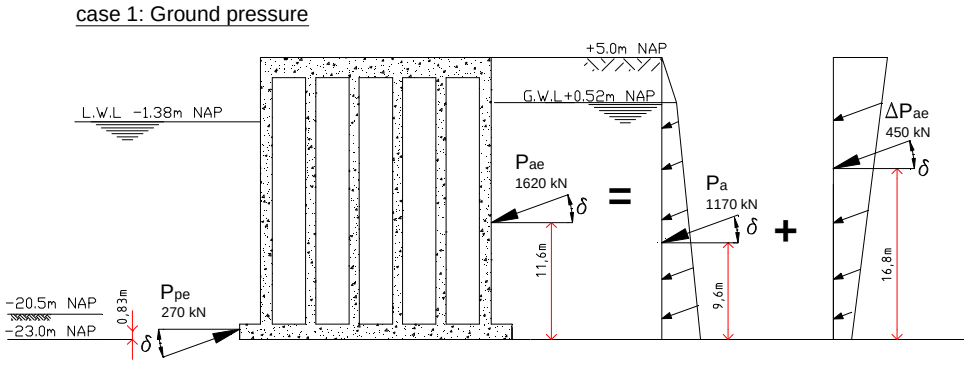

Figure O-3 Dynamic earth pressures for case 1

Surcharge load

The impact of this one-sided limited surcharge load on the wall can be estimate using the method created by Ohde **Error! Reference source not found.** which is illustrated in Figure O-4. The area of influence begins where the line at angle φ cuts the axis of the sheet pile. The full influence is valid when the line at angle ϑ_a cuts the axis. The angle of the sliding plane angle ϑ_a depends on the angle of internal friction φ, the slope of the ground surface β and the inclination of the sheet pile α.

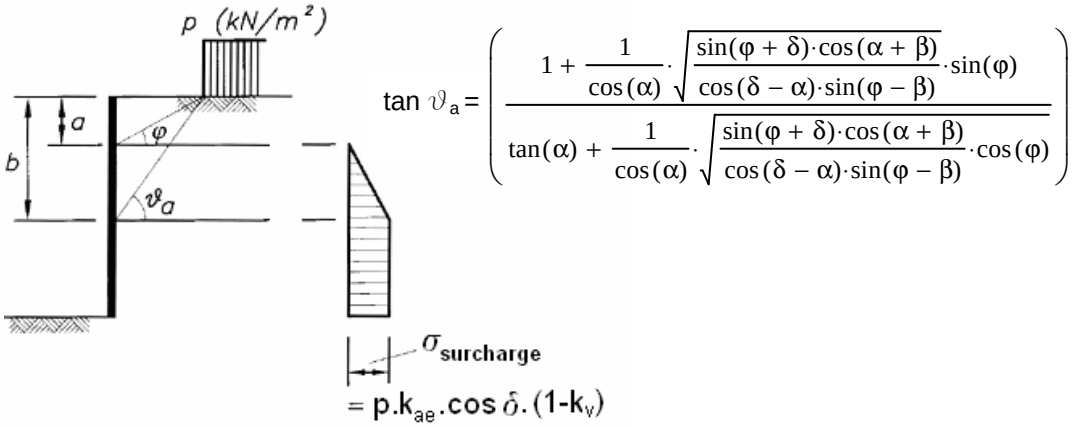

$$\tan\vartheta_a = \left(\frac{1+\frac{1}{\cos(\alpha)}\cdot\sqrt{\frac{\sin(\varphi+\delta)\cdot\cos(\alpha+\beta)}{\cos(\delta-\alpha)\cdot\sin(\varphi-\beta)}}\cdot\sin(\varphi)}{\tan(\alpha)+\frac{1}{\cos(\alpha)}\cdot\sqrt{\frac{\sin(\varphi+\delta)\cdot\cos(\alpha+\beta)}{\cos(\delta-\alpha)\cdot\sin(\varphi-\beta)}}\cdot\cos(\varphi)}\right)$$

Figure O-4 Horizontal ground pressure for one- sided limited surcharge load

Forces acting on the wall due to of surcharge load is shown in **Error! Reference source not found.**.

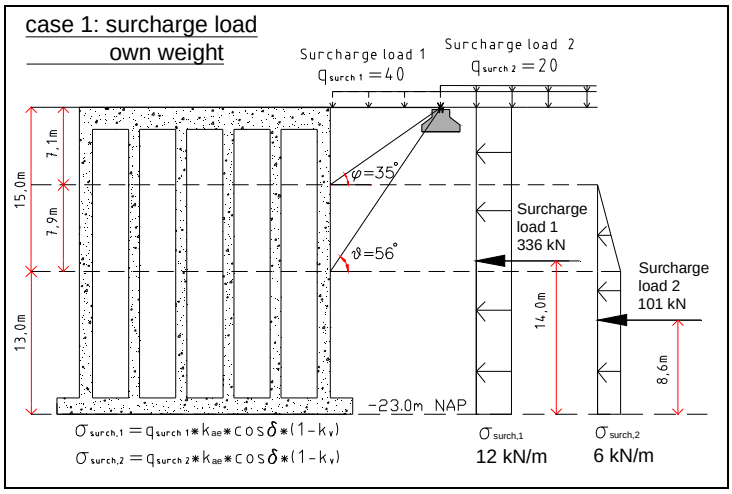

Figure O-5 Horizontal ground pressure as result of surcharge load behind caisson

Crane load

The landside crane load is schematized as a two-sided limited distributed load with a width of the crane rail foundation of 3,5m and a loading of the crane load divided by the width. The bolder load, seaside crane load and the horizontal thrust on the wall due the presence of the two-sided limited distributed crane load can be determined using the method shown in Figure O-6 **Error! Reference source not found.**.

Thrust acting on the wall due to the landside crane load is shown in Figure O-7.

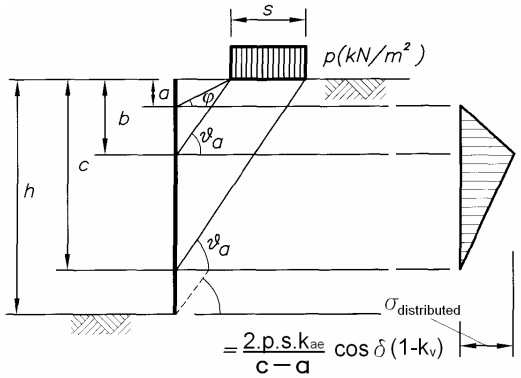

Figure O-6 Horizontal ground pressure for two - sided limited distribution load

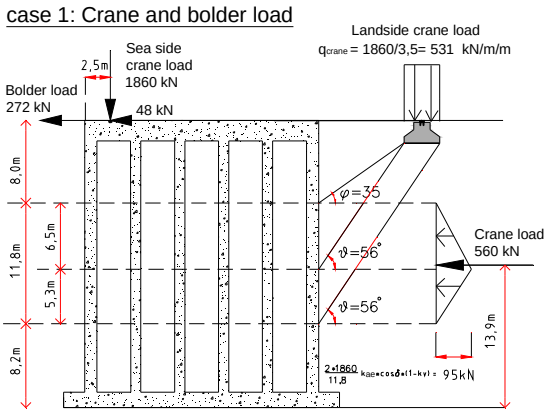

Figure O-7 Horizontal ground pressure due to the landside crane load

Own weight caisson during earthquake

When the vertical acceleration is directed downward (normative earthquake direction) the own weigth of the caisson structure will become less. It can be determined by multiplying the own weight by (1-k_v) as shown below.

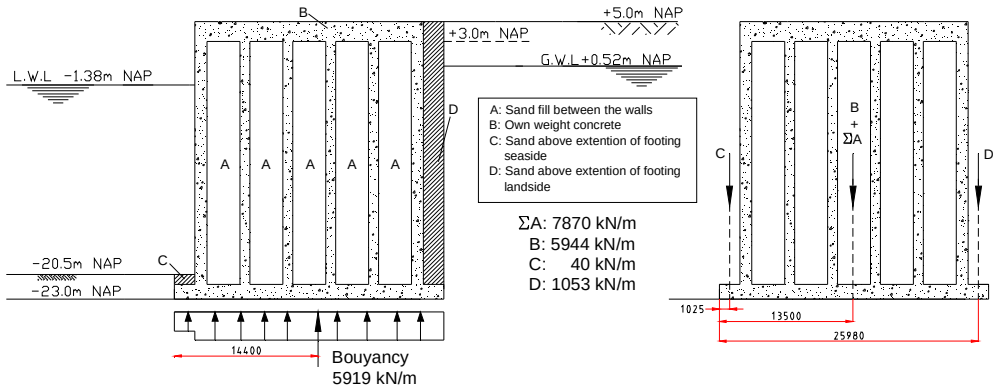

Figure O-8 Own weight of caisson

A= $A_{A,sand,dry}$*γ_d + $A_{A,sand,wet}$*γ_s *(1-k_v)= (3,3*2,48)*19+(3,3*22,02)*20*(1-0,022) = 1574 kN/m
B= $A_{concrete}$*$\gamma_{concrete}$*(1-k_v) = (22,9*2+27*1,5+2*1,2*24,5+4*1*24,5)*25 *(1-0,022) = 5944 kN/m
C= $A_{,c,sand}$*γ_s*(1-k_v) = 1*2,05*20*(1-0,022) = 40 kN/m
D= ($A_{D,sand,dry}$*γ_d + $A_{D,sand,wet}$*γ_s)(1-k_v) = ((4,48*2,05)*19+(22,02*2,05)*20)*(1-0,022)= 1053 kN/m

Bouyancy
Bouyancy is an upward acting force exerted by a fluid, that opposes an object's weight. Any object, wholly or partially immersed in a fluid, is buoyed up by a force equal to the weight of the fluid displaced by the object.

Bouyancy = $A_{below\ water}$* γ_w = (24,95*23,52+2,5*2,05)*10 = 5919 kN/m

Seismic inertia forces caisson
The seismic inertia force of the caisson is determined by multiplying the weight of the caisson during static conditions as determined in appendix M2 by the horizontal seismic coefficient k_h=0,067. The own weight of the caisson including sand fill is 15241 kN/m. This results in a horizontal inertia force of $F_{inertia,hor}$ = 1021 kN/m towards the sea located at NAP- 9m.

O.1.2 Stability of the caisson case 1

There are two main deformations for a gravity retaining wall, namely sliding and rotation. The former is due to inadequate sliding resistance, whilst the outward tilting of a wall may be caused by inadequate resistance to overturning and or bearing.

Under the action of the in section O.1.1 mentioned forces, the stability of the wall is checked for both the sliding and overturning failure making use of force equilibriums.

Safety factors
No safety factors are used because real occurring forces need to be used to see whether or not the caisson is stable or not.

Load combinations and combination factors
Two load combinations are checked for the caisson quay wall and are listed in Table 9-2. Combination factors Ψ for separate loads are also listed in Table 9-2.

Sliding stability
The friction force must withstand the horizontal forces acting on the caisson otherwise the caisson will start to slide. Calculations have been made to check whether the width of caisson is sufficient enough. Sliding stability is checked for only the normative load combination which is load combination 4.

$\sum(F_h*\Psi) \leq F_{friction}$
$F_{friction} = (\mu)* \sum(F_v*\Psi)$

$\sum F_h$: Sum of horizontal forces acting on caisson
$F_{friction}$: Frictional force between caisson floor and the sand beneath with safety coefficient included
Ψ : Combination factor
μ : Dynamic friction coefficient (tan φ)
F_v : Vertical forces acting on the caisson

$\sum F_h$ = -2337*1+2766*1+183*1+151*1–270*1+1620*1+336*0,7+101*0,7+560*0,7+272*1+48*0,7+1021
= 4066 kN/m
$F_{friction}$ = tan 35 ((7870+5944+40+1053-5919+1860)*0.7) = 5317 kN/m

Factor of safety against sliding: $\frac{5317kN/m}{4066kN/m} = 1{,}31 > 1$ ➔ Caisson will not slide

Overturning stability

When seismic loading is exerted on a retaining wall, moment and bearing pressure will increase. When the overturning moment exceeds the restoring moment, the caisson will rotate and overturning instability occurs. When the overturning moment becomes close to the restoring moment, very high and concentrated bearing pressure will be generated near the wall heel. Therefore, unless the founding material is very strong the wall will tend to rotate about the heel due to inadequate bearing capacity. The founding material of the caisson quay wall consists of dense sand which it bearing capacity is sufficient enough (section M3) to prevent rotation due to bearing instability.

Overturning stability is checked by taking the moment around point M.

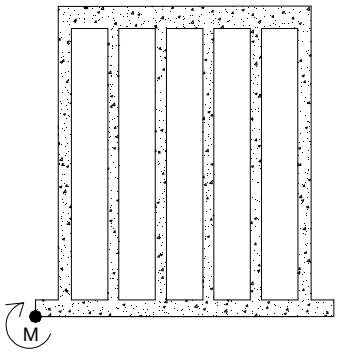

bouyancy	-5919*14,40	=	-85234 kNm/m
own weight	7870*13,5	=	106245 kNm/m
	5944*13,5	=	80244 kNm/m
	40*1,025	=	41 kNm/m
	1053*25,98	=	27357 kNm/m
			----------+
			128653 kNm/m

water pressure	2337*7,2	=	16826 kNm/m
	-2766*7,8	=	-21575 kNm/m
	-183*8,6	=	-1534 kNm/m
	-151*9,4	=	-1419 kNm/m
earth pressure	270*0,833	=	225 kNm/m
	-1620*11,6	=	-18792 kNm/m
surcharge load	-336*14*0,7	=	-3293 kNm/m
	-101*8,6*0,7	=	-608 kNm/m
crane load	1860*4,55*0,7	=	5924 kNm/m
	-560*13,9*0,7	=	-5449 kNm/m
	-48*28*0,7	=	-941 kNm/m
bolder load	-272*28*1	=	-7616 kNm/m
inertia force	-1021*9	=	-9189 kNm/m
			----------+
			-47441 kNm/m

Factor of safety against overturning: $\frac{128653kN/m}{47441kN/m} = 2,71 > 1$ ➔ Caisson will not overturn

The Caisson quay wall is stable for case 1.

O2 Case 2 (50% excess pore water pressure)

This analysis, describes as case 2, assumes that the excess pore water pressure is 50% of the initial vertical effective stress. Just like case 1, an earthquake acceleration of 0,5 m/s^2 is chosen.

O.2.1 Loads case 2

The static and additional seismic forces during an earthquake are determined in this section for case 2. The structure will be calculated per running meter.

Static water pressure
Static water pressures stays the same like case 1 and are shown in Figure O-1.

Dynamic water pressure
Dynamic water pressure results from the dynamic response of a body of water. Distinction is made for free standing water on the seaside of the wall and water in backfill. These water pressures are determined using the Westergaard solution mentioned in chapter 5.4. For saturated backfill, development of dynamic pore water pressure only occurs for free pore water conditions. Water in the pores cannot escape quickly enough to accommodate instantaneously compaction which results in

excess pore water pressure build up. Therefore, no free pore water conditions are present during the presence of excess pore water build up which results in no dynamic water pressure.

The dynamic water pressure for the free standing water on the seaside is the same as calculated for case 1 assuming no excess pore water pressure is generated in the soil front of the caisson, while for the saturated backfill soil it becomes zero due to excess pore water generation as shown in Figure O-9.

Case 2: hydrostatic/dynamic water pressure

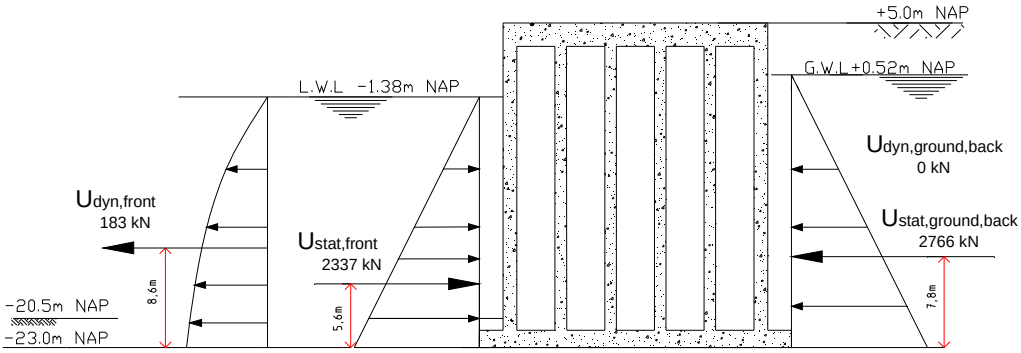

Figure O-9 Hydrostatic and dynamic water pressure for case 2

Dynamic ground pressure
For restrained pore water conditions, the M-O method can be modified to account for the presence of excess pore water within the backfill by replacing γ_{eff} and ψ by $\gamma_{eff,1}$ and ψ_1 respectively (chapter 5.4.1).

$$\gamma_{eff,1} = (\gamma - \gamma_w)(1 - r_u)$$

$$\psi_1 = \tan^{-1}\left[\frac{\gamma \cdot k_h}{\gamma_{eff,1}(1-k_v)}\right]$$

where
$\gamma_{eff,1}$ effective unit weight of soil with excess pore pressure
ψ_1 seismic inertia angle with excess pore pressure
r_u excess pore ratio = 0,5 (for 50% excess pore build up)

The dynamic active earth pressure coefficient k_{ae} and seismic inertia angle ψ_1 for case 2 is determines using Eq. C-2 and Eq. C-3.

$$\psi_1 = \tan^{-1}\left(\frac{k_h}{1-k_v}\frac{\gamma_d}{\gamma_{eff,1}}\right) = \tan^{-1}\left(\frac{0{,}067}{1-0{,}022}\frac{19}{(20-10)(1-0{,}5)}\right) = 14{,}7$$

$$k_{ae} = \frac{\cos^2(\varphi-\beta-\psi)}{\cos\psi\cos^2\beta\cos(\delta+\beta+\psi)\left[1+\sqrt{\frac{\sin(\delta+\varphi)\sin(\varphi-\alpha-\psi)}{\cos(\delta+\beta+\psi)\cos(\alpha-\beta)}}\right]^2}$$

$$= \frac{\cos^2(35-0-14{,}7)}{\cos 14{,}7\cos^2 0\cos(23+0+14{,}7)\left[1+\sqrt{\frac{\sin(23+35)\sin(35-0-14{,}7)}{\cos(23+0+14{,}7)\cos(0-0)}}\right]^2} = 0{,}44$$

Hence the dynamic active pressure thrust P_{ae} is:

$$P_{ae} = \frac{1}{2}k_{ae}\gamma_{dry}H_1^{\,2}(1-k_v) + k_{ae}\gamma_{dry}H_1H_2(1-k_v) + \frac{1}{2}k_{ae}\gamma_{eff,1}H_2^{\,2}(1-k_v)$$

$$= \frac{1}{2}*0{,}44*19*4{,}48^2*(1-0{,}022) + 0{,}44*19*4{,}48*23{,}52*(1-0{,}022) +$$

$$\frac{1}{2}*0{,}44*(20-10)(1-0{,}5)(23{,}52)^2*(1-0{,}022) = 1539kN/m$$

P_{ae}, can be divided into a static component, P_a, and a dynamic component, ΔP_{ae}. The static component can be calculated using Eq. B-7 and Eq. B-8 which is based on the Coulomb Theorem.

$$k_a = \frac{\cos^2(\varphi-\beta)}{\cos^2\beta\cos(\delta+\beta)\left[1+\sqrt{\frac{\sin(\delta+\varphi)\sin(\varphi-\alpha)}{\cos(\delta+\beta)\cos(\alpha-\beta)}}\right]^2} = 0{,}244$$

$$P_a = \frac{1}{2}k_a\gamma_{dry}H_1^{\,2}(1-k_v) + k_a\gamma_{dry}H_1H_2(1-k_v) + \frac{1}{2}k_a\gamma_{eff}H_2^{\,2}(1-k_v) = 1170kN/m$$

The dynamic component ΔP_{ae} is

$$\Delta P_{ae} = P_{ae} - P_a = 1539 - 1170 = 369kN/m$$

The static component is known to act at H/3 above the base of the wall. Seed & Whitman (1970) recommended that the dynamic component be taken to act at approximately 0.6 H. On this basis, the total dynamic active thrust P_{ae} will act at a height h from the base of the wall.

$$h = \frac{P_a \cdot 9{,}6 + \Delta P_{ae}(0.6H)}{P_{ae}} = \frac{1170*9{,}6 + 396*(0.6*28)}{1539} = 11{,}6m$$

The dynamic passive earth pressure coefficient k_{pe} and seismic inertia angle ψ_p for case 2 is determined the same way like for the case 1 which results in the following dynamic earth pressures:

$$P_{pe} = \frac{1}{2}k_{pe}\gamma_{eff}H^2(1-k_v) = 270kN/m$$

P_{pe} is acting at 1/3H above the base of the wall.

Figure O-10 shows an illustration of the dynamic earth pressure thrusts and the excess pore water pressure together with their point of application for case 2.

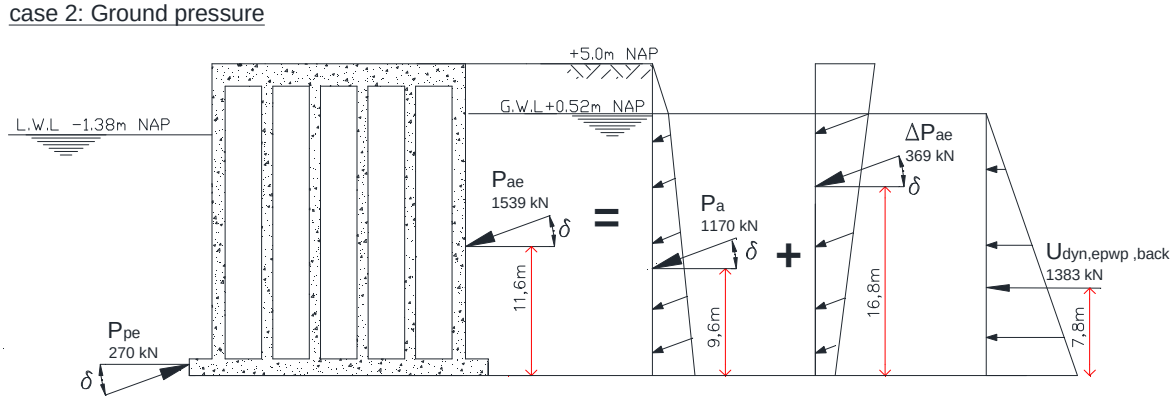

Figure O-10 Ground pressure and excess pore water pressure for case 2

Surcharge load
Just like case 1, the surcharge load can behind the landside crane can be schematized as a one-sided limited surcharge load. The impact of this one-sided limited surcharge load on the wall is estimated using the method created by Ohde **Error! Reference source not found.** which is illustrated in Figure I-6. Forces acting on the wall due to of surcharge load behind the caisson structure are shown in Figure O-11.

Crane load
The landside crane load is schematized as a two-sided limited distributed load with a width of the crane rail foundation of 3,5m and a loading of the crane load divided by the width. The total extra horizontal thrust on the wall due the presence of the two-sided limited distributed crane load can be determined using the method shown in Figure I-8 **Error! Reference source not found.**.

Thrust acting on the wall due to the landside crane load is shown in Figure O-12.

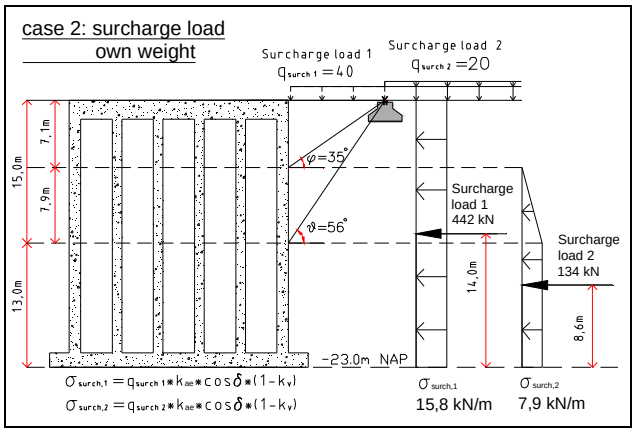

Figure O-11 Horizontal ground pressure as result of surcharge load and own weight behind relieving structure case 2

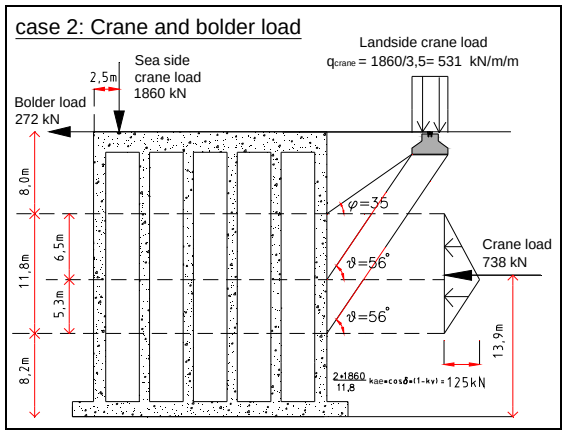

Figure O-12 Horizontal ground pressure as result of landside crane case 2

Own weight caisson during earthquake
Own weight of the caisson is the same as case 1 and shown in Figure O-8.

Bouyancy
Bouyancy for case 2 is the same as case 1 and shown in Figure O-8.

Seismic inertia forces caisson
The seismic inertia force of the caisson is the same as case 1. This is a horizontal inertia force of $F_{inertia,hor}$ = 1021 kN/m towards the sea located at NAP- 9m.

O.2.2 Stability of the caisson case 2

There are two main deformations for a gravity retaining wall, namely sliding and rotation. The former is due to inadequate sliding resistance, whilst the outward tilting of a wall may be caused by inadequate resistance to overturning and or bearing.

Under the action of the in section O.2.1 mentioned forces, the stability of the wall is checked for both the sliding and overturning failure making use of force equilibriums.

Safety factors
No safety factors are used because real occurring forces need to be used to see whether or not the caisson is stable or not.

Load combinations and combination factors

Two load combinations are checked for the caisson quay wall and are listed in Table 9-2. Combination factors Ψ for separate loads are also listed in Table 9-2.

Sliding stability

The friction force must withstand the horizontal forces acting on the caisson otherwise the caisson will start to slide. Calculations have been made to check whether the width of caisson is sufficient enough. Sliding stability is checked for only the normative load combination which is load combination 4.

$\sum(F_h * \Psi) \leq F_{friction}$

$F_{friction} = (\mu) * \sum(F_v * \Psi)$

$\sum F_h$: Sum of horizontal forces acting on caisson
$F_{friction}$: Frictional force between caisson floor and the sand beneath with safety coefficient included
Ψ : Combination factor
μ : Dynamic friction coefficient (tan φ)
F_v : Vertical forces acting on the caisson

$\sum F_h$ = -2337*1+2766*1+183*1–270*1+1539*1+1383*1+442*0,7+134*0,7+738*0,7+272*1+ 48*0,7+1021*1 = 5513 kN/m

$F_{friction}$ = tan 35 ((7870+5944+40+1053-5919+1860)*0.7) = 5317 kN/m

Factor of safety against sliding: $\frac{5317 kN/m}{5513 kN/m} = 0{,}96 > 1$ ➔ Caisson will slide

Overturning stability

When seismic loading is exerted on a retaining wall, moment and bearing pressure will increase. When the overturning moment exceeds the restoring moment, the caisson will rotate and overturning instability occurs. When the overturning moment becomes close to the restoring moment, very high and concentrated bearing pressure will be generated near the wall heel. Therefore, unless the founding material is very strong the wall will tend to rotate about the heel due to inadequate bearing capacity. The founding material of the caisson quay wall consists of Pleistocene medium dense sand which it bearing capacity is assumed to be sufficient enough to prevent rotation due to bearing instability.

Overturning stability is checked by taking the moment around point M.

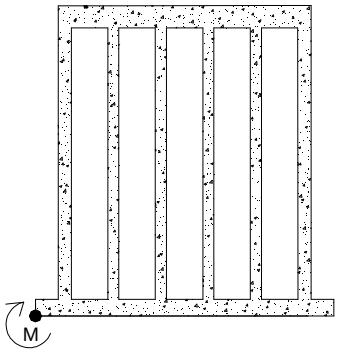

bouyancy	-5919*14,40	=	-85234 kNm/m
own weight	7870*13,5	=	106245 kNm/m
	5944*13,5	=	80244 kNm/m
	40*1,025	=	41 kNm/m
	1053*25,98	=	27357 kNm/m
			----------+
			128653 kNm/m
water pressure	2337*7,2	=	16826 kNm/m
	-2766*7,8	=	-21575 kNm/m
	-183*8,6	=	-1534 kNm/m
earth pressure	270*0,833	=	225 kNm/m
	-1539*11,6	=	-17852 kNm/m
Excess pore pres.	-1383*7,8	=	-10787 kNm/m
surcharge load	-442*14*0,7	=	-4332 kNm/m
	-134*8,6*0,7	=	-807 kNm/m
crane load	1860*4,55*0,7	=	5924 kNm/m
	-738*13,9*0,7	=	-7181 kNm/m
	-48*28*0,7	=	-941 kNm/m
bolder load	-272*28*1	=	-7616 kNm/m
inertia force	-1021*9	=	-9189 kNm/m
			----------+

-58839 kNm/m

Factor of safety against overturning: $\frac{128653kN/m}{58839kN/m} = 2{,}19 > 1$ ➔ Caisson won't overturn

O3 Case 3 (Liquefied backfill)

This analysis, describes as case 3, assumes a fully liquefied backfill. Just like case 1 and case 2, an earthquake acceleration of 0,5 m/s^2 is chosen. Assumed was that no liquefaction occurs in front of the wall. Here, a generation of 50% excess pore water is generated just like case 2. Therefore, the forces acting in front of the wall are the same as case 2.

O.3.1 Loads case 3

The static and additional seismic forces during an earthquake are determined in this section for case 3. The structure will be calculated per running meter. In the case of a liquefied backfill, soil behaves like a heavy fluid with an equivalent unit weight of $\gamma_{LF} = \gamma_{saturated\ sand}$.

Static water pressure
No liquefaction was assumed in front of the diaphragm wall. The static water pressure in front of the quay wall stays the same as case 2 and case 1. On the contrary, saturated soils behind the quay wall are assumed to be liquefied. This means that they behave like a heavy fluid. An equivalent hydrostatic thrust based on a fluid of unit weight γ_{LF} is replacing the ground pressure thrust and is determined as follows:

$$LF_{hydrostatic} = \frac{1}{2}k_{ae}\gamma_{dry}H_1{}^2(1-k_v) + k_{ae}\gamma_{dry}H_1H_2(1-k_v) + \frac{1}{2}\gamma_{LF}H_2{}^2(1-k_v)$$
$$= \frac{1}{2}*0{,}44*19*4{,}48^2(1-0{,}022) + 0{,}44*19*4{,}48*23{,}52(1-0{,}022) + \frac{1}{2}20*23{,}52^2(1-0{,}022)$$
$$= 6354kN$$

Dynamic water pressure
The dynamic water pressure for the free standing water outboard is the same as calculated for case 1 and case 2 while for the saturated backfill soil in front of the wall it becomes zero just like case 2. Behind the quay wall, soil behaves like a free standing heavy fluid. Dynamic response of this free standing heavy fluid can be determined using the Westergaard's solution mentioned in section 5.4.1.

$$LF_{hydrodynamic} = \frac{7}{12}k_h\gamma_{LF}H^2 = \frac{7}{12}*0{,}067*20*(23{,}52)^2 = 432kN/m$$

Dynamic ground pressure
Passive earth pressure is the same as case 2. No active earth thrust will act on the wall because the soil behind the wall is fully liquefied.

Surcharge load and crane load
No cranes or surcharge load is present due to the liquefied backfill. Objects on the surface behind the quay wall will sink into the heavy fluid or just float on top of it.

Own weight caisson during earthquake
Own weight of the caisson is the same as case 1 and shown in Figure O-8.

Bouyancy
Bouyancy for case 2 is the same as case 1 and shown in Figure O-8.

Seismic inertia forces caisson
The seismic inertia force of the caisson is the same as case 1. This is a horizontal inertia force of $F_{inertia,hor}$ = 1021 kN/m towards the sea located at NAP- 9m.

The horizontal force components acting on the diaphragm wall due to water and earth pressure for case 3 is shown in Figure O-13.

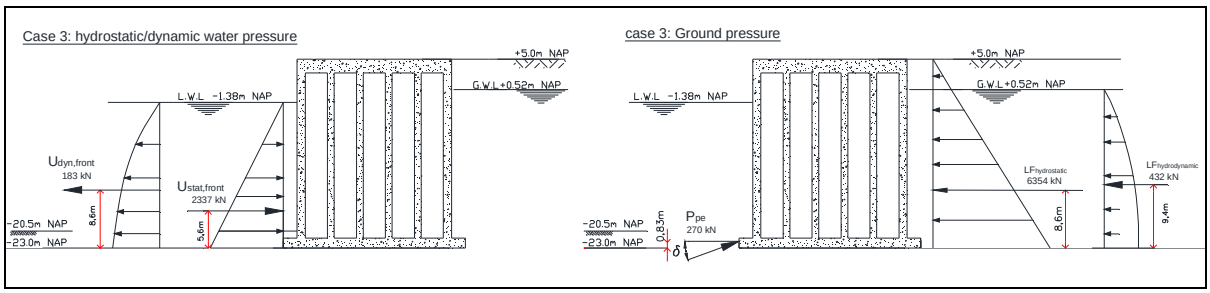

Figure O-13 Horizontal force components on diaphragm wall for case 3

O.3.2 Stability of the caisson case 3

Under the action of the in section O.3.1 mentioned forces, the stability of the wall is checked for both the sliding and overturning failure making use of force equilibriums.

Safety factors
No safety factors are used because real occurring forces need to be used to see whether or not the caisson is stable or not.

Load combinations and combination factors
Two load combinations are checked for the caisson quay wall and are listed in Table 9-2. Combination factors Ψ for separate loads are also listed in Table 9-2.

Sliding stability
The friction force must withstand the horizontal forces acting on the caisson otherwise the caisson will start to slide. Calculations have been made to check whether the width of caisson is sufficient enough. Sliding stability is checked for only the normative load combination which is load combination 4.

$\sum(F_h * \Psi) \leq F_{friction}$
$F_{friction} = (\mu) * \sum(F_v * \Psi)$

$\sum F_h$: Sum of horizontal forces acting on caisson
$F_{friction}$: Frictional force between caisson floor and the sand beneath with safety coefficient included
Ψ : Combination factor
μ : Dynamic friction coefficient (tan φ)
F_v : Vertical forces acting on the caisson

$\sum F_h$ = -2337*1+183*1–270*1+6354*1+432*1+272*1+1021*1 = 5655 kN/m
$F_{friction}$ = tan 35 ((7870+5944+40+1053-5919)*0.7) = 4405 kN/m

Factor of safety against sliding: $\frac{4405 kN/m}{5655 kN/m} = 0,78 > 1$ ➔ Caisson will slide

Overturning stability
Overturning stability is checked by taking the moment around point M.

bouyancy -5919*14,40 = -85234 kNm/m

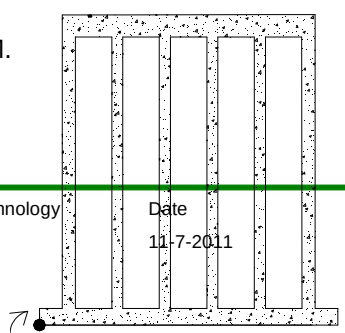

own weight	7870*13,5	= 106245 kNm/m
	5944*13,5	= 80244 kNm/m
	40*1,025	= 41 kNm/m
	1053*25,98	= 27357 kNm/m
		----------+
		128653 kNm/m

water pressure	2337*7,2	= 16826 kNm/m
	-183*8,6	= -1534 kNm/m
earth pressure	270*0,833	= 225 kNm/m
Liquefied backfill	-6354*8,6	= -54644 kNm/m
	-432*9,4	= -4061 kNm/m
bolder load	-272*28*1	= -7616 kNm/m
inertia force	-1021*9	= -9189 kNm/m
		----------+
		-56393 kNm/m

Factor of safety against overturning: $\frac{128653kN/m}{56393kN/m} = 2{,}28 > 1$ ➔ Caisson won't overturn

Appendix P Dynamic calculation Plaxis Caisson

The procedure to perform a dynamic analysis with Plaxis is somehow similar to that for a static analysis. This entails creation of a geometry model, mesh generation, initial stress generation, defining and executing calculation and evaluation of results. In addition to the static model, the dynamic model makes use of the Plaxis dynamic analysis module to analyze the vibration of soil. In modeling the dynamic response of a soil structure, the inertia of the subsoil and the time dependence of the load are considered. Also, damping due to material and geometry is taken into account. Initially the HSsmall model is utilized for the simulation of the dynamic effects.

P1 Dynamic model Plaxis

The same Plaxis model of the caisson like the static Plaxis calculation is used during this dynamic calculation, see section N1.

P2 Dynamic loading

The soil retaining function of the caisson quay wall is derived from the self-weight of the wall that is so heavy that sufficient resistance to shearing is generated in the soil and it cannot tilt or slide. Vertical earthquake acceleration will cause changes in self weight of the caisson and for that reason, vertical earthquake acceleration was included in this analysis. It is kept 1/3 of the horizontal acceleration which is a reasonable assumption according to the Eurocode 8. The earthquake is modeled by imposing a prescribed acceleration at the bottom boundary resulting to shear waves that propagate upwards.

Besides harmonic loading there is also the possibility to read data from digitized load signal. Variations of different real accelerograms of earthquakes are used for this analysis. These accelerograms varies in magnitude caused by different earthquakes and are recorded at different stations over the United States by the United States Geological Survey [K.1]. To make a good comparison, the same earthquake accelerograms used during seismic analysis of the diaphragm wall are used in this Plaxis analysis.

P3 Simulating excess pore water and liquefaction in Plaxis

No excess pore pressure due to backfill is Pleistocene sand and therefore good compacted

P4 Construction method

The quay wall has been built in a certain way. To take the building sequence into account in Plaxis the option “staged construction” can be used. This option allows users to (de)activate weight, strength, stiffness and to change material properties or water pressures. Just like the static analysis, the diaphragm quay wall is created in 9 phases, see section H.2.1. For the purpose of dynamic analysis, a dynamic calculation phase is added. The function “update mesh” will not be used. This function allows the mesh to update after each phase calculation, which will lead to a more accurate second order effect. Since the deformations are very small which result in small second-order-effects this effect is negligible.

P5 Plaxis output

Results of the Plaxis calculation for different earthquake accelerations are given in this section.

Earthquake 1 (a=0,1 m/s^2):

Displacements

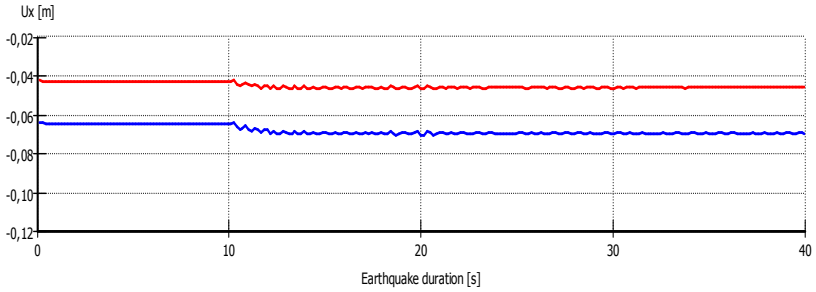

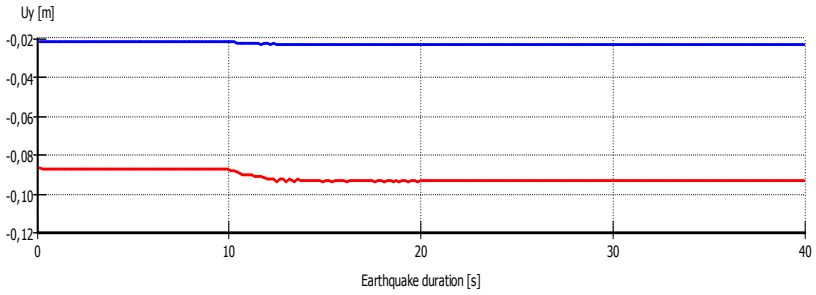

Plaxis Displacement	Hor. displacement After last phase	Vert. displacement After last phase
Seaside crane rail	-0,069 m	-0,023 m
Landside crane rail	-0,046 m	-0,093 m

Stresses

Plaxis Stresses	Depth M_{max} m NAP	M_{max} kNm/m	Max. axial force kN/m
Front wall	-7	-3420	-1900
Wall 1	3	-2450	-1600
Wall 2	3	-2810	-1170
Wall 3	3	-3040	-975
Wall 4	3	-2830	-799
Back wall	-6	-2500	-693

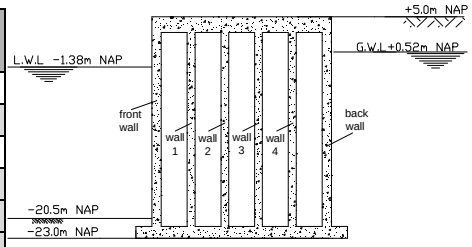

The Bending moment capacity of the walls depends on the amount of reinforcement steel placed in the wall and the axial force within the wall. The same method as mentioned in appendix M3 was used to determine the maximum bending capacity of the caisson walls. Notion must be made that during this calculation no safety factors was included because the real behavior of the wall is investigated. The maximum bending moment of each wall are determined and listed in the table below.

Plaxis Stresses	Max. axial force kN/m	M_{max} kNm/m	M_{cap} kNm/m
Front wall	-1900	-3420	-5211
Wall 1	-1600	-2450	-4168
Wall 2	-1170	-2810	-4273
Wall 3	-975	-3040	-4318
Wall 4	-799	-2830	-4357
Back wall	-693	-2500	-5622

Bending moments of the walls

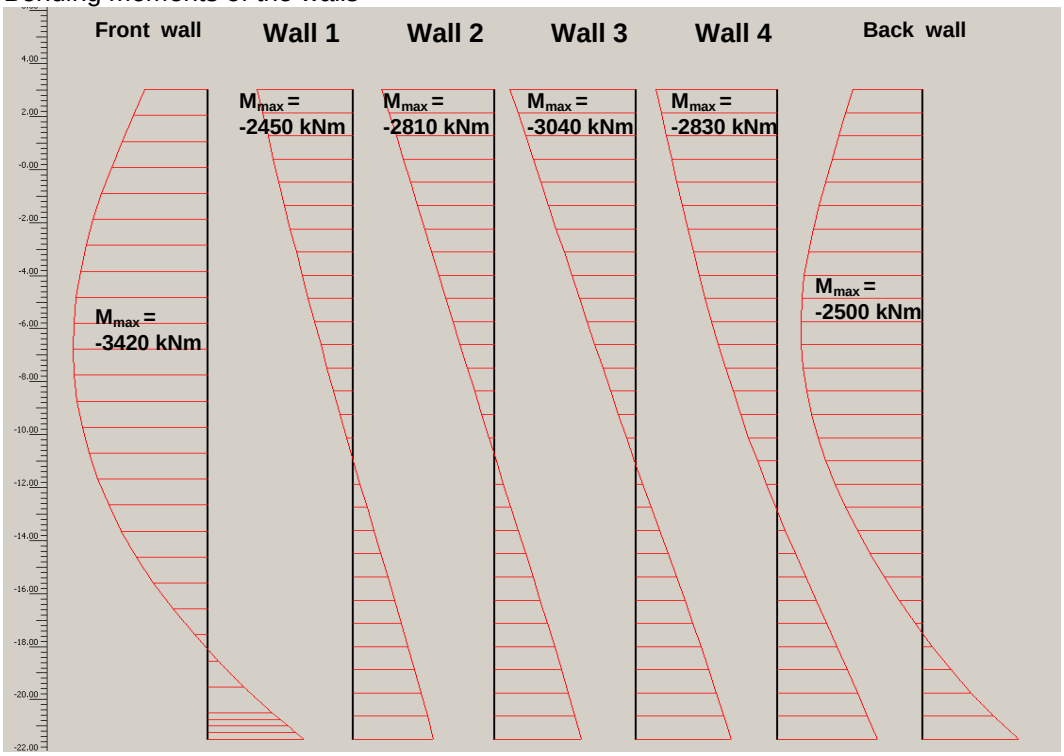

Axial forces of the walls

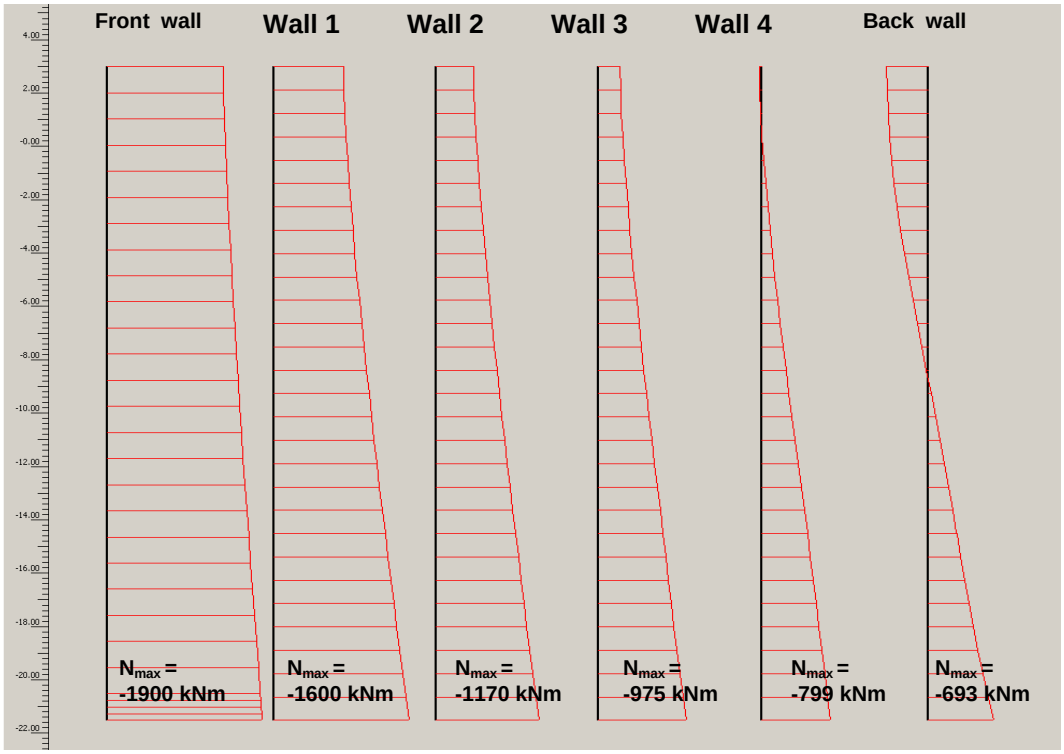

Earthquake 2 *(a=0,2 m/s^2)*:

Displacements

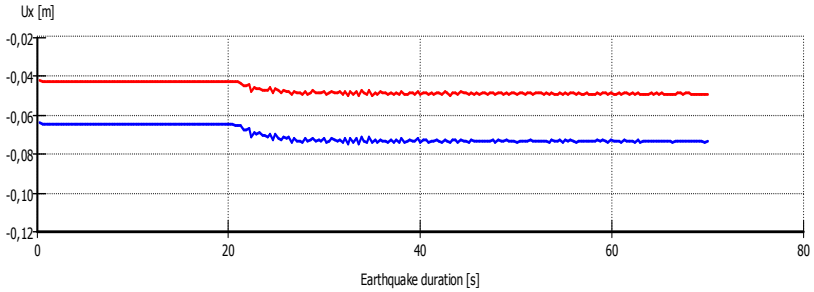

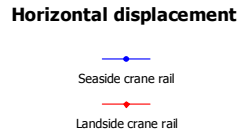

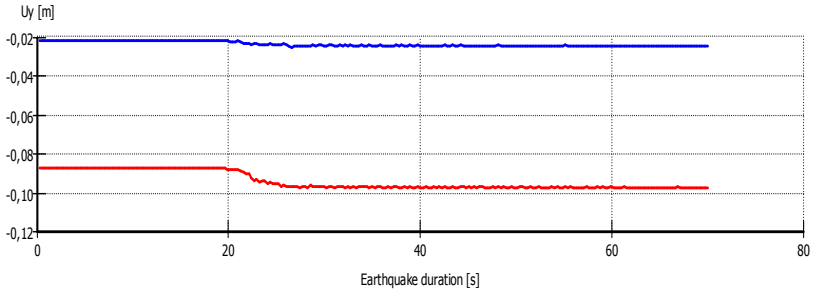

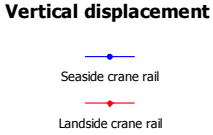

Plaxis Displacement	Hor. displacement After last phase	Vert. displacement After last phase
Seaside crane rail	-0,073m	-0,025m
Landside crane rail	-0,049m	-0,097m

Stresses

Plaxis Stresses	Depth M_{max} m NAP	M_{max} kNm/m	Max. axial force kN/m
Front wall	-7	-3450	-1890
Wall 1	3	-2460	-1610
Wall 2	3	-2840	-1180
Wall 3	3	-3090	-977
Wall 4	3	-2880	-790
Back wall	-6	-2540	-662

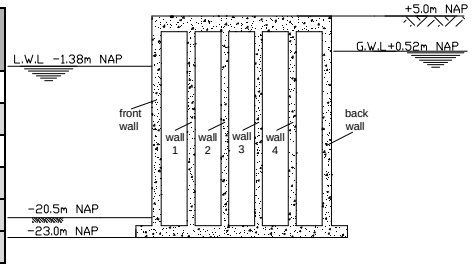

The Bending moment capacity of the walls depends on the amount of reinforcement steel placed in the wall and the axial force within the wall. The same method as mentioned in appendix M3 was used to determine the maximum bending capacity of the caisson walls. Notion must be made that during this calculation no safety factors was included because the real behavior of the wall is investigated. The maximum bending moment of each wall are determined and listed in the table below.

Plaxis Stresses	Max. axial force kN/m	M_{max} kNm/m	M_{cap} kNm/m
Front wall	-1890	-3450	-5215
Wall 1	-1610	-2460	-4166
Wall 2	-1180	-2840	-4271
Wall 3	-977	-3090	-4318
Wall 4	-790	-2880	-4359
Back wall	-662	-2540	-5631

Bending moments of the walls

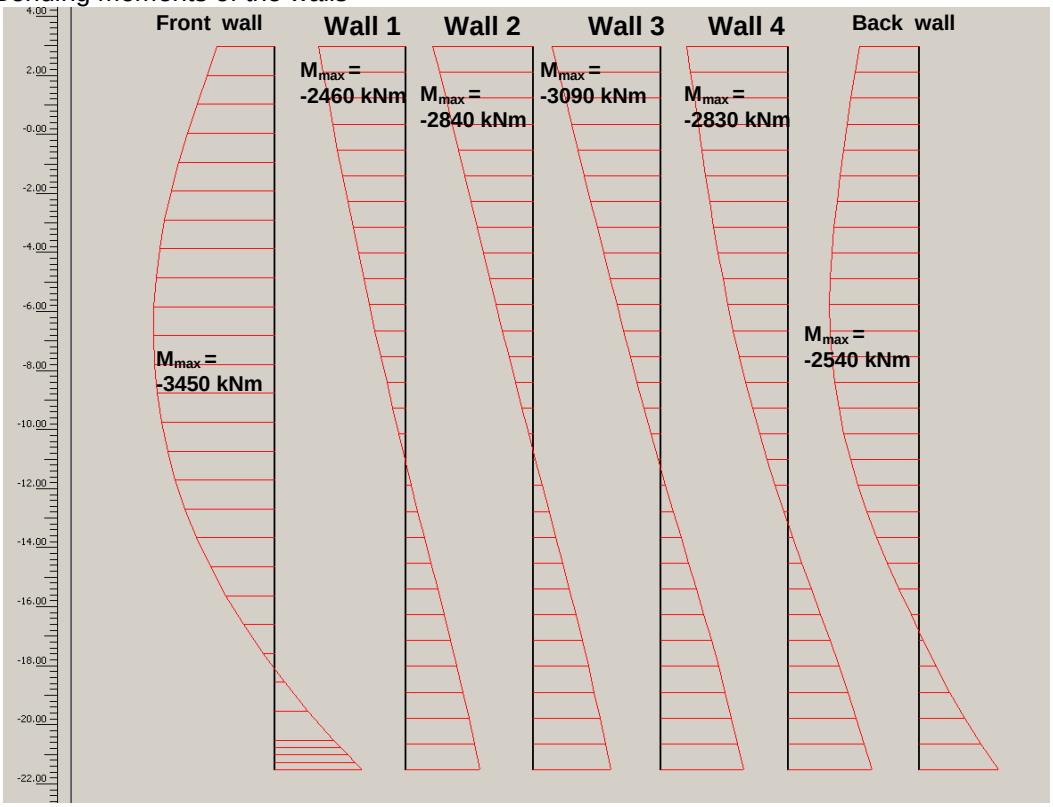

Axial forces of the walls

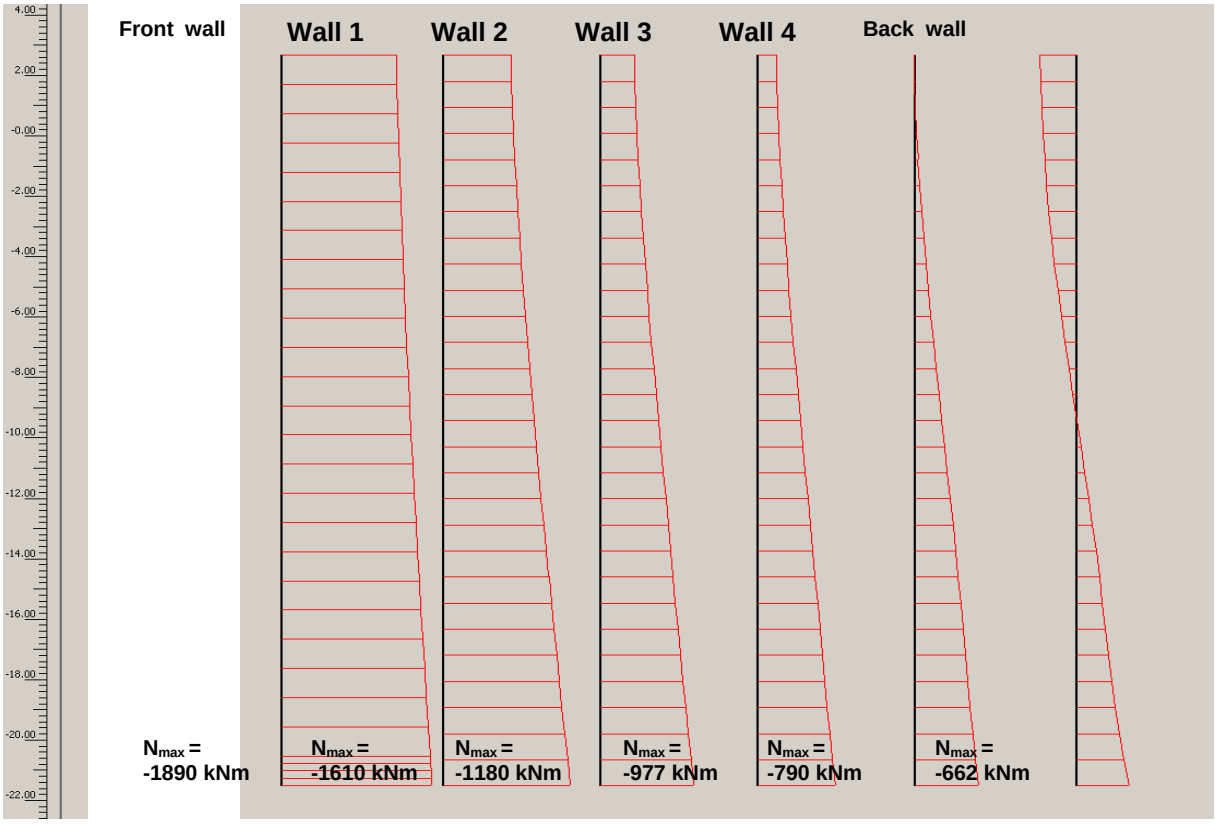

Earthquake 3 (a=0,3 m/s^2):

Displacements

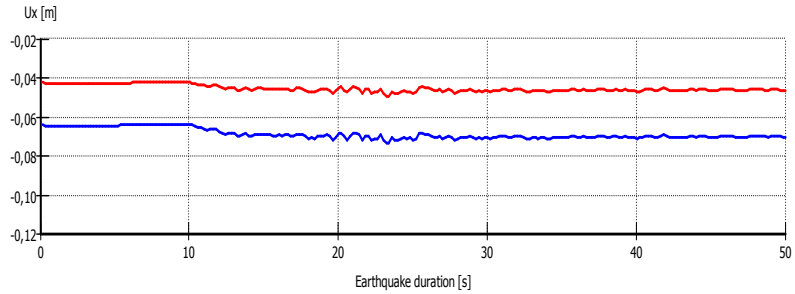

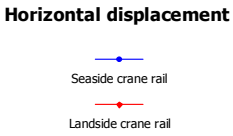

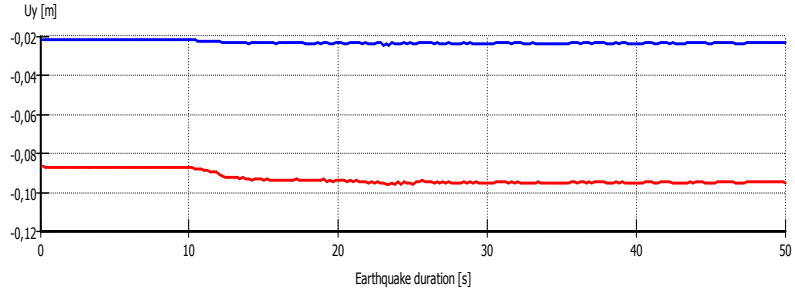

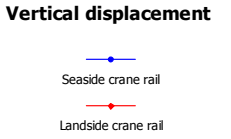

Plaxis Displacement	Hor. displacement After last phase	Vert. displacement After last phase
Seaside crane rail	-0,070m	-0,024m
Landside crane rail	-0,046m	-0,095m

Stresses

Plaxis Stresses	Depth M_{max} m NAP	M_{max} kNm/m	Max. axial force kN/m
Front wall	-6,8	-3440	-1900
Wall 1	3	-2440	-1610
Wall 2	3	-2810	-1170
Wall 3	3	-3060	-975
Wall 4	3	-2850	-793
Back wall	-5,8	-2510	-666

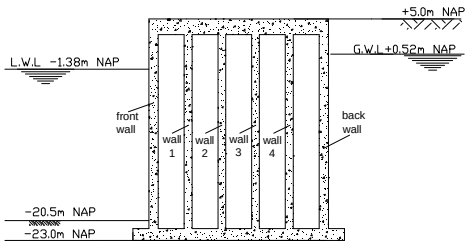

The Bending moment capacity of the walls depends on the amount of reinforcement steel placed in the wall and the axial force within the wall. The same method as mentioned in appendix M3 was used to determine the maximum bending capacity of the caisson walls. Notion must be made that during this calculation no safety factors was included because the real behavior of the wall is investigated. The maximum bending moment of each wall are determined and listed in the table below.

Plaxis Stresses	Max. axial force kN/m	M_{max} kNm/m	M_{cap} kNm/m
Front wall	-1900	-3440	-5211
Wall 1	-1610	-2440	-4166
Wall 2	-1170	-2810	-4273
Wall 3	-975	-3060	-4318
Wall 4	-793	-2850	-4358
Back wall	-666	-2510	-5630

Bending moments of walls

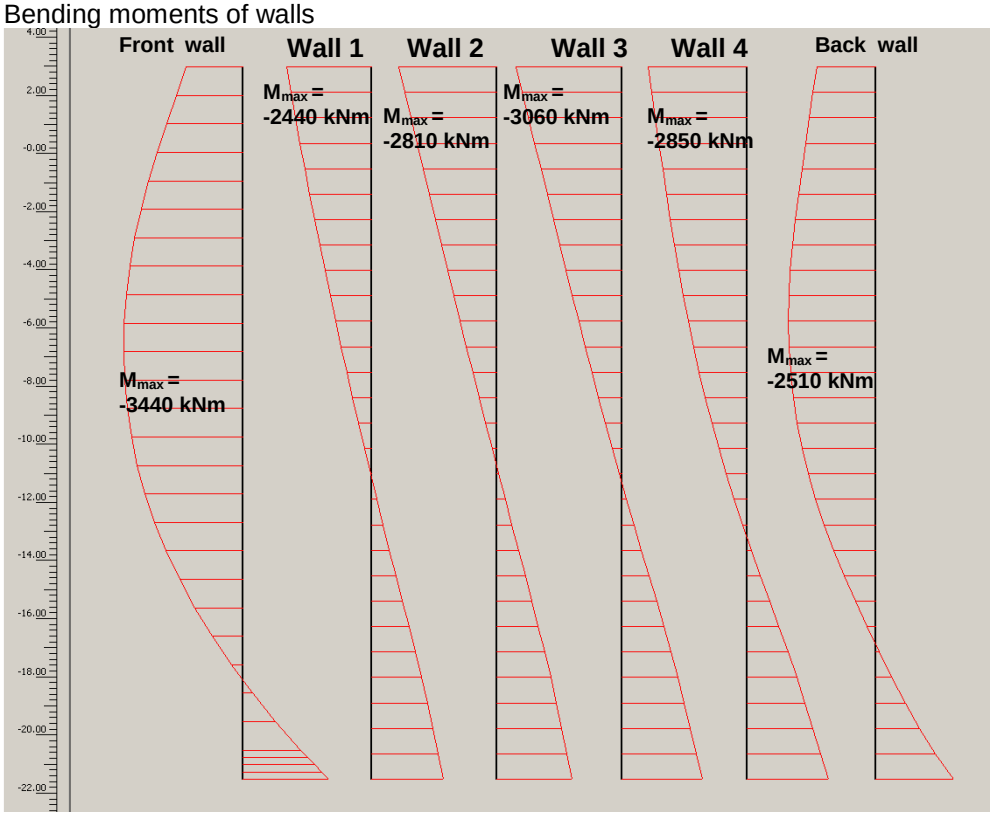

Axial forces of walls

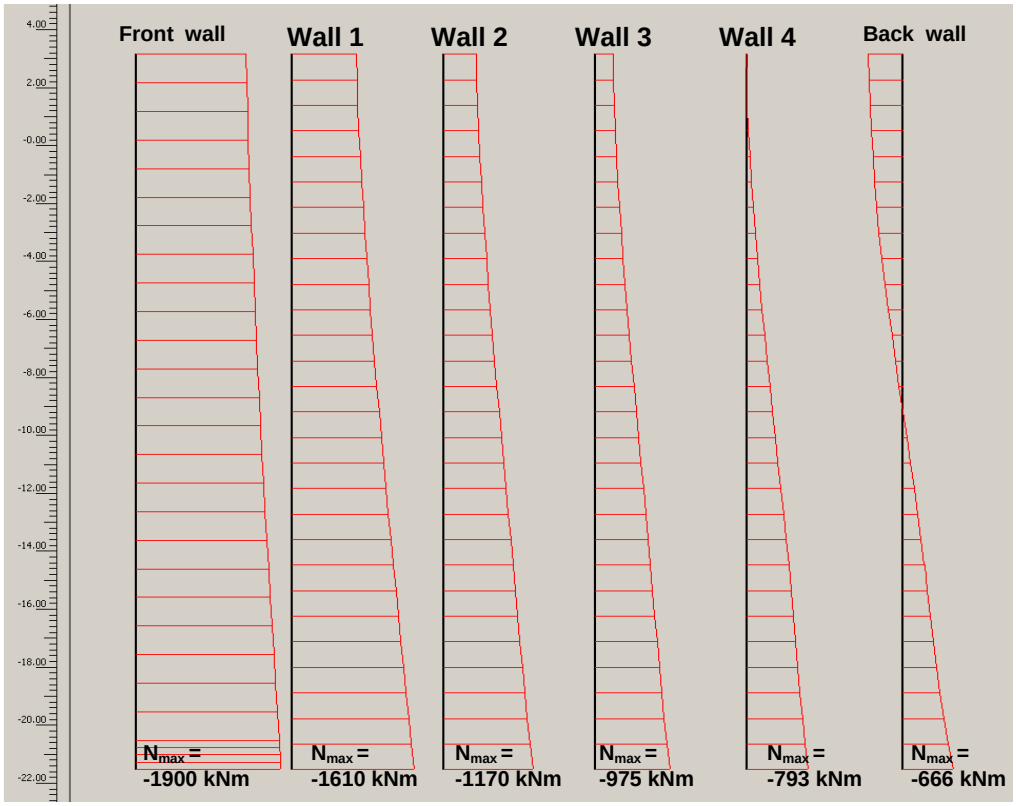

Earthquake 4 (a=0,4 m/s^2):

Displacements

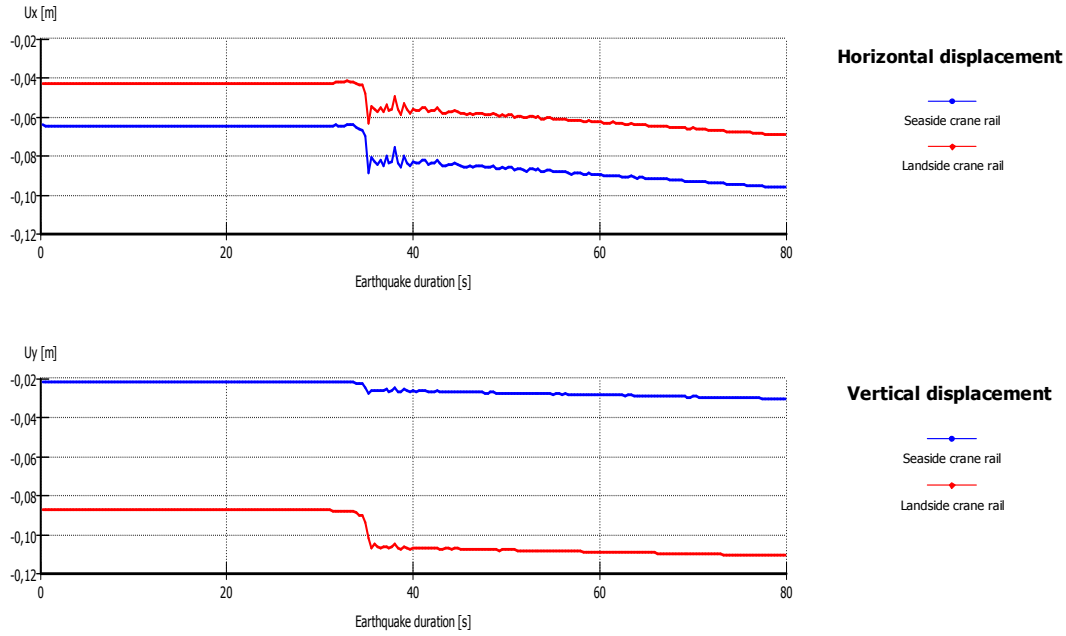

Plaxis Displacement	Hor. displacement After last phase	Vert. displacement After last phase
Seaside crane rail	-0,096m	-0,031m
Landside crane rail	-0,069m	-0,109m

Stresses

Plaxis Stresses	Depth M_{max} m NAP	M_{max} kNm/m	Max. axial force kN/m
Front wall	-6,8	-3540	-1910
Wall 1	3	-2660	-1600
Wall 2	3	-3090	-1160
Wall 3	3	-3350	-941
Wall 4	3	-3120	-743
Back wall	-5,8	-2770	-603

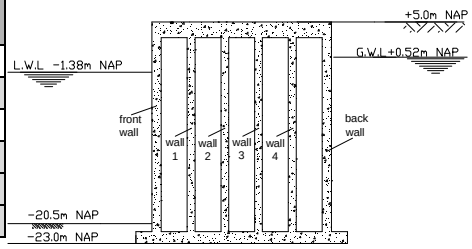

The Bending moment capacity of the walls depends on the amount of reinforcement steel placed in the wall and the axial force within the wall. The same method as mentioned in appendix M3 was used to determine the maximum bending capacity of the caisson walls. Notion must be made that during this calculation no safety factors was included because the real behavior of the wall is investigated. The maximum bending moment of each wall are determined and listed in the table below.

Plaxis Stresses	Max. axial force kN/m	M_{max} kNm/m	M_{cap} kNm/m
Front wall	-1910	-3540	-5208
Wall 1	-1600	-2660	-4168
Wall 2	-1160	-3090	-4276
Wall 3	-941	-3350	-4326
Wall 4	-743	-3120	-4369
Back wall	-603	-2770	-5650

Bending moments of walls

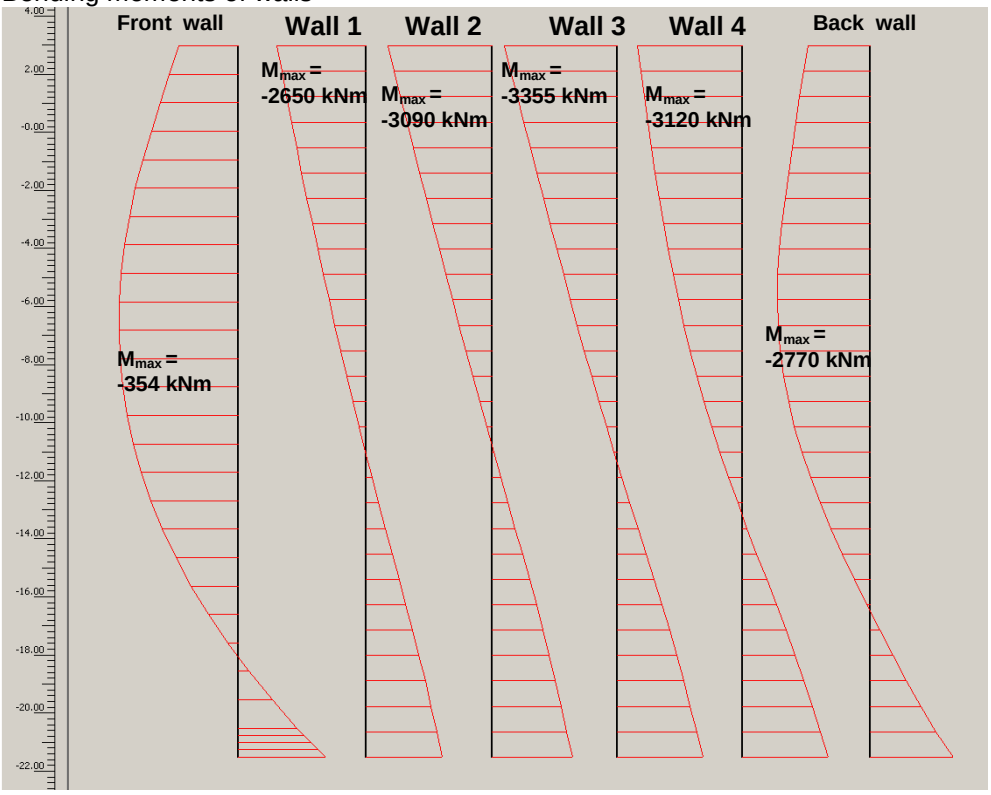

Axial forces of walls

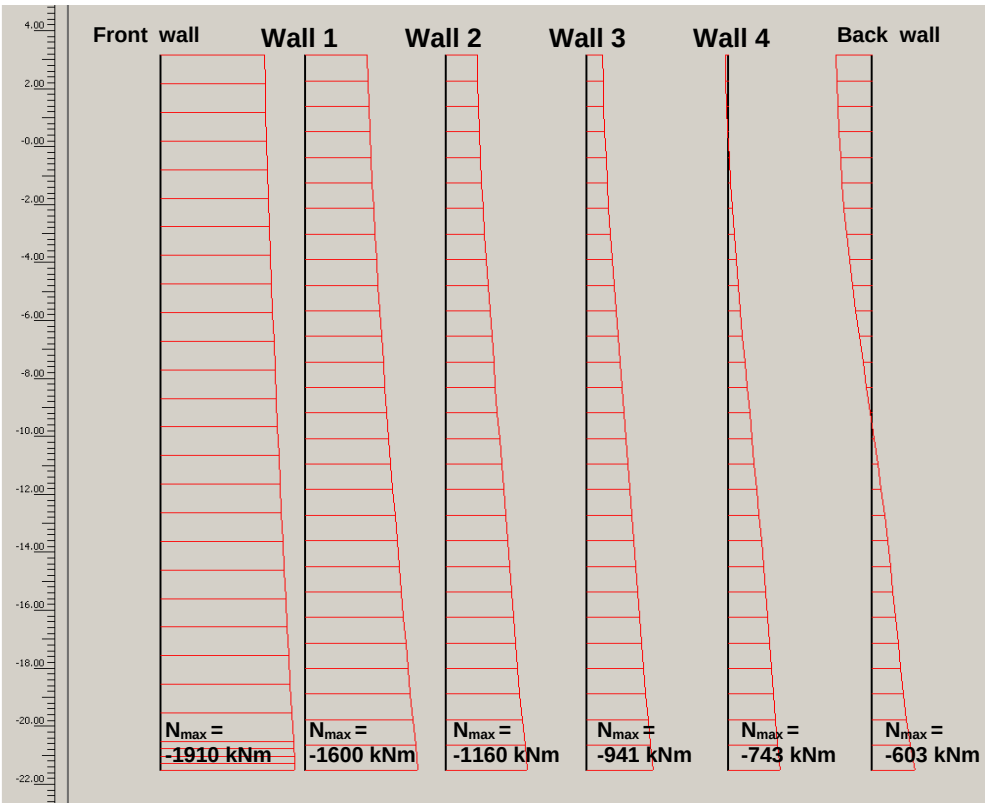

Earthquake 5 (a=0,5 m/s^2):

Displacements

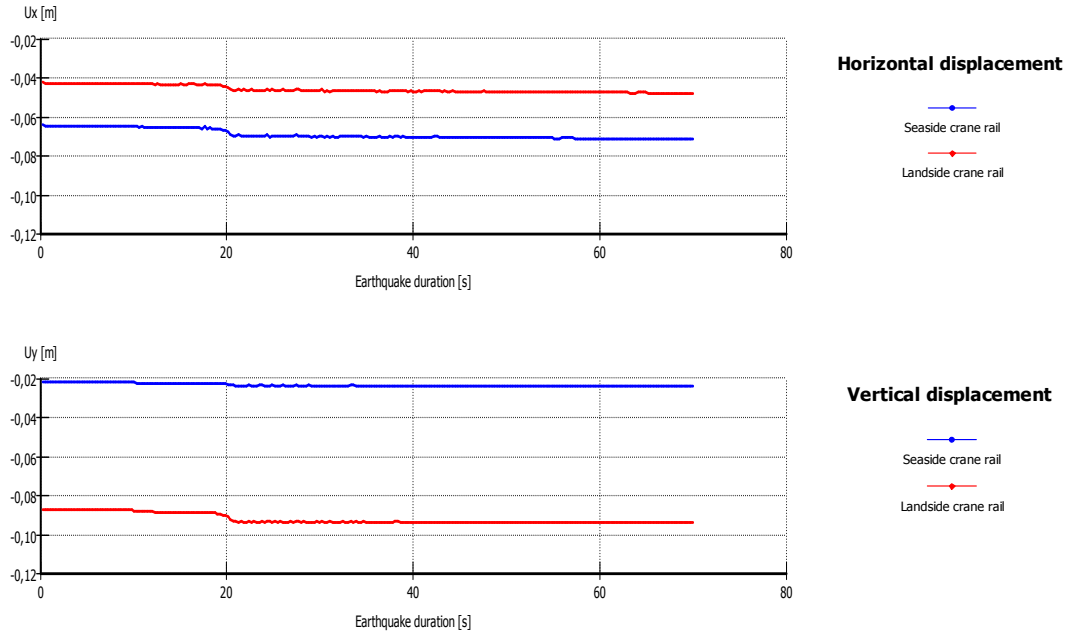

Plaxis Displacement	Hor. displacement After last phase	Vert. displacement After last phase
Seaside crane rail	-0,071m	-0,024m
Landside crane rail	-0,048m	-0,094m

Stresses

Plaxis Stresses	Depth M_{max} m NAP	M_{max} kNm/m	Max. axial force kN/m
Front wall	-6,8	-3430	-1880
Wall 1	3	-2390	-1610
Wall 2	3	-2760	-1180
Wall 3	3	-3010	-980
Wall 4	3	-2820	-797
Back wall	-5,8	-2460	-710

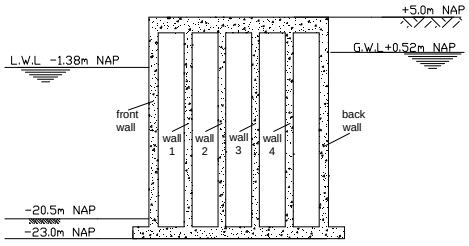

The Bending moment capacity of the walls depends on the amount of reinforcement steel placed in the wall and the axial force within the wall. The same method as mentioned in appendix M3 was used to determine the maximum bending capacity of the caisson walls. Notion must be made that during this calculation no safety factors was included because the real behavior of the wall is investigated. The maximum bending moment of each wall are determined and listed in the table below.

Plaxis Stresses	Max. axial force kN/m	M_{max} kNm/m	M_{cap} kNm/m
Front wall	-1880	-3430	-5219
Wall 1	-1610	-2390	-4166
Wall 2	-1180	-2760	-4271
Wall 3	-980	-3010	-4317
Wall 4	-797	-2820	-4357
Back wall	-710	-2460	-5617

Bending moments of wall

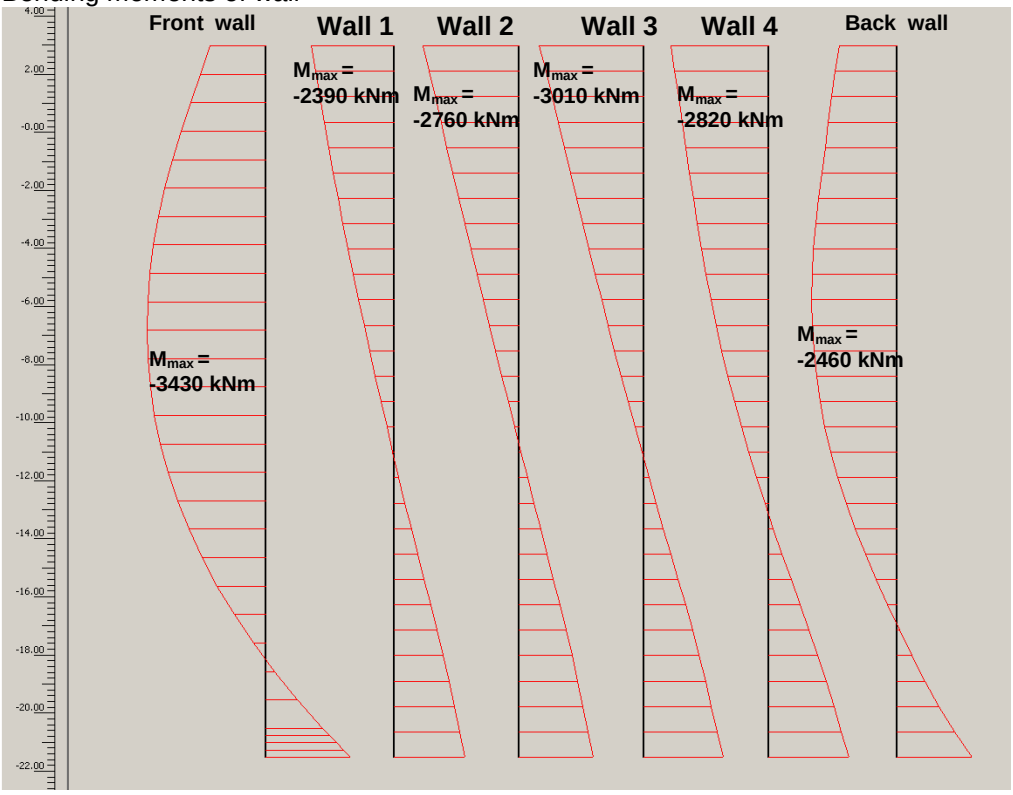

Axial forces of wall

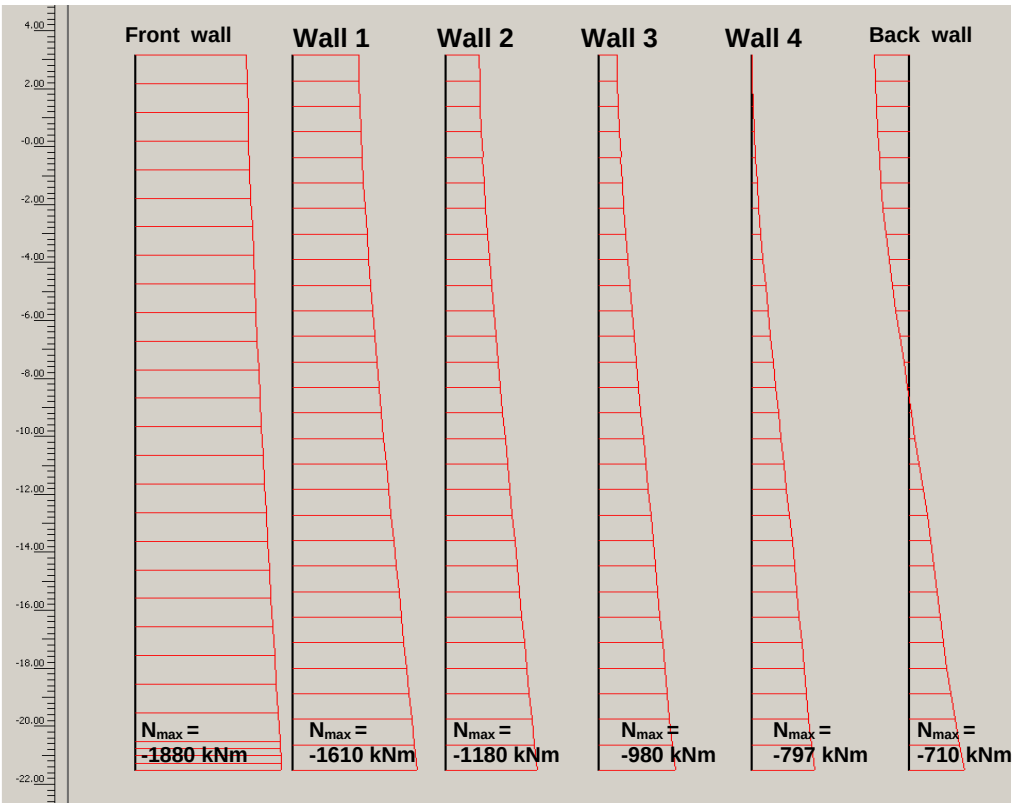

Earthquake 6 (a=0,6 m/s^2):

Displacements

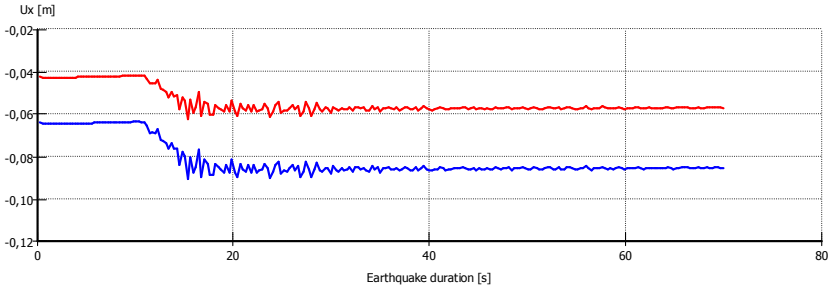

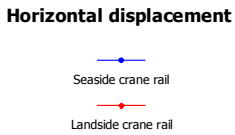

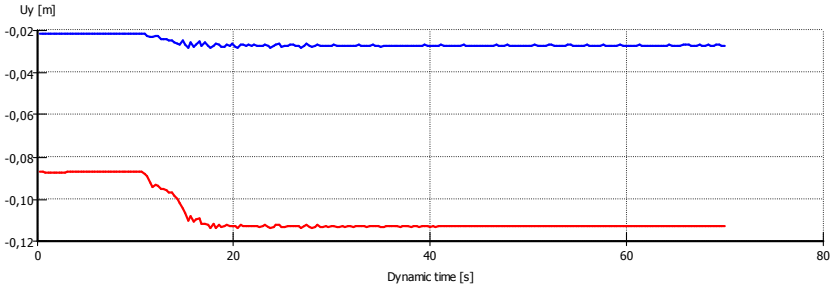

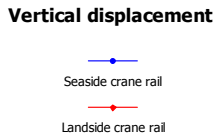

Plaxis Displacement	Hor. displacement After last phase	Vert. displacement After last phase
Seaside crane rail	-0,085	-0,028
Landside crane rail	-0,057	-0,111

Stresses

Plaxis Stresses	Depth M_{max} m NAP	M_{max} kNm/m	Max. axial force kN/m
Front wall	-6,8	-3580	-1900
Wall 1	3	-2690	-1620
Wall 2	3	-3160	-1170
Wall 3	3	-3450	-947
Wall 4	3	-3220	-738
Back wall	5,8	-2970	-539

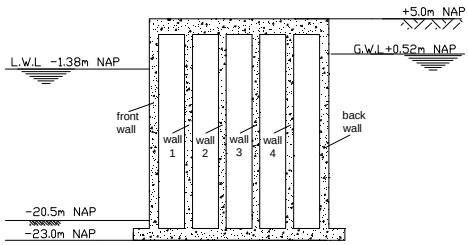

The Bending moment capacity of the walls depends on the amount of reinforcement steel placed in the wall and the axial force within the wall. The same method as mentioned in appendix M3 was used to determine the maximum bending capacity of the caisson walls. Notion must be made that during this calculation no safety factors was included because the real behavior of the wall is investigated. The maximum bending moment of each wall are determined and listed in the table below.

Plaxis Stresses	Max. axial force kN/m	M_{max} kNm/m	M_{cap} kNm/m
Front wall	-1900	-3580	-5211
Wall 1	-1620	-2690	-4163
Wall 2	-1170	-3160	-4273
Wall 3	-947	-3450	-4324
Wall 4	-738	-3220	-4370
Back wall	-539	-2970	-5669

Bending moments of walls

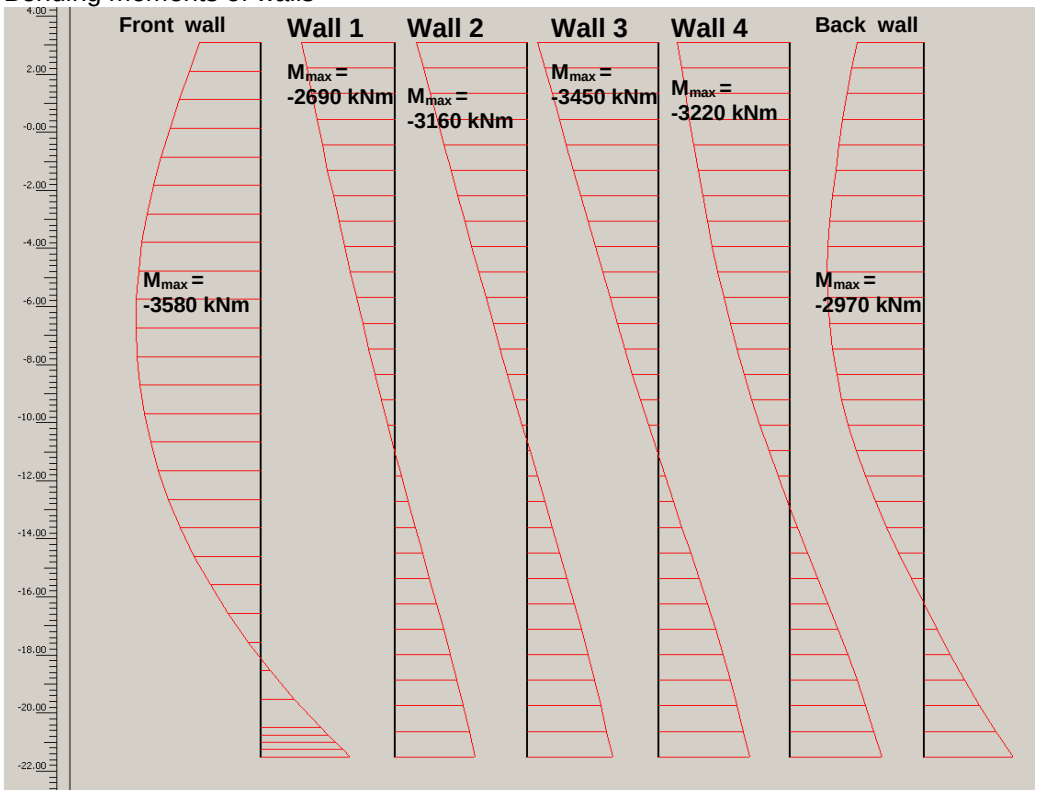

Axial forces of walls

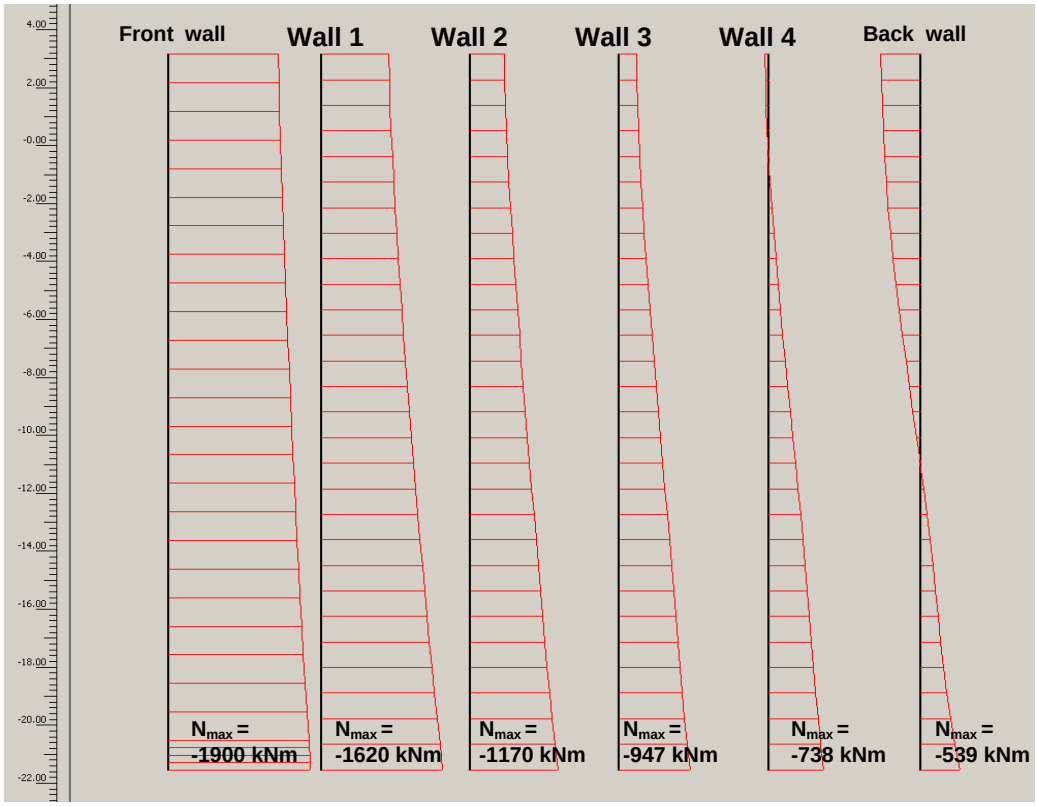

Earthquake 7 (a=0,7 m/s^2):

Displacements

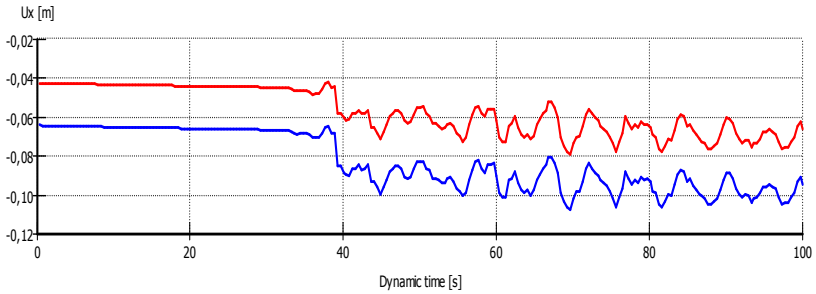

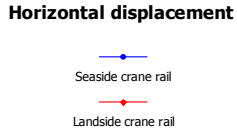

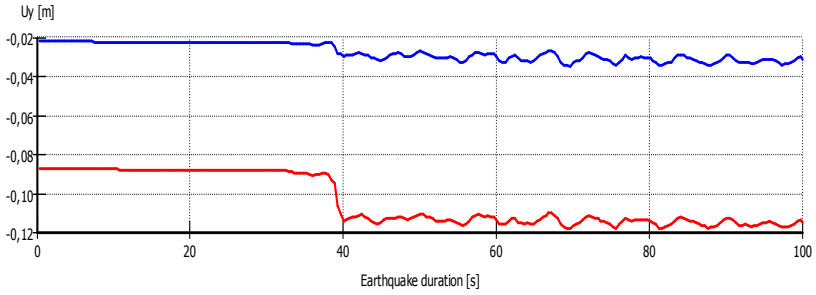

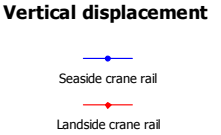

Plaxis Displacement	Hor. displacement After last phase	Vert. displacement After last phase
Seaside crane rail	-0,094	-0,031
Landside crane rail	-0,066	-0,114

Stresses

Plaxis Stresses	Depth M_{max} m NAP	M_{max} kNm/m	Max. axial force kN/m
Front wall		-3610	-1890
Wall 1	3	-2560	-1620
Wall 2	3	-3020	-1160
Wall 3	3	-3310	-944
Wall 4	3	-3100	-739
Back wall		-2700	-570

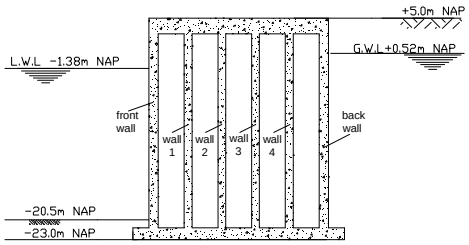

The Bending moment capacity of the walls depends on the amount of reinforcement steel placed in the wall and the axial force within the wall. The same method as mentioned in appendix M3 was used to determine the maximum bending capacity of the caisson walls. Notion must be made that during this calculation no safety factors was included because the real behavior of the wall is investigated. The maximum bending moment of each wall are determined and listed in the table below.

Plaxis Stresses	Max. axial force kN/m	M_{max} kNm/m	M_{cap} kNm/m
Front wall	-1890	-3610	-5215
Wall 1	-1620	-2560	-4163
Wall 2	-1160	-3020	-4276
Wall 3	-944	-3310	-4325
Wall 4	-739	-3100	-4369
Back wall	-570	-2700	-5660

Bending moment of walls

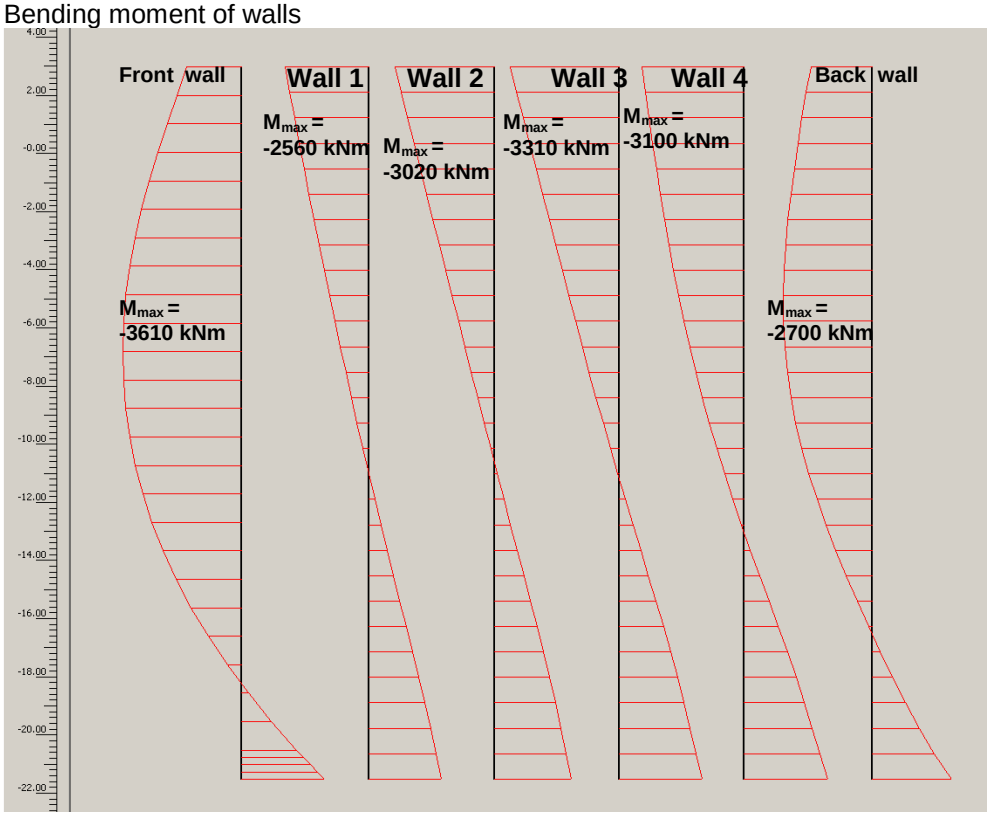

Axial forces of walls

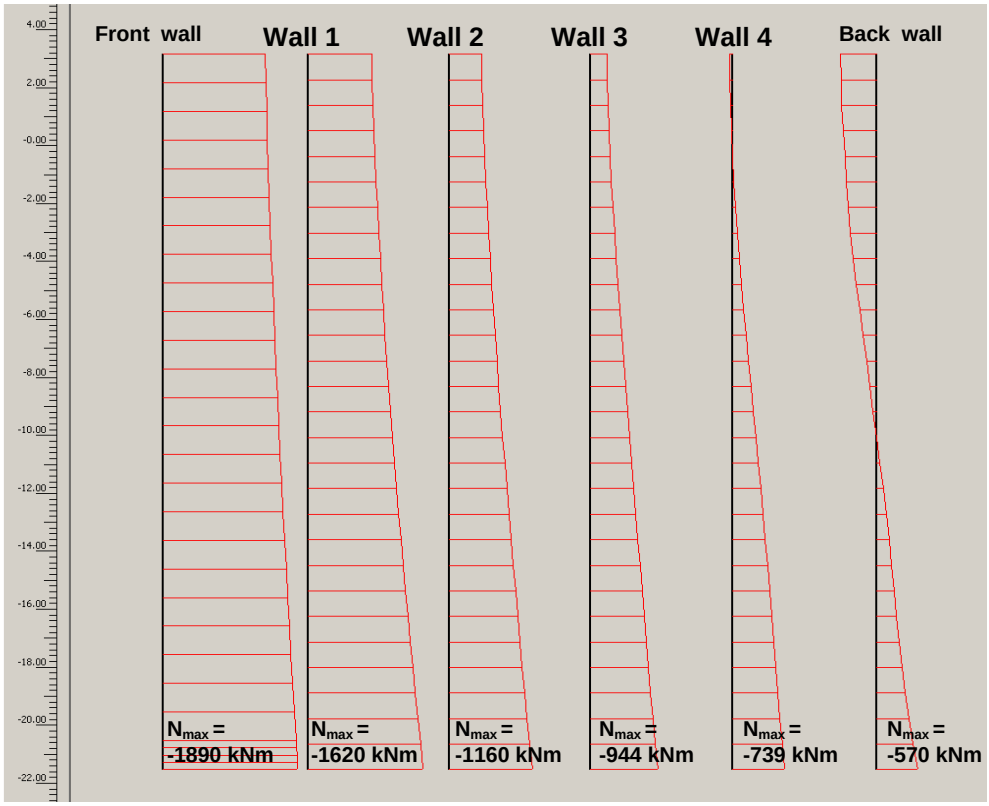

Earthquake 8 (a=0,8 m/s^2):

Displacements

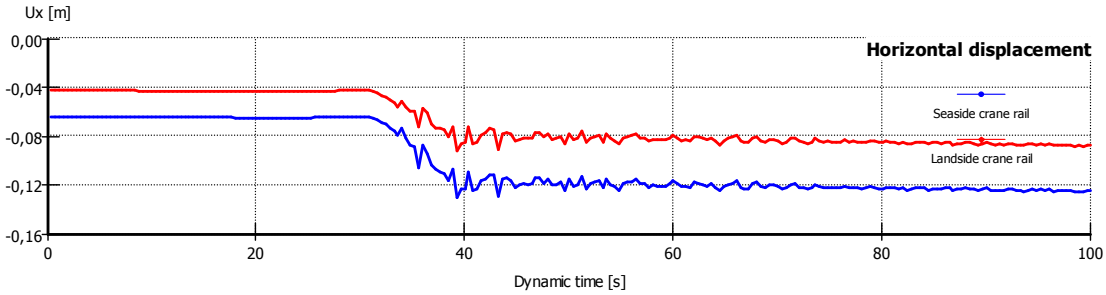

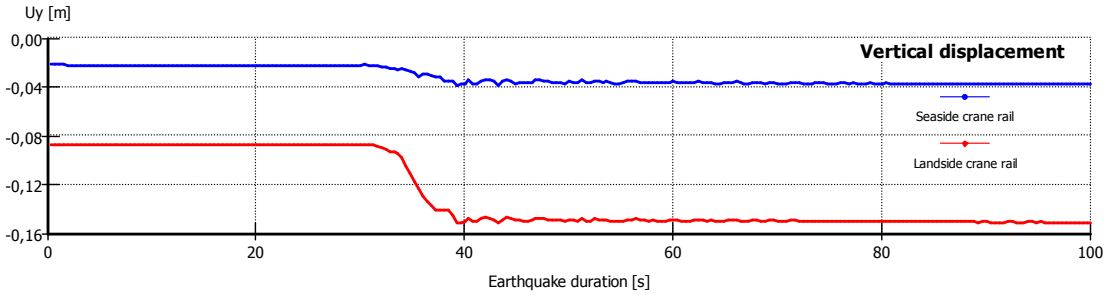

Plaxis Displacement	Hor. displacement After last phase	Vert. displacement After last phase
Seaside crane rail	-0,125	-0,038
Landside crane rail	-0,087	-0,151

Stresses

Plaxis Stresses	Depth M_{max} m NAP	M_{max} kNm/m	Max. axial force kN/m
Front wall		-3810	-1880
Wall 1	3	-2980	-1670
Wall 2	3	-3620	-1170
Wall 3	3	-4000	-891
Wall 4	3	-3740	-649
Back wall		-3140	-661

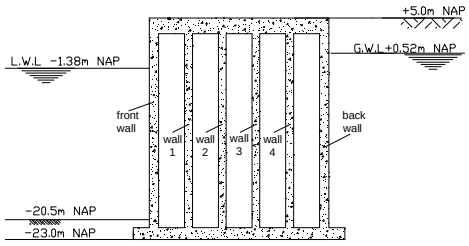

The Bending moment capacity of the walls depends on the amount of reinforcement steel placed in the wall and the axial force within the wall. The same method as mentioned in appendix M3 was used to determine the maximum bending capacity of the caisson walls. Notion must be made that during this calculation no safety factors was included because the real behavior of the wall is investigated. The maximum bending moment of each wall are determined and listed in the table below.

Plaxis Stresses	Max. axial force kN/m	M_{max} kNm/m	M_{cap} kNm/m
Front wall	-1880	-3810	-5219
Wall 1	-1670	-2980	-4150
Wall 2	-1170	-3620	-4273
Wall 3	-891	-4000	-4337
Wall 4	-649	-3740	-4388
Back wall	-661	-3140	-5632

Bending moments of walls

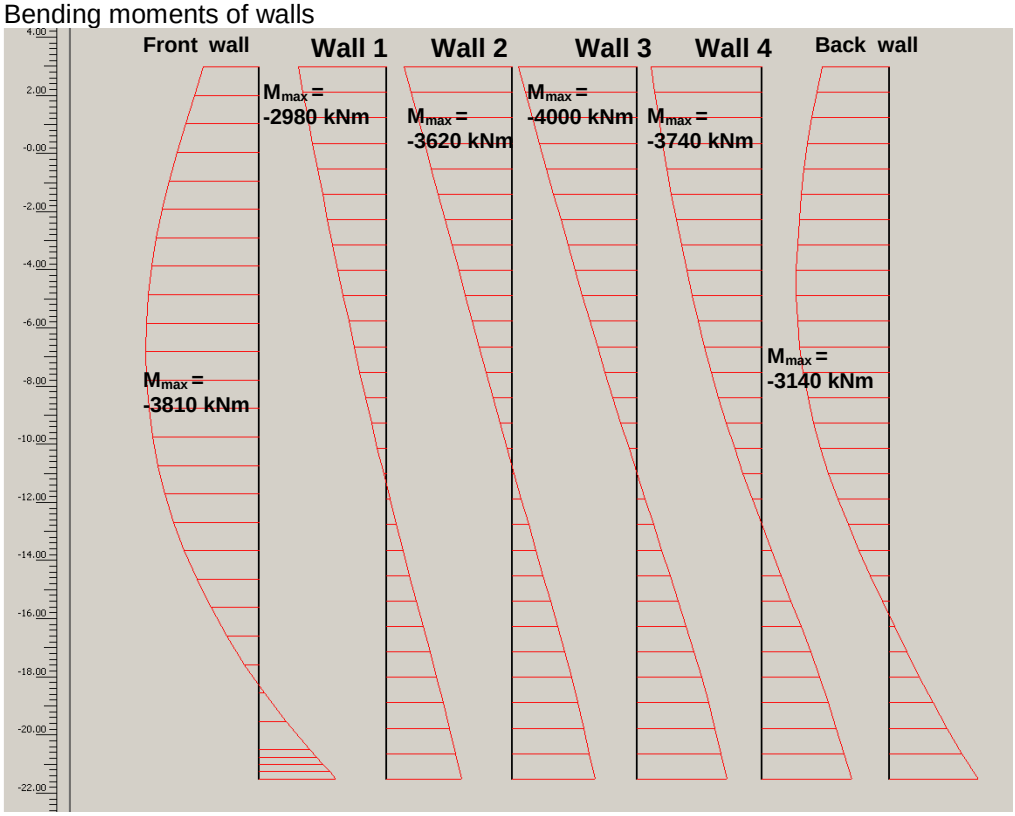

Axial forces of walls

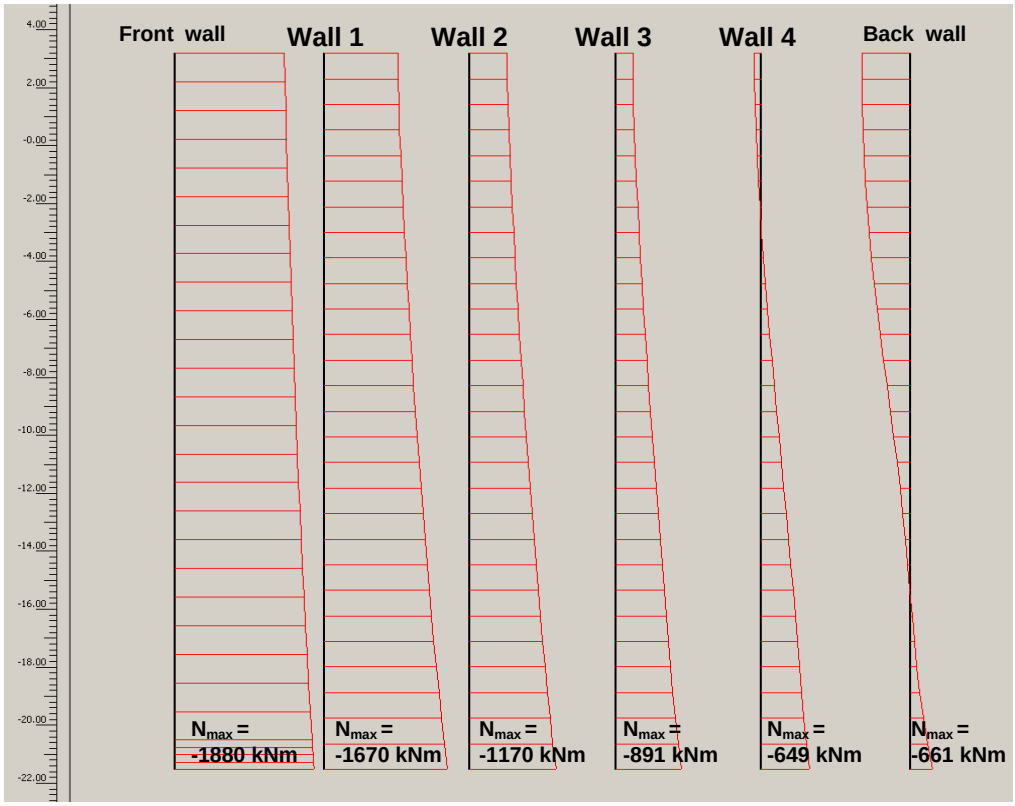

Earthquake 9 (a=0,9 m/s^2):

Displacements

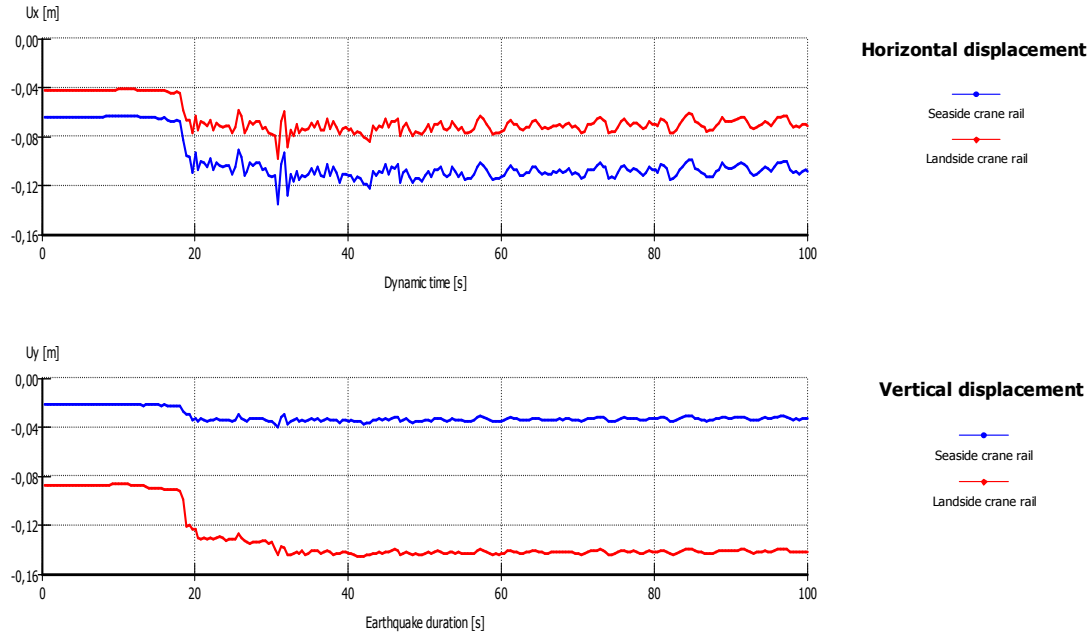

Plaxis Displacement	Hor. displacement After last phase	Vert. displacement After last phase
Seaside crane rail	-0,109	-0,033
Landside crane rail	-0,071	-0,142

Stresses

Plaxis Stresses	Depth M_{max} m NAP	M_{max} kNm/m	Max. axial force kN/m
Front wall		-3840	-1870
Wall 1	3	-2850	-1670
Wall 2	3	-3480	-1180
Wall 3	3	-3900	-920
Wall 4	3	-3710	-690
Back wall		-3040	-673

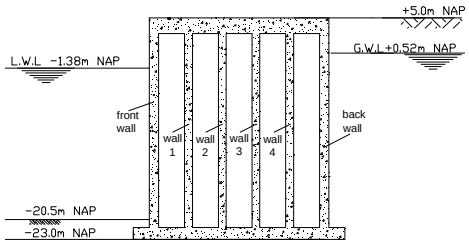

The Bending moment capacity of the walls depends on the amount of reinforcement steel placed in the wall and the axial force within the wall. The same method as mentioned in appendix M3 was used to determine the maximum bending capacity of the caisson walls. Notion must be made that during this calculation no safety factors was included because the real behavior of the wall is investigated. The maximum bending moment of each wall are determined and listed in the table below.

Plaxis Stresses	Max. axial force kN/m	M_{max} kNm/m	M_{cap} kNm/m
Front wall	-1870	-3840	-5222
Wall 1	-1670	-2850	-4150
Wall 2	-1180	-3480	-4271
Wall 3	-920	-3900	-4330
Wall 4	-690	-3710	-4380
Back wall	-673	-3040	-5628

Bendin moments of walls

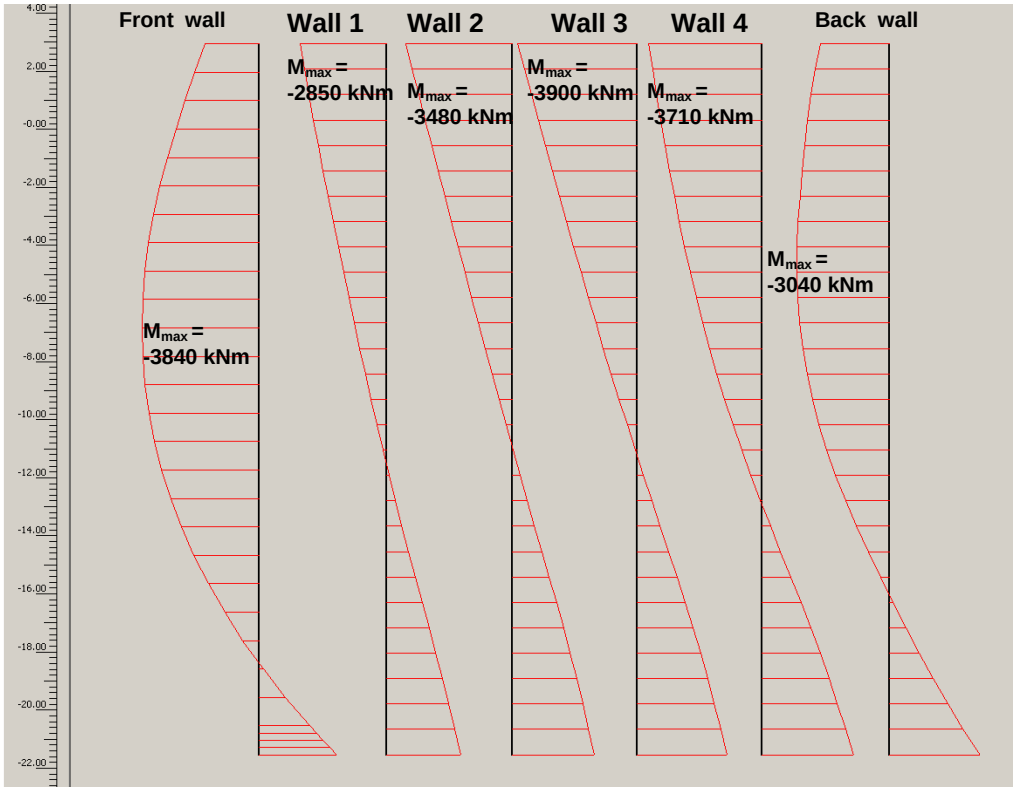

Axial forces of walls